ESRF
The European Synchrotron

ESRF UPGRADE PROGRAMME PHASE II (2015-2022)
TECHNICAL DESIGN STUDY

ESRF
The European Synchrotron

THE ORANGE BOOK

ESRF UPGRADE PROGRAMME PHASE II (2015 - 2022)

TECHNICAL DESIGN STUDY

PRESENTED BY:

Rudolf Dimper,
Harald Reichert,
Pantaleo Raimondi,
Luis Sánchez Ortiz,
Francesco Sette,
and Jean Susini.

This document contains contributions from many members of the ESRF staff, external experts and the scientific community, including:

D. Andrault, R. Barrett, S. Bayat, P. Berkvens, J.-C. Biasci, S. Billinge, B. Boulanger, J.-F. Bouteille, A. Bravin, E. Brun, F. Carla, N. Carmignani, H. Castillo-Michel, J.-M. Chaize, J. Chavanne, F. Cianciosi, P. Cloetens, P. Coan, S. Corr, M. Cotte, D. Coulon, Y. Dabin, I. Daniel, D. de Sanctis, M. DiMichiel, R. Dimper, J. Drnec, L. Dubrovinski, L. Ducotté, F. Ewald, P. Fajardo, L. Farvaque, R. Felici, C. Ferrero, G. Fiquet, A. Götz, L. Goirand, Y. Gouez, M. Hahn, J. Härtwig, P.F. Henry, O. Hignette, J. Hudspeth, S.D.M. Jacques, J. Jacob, N. Janvier, J. Kieffer, S.A.J. Kimber, C. Knabe-Ducheyne, M. Kocsis, M. Krisch, B. Lebayle, G. Le Bec, G. Le Duc, G. Leonard, S. Liuzzo, P. Loubeyre, P. Mackrill, T. Marchial, T. Mairs, P. Marion, D. Martin, T. Martin, M. McMahon, J. Meyer, M. Mezouar, E. Mitchell, C. Morawe, J. Morse, B. Müller, C. Müller-Dieckmann, T. Narayanan, B. Nash, B. Ogier, S. Pascarelli, H. Pedroso Marques, P. Pernot, T. Perron, F. Pfeiffer, E. Plouviez, C. Ponchut, A. Popov, A. Poulin, A. Rack, P. Raimondi, J.-L. Revol, H. Reichert, A. Royant, L. Sánchez Ortiz, M. Sanchez del Rio, M. Santoro, M. Scandella, K. Scheidt, T. Schülli, V. Serriere, F. Sette, A. Snigirev, V.A. Sole, J. Susini, O. Svensson, P. Tafforeau, G. Vaughan, F. Villar, B. Winkler, J. Wright, L. Zhang.

Editors: **Gary Admans, Paul Berkvens, Axel Kaprolat, Jean-Luc Revol**

THE ORANGE BOOK

ESRF UPGRADE PROGRAMME PHASE II (2015 - 2022)

TECHNICAL DESIGN STUDY

TABLE OF CONTENTS

FOREWORD

ESRF UPGRADE PROGRAMME PHASE II (2015 - 2022)

TECHNICAL DESIGN STUDY

THE UPGRADE PROGRAMME CONTEXT

The strength of modern X-ray science is its endeavour to provide unique tools and methods to understand and picture how atoms make and evolve the living matter and the materials that both surround us and of which we are constituted. Understanding materials for electronic devices and for storing and producing new forms of renewable and non-polluting energy, and unravelling the mysteries of biological reactions are examples of key challanges for which we need to improve our capacity to design future materials, processes, drugs, etc. These ambitious goals of 21st century science require fundamental understanding and visualisation of the hierarchical static and dynamic organisation of complex and functionalised matter with full continuity from macroscopic objects down to interactions among single atom pairs.

Future X-ray science at modern synchrotrons and XFELs will bridge the gap between visible light and electron microscopy, *i.e.* it will give full access to study changes within heterogeneous atomic assemblies from ~10^{12} atoms down to only a few atoms; all of this with spatial and temporal resolutions that will be approaching a few atoms in space (nanometre) and inter-atomic motion in time (femtosecond) respectively. Such incredible resolution and range in space and time are made possible by the absolutely impressive and never-ending improvements of brightness, spectral range and degree of spatial and temporal coherence and resolution of accelerator-based X-ray sources. During the last ~50 years peak-brightness has increased up to 22 orders of magnitude when compared to conventional laboratory sources.

In 2009, the ESRF launched an ambitious Upgrade Programme (UP) after a 15 year period (1994-2009) of successful user operation, aiming to provide new opportunities to address the new scientific challenges.

The Upgrade Programme builds on the widely recognised world-leading role of the ESRF in the development of synchrotron science. The ESRF's excellence is acknowledged today by: outstanding scientific record (~2 000 peer-reviewed publications/year and ~24 000 since the beginning, ~11 000 PIs in the last four years and ~6 000 users visits/year, directly contributing to work leading to the 2009 and 2012 Nobel Prize in Chemistry, etc.); unsurpassed reliability, flexibility and quality in the user operation mode of its accelerator and beamlines facilities; a unique instrumentation development programme for the benefit of its users in their exploitation of the facility, and for the national facilities in the Member Countries; the pioneering use of synchrotron science and techniques to support industry and innovation; the excellent training and education of young scientists and engineers for the benefit of science and other large scale analytical research infrastructures. Work at the ESRF has revolutionised the world perception and role of synchrotron science, as well as the European landscape of synchrotron and light source user facilities. It has become a reference model, inspiring

the construction of other first class national and international synchrotron, XFEL, extreme-light and neutron source facilities.

The ESRF UP objective is to maintain and strengthen the existing collaboration among its Member and Scientific Associate Countries to efficiently continue sharing knowledge, expertise and resources for the advancement of X-ray science in both fundamental and applied research fields for the benefit of their scientific communities. This collaboration and shared vision is critical for enabling scientists to work together and in competition with each other on the urgently needed breakthroughs which are necessary to ensure better long-term sustainability and the quality of our modern standard of living.

The ESRF UP aims to provide its scientific users with a new generation of instruments and beamlines coupling established scattering, diffraction and spectroscopy measurements to real space microscopy and 3-D imaging capabilities at the nanometre scale – *i.e.* well below the visible light diffraction limit of ~500 nm – and real-time dynamics down to ~100 ps. Breakthroughs are expected – and in some cases already within reach – in nano-science and nano-technologies, complex biological and soft-matter systems, time-resolved dynamical processes in complex materials, matter at extreme conditions, and in X-ray imaging techniques and applications. The whole of the UP is centred on the development of new instruments for the exploitation of new X-ray optics and nano-mechanics technologies, critically better X-ray detection, drastically improved on- and off-line data analysis and handling capabilities, and a qualitative increase in brightness and the degree of coherence of the X-ray source without the excessive increase in the total power load on critical instrument components.

Published at the end of 2007, the ESRF Purple-Book "Science and Technology Programme 2008-2017" sets the context of the ESRF Upgrade Programme by thoroughly reviewing the compelling science case, and the technology developments necessary for its implementation. The whole Upgrade Programme builds on the unique expertise of the ESRF staff, characterised by their scientific and technical understanding of state-of-the-art beamlines and their end-station capabilities and scientific exploitation, world-class accelerator and source development and operation capacities, unique and specially adapted instrumentation development know-how, and first-class overall technical and IT infrastructure support.

On the basis of the Purple Book, the ESRF Council decided in June 2008 to launch the ESRF UP by establishing a two-phase process. The Upgrade Programme Phase I (UP PI) for the period 2009-2015, and the Upgrade Programme Phase II (UP PII) to be prepared in the period 2012-2014, and to be presented to the Council for consideration in 2014 and launch in 2015.

THE UPGRADE PROGRAMME PHASE I

The Upgrade Programme Phase I has been on the ESFRI Roadmap since its first publication in 2006, and is today heading towards its successful completion by the end of 2015. In fact, it is considered as one of the ESFRI successes, thanks to its full realisation within ten years of the Roadmap's publication. The UP PI is centred on the construction of the new generation of X-ray instruments and beamlines briefly discussed above: 19 out of 30 public beamlines and end stations are under complete

reconstruction or major refurbishment; necessitating the recently delivered ~8 000 m^2 of new experimental hall premises with critical temperature and mechanical stability specifications, optics and nano-mechanics development, new state-of-the-art detectors, and improved computing and laboratory infrastructure. The accelerator complex also underwent extremely important developments to improve its brightness, reliability and stability. This included: a new beam monitoring and feedback system drastically reducing the vertical emittance; the lengthening and canting of insertion device straight sections; a new compact and powerful magnet design and its implementation; new single-mode RF cavities for further improvements in operation stability and reliability; a new solid-state-amplifier based RF power system; new topping-up injector operation. Considered as a whole, the UP PI – on average – allows ESRF beamlines to perform X-ray microscopy and imaging experiments at least 5 000 times better than before thanks to a brighter source (~x5), a smaller beam at the sample (~x100) and more efficient detectors (~x10).

The new features delivered by UP PI are very important for demonstrating that a new era of X-ray science is indeed emerging. Its strengthening effect and its impact will critically depend on the ultimate technical performances of the beamlines. To this purpose, the study and preparation of UP PII during UP PI is of pivotal importance for its launch. As reported in the Purple Book, the overarching questions for the UP PII are the following: 1) can one conceive a new storage ring at the ESRF with qualitative improvements to the present X-ray source parameters such as brightness, degree of coherence and temporal bunch length? 2) Does it make sense from a socio-economic point of view: required investment costs, expertise of ESRF staff, utilisation of existing infrastructure (storage ring tunnel, beamlines, insertion devices, facilities, etc.), new operation costs, impact on the user community (new scientific opportunities vs. shutdown periods, etc.)?

Answers to these questions in 2008 were not at all clear although they have been under close scrutiny for a long time, and this has been a key element leading the ESRF to opt for a two-phase process for the ESRF UP.

The ESRF Council, in 2011, formed an experts' Working Group, chaired by the then Council vice-Chair M. Van der Rest, with the charge of studying "The Strategic Mission of the ESRF for the forthcoming 20 years". A structured report concluded that, in line with the Purple Book's objectives, the ESRF should continue to represent a leading asset in synchrotron science for Europe and at the world level. To this purpose, it should actively pursue the goal of a storage ring upgrade in the existing tunnel capable of qualitatively increasing the X-ray source brightness and transverse coherence. This endeavour should consider the use of modern accelerator technologies developed during the last few years and must be a key deliverable of Phase II of the ESRF Upgrade (http://www.esrf.eu/news/general/strategic-mission/index_html).

THE QUEST FOR "THE ULTIMATE DIFFRACTION-LIMITED STORAGE RING X-RAY SOURCE"

The technical approach to provide a suitable answer to the two questions above has challenged the accelerator community for many years, and many studies on the development of an ultimate low-emittance storage ring have been scrutinised for a long time. In fact, within the storage ring parameters space, the parameter that could in principle be substantially reduced with the effect of dramatically increasing the

X-ray source brightness is the electron beam equilibrium horizontal emittance. This is particularly true in the most advanced operating machines which have reached the diffraction limit in the vertical plane, but do have – as at the ESRF - a horizontal emittance ~1 000 times larger than the vertical emittance.

Methods to substantially reduce the horizontal emittance in a storage ring have been a regular topic of discussion among accelerator scientists since D. Einfeld's pioneering work (Einfeld *et al.*, 1996), and would require radical changes to the storage ring magnet lattice optics design. Discussions and presentations have taken place regularly on this topic since the ICFA 10th Beam Dynamics Workshop on Future Light Sources (Laclare, 1996), and in particular in dedicated ICFA Workshops in 1999, 2002, 2006, 2010 and 2012. Papers on the concept of an "Ultimate Storage Ring" (Ropert *et al.*, 2000; Elleaume *et al.*, 2003; Borland, 2008) have been published regularly. Moreover, at some of these workshops, machine designs with dramatically improved horizontal emittance were presented (PEP-X and SPring-8 II, Hettel and Soutome, 2011). Similarly, for applications other than the production of synchrotron radiation, the concept of using radiation damping for electron emittance cooling has also been studied for high energy physics programmes in a series of "Low Emittance Rings" workshops (CERN, 2010; Heraklion, 2011; Oxford, 2013).

The two main technical approaches for emittance reduction being an increase of the number of bending magnets (multiple bends with often major increases of the storage ring circumference) and the extensive use of damping wigglers (with increased electricity costs, and a reduction of the available straight sections for insertion devices), developed the feeling that perhaps the storage ring concept had already reached ideal performances from a practical point of view, and was not the best option for realising an X-ray source approaching the diffraction limit both in horizontal and vertical directions. This justifies, among other aspects, the interest of the accelerator community in the study of low emittance Linacs and single pass circular devices with energy recuperation (ERLs), where the concept of a diffraction limited source can be developed, giving up – at least partially – the energy-consumption efficiency and operation stability of a storage ring. The advent of reliable low-emittance Linacs, however, brought the concept of an ultimate storage ring to the forefront once again, especially for electron beam energies required for a soft X-ray source. In fact, the design of a multiple bend lattice coupled to a top-up injection sequence using such a Linac has been successfully developed, and adopted for the construction of the new MAX IV facility (https://www.maxlab.lu.se/node/1136), which is presently under implementation on the basis of a seven-bend achromat design. Moreover, the Sirius project (Campinas, Brazil), operating at energies similar to MAX IV, is currently under design, like similar programmes under consideration at other facilities.

The ESRF in the period 2007-2009 considered options for a three- and a four-bend achromat lattice design (Elleaume, 2009) to be constructed in the existing tunnel. It was concluded, however, that the project was risky and expensive due to the challenges related to a reliable top up injection and the operation of such a storage ring. The case for high energy storage rings like ESRF, APS, Spring-8 and Petra III was reviewed by P. Elleaume at the DOE workshop on "Physics of future light sources" (Gaithersburg, 2009).

In 2011, at the Gordon Research Conference on X-ray Science, scientists discussed the needs for future competitive scientific use of synchrotron sources. They concluded that

indeed the possibility of a storage ring based diffraction limited hard X-ray source, with a factor 10-100 increase in source brightness, would be extremely attractive in supporting the X-ray science case such as that first presented in the ESRF Purple Book. A core of these X-ray scientists (H. Dosch, J.B. Hastings, T. Ishikawa, C.C. Kao, H. Reichert and F. Sette) decided to launch three workshops on storage ring based future light sources (ESRF, February 2012; SPring-8, December 2012; SLAC, December 2013), with the principal aim of bringing together the accelerator and synchrotron user scientific communities to discuss the prospects in terms of brightness increase from either a new "green-field" ultimate storage ring facility, or from the best lattice upgrade design of an existing storage ring, and how this would enable new science.

P. Raimondi, the newly appointed Director of the ESRF Accelerator and Source Division, proposed a new lattice concept based on a hybrid multiple bent achromat design, where the concept of multiple bends to reduce the horizontal emittance is maintained, but the cell design contains three families of bending dipoles: a central one and two identical but mirror symmetric at the entrance and at the exit of the cell respectively. This design, coupled to strong sextupole magnets at the entrance and exit of the arc and strong quadrupole magnets in the centre of the arc, simultaneously leads to a dramatically reduced horizontal emittance – almost a factor of two better than in a standard multiple bend design – and with efficient injection from existing full energy injector booster rings. This innovative design has been carefully studied by the ESRF Beam Dynamics Group, and benchmarked at SLAC (Cai *et al.*, 2012), where it has been amply validated. Since 2012, the ESRF has been working on the design of the upgrade of the existing ESRF storage ring lattice based on the Raimondi proposal. A White Paper was presented in November 2012 to the ESRF Council, proposing that: i) this new lattice concept will be used to upgrade the existing ESRF storage ring and thus represent one of the core deliverables of the UP PII, and ii) the immediate ESRF objective should be to prepare, by June 2014, a full scale Technical Design Study (TDS) to allow the Council to consider the UP PII implementation as of 2015 and delivery by 2020.

We are proud to present here, on behalf of all our colleagues at the ESRF and of the many people from the world accelerator and X-ray science communities, the Technical Design Study Report presenting the proposal for the implementation of the ESRF Upgrade Programme Phase II.

THE ORANGE BOOK

The present Technical Design Study Report is the proposal for the implementation of the ESRF Upgrade Programme Phase II, and we will refer to it often as "The Orange Book". It follows the tradition at the ESRF to refer to a colour for papers which have marked its history: "The Black Book" in 1975, "The Blue Book" in 1979, "The Yellow Book" in 1982, "The Green Book" in 1984, "The Red Book" in 1987 and "The Purple Book" in 2007.

The deliverables of the UP PII are:

1. The procurement, pre-assembly, construction and commissioning of a new low-emittance storage ring lattice substituting the present one in the existing storage ring tunnel during the period 2015-2020. The horizontal emittance will be reduced by at least a factor of 30, with consequent similar increases in X-ray source

brightness and coherence – especially at hard X-ray energy. Even higher increases will be provided by the envisioned new insertion device technologies and other storage ring improvements that could improve source properties by up to a factor of 100 compared with those of today.

2. The identification, design, construction and commissioning of four new state-of-the-art insertion device beamlines to fully exploit the brightness and coherence properties of the new upgraded X-ray source in the period 2020-2022.

3. The implementation of an aggressive scientific instrumentation roadmap, with the delivery of an ambitious detector programme and of a new computing infrastructure to handle the massive amount of data expected from the scientific exploitation of the new X-ray source. The new detectors and data collection strategies will boost present performances – especially in large data volume experiments such as serial nano-crystallography and X-ray microscopy and imaging – by at least a factor of 10-100.

The Orange Book is divided into 4 chapters.

Chapter 1 of The Orange Book reviews the science case that will be enabled by the delivery of the proposed ESRF storage ring upgrade. The scientific areas and objectives are the same as those presented in 2007 in The Purple Book. However, their evolution during the last seven years has been very significant thanks to new scientific results, and to the advent of new instrumentation capabilities including the first opportunities offered by the new ESRF UP PI beamlines, and the first exciting results at the LCLS and SACLA XFELs. Therefore, we have decided to present its update in The Orange Book.

The updated science case has greatly benefitted from thorough discussions with the international synchrotron user community and also from the input of both accelerator and scientific instrumentation communities who have been solicited to work together to assess the new science opportunities. The ESRF's 2013 and 2014 Users Meetings, more than 10 dedicated workshops and meetings organised at the ESRF in 2013 and 2014, the ESRF Science and Students Days in October 2013, the Gordon Research Conference on " X-ray Science" in August 2013, the " Future Light Sources" Workshop at SLAC in December 2013, discussions with the ESRF SAC at its spring and autumn 2013 meetings are just a few examples of the widespread international interest in the new scientific opportunities that the ESRF lattice upgrade will enable. The scientific community at large is very interested in the new horizons opening up in X-ray science, where *X-ray microscopy techniques* will be able to bridge the presently existing gap between *optical microscopy* and *electron microscopy*. It sees "almost infinite" applications in condensed matter science, innovative materials research and life science.

Chapter 2 of The Orange Book presents the Technical Design Study of the proposed ESRF storage ring lattice upgrade. It constitutes, with **Chapter 4**, the main technical bulk of the present Orange Book. The lattice study, launched at the beginning of 2013, has evolved into that of the present proposal thanks to the motivation and dedication of many people at the ESRF. We estimate that approximately 28 full-time equivalent ESRF staff have worked on these topics during the last 15 months. The ESRF has benefitted enormously from the critical advice of the Accelerator Programme Advisory Committee (APAC) created by the Council in spring 2013. The APAC met in September 2013,

January 2014 and in May 2014 to review the lattice upgrade preparation work reported here. **Chapter 2** sets the framework for the upgraded storage ring objectives, presents the properties of the upgraded X-ray source, describes the new lattice design, and reviews the engineering design challenges and the planned solution. The last section of **Chapter 2** is dedicated to the implementation programme. It describes the procurement and preparatory work – which will take place in the period between 2015 and Mid October 2018 in parallel to the normal operation of the ESRF – and the construction and commissioning work, which will take place during a shutdown period lasting from 15 October 2018 until 31 May 2020, at which time user operation will be resumed.

Chapter 3 of The Orange Book reviews the procedures for the identification of the most attractive scientific opportunities to be addressed, with the construction by 2022 of four new state-of-the-art beamlines. With the construction of these new beamlines, the nominal ESRF public beamline portfolio will return to its ideal value of 30 beamlines from the present 28 beamlines. This reduced number of beamlines is dictated by the need to transfer a fraction of the operation budget resources to the UP PII construction budget. It has already been the case since 2011, to address budget pressure in the delivery of the UP PI, and with the support of the ESRF Science Advisory Committee, the Council decided upon the temporary closure of two public beamlines. These resources will be transferred back to operation at the end of the UP PII in 2022 to enable the reinstatement of the full beamline portfolio. The chapter also thoroughly reviews the impact of the new source on the existing beamlines, and in particular on the new beamlines and stations constructed during UP PI and on the bending magnet beamlines.

Chapter 4 of The Orange Book presents the outcome of a detailed survey on the scientific instrumentation needs that are necessary to fully exploit the new source properties. The scientists and engineers involved in this thorough analysis, led by the ESRF instrument development and technical infrastructure support divisions, have considered the impact of the new source properties on all of the different steps from X-ray generation, transport, delivery and detection to data storage. The many challenges of X-ray nano-optics, precision mechanics, sample environment and positioning, detectors and data storage are considered in detail in the context of addressing the scientific challenges presented in **Chapter 1**. We highlight how important and necessary it is to invest in a powerful instrumentation programme, and a proposal for two ambitious programmes is presented. One focuses on a new detector plan for the exploitation of coherent scattering and nano-imaging. The second deals with the imperative need to develop a powerful and user friendly computing infrastructure to allow on-line data analysis, and to handle the very large amount of data that will be produced by the future beamlines and stations.

The TDS Report has been prepared during the last 18 months thanks to the excitement and dedication of many people at the world level together with the motivation, skill and experience of the ESRF staff in all Divisions and Services, and in particular thanks to the input and critical views of the ESRF user communities, and the different advisory panels: AFC, APAC and SAC.

CONCLUSION

The UP PII of the ESRF proposes the design and implementation of a new low emittance lattice storage ring to be constructed and commissioned in the existing storage ring tunnel as a substitute for the present storage ring. This challenging programme will be carried out in the period 2015-2020, to be followed in the period 2020-2022 by the construction of four new state-of-the-art beamlines. During the whole 2015-2022 UP PII implementation period – in line with the UP PII scientific goals, the new and existing beamlines, and the scientific instrumentation roadmap to fully exploit the new X-ray source potential – the UP PII will deliver breakthrough developments in X-ray detection technology and large data handling infrastructure.

Compared to present third generation source capabilities, the ESRF Upgrade Programme as a whole, will enable in the next decade completely new X-ray microscopy, imaging and nano-crystallography applications with a performance enhancement that can go all the way up by a factor of 10^6. This is through its average upgraded beamline performance improvements in X-ray microscopy applications in the *meso*-scale of approximately 5000 provided by the UP PI, and the further improvements planned through UP PII due to the enhancement of source properties and scientific instrumentation.

The UP PII will conclude the ESRF Upgrade Programme, and deliver by 2022 a fully renewed facility, which will be able to address the most challenging X-ray science questions at least for the subsequent 10-20 years. This is through its average upgraded beamline performance improvements in X-ray microscopy applications in the meso-scale of approximately 5000 provided by the UP PI, and the further improvements planned through UP PII, due to the enhancement of source properties and scientific instrumentation.

The ESRF Upgrade Programme, thanks to the strong collaboration existing among the ESRF Member and Scientific Associate Countries, will pave the way for future synchrotron science, and contribute at a global level to an exciting time for fundamental discoveries and innovative applications. The new opportunities in X-ray science, complementing and extending other advanced analysis tools for material and living matter, will contribute with key discoveries to the sustainable well-being of our society: new smart materials will optimise the use of existing natural resources and provide better production and management of clean energy, new understanding of biological processes at the mesoscopic and cellular levels will introduce new drugs and create new diagnostic and therapeutic programmes, and studies of exotic natural thermodynamic states will help us to better understand our planet, its resources and evolution. These far-sighted plans will attract a new generation of scientists who, with the use of a new generation of X-ray probes, will be able to explore and understand more effectively than today many of the mysteries of the world surrounding us.

Rudolf Dimper,
Harald Reichert,
Pantaleo Raimondi,
Luis Sánchez Ortiz,
Francesco Sette
and Jean Susini

References

Einfeld D., Schaper J., Plesko M., A lattice design to reach the theoretical minimum emittance for a storage ring, Proceedings EPAC 1996, Sitges 1996.

Ropert A., Filhol J.M., Elleaume P., Farvacque L., Hardy L., Jacob J., Weinrich U., Towards the ultimate storage ring-based light source, Proceedings EPAC 2000, Vienna 2000.

Elleaume P., Ropert A., The ultimate hard X-ray storage-ring-based light source, *Nucl. Instr. and Meth. A* 500, 18 (2003) .

Summary of NSLS II Source Properties, 2007, http://www.bnl.gov/nsls2/project/source_properties.asp

Borland M., Ultimate Storage Ring Light Sources, LSU Grand Challenge Workshop, 2008, Louisiana State University, Jan 2008.

Hettel R. *et al.*, Concepts for the PEP-X Light Source, Proceedings of PAC09, Vancouver 2009.

Elleaume P., Overview of ultimate storage ring: status and challenges, DOE Workshop on "Physics of future light sources", Gaithersburg, 2009.

Bei M., Borland M., Cai Y., Elleaume P., Gerig R., Harkay K., Emery L., Hutton A., Hettel R., Nagaoka R., Robin D., Steier C., The Potential of an Ultimate Storage Ring for Future Light Sources, *Nucl. Instr. and Meth. Phys. Research A*, **622**, 518-535 (2009) .

Detailed Design Report on the MAX IV Facility, 2010 https://www.maxlab.lu.se/node/1136, 2010.

Nosochkov Y., Bane K., Cai Y., Hettel R., Wang M.W., Lattice design for PEP-X ultimate storage ring light source, Proceedings IPAC 2011, San Sebastian, 2011.

Shimosaki Y., Kaneki K., Nakamura T., Ohkuma H., Schimizu J., Soutome K., Takao M., Design study of nonlinear optics for a very loe-emittance lattice of the Spring8-II, Proceedings IPAC 2011, San Sebastian, 2011.

SPring-8 Upgrade Plan Preliminary Report, 2012, http://www.spring8.or.jp/pdf/ja/sp8II/pr/preliminaryreport.pdf

The Strategic Mission of the ESRF for the forthcoming 20 years, 2012
http://www.esrf.eu/news/general/strategic-mission/index_html

ESRF Upgrade Programme Phase II (2015-2019) White Paper, 2012, http://www.esrf.eu/files/live/sites/www/files/about/upgrade/documentation/whitepaper-upgrade-phaseII.pdf

Cai Y., Hettel R., Rabedau T., Evaluation of the ESRF lattice upgrade proposal, SLAC, 2012.

The First Workshop: ICFA 10th Beam Dynamics Workshop on Future Light Sources, January 22-25, 1996, Grenoble, France, organised at ESRF by JL Laclare.

The Second Workshop: ICFA 17th Advanced Beam Dynamics Workshop on Future Light Sources, April 6-9, 1999, Argonne National Laboratory, Argonne, IL USA.

The Third Workshop: ICFA 24th Advanced Beam Dynamics Workshop on Future Light Sources, May 1-4, 2002, SPring-8, Japan.

The Fourth Workshop: ICFA 37th Advanced Beam Dynamics Workshop on Future Light Sources (FLS2006), May 15-19, 2006, DESY, Hamburg, Germany, organised by J. Rossbach and K-J. Kim.

The Fifth Workshop: 48th ICFA Advanced Beam Dynamics Workshop on Future Light Sources (FLS2010), March 1-5, 2010, SLAC, Menlo Park, CA, USA.

The Sixth Workshop: International ICFA Workshop on Future Light Sources (FLS2012), March 5-9, 2012, JLAB, Newport News, VA, USA, organised by S. Chattopadhyay, G.R. Neil and G.P. Williams.

Low Emittance Rings 2010 Workshop, CERN 2010.

Low Emittance Rings 2011 Workshop, Heraklion, 2011.

Low Emittance Ring 2013 Workshop Oxford, 2013.

ESRF
The European Synchrotron

PART 1
Science Drivers

INTRODUCTION

The science drivers for the Upgrade Programme of the ESRF were laid out in detail in the Purple Book that served as a guide for the definition of the UP PI. Its publication in 2007 identified new opportunities in both frontier and applied research that were summarised in five broad reference areas (**Figure 1.01**).

These areas still serve as a valuable guide for the development of a science case that goes far beyond the goals set out for UP PI.

Figure 1.01: Areas of opportunity identified in The Purple Book in 2007.

The UP PII will deliver X-ray beams of qualitatively higher brightness and transverse coherence (see **Chapter 2**) allowing a smaller X-ray beam size down to the nanoscale with a further improved level of stability and reliability. This will provide unprecedented tools for the investigation of matter and its dynamical properties from the atomic length scale all the way up to the size of real devices. Already in 2015, the ESRF beamlines will offer a beam size from 14 nm to 100 mm (and unsurpassed parallel collimation), thus covering a range of 7 orders of magnitude, but limited in brilliance and coherence. It is the prime goal of the UP PII to substantially overcome these limitations.

X-ray science has taken great strides towards characterising *isolated* objects down to the nanoscale thanks to recent developments in nano-beams and coherent scattering techniques such as ptychography and coherent X-ray diffraction imaging. The next big challenge is the development of new methodologies for characterising *embedded* nanoscale structures down to the atomic level within multi-scale structural hierarchies on all relevant time scales that govern the function of any material, be it organic or inorganic.

The second parameter where the synchrotron radiation source performance will be improved dramatically is the transverse horizontal coherence of the beam which is today at the level of a few per thousand in the energy range up to 8 keV; it decays rapidly to even lower values with increasing X-ray energy. Similarly to the brightness, the coherent fraction of the X-ray beam grows linearly with decreasing emittance. The unmatched coherence properties of the new source, with a gain in excess of a factor of 40 at higher energies, will open new avenues in the exploitation of coherence. This will be mainly due to the fact that coherent scattering carries information on the micro- and nano-structure of materials below the size of the probing beam without averaging, and this should in principle allow us to reach a detection limit close to single atoms.

The unique possibilities in the five areas that are presented in this chapter are intimately linked to the major societal challenges we are facing today: progress in biology and life sciences has a direct impact on human health; *in situ* materials chemistry is a key area in energy-related technologies; nano-science and nano-technology are at the heart of information technology; and the understanding of matter at extreme conditions provides new opportunities for the development of new high-performance materials. The five scientific key areas also have profound implications for applied and industrial applications.

To reach the goals described in the science case below, a new generation of scientific instrumentation is required, which the ESRF sets out to develop in the coming years. Advanced instrumentation is the key to dealing with one of the most challenging aspects for the exploitation of the potential of the new source: radiation damage induced by the intense, focused X-ray beams. Today's experiments suffer not only from primary radiation damage directly induced by the interaction of high energy photons with the sample material, but also from secondary radiation damage spreading throughout the sample in the course of an experiment. The advent of XFELs supplying extremely short and intense pulses of photons has shown the way to beat secondary radiation damage by performing experiments faster than the damage can spread in the material. The increase in peak brightness of a (near-) diffraction limited source together with well-suited instrumentation for fast data collection will enable synchrotron-based experiments to counter radiation damage in a similar way.

New instrumentation is the key to building completely new instruments that offer scientific opportunities not available today. For instance, new beamlines for serial synchrotron crystallography or hard X-ray diffraction microscopy (the X-ray analogue of transmission electron microscopy) will provide deep insight into materials and their properties that is not available today. New instrumentation will also help to adapt the existing beamline portfolio to the full potential of the new source (see **Chapter 3**). The corresponding instrumentation programme includes all aspects of X-ray technology from photon beam transport, sample handling and manipulation, detection of photons with the highest efficiency and resolution, to the analysis of large quantities of raw data acquired in a very short time. A roadmap to achieve these ambitious goals is described in detail in **Chapter 4** of this document.

In line with the science case laid out in the Purple Book, new scientific opportunities are presented in detail in the following chapter for:

- interactions between biological systems and exogenous materials
- structural and functional biology: new opportunities at cellular and molecular levels
- *in situ* materials chemistry
- nanomaterials for technology
- matter at extreme pressures and temperatures
- enhanced industrial applications and exploitation of synchrotron science

These areas serve as a valuable guide for the development of a science case that goes far beyond the goals set out for UP PII.

1.1. INTERACTIONS BETWEEN BIOLOGICAL SYSTEMS AND EXOGENOUS MATERIALS: FRIEND OR FOE?

Opportunities

- Probing the bioresponse to exogenous materials with the ultimate sensitivity and resolution
- Multiscale analysis of heterogeneous materials
- Low-dose *in vivo* tomography of living organisms

1.1.1. INTRODUCTION

Bio-interaction with exogenous materials is part of our everyday life. Natural and synthetic materials can enter into individual organisms both intentionally (*e.g.* medical treatment) as well as accidentally (*e.g.* indirect uptake from air, water, soil or food). The bio-response to exogenous materials is intrinsically complex, requiring powerful non-invasive techniques such as X-ray imaging based on synchrotron sources of ultimate performance in order to evaluate whether the interaction of materials with living organisms will be friend or foe.

The public perception of exogenous materials in living organisms is usually linked to biomedical applications: in 2013, two major breakthroughs in medicine were the first implant of an artificial heart and the development of anti-cancerous nano-capsules, the latter receiving the European Inventor Award 2013. Both cases represent, at two opposite length scales, the development of complex, structured and functionalised devices to support life. In the coming decade, 3D (bio)-printers are expected to revolutionise daily life and medicine, more particularly "in the same way as the printing press revolutionised conventional printing" (Schubert *et al.*, 2014). In general, the use of synthetic materials for medical purposes, in particular nano-metric objects, is burgeoning in the same way as the production of other commodities (*e.g.* cosmetics, electronics, fertilisers) in the past, increasing their potential interaction with living organisms. In all cases, a full life-cycle analysis is important to understand the interplay between human life and the environment. Whenever this understanding is lacking or ignored, enormous negative effects may be observed as exemplified by well-known cases of asbestos, CFCs, and the recent case of PIP breast implants. A transition from a reactive approach towards a more proactive approach would be highly appropriate in a science-driven society.

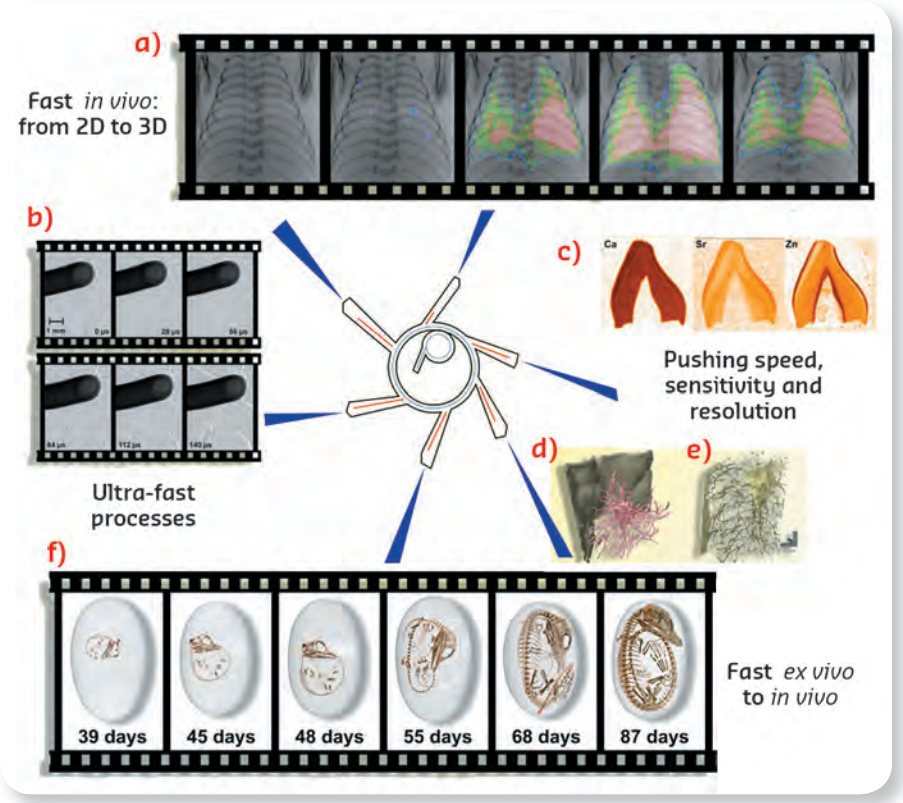

Figure 1.02: Benefits of Phase II of the ESRF Upgrade Programme for X-ray imaging: from *in vivo* radiography (a) to *in vivo* tomography (e), from static structures and devices (c,d,e) to in operando research (b) up to the ultimate spatial, temporal and chemical resolution.
Credits: a) Marcus Kitchen, Monash University. te Pas AB et al., 2009. b) Rack A. *et al.*, 2014. c) Bonnin A., Tafforeau P., Bohic S., Tack P. and Garrevoet J., unpublished. d) Langer M. *et al.*, 2012. e) Reprinted by permission from Macmillan Publishers Ltd: Dierolf M. *et al.*, *Nature* **467**, 436-440, copyright 2010. f) Tafforeau P., Kundrát M. and La *Ferme aux Crocodiles* (Pierlatte, France), unpublished.

X-ray imaging as a multipurpose multimodal platform at the ESRF is a unique tool which provides insight into the complex interplay between living host organisms and exogenous materials. The current and future ESRF X-ray imaging beamlines offer unique instruments for studying complex systems, from soft materials such as proteins and cells to hard materials such as nano-electronics and catalysts. The diversity of techniques also facilitates the study of the frontier between soft and hard materials to understand how both systems (living organisms and materials) interact at different length and time scales. This simple description encompasses a very large number of cases that can be divided into two main categories based on origin: either the interaction is on purpose, and usually designed and controlled by humans (*e.g.* medical treatments, cosmetics, or fertilisers) or it is accidental, with natural or human origins (*e.g.* side effects of medical treatments (Li *et al.*, 2014) or pollution in the working or living environment (Pascolo *et al.*, 2013). While the material part can be relatively simple (as in the case of nano-particles or gas), the biological system (cells, tissues and organs) is by default complex. Accordingly, imaging capabilities are required to follow endogenous and exogenous components simultaneously. The multi-scale character of the phenomena requires versatile imaging solutions. The present X-ray beams can be tailored to cover a field of view as large as a decimetre, while lateral resolution can reach the nanometre scale (not necessarily on the same experimental station). The new source, combined with the existing beamlines, will allow the consecutive characterisation of the same system over several length scales by providing access to different complementary experimental stations or by offering length-scale flexibility at one beamline.

In the following sections, several examples of interaction between living organisms and materials are presented (*cf.* the generic **Figure 1.02**). The main benefit for X-ray imaging offered by the proposed new source is the increased amount of coherent photons (especially at higher energies) that allows shorter acquisition times while phase-contrast imaging techniques maintain a high sensitivity, thus enabling X-ray cinematography even for dose-sensitive samples in a hierarchical manner. The increased brilliance will also give rise to a substantially enlarged photon flux density. Both, multiscale characterisation and nanometric resolution when combined with large penetration depth are unique properties of X-ray imaging which will greatly benefit from the improved synchrotron source.

Further to the examples presented here, X-ray imaging will also provide new insight in other areas such as micro- and nano-technologies, applied industrial research, life sciences (*e.g.* evolutionary biology, bionics and/or biomimicry), and energy research.

1.1.2. *Ex vivo* NANOCHEMISTRY

Nanomaterials are increasingly being used in medicine, cosmetics and even in agriculture, and deserve particular attention. The uptake of nanoparticles in cells and tissue is of major interest. Both the potential and risk associated with these ubiquitous systems must be evaluated (Lewinsky *et al.*, 2008). Advanced nanoscale three-dimensional imaging, in both full-field and scanning modes, at subcellular and tissue level will be fundamental in order to understand the mechanisms controlling nanoparticle uptake, partitioning and aggregation. Pushing the resolution limit as much as possible was the main objective of the Nano-imaging/Nano-analysis project within Phase I of the Upgrade Programme. With Phase II, nanobeams will become a common commodity at many beamlines and studies of nanoscale materials will become routine. In particular, such studies will increase the level of detail in investigations of biological systems (Dierolf *et al.*, 2010).

The increased brightness of the source will allow us to shift the detection limits a long way towards single atom detection using X-ray fluorescence at the most advanced beamlines such as the ID16A/B NanoImaging/NanoAnalysis complex. Among the many potential applications are the visualisation of action mechanisms of therapeutic agents and nanovectors (at therapeutic concentrations). Promising examples are small interfering RNA based drugs. The best resolution in X-ray imaging achieved today is about 5 nm in coherent imaging from strongly scattering objects. Even though it is obvious that X-ray microscopy will never achieve the spatial resolution of electron microscopy, the true strength of hard X-ray techniques lies in their large penetration depth while preserving the resolution. It is thus possible to produce high resolution images from extended objects with the structure of interest deeply buried inside the object. The improved nanometric spatial resolution and detection of features through (pink beam) ptychography and magnified holotomography will enable the detection of defects in almost any object, for example in artificial organs. Of particular interest is the development of a bio-compatible sheet to encapsulate beta cells in

an artificial pancreas. This requires the detection of defects in polymer structures which are smaller than 10 nm and several hundred µm thick.

In addition to the gains from exploiting the smaller beam with higher coherence, the increase in brightness will offer a major step towards multi-scale analysis. When nano-particles interact with plants, they are frequently distributed inhomogeneously over millimetric regions within the plants. The large scale localisation of these particles is as important as their local (submicrometric) chemical study. Presently, when working on diluted systems, the limited brightness forces researchers to accept a compromise between number of data (number of samples, of conditions, of pixels) and data quality. As an example, an X-ray microspectroscopy (µXRF/µXANES) study has demonstrated the translocation of TiO_2 nano-particles into the leaves and fruit of cucumber plants. However, scanning such large samples with a sub-micrometre beam has limited the scanned area to a small fraction of the tissues and limited the replication of the experiment (Servin *et al.*, 2013). By increasing the flux, and also using a new generation of X-ray fluorescence detectors, larger regions could be mapped, on a larger number of compartments of the living organisms, submitted to a broader range of conditions (more data points along a kinetic study, comparison of the effect of various exogenous chemicals, etc.) (**Figure 1.02, right**). The new source will also offer new possibilities by increasing by at least one order of magnitude the number of samples studied with the same amount of beamtime. This will allow much more complete and statistically relevant studies, not feasible today.

In addition to localising the endo- and exogenous components and monitoring the changes in their morphology, these examples also illustrate that it is essential to assess the chemical modification. This is fundamental in understanding how the living organisms will react chemically to a controlled or accidental intrusion of a foreign body. Scanning fluorescence-techniques with micrometre resolution (µXRF) are increasingly being used to reveal modifications (in distribution and concentration) of constitutive elements in cells or tissues exposed to external agents (Bohic *et al.*, 2012). As an example, lung tissues from shipyard workers exposed to asbestos showed a particular concentration of Fe, confirming that asbestos fibres mobilise iron, and cause an alteration of the homeostasis of this element in the tissue (Pascolo *et al.*, 2013). Studying the chemical modification of the exogenous components is equally important. For instance, the way in which (nano)fertilisers and (nano)pollutants are absorbed by plants can have dramatic subsequent effects. They may be modified during the process of uptake and migration within plants. One would like to know whether the particles are modified: for example reduced solubility can lead to agglomeration in specific parts of a plant which can be important for phytoremediation purposes. The changes could have an influence on whether they can enter the food chain. It is also possible that the final form(s) are more or less toxic than the original species. X-ray absorption spectroscopy is currently used to study such systems and it is capable of monitoring even a slight chemical modification of exogenous materials when "absorbed" or "digested" by living organisms. For such studies, in addition to the decreased beam size, the new source will offer the possibility of reaching lower detection limits thanks to the expected higher flux. Detection limits could be enhanced with the use of wavelength dispersive detectors (Cotte *et al.*, 2011) that offer higher energy resolution and allow the selection of a particular emission line eliminating the background from overlapping emission lines. Particularly, in the soft X-ray domain (4-9 keV) where the input count rate of an energy dispersive detector is determined mainly by the fluorescence yield of Ca and K in biological samples, improving the detection limits for elements present in trace concentrations (S, P, Ti, Ce, Mn, Fe) would be an important step forward. Along with detector developments, higher flux and smaller undulator bandwidth could render sub-micro or even nano- X-ray emission analyses and high resolution XANES feasible (Cafun *et al.*, 2013). This would offer a real step forward in many cases where the identification of the chemical environment through classical X-ray absorption spectroscopy is tedious.

1.1.3. *In vivo*, TIME-RESOLVED IMAGING

The examples above highlight another major issue: the multi-scale character of these phenomena. Most of the phenomena are based on microscopic or even nanoscopic interactions, which end as macroscopic (positive or negative) effects in macroscopic systems. Consequently, the full understanding of these processes requires a multi-scale characterisation, as outlined in **Figure 1.03** which presents the example of bone's hierarchical structure and the corresponding X-ray imaging techniques. This multi-scale characterisation is not accessible by other laboratory-based techniques such as positron-emission-tomography (PET-CT), magnetic resonance imaging (MRI) or optical-coherence-tomography (OCT), but is in strong demand, especially for recent approaches such as integrated medicine where the complete organism is considered for a treatment rather than isolated parts at a specific length-scale.

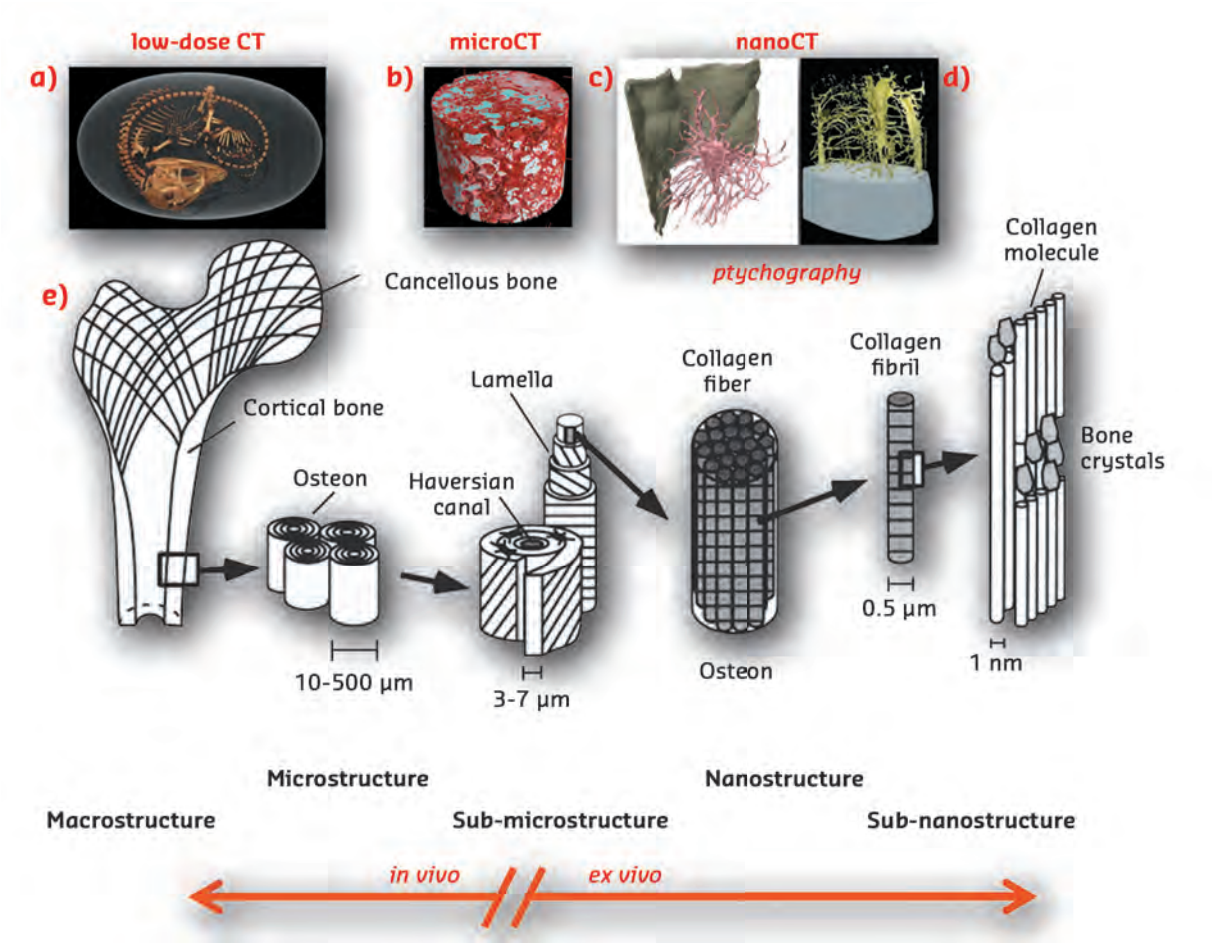

Figure 1.03: Bone's hierarchical structure and the corresponding X-ray imaging techniques. Credits: a) Tafforeau P., Kundrát M. and La Ferme aux Crocodiles (Pierlatte, France), unpublished. b) A. Rack/ESRF; M. Stiller, C. Berlin, C. Knabe/University of Marburg. c) Langer M. *et al.*, 2012. d) Reprinted by permission from Macmillan Publishers Ltd: Dierolf M. *et al.* 2010, copyright 2010. e) Reprinted from Rho J.-Y. *et al.*, 1998, Copyright 1998, with permission from Elsevier.

This feature sets X-ray imaging apart from the other techniques and will thus be further exploited with the new machine after Phase II of the ESRF Upgrade Programme.

When dealing with the interaction between materials and living organisms, an important consideration is the time factor. All of these systems are evolving with time, and here again on extremely diverse scales. For example, sarin gas can lead to death in a few minutes, while the effects of exposure to asbestos can take decades to materialise. Quite surprisingly, most imaging studies are currently carried out in a static way. Time-resolved studies need to be developed further in order to access the big picture, while dose issues will limit the range of techniques that can be applied to *in vivo* studies, restricting use of some of the length scales. The importance of time-resolved X-ray imaging was identified during the dedicated Phase II X-ray Cinematography Workshop. Phase II of the ESRF Upgrade Programme will enable us to reach new frontiers in X-ray imaging: the increased brilliance and photon flux, in particular at higher energies, as well as the higher fraction of coherent photons will open a variety of new possibilities for the existing techniques (*cf.* Figure 1.02). For sensitive (biological) specimens, higher energies will be highly beneficial in order to reduce the dose received by the sample. High sensitivity will be reached through a combination of both the existing and coherent X-ray imaging techniques. The great potential of time-resolved X-ray imaging covers all techniques and therefore a very broad range of length and time scales, from the observation of a rabbit lung while breathing to a spinning nano-needle in an assembly of semiconductor-nanostructures.

Above, we have emphasised that the current, and even more so, the future ESRF XRI beamlines are unique instruments for studying complex systems, in a static or dynamic manner, from hard materials (*e.g.* nano-electronics, catalysts) to soft materials (such as proteins and cells). The following scientific showcase is an application where multi-scale characterisation would be highly beneficial. It is inspired by the success of the multi-scale study of osteoporosis (Peyrin *et al.*, 2009), including X-ray imaging to reveal bone morphology, mechanics and pathology.

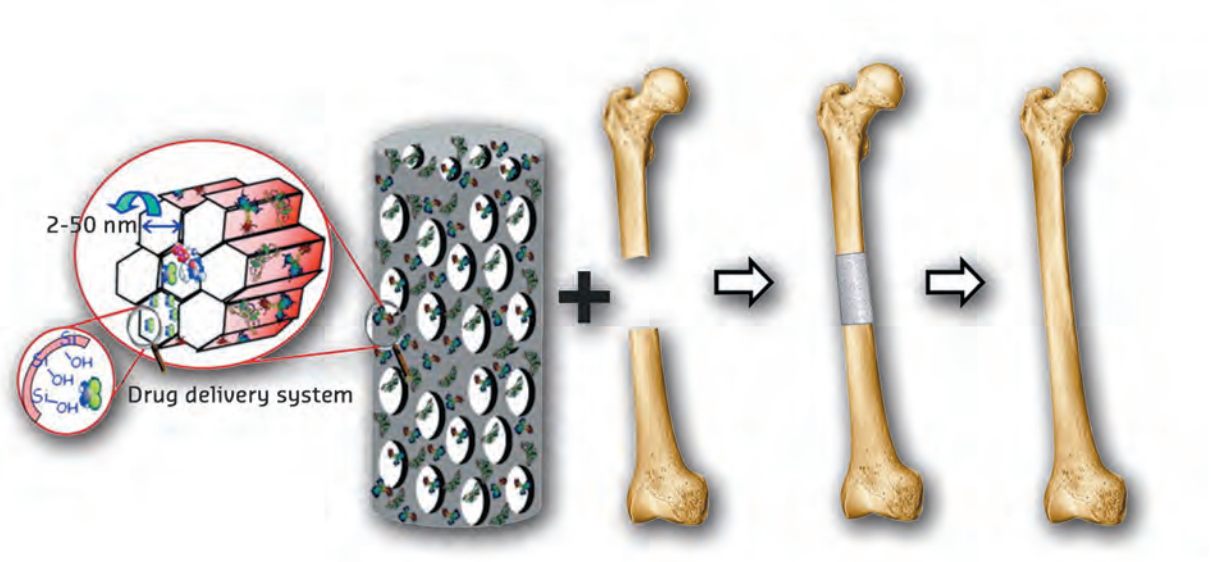

Figure 1.04: Schematic representation of the bioceramic-supported bone regeneration using scaffolds functionalised with biomolecules to promote bone growth. Credit: Adapted from Manzano *et al.*, 2012, Copyright 2012, reprinted with permission from Elsevier.

1.1.4. GUIDED BONE TISSUE ENGINEERING

Bone diseases are of foremost societal importance as they affect a huge number of people either through bone loss by complex fractures, tooth extraction or cancer surgery, by osteoporosis, which leads to loss of bone mass and bone density, or via spinal cord injuries. Such devastating injuries can impact mobility, are a potential cause of death and present a huge burden to healthcare systems. For example osteoporosis, a major bone disease, is estimated to affect 200 million women worldwide. The cost of osteoporosis, including pharmacological intervention in the EU in 2010 was estimated at €37 billion (International Osteoporosis Foundation, 2014).

Among the various techniques to reconstruct severe bone defects, the concept of guided bone regeneration has become a well-established surgical approach, *e.g.* by implanting bio-degradable ceramics which support bone formation (Ducheyne *et al.*, 2011) and provoke a bio-response of the living host organism. Bio-ceramic scaffolds combined with stem cells are well suited as implants for large bone defects as depicted in **Figure 1.04**. Ultimately, the dream is to develop guided bone regeneration further, towards a generic bone-tissue engineering technique, with rapid prototyping-like techniques delivering the replacements in an on-the-fly manner (Schubert *et al.*, 2013).

Living bone tissue reacts to physical stimuli, growing in response to imposed loads, and capable of detecting damaged (but not yet completely fractured) areas of tissue and replacing them through a process called remodelling. Bone regeneration is thus guided by exogenous bio-material in a complex interplay. To study the nature of the process in three dimensions requires sensitive techniques. Additionally, the nature of the process will only really be known once time has been added as the fourth dimension. To determine the biodegradation characteristics of bone substitute materials, one is limited to animal studies where the resulting specimens are typically visualised *ex vivo*, *e.g.* by histological sectioning (two-dimensional histomorphometry) or computed tomography (CT) of organs. Frequently *ex vivo* animal studies are correlated with *in vitro* studies of the biomaterial alone. These studies of degradation kinetics are rather limited in their informative value as the specimens can only be extracted at one pre-defined time point, and therefore it only provides a snapshot of the entire degradation and remodelling (Ducheyne *et al.*, 2011). Today, there is an increasing demand for *in vivo* monitoring of animals in a three-dimensional manner for longitudinal studies, leading to the possibility of studying a given parameter and its potential changes in the very same body as a function of time (Bayat *et al.*, 2005). One can therefore assess changes in location in the animal, concentration or interaction with matter for exo- or endogenous elements, while comparison between time intervals is not relevant if performed on different individuals. As an example, *in vivo* X-ray imaging performed at different time intervals in a longitudinal manner may reveal modification in joints and especially an osteoarthritis pattern, due to aging (Coan *et al.*, 2010). Furthermore, *in vivo* experiments (if compared to *post-mortem* or *ex vivo* experiments) allow functional parameters to be assessed for soft tissues (*e.g.* perfusion of

organ tissue by blood in normal and pathological conditions such as cancer, lung filling during respiration and under pathological conditions such as asthma or chronic obstructive diseases).

A few technical constraints are inherent to *in vivo* imaging such as: (i) monitoring of the animal: vertical positioning of the sample, monitoring the anaesthesia and physiological parameter during the acquisition; (ii) adaptation of the image acquisition sequence to *in vivo* constraints: heart/lung motion, anesthesis duration, compromise between temporal and spatial resolution at the detector level; (iii) careful management of the radiation dose as a function of the animals future (survival or euthanasia).

1.1.5. *In vivo* HISTOVOLUMETRY

Phase II of the ESRF Upgrade Programme offers the unique potential to overcome limitations of common *ex vivo* techniques and laboratory-based *in vivo* CT animal studies. Such studies are restricted to absorption contrast and, hence, can typically depict only hard tissue while important soft tissue remains invisible. With the increased coherent photon flux density, especially at higher energies, phase-sensitive imaging will become feasible at shorter wavelengths than today. Progressing towards higher energies has important implications: i) an increase in X-ray transmission through the sample and thus the possibility of investigating larger samples or more dense tissues, and ii) more importantly, the reduction in X-ray absorption and consequently, the dose to the sample. For a given sample, the photoelectric effect drastically decreases with the radiation wavelength with a consequent reduction of the dose deposited. This trend changes at photon energies for which the Compton effect becomes predominant and results in a new increase in dose. It is therefore possible to define an optimal energy for which the radiation dose is minimised for a given incoming photon flux. In the case of biomedical samples, this optimal energy is in the range 60 to 100 keV (ICRU, 1980). The improved sensitivity offered by the use of hard X-ray phase contrast imaging compared to the standard absorption signal is an important benefit for biomedical imaging and makes it possible to perform "low-dose *in vivo* phase-sensitive X-ray cinematography" depicting hard and soft tissue in a simultaneous manner and hence, opens a new world of possibilities through studying living organisms.

A recent demonstration study carried out at the ESRF with phase-sensitive tomography at varying photon energies is depicted in **Figure 1.05, left**. Excellent image quality was obtained for 60 keV as well as 96 keV: both soft tissue and mineralised tissue such as bone are depicted. The dose delivered to the sample is still significant, *i.e.* such scans are not compatible with *in vivo* studies. Bearing in mind that the dose-relevant mass energy-absorption coefficient μ_{en}/ρ drops by almost an order of magnitude for water with respect to the mass attenuation coefficient μ/ρ when tuning the photon energy from 19 keV to 96 keV (see **Figure 1.05, right**), this demonstration of hard X-ray phase-sensitive tomography around 100 keV with excellent image quality defines a first step towards *in vivo* compatible low-dose phase contrast tomography for longitudinal animal studies: *in vivo* histovolumetry. Phase II of the ESRF Upgrade Programme will provide the missing step in establishing a protocol for real investigations as it will significantly increase the coherent photon flux density at these energies, *i.e.* increasing the sensitivity as well as reducing the dose to the sample. Phase II will enable phase-contrast tomography at 100 keV photon energy as a routine tool for low-dose *in vivo* studies of living organisms.

Being able to apply such low-dose tomography protocols to *in vivo* imaging of bone regeneration in longitudinal studies, preferably in a hierarchical manner, would provide fundamental knowledge about the stimulation of bone growth on the surface of artificially introduced exogenous materials, *e.g.* bioceramics. Furthermore, external stimuli as well as the bone strength could be tested in a true *in vivo* manner. This would be a revolutionary approach for the development of surgery strategies and recovery roadmaps. While medical imaging techniques (such as X-ray radiography, MRI, ultrasound) are usually sensitive to specific bio-components, phase-contrast will allow not only the bioceramics to be depicted, but also the bone tissue, from the early soft and spongy stages to the final dense mineralised state.

Bone regeneration is one of the many examples where Phase II will allow new frontiers to be reached by means of low-dose X-ray imaging. There are many more biomedical *in vivo* imaging applications that require the three-dimensional structure of organs to be elucidated at a spatial resolution and sensitivity inaccessible to conventional sources, and to perform dynamic functional imaging. A few examples are gas transport and exchange mechanisms of pathologic processes, adverse effects of mechanical ventilation on the lung and strategies to prevent them, aerosol transport and deposition (**Figure 1.02, top**). Much of the current knowledge on organ and tissue function at small length scales remains theoretical, and there

is a tremendous need for such whole-organ imaging in small animal models.

Finally, out of the medical context, *in vivo* low dose longitudinal studies could have a major outcome for evolutionary biology (**Figure 1.02, bottom**). Until now the only way to visualise the formation of organs in three dimensions was through *post-mortem* imaging to circumvent any motion artefacts during imaging acquisition. To reduce the individual variability, the results of developmental studies are significantly stronger if measurements are made on the same specimen at different growth stages. This implies keeping the animals alive and that they are unaffected by repetitive analyses. Moreover, some biological events are complex and every small and rapid developmental step has to be carefully studied. This is the case of the metamorphosis of amphibians or the development of amniote embryos *in ovo,* for example. Additionally, longitudinal studies would be the only possibility in the case of protected or wild species not available at laboratories.

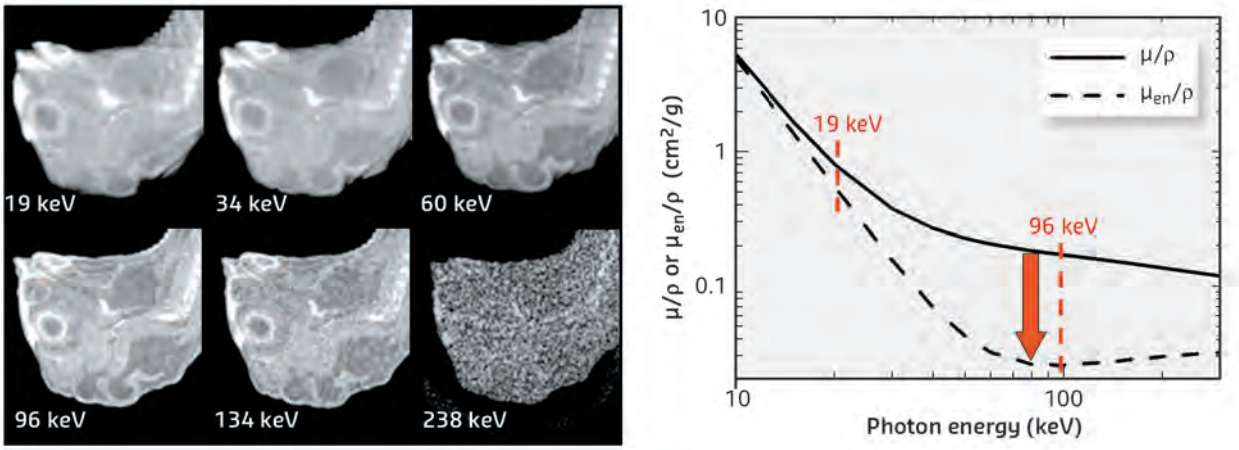

Figure 1.05: Left: tomographic slices of the head of a crocodile embryo (*crocodylus niloticus*) acquired *ex-vivo* with phase-sensitive X-ray tomography at different photon energies (ID19, ESRF). Right: absorbed energy vs. deposited dose (water). Source: http://physics.nist.gov/PhysRefData/XrayMassCoef/ComTab/water.html.

1.1.6. REALTIME IMAGING FOR APPLIED AND MATERIALS RESEARCH

Another important application of X-ray imaging is the full characterisation of man-made materials during the production process. The aim is to understand the impact the material may have during its entire life cycle. In this case, dose issues are less of a problem than for biological systems and existing techniques will be enhanced through Phase II of the Upgrade Programme. High spatial resolution in the nano-regime can be combined with time-resolution to study effects such as electromigration in a hierarchically structured device *in operando*. The time resolution for X-ray imaging at a synchrotron light source is ultimately given by the bunch structure in the storage ring (**Figure 1.02, left**). Hence, X-ray images representing a frozen moment in time as short as 100 ps can be acquired in order to track ultra-fast process such as crack propagation in solids, be it a bio-ceramic, regenerated bone or semiconductor wafer (Rack *et al.*, 2014).

As the ESRF revolutionised imaging techniques over the last decade in fields as diverse as nano-electronics, environmental sciences and palaeontology, we anticipate Phase II of the Upgrade Programme will revolutionise medical imaging, evolutionary biology and many other domains.

References

Bayat S., Apostol L., Boller E., Brochard T., Peyrin F., *In vivo* imaging of bone micro-architecture in mice with 3D synchrotron radiation micro-tomography, *Nuclear Instruments and Methods in Physics Research A* **548**, 247–252 (2005).

Bohic S., Cotte M., Salome M., Fayard B., Kuehbacher M., Cloetens P., Martinez-Criado G., Tucoulou R., Susini J., Biomedical applications of the ESRF synchrotron-based microspectroscopy platform, *Journal of Structural Biology* **177**, 248-258 (2012).

Cafun J.D., Kvashnina K.O., Casals E., Puntes V.F., Glatzel P., Absence of Ce^{3+} sites in chemically active colloidal ceria nanoparticles, *ACS Nano* **7**, 10726-10732 (2013).

Cotte M., Szlatchetko J., Lahill S., Salome M., Sole V.A., Biron I., Susini J., Coupling a wavelength dispersive spectrometer with a synchrotron-based X-ray microscope: A winning combination for micro-X-ray fluorescence and micro-XANES analyses of complex artistic materials, *Journal of Analytical Atomic Spectrometry* **26**, 1051-1059 (2011).

Coan P., Wagner A., Bravin A., Diemoz P.C., Keyriläinen J., Mollenhauer J., *In vivo* X-ray phase contrast analyzer-based imaging for longitudinal osteoarthritis studies in guinea pigs, *Physics in Medicine and Biology* **55**, 7649-7662 (2010).

Dierolf M., Menzel A., Thibault P., Schneider P., Kewish C.M., Wepf R., Bunk O., Pfeiffer F., Ptychographic X-ray computed tomography at the nanoscale, *Nature* **467**, 436-440 (2010).

Ducheyne P., Kealy K.E., Hutmacher D.E., Grainger D.E., Kirkpatrick C.J. (eds.), *Comprehensive Biomaterials*, Elsevier (2011).

International Commission on Radiation Units and Measurements, Radiation Quantities and Units, *ICRU Report* **33** (1980).

International Osteoporosis Foundation (2014), www.iofbonehealth.org/facts-statistics

Langer M., Pacureanu A., Suhonen H., Grimal Q., Cloetens P., Peyrin F., X-Ray Phase Nanotomography Resolves the 3D Human Bone Ultrastructure. *PLoS ONE* **7**, e35691 (2012).

Li J., Chang X., Chen X., Gu Z., Zhao F., Chai Z., Zhao Y., Toxicity of inorganic nanomaterials in biomedical imaging, *Biotechnology Advances*, in press (2014).

Lewinsky N., Colvin V., Drezek R., Cytoxicity of Nanoparticles, *Small* **4**, 26-49 (2008).

Manzano M. and Vallet-Regí M., Revisiting bioceramics: Bone regenerative and local drug delivery systems, *Progress in Solid State Chemistry* **40**, 17-30 (2012).

May M. (editor), The Spine, *natureOUTLOOK* **503** (2012).

Pascolo L., Gianoncelli A., Schneider G., Salomé M., Schneider M., Calligaro C., Kiskinova M., Melato M., Rizzardi C., The interaction of asbestos and iron in lung tissue revealed by synchrotron-based scanning X-ray microscopy, *Scientific Reports* **3**, 1123 (2013).

Peyrin F., Investigation of bone with synchrotron radiation imaging: from micro to nano, *Osteoporosis International* **20**, 1057-1063 (2009).

Rack A., Scheel M., Hardy L., Bonnin A., Curfs C., Reichert H., Exploiting coherence for realtime studies by single-bunch imaging, *Journal of Synchrotron Radiation* **21**, 815-818 (2014).

Rho J.-Y., Kuhn-Spearing L., Zioupos P., Mechanical properties and the hierarchical structure of bone, *Medical Engineering & Physics* **20**, 92-102 (1998).

Servin A., Morales M.I., Castillo-Michel H., Hernandez-Viezcas J.A., Munoz B., Zhao L., Nunez J., Perlata-Videa J.R., Gardea-Torresdey J.L., Synchrotron verification of TiO_2 accumulation in cucumber fruit: possible pathway of TiO2 nanoparticle transfer from soil into the food chain, *Environmental Science and Technology* **47**, 11592-11598 (2013).

Schubert, C., van Langeveld M.C., and Donoso, L.A., Innovations in 3D printing: a 3D overview from optics to organs, *British Journal of Ophthalmology,* **98***:159–16* (2014).

te Pas A.B., Siew M., Wallace M.J., Kitchen M.J., Fouras A., Lewis R.A., Yagi N., Uesugi K., Donath S., Davis P.G., Morley C.J., Hooper S.B., Effect of sustained inflation length on establishing functional residual capacity at birth in ventilated premature rabbits, *Pediatr Res.* **66**, 295-300 (2009).

1.2. STRUCTURAL AND FUNCTIONAL BIOLOGY: NEW OPPORTUNITIES AT CELLULAR AND MOLECULAR LEVELS

Opportunities

- Room temperature serial protein crystallography of microcrystals
- High resolution imaging of cells and the investigation of protein structural dynamics during physiological activity
- *Ab initio* crystal structure determination of large protein complexes and membrane proteins

1.2.1. INTRODUCTION

Structural biology using synchrotron X-rays provides a basic insight into a plethora of fundamental biological processes, and it is also at the forefront of applied research, much of which has a direct impact on society. Medicine is an area where the benefit to society is particularly evident, for example in providing information concerning the mode of action of many drugs and their protein targets and in elucidating structural information for use in pipelines for rational drug design (*i.e.* Murray & Blundell, 2010; Kobilka, 2013) thus paving the way for improved treatment of diseases. However, structural biologists are also turning their attention to other topics. The study of proteins and protein complexes that play key roles in many metabolic processes are often of direct relevance for renewable energy sources or in the bioremediation of pollution caused by industrial waste. Advances in fields such as health, bioenergy and ecology clearly contribute to the wellbeing of society at large and are major goals of the Framework Programme of Horizon 2020 (ref. Horizon 2020). In the future, structural biology will continue to have an impact on all of these areas.

While macromolecular crystallography allows crucial atomic level descriptions of the mechanisms of action of biological systems, many biological experiments need to be performed at the cellular level under appropriate physiological conditions. Such studies are important to gain a deeper understanding of biological functions, to elucidate molecular pathology and to further develop nanomedicine. Here, a direct imaging technique with nanometre resolution is clearly lacking and one of the goals of the Upgrade Phase II is to enhance existing scattering and coherent diffractive imaging techniques to reach this new level of precision.

In the following subsections, representative case studies relating to health, bio-energy and ecology, and bio-remediation are presented. The main experimental techniques involved are microbeam macromolecular crystallography, serial macromolecular crystallography, high resolution low angle X-ray diffraction, and coherent scattering and spectroscopy.

1.2.2. SELECTED APPLICATIONS

1.2.2.1. HEALTH

Improvements in living standards across Europe have led to a continuous increase in life expectancy. As a direct consequence, so-called "first world" diseases have become the major causes of death in Europe. In particular, cardiovascular and neurological conditions have a major impact (**Figure 1.06**). Among the latter are Alzheimer's and Parkinson's diseases which are not only major causes of death but also have a major impact on the quality of life in an increasingly ageing population. While the triggers for these diseases are as yet unknown, their impact can be reduced by identification of the biomolecules responsible. Determination of the atomic structures of such molecules may then lead to the identification of appropriate treatments. Most of the interesting targets in this area are membrane proteins, in particular receptors that belong to the G-protein coupled receptor family (GPCRs). The crystallisation of GPCRs often results in small, poorly diffracting crystals. The highly intense,

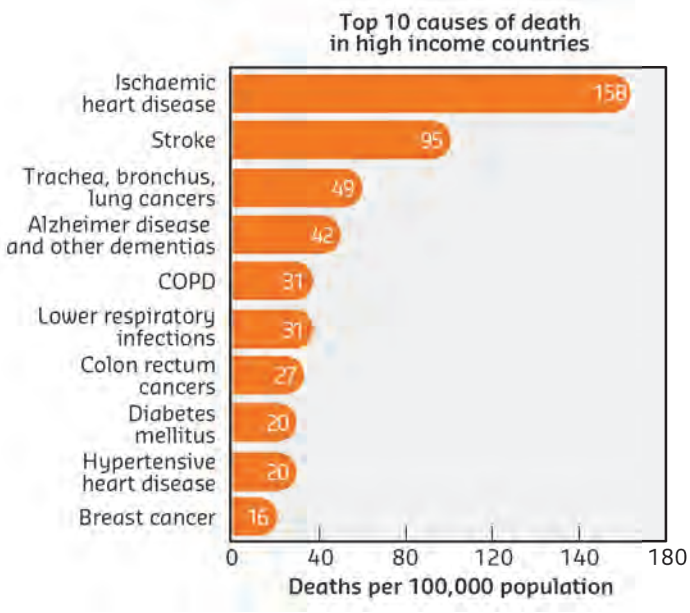

Figure 1.06: The major causes of death in high income countries, figures for 2012. Data: World Health Organization (http://www.who.int/mediacentre/factsheets/fs310/en/index1.html)

microfocus X-ray beams that will be produced by the upgraded X-ray source will prove crucial in the determination of the three-dimensional structures of these highly medically relevant drug targets. Moreover, information on the dynamics of these receptors and other molecules of interest will also aid in the design of efficient therapeutic agents against debilitating cardiovascular and neurological diseases.

While macromolecular crystallography (MX) will almost certainly prove the most useful technique in future drug design pipelines, a full understanding of cardiovascular disease and illnesses such as Alzheimer's and Parkinson's will result only from an integrated approach incorporating other techniques. For example, X-ray fluorescence microscopy can be used to probe the role of metal ions in neurological diseases (**Figure 1.07**; Davies *et al.*, 2014). To better understand cardiovascular regulation, nuclear inelastic scattering can be employed to study the role of molecules such as nitric oxide in cardiovascular regulation (Moeser *et al.*, 2012).

Cardiovascular diseases are the leading cause of death worldwide (about 30%). Most treatments are preventive (*i.e.* control of tobacco consumption, reduction in cholesterol, sugar and total body fat levels). The main roadblock for developing effective medicine for cardiomyopathies is the lack of a complete understanding of the molecular events governing the pathway of cardiac muscle cell regulation (Spudich, 2014). There is a direct relationship between the pump function of the heart and the properties of the cardiac contractile system involving the filamental proteins myosin, actin and other regulatory proteins such as tropomyosin, myosin binding protein C, troponin (Spudich, 2014). Currently there is insufficient knowledge about the underlying mechanisms of dysfunction of the contractile apparatus in cardiac

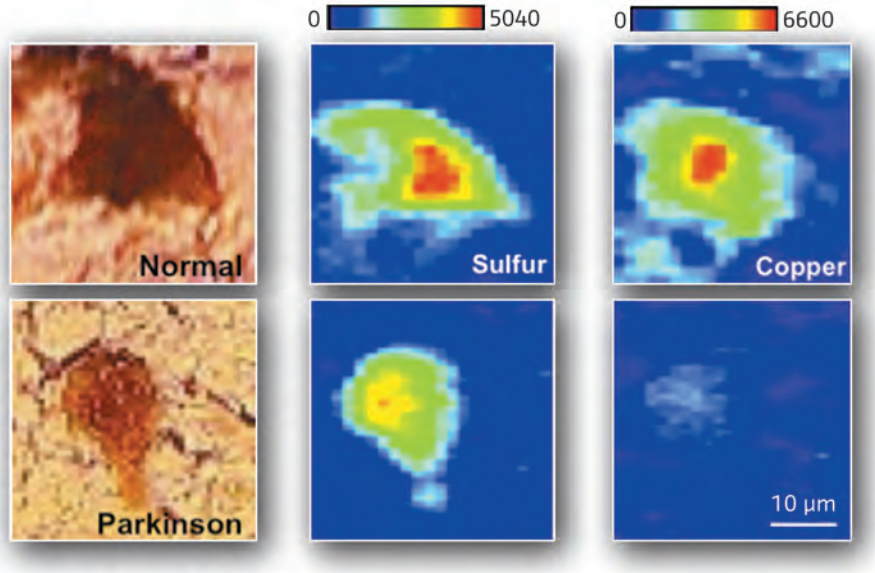

Figure 1.07: Sulphur and copper levels, determined by synchrotron X-ray fluorescence microscopy, in fresh frozen tissue sections of the substantia nigra (SN) of a Parkinson's disease patient and a control case. Credit: Reprinted from Davies *et al.*, 2014, Copyright (2014), with permission from Elsevier.

diseases and heart failure (de Tombe *et al.*, 2010). This is despite the availability of crystal structures for many of the proteins involved.

Low-angle X-ray diffraction has been widely used in structure-function studies of both mammalian and non-mammalian skeletal muscle fibres. In particular, the interference fine structure in the high resolution low-angle diffraction diagram turned out to be a powerful method to follow myosin motor movement with sub-nanometre and sub-millisecond resolution during physiological activation (Recondeti *et al.*, 2011). At present, the same approach cannot be applied to cardiac muscle because the striations in the cardiac muscle, unlike those in skeletal muscles, are branched creating a more tenacious structure, as depicted in **Figure 1.08**. To circumvent this tenacious architecture of cardiac muscle, the X-ray beam size will have to be less than 5 µm, while the divergence should be low enough to resolve spacings of 1.1 µm and with sufficient flux to record diffraction patterns with millisecond resolution. The improved brilliance of the Phase II X-ray beams will make the above requirements technically feasible thus opening the door for detailed structural-dynamics studies of small mammalian cardiac muscle preparations and even for single myocites as shown in **Figure 1.08**. Furthermore, by combining with transgenesis or transfection methods, it will be possible to determine the structural consequences of specific protein modifications that will shed light on the molecular basis of cardiomyopathies and heart failure. The knowledge thereby gained could pave the way for the development of effective medicines for the treatment of heart failure (Spudich 2014).

1.2.2.2. BIOENERGY AND ECOLOGY

To reduce dependency on fossil resources without affecting food procurement, the production of energy from renewable sources and of biofuel from non-food crops has been identified as a major goal for the near future (ref. Horizon 2020). The fabrication of biofuels will almost certainly involve the structural study of enzymes such as membrane-bound hydrogenases as well as investigations of the structures of catalytic enzymes that are involved in, for example, complex sugar degradation.

A particular area where structural biology might contribute is in the bioconversion of methane first to methanol, then to formaldehyde for use in future fuel production (Conrado & Gonzalez, 2014). The only available route for this process is the methane monooxygenase (MMO) pathway which suffers the disadvantage that any production of formaldehyde results in ~40% of the energy contained in methane molecules being lost. Moreover, the conversion of methane to fuels such as n-butanol releases about a third of the carbon in methane as CO_2. However, a more efficient engineered pathway based on higher turnover enzymes can be envisioned and is clearly required (**Figure 1.09**). One route to this goal is the creation of more efficient enzymes based on structural knowledge of the mechanism of action of the native enzymes, MMO and methanol dehydrogenase, in the MMO pathway. Combined with improved process design, such engineered enzymes could provide new routes for methane activation and bioconversion.

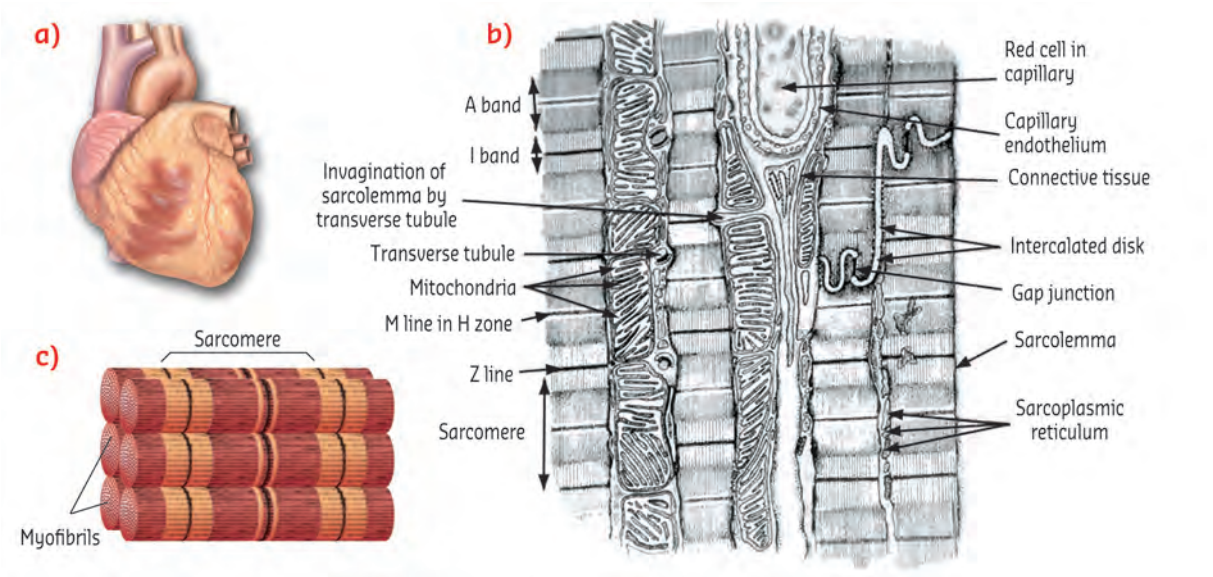

Figure 1.08: (a) Picture of human heart showing the peculiar feature of cardiac muscle (Credit: Patrick J. Lynch, medical illustrator; C. Carl Jaffe, MD, cardiologist). (b) Sketch of an electron micrograph of cardiac muscle showing the striated and non-striated regions (Image published in Berne and Levy, copyright Elsevier (1997) reproduced with permission). (c) Sketch of single cardiac myosite showing the sarcomere and myofibrils in which myofilaments are packed.

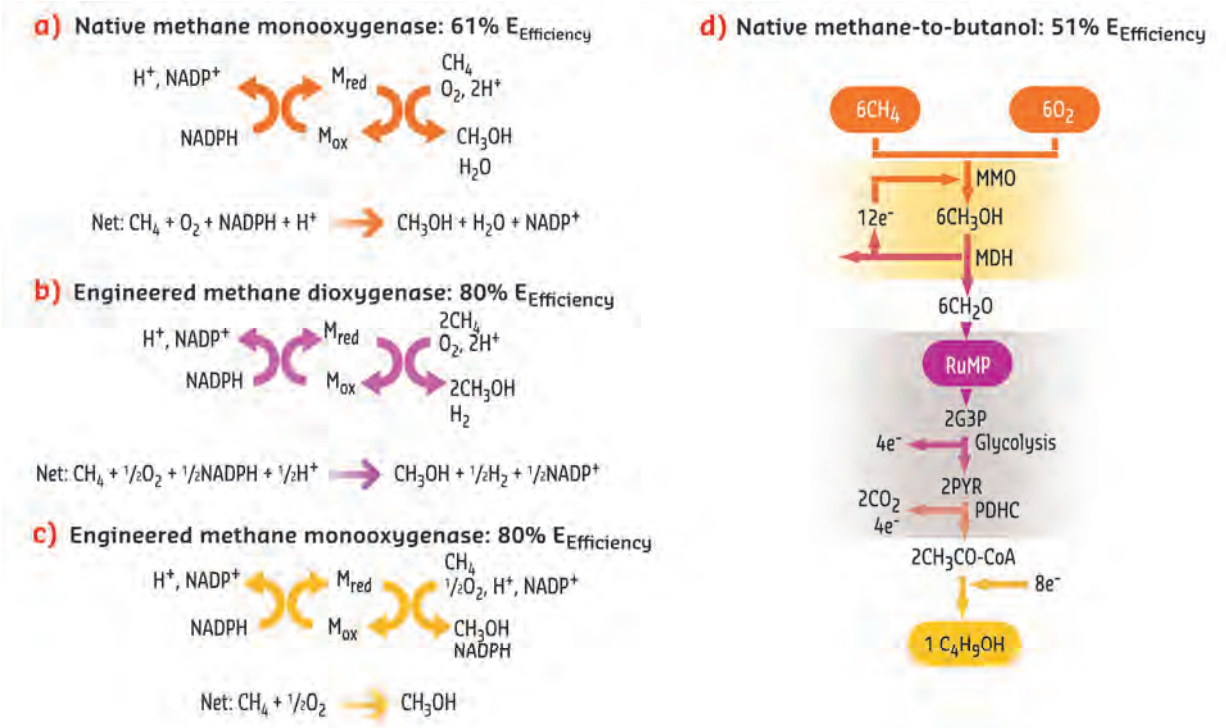

Figure 1.09: Methane to n-butanol bioconversion based on engineered, improved enzymes in the MMO pathway. Figure adapted from (Conrado & Gonzalez, 2014).

1.2.2.3. BIOREMEDIATION

Many organisms have evolved metabolic pathways that allow them to survive in toxic environments such as those polluted, as a result of industrial activity, by xenobiotic organic compounds or heavy metals. Bioremediation (**Figure 1.10a**) exploits these pathways and can be used both in the microorganism-mediated detection of pollutants and their conversion into non- or less toxic substances that can then be safely removed. However, many of the natural pathways exploited are inefficient and protein engineering is used to overcome limitations. Here, and in the case of the development of improved systems for the production of biofuels (see above) a combination of directed evolution and rational protein design will be important to allow a full exploration of the sequence-function space (Böttcher & Bornscheuer, 2010). Targets here will include both the enzymes that make up the metabolic pathways (more efficient conversion) and the proteins (transcription factors) that regulate them. Structural biology when combined with other synchrotron-based techniques, particularly X-ray fluorescence microscopy, will have a central role to play in this endeavour (**Figure 1.10b**).

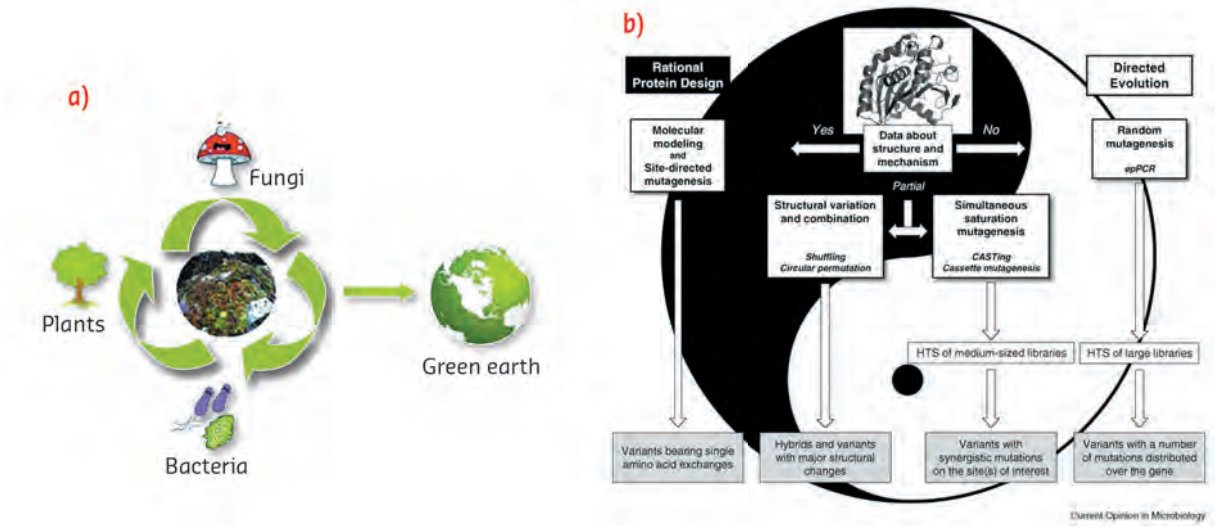

Figure 1.10: a) The process of bioremediation (from Karigar & Rao, 2011). b) Pathways for directed evolution (Reprinted from Böttcher & Bornscheuer, 2010, Copyright 2010, with permission from Elsevier).

1.2.3. TECHNIQUES

1.2.3.1. MACROMOLECULAR CRYSTALLOGRAPHY

Macromolecular crystallography is the major technique for determining the atomic structure of macromolecules at high resolution, the knowledge of which has been pivotal in understanding in detail a wide range of biomolecular mechanisms (**Figure 1.11**). The success of MX has led to a situation where the systems targeted are becoming more and more biologically important, and in many cases the production of well ordered, large crystals has become increasingly difficult. The advent of microcrystallography (*i.e.* MX using small, even micrometre-sized, X-ray beams) has helped to circumvent this problem, allowing the collection of high quality diffraction data from crystals that are ever smaller in size or that present low levels of homogeneity in their diffraction quality. These advantages were crucial in the determination of the crystal structures of GPCRs that are the targets for about 40% of current therapeutic treatments (see, for example, Kobilka, 2013).

1.2.3.2. MACROMOLECULAR CRYSTALLOGRAPHY FOLLOWING PHASE II OF THE UPGRADE PROGRAMME

Multi-crystal data collection and serial crystallography

The proposed Phase II of the ESRF's Upgrade Programme will permit the construction of a new generation of microfocus (or even nanofocus) beamlines for MX. Flux densities at the sample position will increase by nearly 5 orders of magnitude, enabling *de facto* data retrieval even from sub-micrometre-sized crystals. However, even with such flux densities, the resolution of a complete diffraction dataset originating from a single cryo-cooled microcrystal of a biological macromolecule will remain limited by radiation damage and many such crystals will be required for the collection of even moderate resolution diffraction data (**Figure 1.12**). Collecting data in this way is known as multi-crystal data collection.

The ultimate implementation of multi-crystal data collection has recently advanced at X-ray Free Electron Laser sources (X-FELs). At such sources, the extreme brightness of the pulsed X-ray beam produced (~1 billion times higher than at a synchrotron) has led to serial femtosecond crystallography (SFX; Chapman *et al.*, 2011). It has been shown that SFX can be used for the collection of complete data sets from the micro/nanocrystals of a number of different systems with the crystal structure determination of *Trypanosoma brucei* cathepsin B using SFX as applied to *in vivo* grown micro/nano-crystals (**Figure 1.13**; Redecke *et al.*, 2013). This was identified by Science magazine as one of the top-ten scientific breakthroughs of 2012 (see www.sciencemag.org/special/btoy2012). It has since been shown that protein crystal structures can be solved *ab initio* using SFX (Barends *et al.*, 2013).

SFX has many advantages, particularly that data collection is carried out at room temperature and the crystal structures obtained are free from artefacts caused by radiation damage. There are, however, currently a number of limitations to the technique. In particular, many tens of thousands of diffraction images (and thus crystals) are required to build a complete data set and, with current experimental setups, many crystals never 'see' an X-ray pulse and are thus wasted.

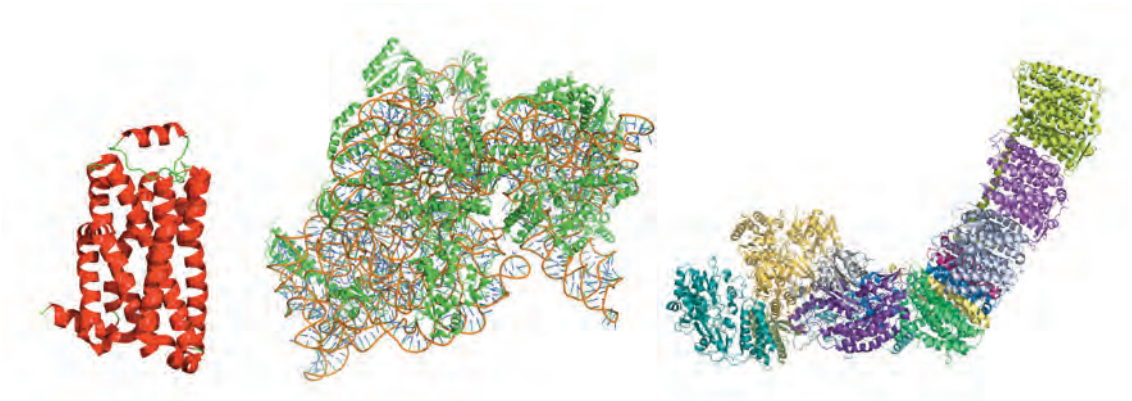

Figure 1.11: Highlights from 15 years of MX at the ESRF. Crystal structures of (from left to right) GPCRs, ribosomes and the entire respiratory complex 1. Figures from Protein Databank entries 2VT4, 1FJG and 4HEA respectively.

Serial crystallography at synchrotron radiation sources

Inspired by the success of serial crystallography as carried out at X-FELs, researchers have been testing the suitability of beamlines at synchrotron sources to carry out similar experiments; in early 2014 it was demonstrated that a complete diffraction dataset could be assembled from microcrystals grown *in vivo* of *T. brucei* cathepsin B using synchrotron serial crystallography (SSX; Gati *et al.*, 2014) (**Figure 1.14**). Consistent with the "diffraction before destruction" principle of the SFX experiment, the resolution of the synchrotron-collected data is lower (2.1 Å for SFX data). Nevertheless, the electron density maps resulting from both techniques are similar in quality (**Figure 1.14**). At the same time, the amount of material required for the SSX experiment was lower by many orders of magnitude.

Test experiments carried out recently on ID13 have also shown that synchrotron beamlines can be used to collect data from crystals delivered, as in SFX experiments, using jet injectors. Here, crystals of the membrane protein bacteriorhodopsin were fed into the path of the X-ray beam using a novel lipid cubic phase (LCP) jet injector developed at Arizona State University by an international team led by Uwe Weierstall. The slower streaming rate of crystals compared to the liquid injectors often used in SFX experiments increases the possibility of obtaining a 'hit' and is more suited to the

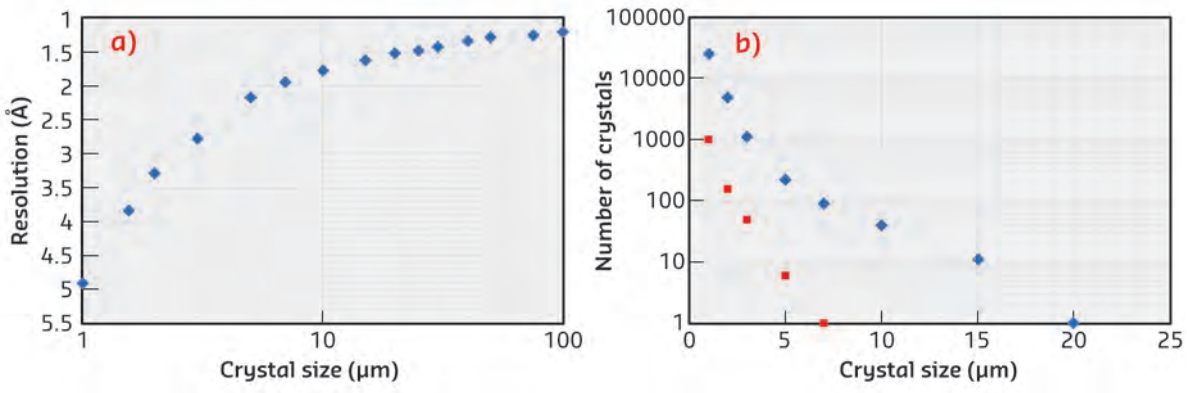

Figure 1.12: a) Complete dataset resolution achievable from a cryocooled single crystal vs. crystal size. b) Number of cryocooled crystals of a given size required to achieve dataset resolutions of 1.5 Å (black) and 2.0 Å (red). Crystals of thermolysin, B-factor = 11.5 Å^2 in both cases. For a crystal 1 µm^3 in dimension, partial data sets from about 1000 crystals would be needed to achieve a final data set resolution of 2.0 Å. Credit: Alexander Popov. ESRF.

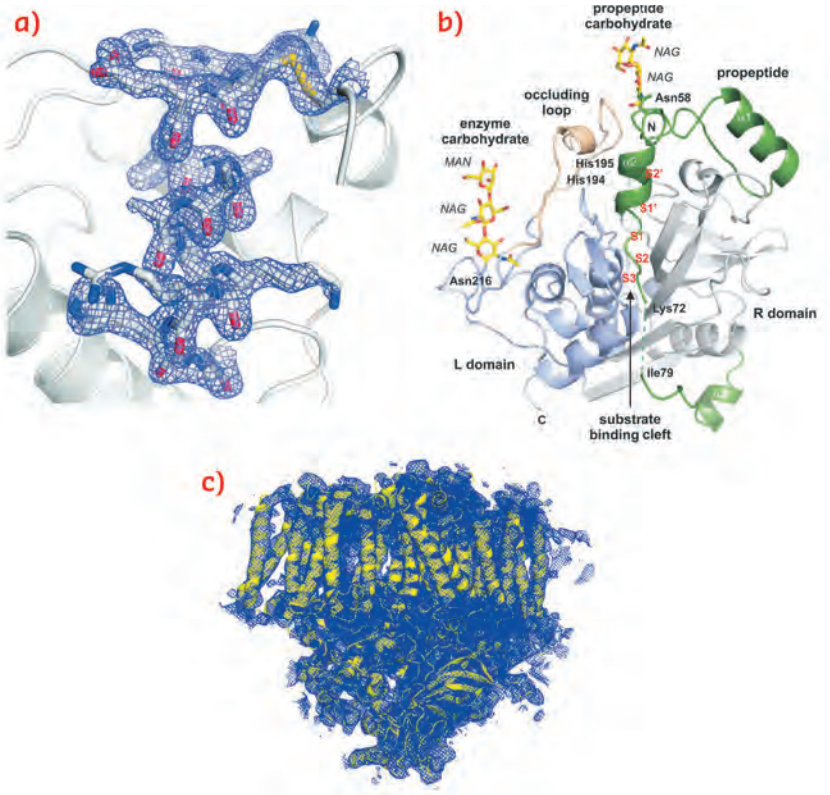

Figure 1.13: Macromolecular crystal structure determination using SFX. a) A section of the refined $2mF_{obs}-DF_{calc}$ electron density map, at 1.9 Å resolution, as obtained from microcrystals of lysozyme. b) The crystal structure, obtained at 2.1 Å resolution, of T. brucei cathepsin B using data obtained from micro-crystals grown *in vivo*. c) 2mFo-DFc electron density map, at ~5.7 Å resolution, obtained from microcrystals of photosystem II. Credits: a) Reprinted from Boutet *et al.* 2012. Reprinted with permission from AAAS. b) Reprinted from Redecke *et al.* 2013. Reprinted with permission from AAAS. c) Reprinted from Kern *et al.* 2013. Reprinted with permission from AAAS.

flux densities currently available at synchrotron beamlines. The test experiment was extremely successful and allowed both the collection of a complete diffraction data set and the solution of the structure of bacteriorhodopsin using the Molecular Replacement technique (see http://www.esrf.fr/home/news/general/content-news/general/novel-injector-allows-x-rays-to-map-membrane-proteins.html for details).

Despite the success of the experiments described above, it is clear that the low flux density of current third generation synchrotron sources when compared to X-FELs is a major limitation to the data quality and the resolution obtainable using SSX. The experiment described above required many hours of beamtime. The submicrometre, ultra-high brilliance beams that will be available for MX at the ESRF after Phase II of the Upgrade Programme will improve data quality and resolution in such experiments and will make SSX more tractable even with more weakly diffracting crystals. Moreover, X-ray beams delivering the radiation damage limiting dose in a submicrometre area within a millisecond, coupled with large area single photon counting detectors with frame rates in the order of 1 kHz, raise the prospect that the time scale of such experiments, including those targeting the structure solution of membrane complexes from higher organisms (*i.e.* photosystem II from plants, respiratory and other mitochondrial complexes) can be reduced to a matter of minutes.

It is worth noting that serial crystallography need not be confined to the compilation of complete datasets from partial ones. Using modified experimental protocols, it will be possible to rapidly collect thousands of complete datasets from different crystals of the same sample. Only rarely are such samples truly isomorphous (*i.e.* same unit cell dimensions, same positions in the crystal for all of the atoms in the macromolecule) and in the future it is highly likely that structural biologists will produce ensembles of crystal structures rather than single snapshots. Such ensembles, perhaps in combination with other techniques such as nuclear magnetic resonance (NMR) and small angle X-ray scattering (SAXS) will help map the conformational space of biological macromolecules and allow access to information concerning protein dynamics. Such information may have important implications for drug design.

Room temperature synchrotron MX

An apparent disadvantage of SSX is that, unlike SFX experiments, radiation damage cannot be outrun. Recent studies aimed at analysing the effect of dose-rate on the radiation damage to crystals of biological macromolecules maintained at room-temperature were carried out at synchrotron MX beamlines (Warkentin *et al.*, 2013). These studies have provided evidence that the use of very high X-ray dose rates (*i.e.* those that will be associated with Upgrade programme Phase II X-ray beams) coupled with very short data collection times may allow most of the radiation damage caused by the diffusion of X-ray induced free radicals through the crystal to be outrun even at synchrotron sources.

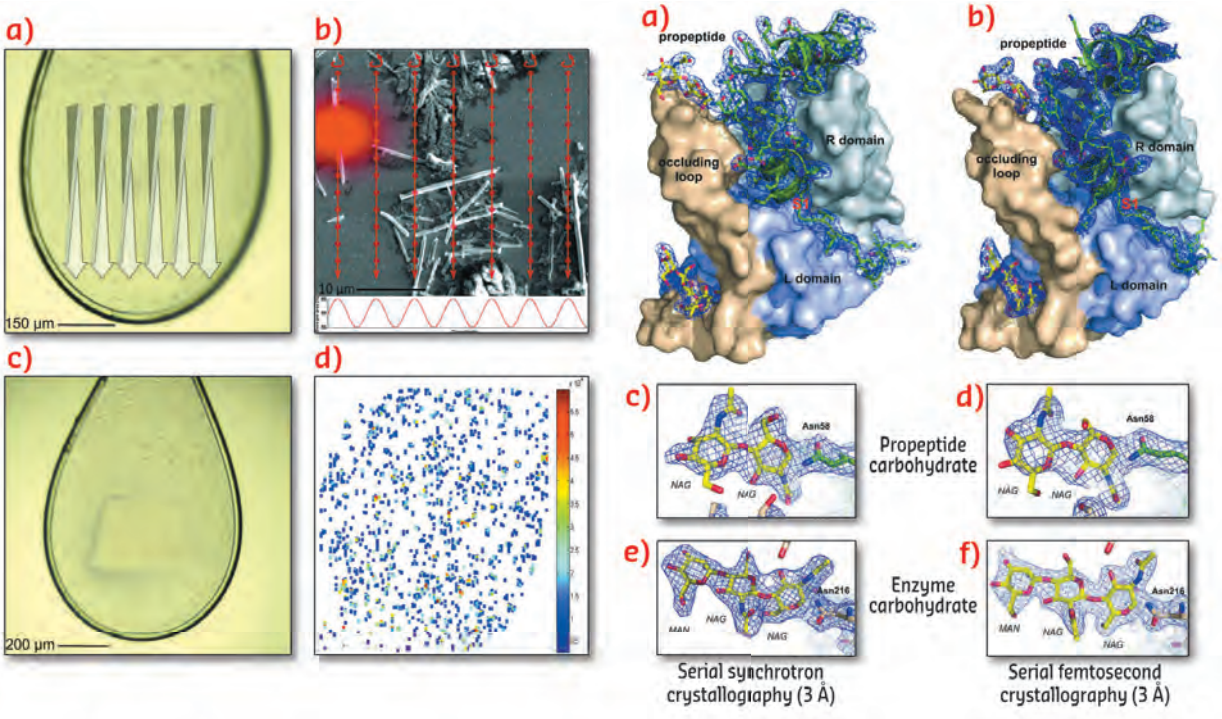

Figure 1.14: Left: Serial synchrotron crystallography (SSX). A sample support is rastered by a 4dscan data collection; frames with positive hits are selected and the diffraction patterns integrated and combined to produce a complete data set. Right: A comparison of the crystal structures obtained using SSX and SFX, both refined at 3.0 Å resolution, of micro-crystals of T. brucei cathepsin B grown *in vivo*. Credit: Gati *et al.*, 2014.

While the time delay before evidence of radiation damage becomes apparent is short (~100 msec; presentation by M. Weik at the ESRF Users' Meeting 2014) this observation raises the possibility of collecting complete diffraction data sets from single crystals of biological macromolecules at extremely high flux density synchrotron MX beamlines. To date, the observation of a time-lag before radiation damage becomes apparent has been limited to only a small number of systems and clearly much more work in this area is required. However, if this does prove to be a general phenomenon, ultrafast, room temperature data collection will provide an exciting new tool, complementary to both SFX and SSX, which will require the development of new data collection protocols, new sample environments and new detector technology.

Studies show that data collection at room temperature has other intrinsic benefits. Crystal structures that are indicators of molecular motion (*i.e.* Debye Waller or 'temperature' factors) will be more realistic than those obtained from cryo-cooled crystals (Figure 1.15). When coupled with the ensembles of crystal structures described above and molecular dynamics calculations, this will provide a new level of understanding of molecular functionality and mechanisms of protein-substrate interaction.

Room temperature diffraction or scattering data collected on ultrafast time scales from either crystals or solutions will also facilitate time-resolved, pump-probe studies of molecular mechanism and function (Figure 1.15). Similarly, the development of enhanced fragment-based screening protocols might be possible. Currently such screening consists of soaking a crystal in solution containing a compound or a cocktail of compounds. This is a tedious and error prone procedure, as it implies crystal transfer into the soaking solution, and subsequent freezing. Performing quick room temperature data collection will permit (both) the collection of data *in situ*, by carrying out direct mixes on the crystal, and a substantial reduction in the quantity of protein and ligand used.

Ab initio structure determination using increased coherence

Above, we have concentrated on the possibilities that will be afforded by the extremely high flux densities that will be available at ESRF MX beamlines after Phase II of the Upgrade Programme. However, the smaller horizontal source size and divergence of the X-ray beam will also lead to a large increase in the coherent fraction of the available X-ray beam. For a beamline such as ID29, this gain will be a factor of ~30.

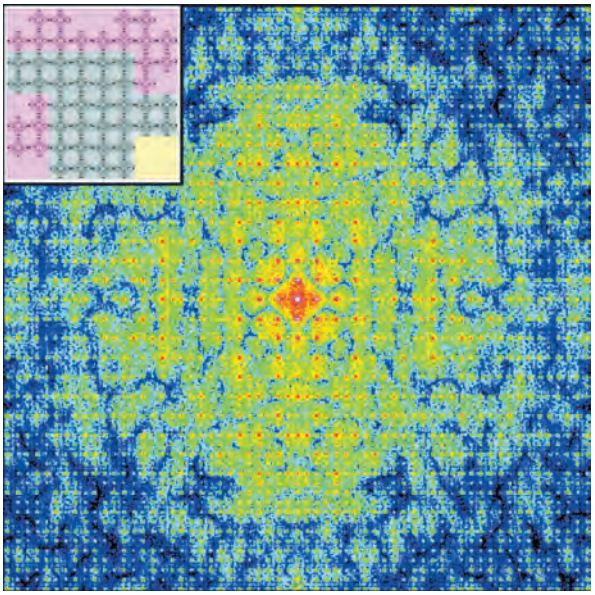

Figure 1.16: A simulated X-ray diffraction pattern of a 2D nanocrystal. An inset shows the structure of the 2D lattice with outer cells labelled as partially occupied (red), unoccupied (yellow) and fully occupied (grey). Credit: Miao & Rodriguez (2014).

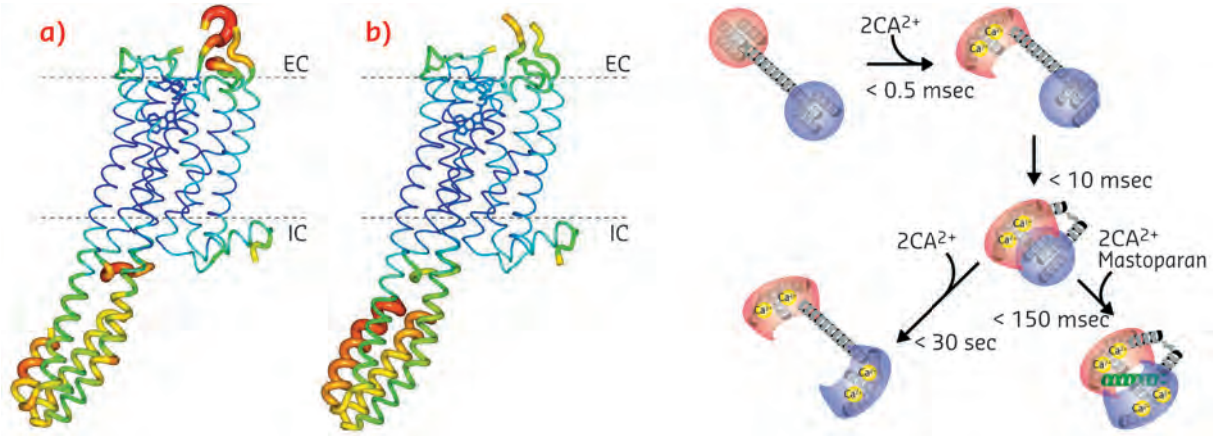

Figure 1.15: Room temperature data collection. Left: a comparison of the crystal structures of a GPCR determined at room-temperature (SFX, a) and at 100 K (synchrotron, multi-crystal diffraction data collection, b). Atomic displacement parameters are shown in heat colours and coil sizes, highlighting differences in the mobility of flexible regions. Right: A schematic illustration of the kinetic reaction of calmodulin upon Ca^{2+} binding obtained from time resolved SAXS measurements. Credit: (Left) Liu *et al.*, 2013; (Right) Reprinted with permission from Yamada *et al.*, 2012. Copyright (2012) American Chemical Society.

Recent publications (Miao & Rodriguez, 2014; Liu *et al.*, 2014) have suggested that the coherence of the X-ray beam at X-FELs might be used in the *ab initio* determination of macromolecular crystal structures (**Figure 1.16**). Although still in its infancy, this technique relies on the measurement of diffraction intensities between Bragg peaks from nanocrystals. Such coherence "hungry" experiments might also be envisaged at ESRF beamlines following Phase II of the Upgrade programme. An ultimate MX beamline might therefore provide, in different experimental setups, the best diffraction data from microcrystals (crystallography), nanocrystals (oversampling of the diffraction pattern for *ab initio* phasing) and, perhaps, even from non-crystalline specimens (*i.e.* cells) using coherent diffractive imaging (CDI).

1.2.4. IMAGING CELLS WITH NANOMETRE RESOLUTION USING COHERENT DIFFRACTION IMAGING

Advances in microscopy techniques have been pivotal in advancing our understanding of biological systems. For example, progress in optical microscopy in the seventeenth century led to the discovery of single cell microorganisms such as algae, bacteria, etc., and to the birth of microbiology. Modern cryoelectron microscopy can image nanostructures such as the ultrastructure of cells and viruses with a resolution of about 3-5 nm. However, a limitation of electron microscopy is that the sample thickness needs to be small, typically less than 0.5 µm.

The high penetration power of X-rays is a major advantage for imaging micrometre sized objects. In this respect, CDI has emerged as a very promising method (J. Miao *et al.*, 1999). In this method, a 2D projectional image is reconstructed from an oversampled 2D speckle pattern and a 3D image is reconstructed from many such 2D projections using tomographic methods (**Figure 1.17**). Currently the resolution of the images obtained using CDI is of the order of 40-60 nm, clearly insufficient for visualising cellular organelles. Two main factors are limiting the resolution; the quality of the recorded speckle

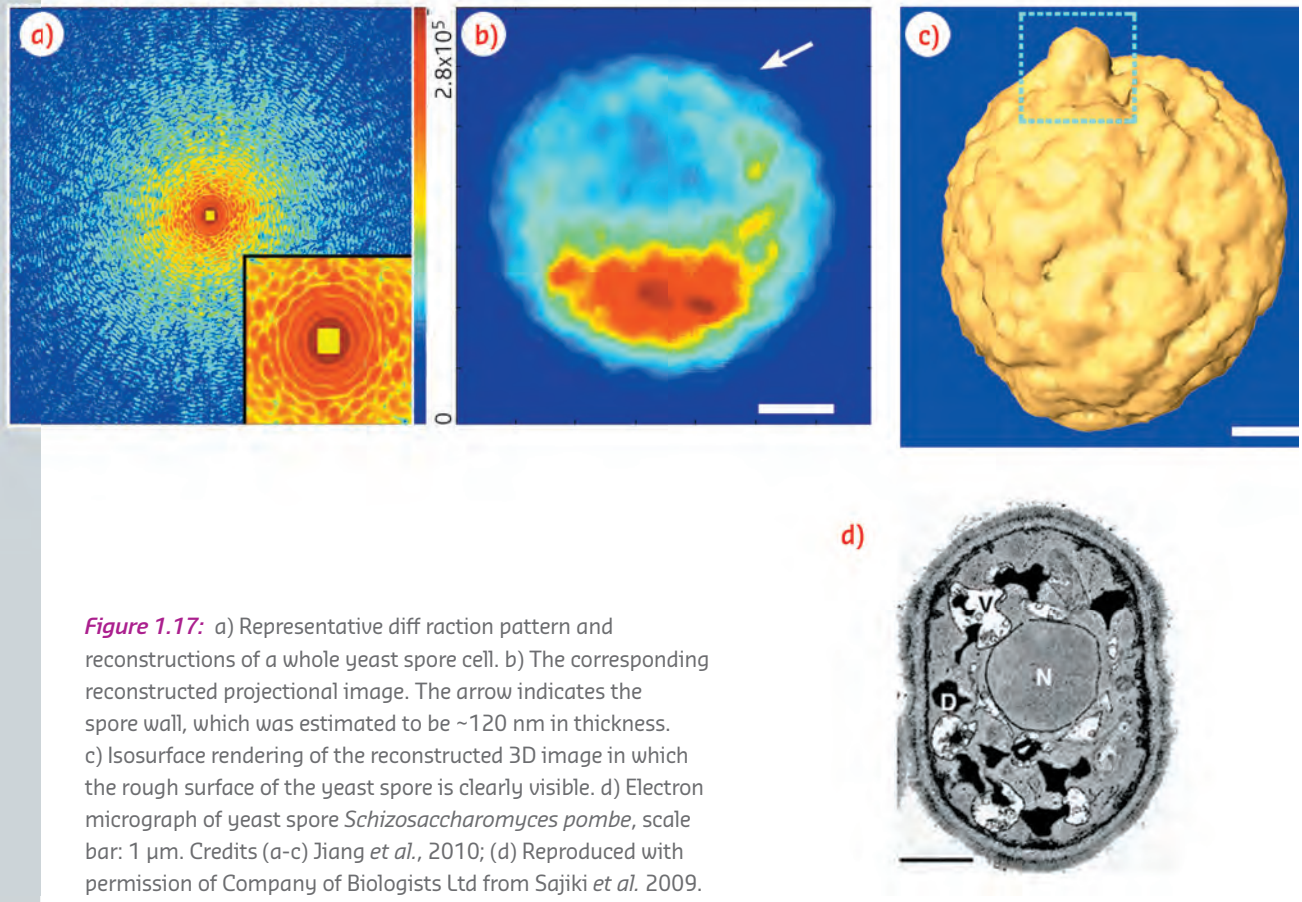

Figure 1.17: a) Representative diff raction pattern and reconstructions of a whole yeast spore cell. b) The corresponding reconstructed projectional image. The arrow indicates the spore wall, which was estimated to be ~120 nm in thickness. c) Isosurface rendering of the reconstructed 3D image in which the rough surface of the yeast spore is clearly visible. d) Electron micrograph of yeast spore *Schizosaccharomyces pombe*, scale bar: 1 µm. Credits (a-c) Jiang *et al.*, 2010; (d) Reproduced with permission of Company of Biologists Ltd from Sajiki *et al.* 2009.

pattern and radiation damage when multiple exposures with different specimen orientations are required for 3D reconstruction. An increase in the degree of coherence by a factor of 30 by Phase II of the Upgrade Programme and a corresponding improvement in 2D detector technology will enable much better speckle patterns to be recorded for the given cumulative X-ray dose on the specimen. An interesting opportunity would be CDI at higher energies (~ 20 keV) which could prolong the lifetime of a biological specimen in the X-ray beam. However, this will require a high resolution detector (ca. 15 µm) to satisfy the oversampling criterion. The ultimate goal would be to push the resolution obtainable from CDI to below 5 nm. This will allow not only the imaging of cellular organelles but also elucidation of the finer structures of cell membranes and channels of cellular transport. Such information is important to understand cellular recognition, especially how nanomedicines interact with a cellular interface.

1.2.5. DIFFUSION OF PROTEINS IN CROWDED MEDIA BY X-RAY PHOTON CORRELATION SPECTROSCOPY

Large scale domain motions are often essential for proteins to perform their biological functions. Such correlated domain motions occur in motor proteins, signalling proteins, genome regulatory proteins, and structural proteins (Bu *et al.* 2005). The interplay between protein dynamics and biological functions remain largely unexplored due to the complexity spanning a broad range of spatial and temporal scales. While NMR and neutron spectroscopies can probe the faster components of the internal domain and diffusive dynamics in concentrated systems, dynamic light scattering is suitable mainly for studying diffusive motions in dilute systems (Biehl *et al.* 2011). Proteins perform their biological function in a crowded cellular environment as depicted in **Figure 1.18** and under these conditions many proteins may form dynamic clusters (McGuffee & Elcock, 2010).

To date, the investigation of protein dynamics by X-ray photon correlation spectroscopy (XPCS) has not been very successful. XPCS covers all the relevant length scales for intra and inter-protein dynamics but accessing the corresponding time scales has been hampered due to limited coherent flux. An increase in coherence by a factor of 30-50 would place XPCS in the microsecond range and thereby reduce the gap with neutron spin-echo spectroscopy. This will make XPCS suitable for probing long time diffusive behaviour, cluster dynamics, ageing processes, etc., in concentrated protein solutions of relatively large complexes. Another limiting factor of XPCS for proteins is radiation damage. Here again using energies higher than the usual 8 keV will be an advantage provided that the coherent flux is high enough to access the short time scales of microseconds and below. If this can be achieved, XPCS will become a suitable technique to explore the diffusive dynamics of proteins in crowded media. A detailed understanding of these dynamics is important for many practical applications such as food and pharmaceutical industries involving processing (*e.g.* freeze drying) and long term storage of concentrated protein systems.

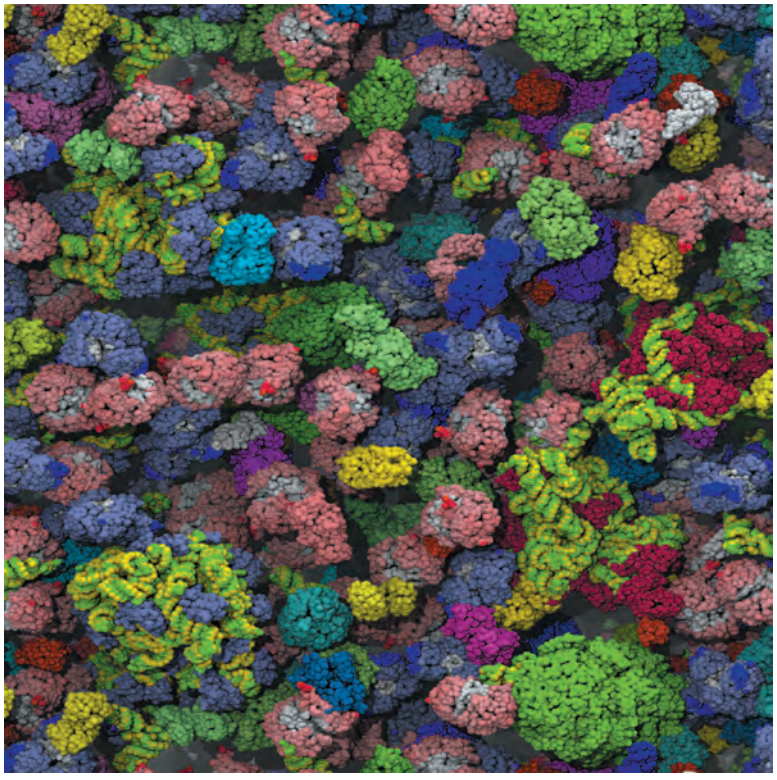

Figure 1.18: Bacterial cytoplasm model from Brownian dynamics simulation illustrating the important role of crowding on the behaviour of macromolecules in the cellular medium (McGuffee & Elcock, 2010). Different colours show the main proteins found in the cytoplasm and RNA is shown as green and yellow. Source: PLoS Computational Biology; image credit: A.H. Elcock, University of Iowa.

1.2.6. SUMMARY

The proposed upgrade of the storage ring would facilitate the construction of MX beamlines producing, at the sample position, a (sub-) micrometre beam size with an extremely high flux density. Such experimental resources would enable new paradigms for synchrotron-based MX experiments. The most obvious application is serial crystallography used in the determination of the crystal structures of membrane proteins and large macromolecular complexes. Ultrafast room temperature data collection would also be enabled by such experimental facilities. This raises the prospect of outrunning radiation damage even at synchrotron sources as well as providing exciting possibilities for pump-probe, time-resolved experiments and studies of the dynamics of macromolecular structure. These, coupled with molecular dynamics calculations and information from other synchrotron-based techniques that will also benefit from the Upgrade Programme Phase II, will provide a hitherto unobtainable picture of macromolecular action and mechanism that will find application not only in a better understanding of fundamental biological processes but also in areas essential to the wellbeing of society at large. Such areas include the design of improved therapeutic agents against first-world diseases such as cardiovascular and neurological conditions, the improved production of biofuels and the microorganism-assisted remediation of pollution caused by industrial activity.

The tremendous increase in the degree of transverse coherence will help to significantly enhance the performance of coherent imaging methods for imaging larger biological cells towards the spatial resolution of electron microscopy. Much higher brilliance will permit microbeam high resolution low angle diffraction experiments on biological cells and probe cellular functions under physiological conditions. Improvement in the transverse coherence will equally benefit the XPCS technique allowing access to microsecond range dynamics in crowded biological systems.

References

Barends T.R.M. *et al.* & Schlichting I., De novo protein crystal structure determination from X-ray free-electron laser data, *Nature*, **505**, 244-247 (2013).

Berne R.M. and Levy M.N., Cardiovascular Physiology, Mosby-Year Book (1997).

Biehl R., Monkenbusch M. and Richter D., Exploring internal protein dynamics by neutron spin echo spectroscopy, *Soft Matter* **7**, 1299–1307 (2011).

Böttcher D. & Bornscheuer U.T., Protein engineering of microbial enzymes, *Current Opinion in Microbiology* **13**, 274–282 (2010).

Boutet S., *et al.*, High-Resolution Protein Structure Determination by Serial Femtosecond Crystallography, *Science* **337**, 362-364 (2012).

Bu R. *et al.*, & Callaway D.J.E., Coupled protein domain motion in Taq polymerase revealed by neutron spin-echo spectroscopy, *Proc Natl Acad Sci U S A*, **102**, 17646–17651 (2005).

Conrado R.J. & Gonzalez R., Envisioning the Bioconversion of Methane to Liquid Fuels, *Science* **343**, 621-623 (2014).

Chapman H.N., *et al.*, Femtosecond X-ray protein nanocrystallography, *Nature* **470**, 73-77 (2011).

Davies K.M. *et al.* & Double K.L., Copper pathology in vulnerable brain regions in Parkinson's disease, *Neurobiol Aging* **35**, 858-66 (2014).

Gati C., *et al.* & Redecke L., Serial crystallography on *in vivo* grown microcrystals using synchrotron radiation, *IUCrJ* **1**, 87-94 (2014).

Horizon 2020. The EU Framework Programme for Research and Innovation. Societal-challenges: http://ec.europa.eu/programmes/horizon2020/en/h2020-section/societal-challenges

Jiang H. *et al.*, & Miao, J., Quantitative 3D imaging of whole, unstained cells by using X-ray diffraction microscopy, *Proc Natl Acad Sci U S A* **107**, 11234–11239 (2010).

Karigar C.S. & Rao S.S., Role of Microbial Enzymes in the Bioremediation of Pollutants: A Review, *Enz. Res*, 2011, Article ID 805187 (2011).

Kern J. *et al.* & Yano J., Simultaneous Femtosecond X-ray Spectroscopy and Diffraction of Photosystem II at Room Temperature, *Science* **340**, 491-495 (2013).

Kobilka B., The Structural Basis of G-Protein-Coupled Receptor Signaling (Nobel Lecture), *Angew. Chem. Int.* **52**, 6380–6388 (2013).

Liu H., Zatsepin N.A. & Spence J.C.H., Ab-initio phasing using nanocrystal shape transforms with incomplete unit cells, *IUCrJ,* **1**, 19–27 (2014).

Liu W. *et al.*, & Cherezov V., Serial femtosecond crystallography of G protein-coupled receptors. *Science* **342**, 1521-1524 (2013).

McGuffee S.R. and Elcock A.H., Diffusion, Crowding & Protein Stability in a Dynamic Molecular Model of the Bacterial Cytoplasm, *PLoS Computational Biology* **6**, e1000694 (2010).

Miao J., *et al.*, & Sayre D., Extending the methodology of X-ray crystallography to allow imaging of micrometre-sized non-crystalline specimens, Nature **400**, 342–344 (1999).

Miao J. & Rodriguez A., Phasing tiny crystals, *IUCrJ*, **1**, 3-4 (2014).

Murray C.W.1, Blundell T.L., Structural biology in fragment-based drug design, *Curr Opin Struct Biol.* **20** 497-507 (2010).

Nury H. *et al.*, X-ray structures of general anaesthetics bound to a pentameric ligand-gated ion channel, *Nature* **469**, 428-431 (2011).

Reconditi M. *et al.,* & Irving M., Motion of myosin head domains during activation and force development in skeletal muscle, *PNAS* **108**, 7236–7240 (2011).

Redecke L., *et al.* & Chapman H.N., Natively Inhibited Trypanosoma brucei Cathepsin B Structure Determined by Using an X-ray Laser, *Science* **339**, 227-30 (2013).

Sajiki K., Hatanaka M., Nakamura T., Takeda K., Shimanuki M., Yoshida T., Hanyu Y., Hayashi T., Nakaseko Y., Yanagida M., *J Cell Sci* **122**, 1418-1429 (2009).

Spudich J.A., Hypertrophic and Dilated Cardiomyopathy: Four Decades of Basic Research on Muscle Lead to Potential Therapeutic Approaches to These Devastating Genetic Diseases, *Biophys. J.* **106**, 1236–1249 (2014).

de Tombe P.P. *et al.*, & Irving T.C., Myofilament length dependent activation, *J. Mol. Cell. Cardiol.* **48**, 851–858 (2010).

Warkentin M., *et al.*, Global radiation damage: temperature dependence, time dependence and how to outrun it, *J. Synchrotron Rad.* **20,** 7-13 (2013).

Yamada Y. *et al.* & Yagi N., A compact intermediate state of calmodulin in the process of target binding, *Biochemistry* **51**, 3963-3970 (2012).

1.3. *In situ* MATERIALS CHEMISTRY

Opportunities:

- Materials chemistry for devices that helps to solve grand challenges in clean energy provision and transport
- 'Chemically resolved X-ray vision' into working catalysts and devices for a green energy economy
- Understanding and optimising complex devices on realistic time scales

1.3.1. INTRODUCTION

The chemistry of materials shapes the world we live in, from the myriad complex chemical processes that produce the materials used in our daily life, to the advanced devices that convert and store clean energy. Despite this vast diversity, one characteristic is common to all. Systems such as batteries, fuel cells, solar cells and hydrogen storage materials rely upon a synergy between atomic structure on the nano scale and microscopic engineering. Complex heterogeneous systems that require characterisation on multiple length scales are thus the norm rather than the exception.

Perhaps the greatest challenges in materials chemistry lie in understanding and controlling the many-faceted properties of devices crucial to the emerging green energy economy, which offers a chance to escape from our reliance on fossil fuels. By answering this call, we can help to usher in a new era of green, sustainable chemistry. Collectively, the European Union faces ambitious targets on both short and medium time scales. For example, the Horizon 2020 funding programme (ref: Horizon 2020) contains a commitment to reduce greenhouse gas emissions by 20% by 2020 and to achieve a further reduction to 80-95% by 2050. The solution to this challenge clearly lies in the materials domain. As we shall show below, the upgrade of the ESRF storage ring will provide a unique and extremely incisive tool, which will have quantifiable social and economic returns.

In the last few decades, third generation synchrotrons like the ESRF have proven themselves capable of responding to society's grand scientific challenges. X-ray scattering and spectroscopic techniques provide atomic level detail, and with Phase I of the ESRF Upgrade Programme soon completed, this is coupled with nanometre spatial resolution. Together with synthetic advances that provide exquisite control of particle shapes and morphologies, we can now truly say that synchrotron X-rays provide a window into the nano world.

However, these developments, which are driven by intellectual curiosity and practical demand, remain unable to address a vast range of problems. In particular, the jump from 'bottom up' materials chemistry to market-ready high technology products remains a challenge. This arises from unforeseeable difficulties extrapolating from the simplified model systems currently required to facilitate experiments. As devices or chemical processes become more complicated, new phenomena that are more than just the sum of the constituent parts become apparent. Furthermore, maximum performance is often associated with inhomogeneous states or disordered materials. Current experimental methods allow only partial characterisation of real devices; allowing the study of 3D structure, but often only *ex situ*, or of the global chemical state during functioning. Such information is inadequate to provide a real, *in situ* hierarchical characterisation of these systems.

The next-generation *in situ* X-ray experiments therefore needs to provide information on length scales from the chemical bond to the macroscopic, all at realistic time scales and in 3D. Moving from simple models to real devices requires more than just a change in an individual researcher's mindset. In fact, with the synchrotron sources of today, this vision is entirely out of reach, requiring vast increases in X-ray intensity and coherence. The complexity of these devices also currently renders *ab initio* modelling approaches almost impossible; hence only further experimental advances can make progress tractable.

The proposed upgrade of the ESRF storage ring offers the opportunity to invest in a unique super-microscope, which will revolutionise the *in situ* study of materials chemistry, providing 'chemically-resolved X-ray vision'. This possibility arises due to the hundred-fold increase in hard X-ray intensity provided by the new storage ring and new insertion devices. This increase is particularly valuable to *in situ* materials chemistry experiments, where the ability to penetrate complex sample environments is crucial.

1.3.2. SUPERCONDUCTING TECHNOLOGY FOR THE FUTURE GREEN ENERGY GRID

The transmission of electricity through conventional cables causes substantial losses, for example, 6.5% of all power generated is wasted as heat (EIA, 2007). Were this problem removed, as many as 450 polluting power plants could be closed in the United States alone. Superconductivity, discovered in 1911 by cooling mercury to liquid helium temperatures, offers a potentially lossless solution. The immense benefits of using superconducting current carriers are evident, but a hundred years later, superconductors have found widespread use in just one technology, magnetic resonance imaging (MRI). In fact helium-cooled superconductors could not compete with ordinary copper and aluminium wire in more common applications, like transmission cables, where the advantages of superconductivity are not sufficient to compensate the enormous costs.

This is about to finally change with high temperature superconducting cables becoming available that operate at temperatures higher than liquid nitrogen, which costs a fraction of the price of liquid helium. High temperature superconductor (HTS) cables have two main advantages compared to conventional wires: they can carry much higher current per unit area and they reduce the energy losses by up to 90%. The cost of implementation is currently ten times greater than that of copper cable (15-25 $/kA/m) but it is becoming low enough to be commercially viable, as the refrigeration equipment consumes about half the power saved by the elimination of the majority of resistive losses. The first installations of this new technology have already been carried out in high power lines in highly populated areas like New York City where space for new infrastructures is limited.

This technology could one day be used for the European super grid which would interconnect Europe and North Africa with a high voltage power grid (**Figure 1.19**). The super grid would lower the cost of electricity through the sharing of the most efficient power plants; it would lead to a wider use of renewable energy, particularly wind energy and solar energy, allowing the transport over very large distances from the production areas like North Africa (solar) and Atlantic coast (wind) to the rest of Europe.

Lowering the cost of HTS technology is fundamental in order to make it economically feasible. To do this, improvements in the processing of superconducting cables are necessary in order to increase the current density. This can be done by controlling at the nano scale level defect formation, porosity, crystal size, orientation and growth during the high pressure/high temperature heat treatments involved in the manufacturing process. Such diagnostic capabilities are not yet available at synchrotron facilities mainly because the measurement time is longer than the time scale of the processes involved. The enormous increase in flux provided by the new storage ring will make this type of experiment commonplace.

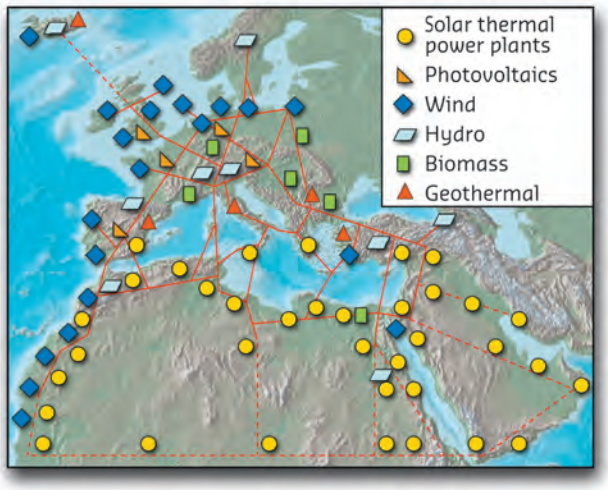

Figure 1.19: A conceptual plan of a European super grid linking renewable energy projects like DESERTEC and Medgrid across North Africa, the Middle East and Europe. Credit: Trans-Mediterranean Renewable Energy Cooperation/CC-BY-2.5.

1.3.3. CHEMISTRY OF LIQUIDS, DISORDERED SYSTEMS AND NANOMATERIALS

The last few decades have also seen impressive progress in understanding the structure of the very small. From the single-crystal structure solution of gold nanoparticles (Jadzinsky *et al.*, 2007) to efforts employing coherent diffraction (Pfeifer *et al.*, 2006), it is clear that we begin to understand the organising principles that govern nanostructure. The improvements proposed in Phase II of the Upgrade Programme will revolutionise the study of chemical reactions in disordered, amorphous and liquid systems. Here conventional crystallographic approaches are blind due to the absence of sharp Bragg reflections. By exploiting the very high energy X-rays produced at the ESRF, it has recently become possible to probe these important states using so-called pair distribution function techniques. Here the complete scattering profile of the sample is measured, before mathematical

processing of the data into real space. The result is a histogram of bond lengths, which is completely model independent and highly complementary to spectroscopic methods such as EXAFS. At present, we are limited by the incident X-ray intensity to frame rates of the order of Hz. This means that we cannot probe the fast-forming intermediates which appear during typical catalyst operation, during the synthesis of nanoparticles, or vast amounts of other chemical reactions of synthetic interest. The new X-ray source will make this tool indispensible for a huge range of chemical reactions. The increased counting statistics mean that very weak signals, such as those from solvated metal clusters or even organic molecules, can be studied directly at the concentrations used in industry. Until now, solid state chemistry has been mainly studied with X-ray scattering methods, due simply to the ease of studying reactions using diffraction techniques. To be able to bring the same level of understanding to much more industrially-common solution chemistry processes will be absolutely revolutionary. For the first time, we will be able to measure the structure of elusive reaction products directly on the time scale of real, irreversible reactions, in actual systems. Furthermore, we anticipate that (sub) microsecond time resolution will be achievable in favourable systems.

1.3.4. STUDY OF REAL DEVICES UNDER OPERANDO CONDITIONS

Perhaps the biggest gains from the Upgrade Programme Phase II will be for *in situ* experiments on real functioning devices like fuel cells and lithium batteries. Current synchrotron experiments for studying real devices under operando conditions fall into two broad categories. The first is computed absorption/phase contrast tomography, where the attenuation/refraction of an X-ray beam is used to extract a materials density. Reconstructed volumes with high spatial resolution can now be routinely achieved. However, no chemical information is obtained and details of bonding, oxidation states and coordination are lost. The second common method used today relies on probes like diffraction and XANES. Here a small region of sample is followed as a function of time, and atomistic structure or oxidation state can be easily obtained. For example, researchers at the ESRF recently tracked solvent-free green reactions inside rapidly moving milling vessels on a time scale of seconds (Friščić *et al,* 2013). However, no 3D spatial information was obtained. A possible route that combines this information (spatial and physico-chemical as a function of time) has recently been demonstrated by pioneering diffraction tomography experiments at the ESRF. Here, spatially resolved diffraction information is provided, making it possible, for example, to map the nanoparticle size distribution which occurs upon processing the active ingredient in a commercial catalyst body (Jacques *et al*, 2013). However, these experiments are extremely flux limited and three-dimensional volumes cannot be reconstructed, nor can they be carried out in operando, due to constraints on the measurement times. The hugely increased high-energy flux offered by Phase II of the Upgrade Programme will allow us to fully unify tomography, diffraction and spectroscopy, providing time-resolved, three-dimensional, atomistic detail in operando. By harnessing the nano revolution of the last decade, we therefore expect a rejuvenated and upgraded ESRF to lead the way in facing up to the grand societal and scientific challenges of 2019 and beyond.

1.3.5. CATALYSIS

Catalysis plays a vital role in providing society with fuels, commodity and fine chemicals, pharmaceuticals, polymers, and means for protecting the environment. Catalysts are the key enabler in 90% of chemical manufacturing processes; they are used in the production of about €1,000 billion worth of products worldwide. The combination of increasing demand and reduced availability of raw materials means it is vital that catalysts and catalytic processes operate as efficiently as possible.

In many catalytic processes, catalyst metal nanoparticles such as Cr, Ni, Co, Au, Pd, Pt and Ag are deposited on millimetre-sized pellets made of porous supports. Since the efficiency of the reactor depends on the efficiency of the catalyst body, its design is of extreme importance. The optimisation of the design depends on an understanding of the factors which influence the physico-chemical nature and spatial distribution of the active phase within the catalyst body during the preparation process. Correlating how parameters that influence catalyst performance, *i.e.* nanoparticle size, shape, redox functionality and metal-support interactions affect and evolve in core catalytic processes is thus mandatory for improving industrial processes.

Unfortunately the characterisation techniques available today (Raman, IR, UV/Vis micro-

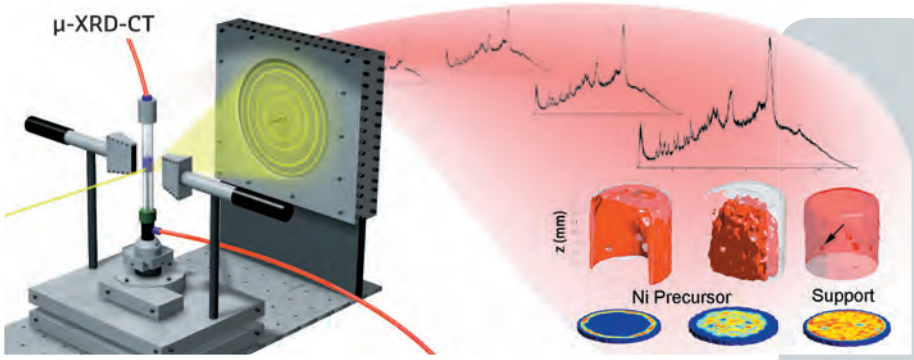

Figure 1.20: Current X-ray tomographic measurements can either supply 3D volumes of the absorption contrast in samples or 2D slices containing atomic level detail. Phase II of the Upgrade will allow the unification of these techniques for the first time. Credit: S.D.M. Jacques, Manchester University.

spectroscopy, MRI, or absorption/phase contrast microtomography) provide incomplete information. Moreover the characterisation is rarely performed under realistic industrial conditions, leading to contrasting conclusions as to what makes a catalyst active.

Time-resolved diffraction microtomography provides information about both the chemical species and nano-particle size evolution as a function of space and time (**Figure 1.20**). The technique is currently limited to 2-dimensional spatial mapping and can only be applied to relatively slow processes due to the limited photon flux available. Nevertheless, the images obtained constitute a totally new way of monitoring intricate chemistry in space and time within materials.

The new X-ray source combined with the use of a new type of crystal-less optics, made feasible by the smaller chromatic dispersion of the new source, will provide a flux increase of more than a factor 100 in the high energy X-ray region. This enormous increase in flux will allow time resolved 3-D characterisation and the study of much faster chemical processes, a tremendous leap towards the study of industrial processes on full size industrial materials. These measurements will prove invaluable for future catalyst optimisation and design.

1.3.6. ATOMISTIC DETAIL IN OPERATING LITHIUM BATTERIES

Achieving the clean production, storage and transportation of energy is the greatest challenge facing humanity in the 21st century. Although intensive research is being carried out along various avenues, no solution which supplies adequate levels of power has yet been found to replace the polluting and dwindling fossil fuels on which our civilisation currently depends.

Automobiles are major consumers of fossil fuels, and thus the application for which energy storage has seen most research. Combinations of batteries and fuel cells are considered to be the most promising solution for clean, fully electric automobiles in the near future. Lithium, as both the lightest metal and most electropositive element, is the obvious choice for use as the ionic conductor for power storage. Lithium batteries consist of a negative anode, and a positive cathode, separated by an electrically insulating, but ion-conducting material ("electrolyte"). The flow of positive ions from the anode to the cathode induces a flow of electrons through an exterior loop, thus providing electricity. However, market-ready systems, based on Li-ion batteries like those used in portable telephones and computers, lack the capacitance, life cycle, and/or recharging times needed to satisfy the minimum requirements of such applications. The complexity of these devices can also lead to surprises like shorting or "thermal runaway" where uncontrolled chemical reactions, triggered by degradation, melt or burn the device (for example, the Boeing 787 Dreamliner fleet was grounded for several months due to such a problem). In spite of 20 years of intensive studies, the energy density of Li-ion battery systems is expected to soon reach its limit, which will not be sufficient for the crucial application of electric vehicles (Armand and Tarascon, 2008).

When used as an anode, Li metal gives far better performances than graphitic carbon; with theoretical energy capacities more than ten times greater, as well as much more rapid recharging times and pulse rates. However, lithium metal anodes are plagued by a variety of technical issues leading to performance loss and failure (**Figure 1.21**). The first step in solving these technical issues is to understand their origin – something which can only be done by studying real working systems. The degradation phenomena are the results of the subtle interplay between chemical and physical processes, so a total characterisation approach is needed to understand them.

Through synchrotron radiation we are already beginning to understand these failure modes. For example absorption tomography has been used (Ebner *et al*, 2013) to image the mechanical degradation that occurs during cycling. This effect, which is due to the volume change of the active material upon lithiation, drives easily distinguishable

cracking and distortion and failures due to short circuit resulting from metal redeposition.

However, understanding more subtle issues, like long term capacity fading, requires chemical information. This is especially true in the case of the passivating layer which forms at the interface between the electrode and electrolyte. Extending over at most a few micrometres, and X-ray amorphous, the origin and make-up of this material are poorly understood. These side reactions are compounded by a year-on-year increase in structural hierarchy in new cell designs. One could argue that the complexity of these devices has been increasing much faster than the brightness of the synchrotron light sources used to study them.

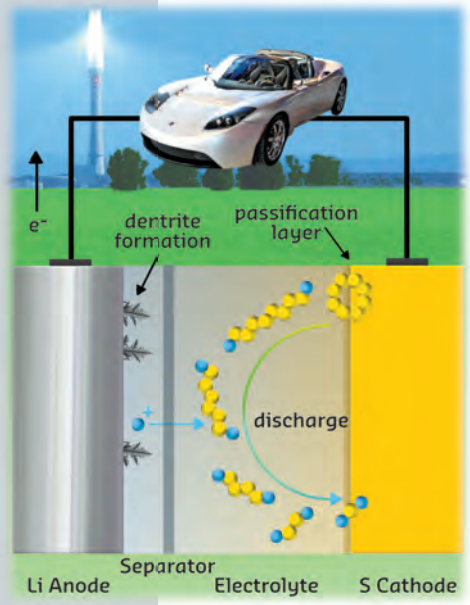

Figure 1.21: Illustration of the structural complexity of a lithium metal – sulphur battery, showing the diverse failure modes possible, including dendrite growth on the anode, the formation of a pacification layer on the cathode, and the complex chemistry occurring between lithium (blue) and sulphur (yellow) in the electrolyte during cycling. Credit: Background: Gemasolar by Ion Tichy / CC-SA-3.0; Tesla Roadster by Plug In America / CC-BY-SA-2.0.

This will change with the many-fold increase in hard X-ray brilliance provided by the Phase II X-ray source. For the first time it will be possible to reconstruct three-dimensional and chemically resolved maps of in operando batteries on time scales relevant to their actual operation. Using advanced techniques like pair distribution function tomography (Jacques *et al*, 2013), 3D volumes of chemical species and their bond lengths, coordination numbers and hence oxidation states will be extracted in a model independent fashion. This means that we can probe chemical bonding and ion-transport in a dynamic system independently of the exact structure formed, the degree of crystallinity, and even the boundaries between the solid and liquid states.

In the case of lithium batteries, these experiments will allow us to provide critical missing information that is required for safe and efficient energy storage. The Upgrade Programme Phase II will thus be the link between microscopic details and global solutions, allowing the development of the high-voltage electrodes needed for an interconnected green energy grid. By providing chemically resolved X-ray vision, we will be able to match the pace of device development for the first time, thus preventing debacles like the 2013 Boeing failures. In time, we believe that the *in situ* techniques developed through the Upgrade Programme Phase II will be regarded in the same light as the pioneering computed tomography experiments of the 1990s. From a laboratory curiosity, computed absorption tomography rose to become an everyday hospital technique in just a few decades. We similarly expect the vision developed here to transform materials chemistry in the years to come.

References

Armand M. and Tarascon J.-M., Building better batteries, *Nature* **451**, 652–657 (2008).

Ebner M., Marone F., Stampanoni M., Wood V., Visualization and quantification of electrochemical and mechanical degradation in Li ion batteries, *Science* **342**, 716-720 (2013).

EIA 2007, Source: U.S. Energy Information Administration, via Wikipedia - Electric power transmission.

Friščić T., Halasz, I., Beldon, P.J., Belenguer A.M., Adams F., Kimber S.A.J., Honkimäki, V., Dinnebier R.E., Real-time and *in situ* monitoring of mechanochemical milling reactions, *Nature Chemistry* **5**, 1505 (2013).

Horizon 2020: http://ec.europa.eu/programmes/horizon2020/

Jacques S.D.M., Di Michiel M., Kimber S.A.J., Yang X., Cernik R.J., Beale A.M., Billinge S.J.L., Pair distribution function computed tomography, *Nature Communications* **4**, 2536 (2013).

Jadzinsky P.D., Calero G., Ackerson C.J., Bushnell D.A., Kornberg R.D., Structure of a thiol monolayer-protected gold nanoparticle at 1.1 Å resolution, *Science* **318**, 430-433 (2007).

Maugeri L., Ladecola A., Joseph B., Simonelli L., Olivi L., Okubo M., Honma I., Wadati H., Mizokawa T., Saini N.L., Local structure of $LiCoO_2$ nanoparticles studied by Co K-edge X-ray absorption spectroscopy, *Journal of Physics: Condensed Matter* **24**, 335305 (2013).

Mizushima K., Jones P.C., Wiseman P.J., Goodenough J.B., Li_xCoO_2 (0<x<1): A new cathode material for batteries of high energy density, *Materials Research Bulletin* **15**, 783-789 (1980).

Nolte P., Stierle A., Jin-Phillipp N.Y., Kasper N., Schulli T.U., Dosch H., Shape changes of supported Rh nanoparticles during oxidation and reduction cycles, *Science* **321**, 1654-1658 (2008).

Pfeifer M.A., Williams G.J., Vartanyants I.A., Harder R., Robinson I.K., Three-dimensional mapping of a distortion field inside a nanocrystal, *Nature* **442**, 63-66 (2006).

1.4. NANOMATERIALS FOR TECHNOLOGY

Opportunities:

- *In situ* imaging of strain and chemical composition in biocompatible sensors
- Device imaging and failure analysis under operating conditions: from solar cells to quantum computers
- Three dimensional imaging of nano-electronic building blocks

1.4.1. INTRODUCTION

We are surrounded by modern materials and devices which have a profound impact on our day-to-day lives. To develop new technologies in the future, we will need to find new materials and new ways to control their properties. At the same time as developing more powerful technologies, there is an ever increasing need to improve energy efficiency and make more efficient use of our planet's resources. Our lives have been revolutionised by the advent of modern high tech devices. With a smart portable telephone we can carry in our pocket a portal to access all of human knowledge. The spread of embedded computing into a wide range of other devices will allow them to perform with ever improved energy efficiency and in more effective ways. Despite these significant technological advances, many aspects of human life can still be improved. Smart houses could regulate heating and lighting, offer improved security and at the same time drastically cut energy consumption. Self driving cars would revolutionise transportation, offering increased safety and efficiency and freeing the drivers from the task of controlling their vehicle. For many medical conditions, the quality of life of a patient can still be ameliorated. As the population of elderly people continues to increase, there is an ever increasing need for medical devices. The challenge in developing many of these devices is to find ways to allow digital electronics to interact with their environment.

The miniaturisation of electronic devices by the semiconductor industry has followed an exponential improvement described by Moore's law. The number of transistors which can be placed on an integrated circuit doubles approximately every 18 months. This growth cannot continue indefinitely and size limitations given by quantum mechanics as well as problems of thermal power dissipation provide great challenges. Simple Si/SiO_2 based structures permitted downscaling with little change in the basic principles of transistor architecture in 40 years. The last decade

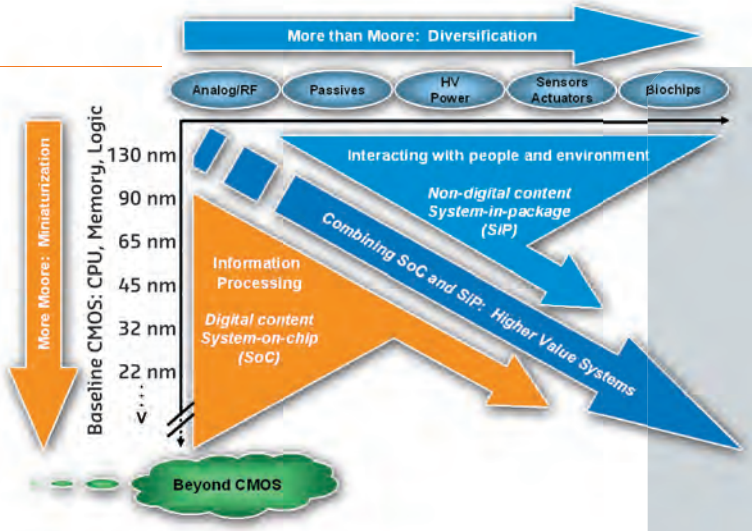

Figure 1.22: The combined need for both digital and non-digital functionality in an integrated system is identified as a dual trend. Miniaturisation of digital electronics ("More Moore") and functional diversification ("More than Moore") are both required. Credit: ITRS "More-than-Moore" White paper (http://www.itrs.net/Links/2010ITRS/IRC-ITRS-MtM-v2%203.pdf).

has seen a rapid increase in the use of many different chemical elements in devices, and with more than fifty different elements present today, chemical innovation on the materials side has become a decisive factor to continue the international technology roadmap for semiconductors (ITRS). To develop useful devices, the increase in transistor density for digital processing is only one part of the story ("more Moore"). A parallel approach to increase device performance and versatility is obtained via a diversification and a functionalisation of devices and the combination of Si technology with high performance semiconductors such as SiC or III-V compounds or with functional oxides such as those used in ferroelectrics or resistive memory (RRAM). A large number of bulky analogue components are also required for the electronics to interact with the environment. The development of such hybrid systems has been labelled "More than Moore" and identified by the IRTS as a key area for future development (**Figure 1.22**). The efforts in the European semiconductor industry will thus concentrate on those techniques bearing a high potential for disruptive technologies leading to

completely new devices or radical improvements of existing functionality. This promises to create valuable technologies by adding new functions ruther than by conventional upscaling. It also presents great opportunities for physicists, chemists and material scientists to open new fields of innovation by collaborative research. Synchrotron radiation already plays a key role in elucidating materials structure-property relationships and the proposed upgrade of the ESRF X-ray source will allow these methods to be applied on the far shorter length scales necessary to study these complex devices.

For both principles, "More Moore", thus smaller structures (5 nm for 2019 on the ITRS) and "More than Moore", through 3D integration and increased complexity, one of the biggest problems will be the power dissipation or the management of local heat-load. This is critical for the more complex devices which contain more interfaces that are subject to interdiffusional or thermal stress. The heat dissipation problem will have an important impact on device failure and thus on their viability for mass production.

Nanotechnology allows us to exploit the changes in the way materials behave at the molecular or atomic length scale. In this microscopic world, many of the properties of materials are quite different from the properties of bulk materials that we are used to. Extreme mechanical forces can be concentrated in tiny devices, which stretch out or compress the atomic bonds and change the way the material behaves. Elastic strain in these devices is often even an intentional part of their functionality as charge carrier mobilities and bandgaps are tuned by changing the strain state. To measure local strains and their evolution under operational conditions, tools are required that can work on samples in their native state without invasive sample preparation. Because of their penetrating power, X-rays are perfectly suited to image devices as a whole or to look at buried layers of a particular material during processing or even during operation.

1.4.2. X-RAY IMAGING OF COMPLEX DEVICES

Many technological challenges need to be met in the development of microelectronic devices pushing the integration of an ever greater variety of materials into the same chip. In particular, this is needed to tackle problems such as current leakage or to introduce and combine other functional materials, *e.g.* ferroelectrics. The "More than Moore" approach also encourages a higher degree of 3D integration of future devices to increase the volumetric device density. The fabrication processes as well as the ageing processes and the functionality itself are reaching a high degree of complexity, calling for characterisation methods at device relevant resolution (typically 1-100 nm). Among the parameters to be resolved are lattice strain and chemistry in the as-grown device since device functionality is controlled by these parameters. Such investigations can be performed today using scanning X-ray diffraction techniques at typical resolution limits of the order of 50-100 nm for simple methods which rely solely on a small X-ray beam size. The resolution can reach 10-20 nm when using reconstruction-based lensless imaging methods that use coherent X-rays. For example in coherent diffraction imaging (CDI) with 2D ptychography, the resolution depends on the atomic weight of the material (Hruszkewycz, 2013).

A 3D integrated device as sketched in **Figure 1.23**, can be scanned in a focused X-ray beam and a map can be created using X-ray diffraction to select a specific layer in the device. A 3D reciprocal space map can be created for every pixel covered by the scan on the sample. The field of view is only limited by the scan range and the time needed to collect the data. The spatial resolution that can be obtained depends on the X-ray source size and focusing optics. By upgrading the ESRF source, the resolution and size of these images will be much improved, allowing smaller device structures to be studied during *in situ* experiments. When no reconstruction algorithms

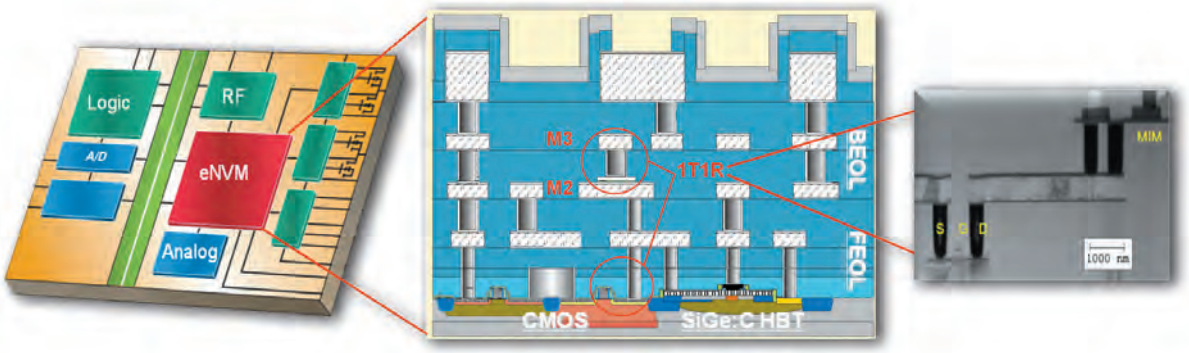

Figure 1.23: Back-end of line integration of non volatile RRAM into a SiGe BiCMOS chip technology for system on chip solutions. Credit: T. Schroeder, IHP Frankfurt/Oder.

are applied, the resulting image has a spatial resolution defined by the beam size itself. Coherent X-rays can be used for reconstruction algorithms in a lensless imaging (CDI or ptychography) approach to significantly improve this resolution, pushing it to the regime of a few nanometres while preserving the advantage of high strain resolution, retaining the absence of sample preparation and permitting the choice of the field of view to be flexible. Currently at the ESRF, lensless imaging methods are rarely used due to the low coherent flux from the X-ray source; the measurement speed is many orders of magnitude slower than conventional methods. The proposed upgrade will increase the coherent flux by a factor of 100 which will make these highest resolution modes routinely available for user experiments. To achieve a sample throughput that is compatible with typical beamtime allocations or industrial experiments, such a dramatic increase in coherent flux is needed in order to study real devices. Typically, the devices studied include novel substrates or other 2D extended systems and it is critical to be able to measure a series of samples or conditions to extract variations and to detect heterogeneities due to the fabrication process.

Currently only low energy X-ray beams are available for coherent diffraction and they have limited spatial resolution, so X-ray methods have yet to develop their potential in this area due to the limitations of X-ray sources. Phase II of the Upgrade will extend spatial resolution and sensitivity to lattice strain to the scales relevant for such devices and allow fundamental questions about microstructure-property relationships to be addressed.

1.4.3. SOLAR ENERGY

Photovoltaic cells offer a way to harvest the sun's energy and convert it directly into electricity. While the most efficient solar cells are based on silicon, polymer-based organic solar cells have the potential to create an inexpensive renewable energy source that would have a low environmental impact. The efficiency of these devices can be improved by adding metallic nanoparticles into the polymer layer to increase the absorption of sunlight and enhance the conversion into electrical energy. Synchrotron X-rays can offer unique insights into the internal structures of these devices. By aligning an organic solar cell parallel to a high energy nanofocused X-ray beam, Paci *et al.* in 2013 were able to measure the distribution of nanoparticles as a function of height inside the device (**Figure 1.24**). Such investigations are at the limit of current technology and constitute only the very first step in the optimisation of device properties by introducing structural complexity.

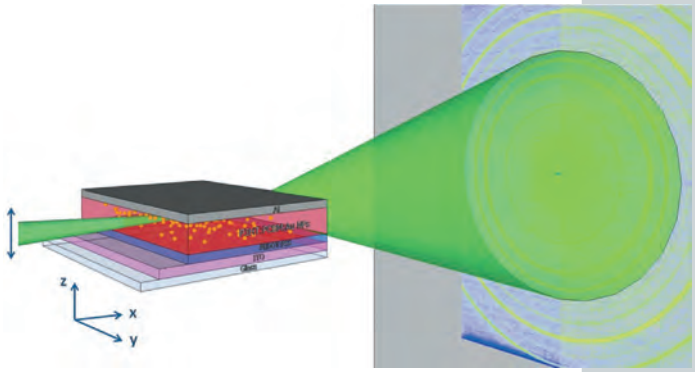

Figure 1.24: Depth profiling of an organic solar cell using synchrotron X-ray to determine the distribution of nanoparticles in an organic layer. Credit: Paci *et al.*, 2013; Copyright © 2013 WILEY-VCH Verlag GmbH & Co. KGaA, Weinheim.

1.4.4. FLEXIBLE ELECTRONICS

Historically most electronics are based on silicon which is not flexible. Today combinations of organic and inorganic thin film electronics can be used to fabricate flexible devices. This opens up a wide field of applications ranging from paper-like displays to biocompatible sensors and devices. **Figure 1.25** shows a mock-up of a flexible display which will allow computing devices to be used as conveniently as paper. Such displays could be used anywhere from car windscreens to eye glasses. The contact lens in the same figure shows a potential bio sensor (Salvatore, 2014) for monitoring excess pressure in the eyeball, responsible for glaucoma.

The multi modal potential of X-ray techniques using small beams, serving on the one hand as an imaging tool and on the other hand as a spectroscopic probe with excellent chemical and electron-state sensitivity, is essential to the study of such complex devices. One critical need for developing biosensors is to track trace element diffusion under implantation conditions.

Flexible electronics must be able to withstand large deformations without degrading their properties. Most of the high performance materials we use today have been optimised through an understanding

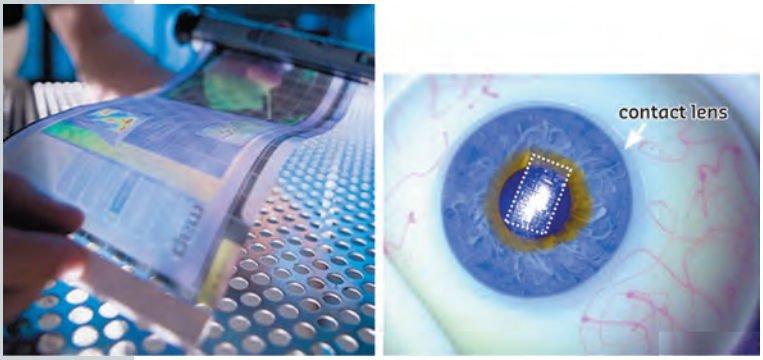

Figure 1.25: Flexible displays and biocompatible sensors are becoming possible with today's technology. Credit: Left: RDECOM / CC-BY-1.0; Right:. Reprinted by permission from Macmillan Publishers Ltd: *Nature Communications* **5**, 2982, copyright 2013.

of structure-property relationships. From atomic structures we can compute electronic properties and relate these to bulk material properties. The microstructure of the material also plays an increasingly important role as devices become smaller. The grain sizes, dislocation and defect structures and the arrangement of domains all combine to influence and control the way a material behaves. Understanding the relationships between microstructure and properties requires analytical tools that can show us the 3D microstructures on relevant length scales. Learning how microstructures change with large deformations will be essential to the development of new devices.

1.4.4.1. QUANTUM COMPUTING

An intensive research effort to realise the potential of quantum computers is currently being made. In a conventional computation, the machine passes through a series of distinct states to arrive at a final answer. The working principle of a quantum computer is that it can simultaneously pass through a multitude of superimposed quantum states during a computation, which would allow new classes of problems to be solved with unprecedented speed. Such devices that potentially exploit individual quantum states of electrons promise to add a new dimension to the capabilities of microelectronics. Although multiple theoretical routes can be proposed, we currently do not know how to build such a machine; a large number of quantum states need to be coupled with each other without being perturbed by their surroundings. The "analog" character of quantum logic is fundamentally different to current digital computers and so a new level of detailed understanding of the microstructure and defects in the constituent materials used to construct devices will be needed to overcome the technical challenges.

Figure 1.26 represents a typical measurement performed on a functional layer in a quantum computing device. One promising route to forming these quantum structures on silicon is to create coupled quantum dots in which electrons are trapped in a thin silicon layer within a stack of layers of an alloy of silicon and germanium. As in conventional electronic devices, the properties of quantum mechanical components based on these silicon two-dimensional electron gases depend very strongly on their structure, and the changes in the structure induced by the formation of the devices.

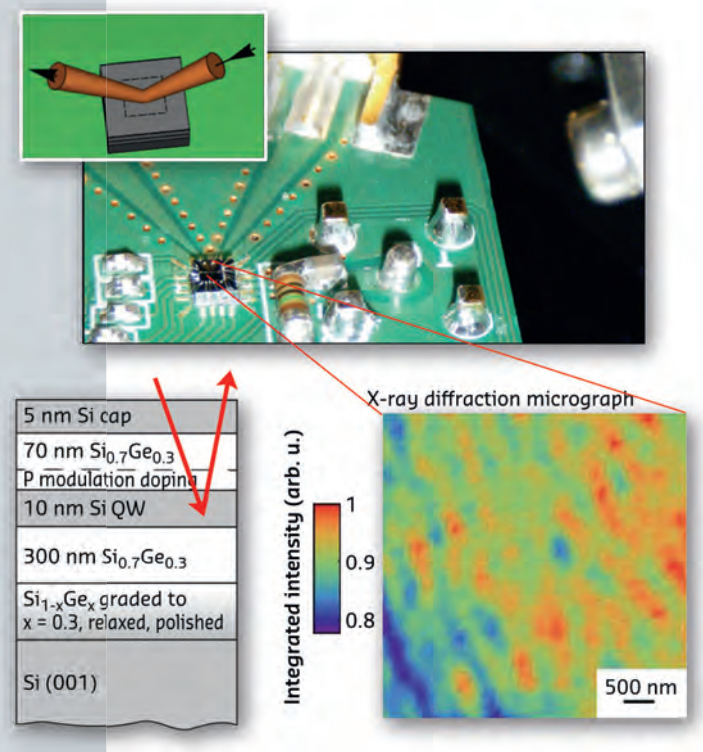

1.4.4.2. DEVICE IMAGING: CURRENT PERFORMANCE AND OUTLOOK

After the proposed upgrade, X-ray diffraction imaging techniques will achieve the resolution required to study real devices in space and time and could be applied during *in situ* thermal treatment or growth of a device. This is possible as the high scanning speed (2D maps of intensity images in less than one minute) would allow researchers to follow strain drifts due to

Figure 1.26: Scanning X-ray diffraction map of a structured thin Si quantum well layer integrated onto a circuit board. The X-ray diffraction micrograph shows sensitivity to thickness variations of the order of a few atoms of the quantum well layer. Credit: Evans 2012, Copyright © 2012 WILEY-VCH Verlag GmbH & Co. KGaA, Weinheim).

local temperature changes. The extraordinary strain resolution obtained with X-rays can image static strain fields at epitaxial interfaces or around defects both after or during processing or under operation conditions. The stability of these interfaces is a major concern and a bottleneck in the development of complex multi-material devices.

This high strain resolution can be applied to a wide range of ageing and reliability studies of high power devices such as lasers, light emitting diodes, and CMOS chips. Local variations of heat load, so-called hot spots that are often caused by fabrication imperfections, are often responsible for limited device lifetime and could be detected in the device interior due to the high strain resolution and the ability to image specific device components based on their X-ray diffraction. A better understanding of these failure mechanisms would increase the longevity of electronic devices, which has a very large potential impact not only in terms of their economic cost, but also on our use of natural resources and the environmental impact of manufacturing replacements for failed equipment.

The characterisation of strain in working 3D devices is not likely to become possible with electron based methods due to the limited penetration depth for electrons in matter. When electron holography is possible, lattice parameter resolution of a few parts in 1000 have already been demonstrated with spatial resolutions of a few nanometres (Béché, 2013). These values, however, can only be obtained in thin polished samples and cover a field of view of about one micrometre. On a macroscopic scale, local strains can be measured destructively by attaching a strain gauge to a sample and then measuring the relaxation when the sample is drilled or cut. At the nanoscale, X-ray diffraction is currently the only method which can image these strains. **Figure 1.27.** presents a summary of strain resolution and length scales reached by current techniques. The application to real devices will remain the domain of X-ray methods and the X-ray source upgrade is essential to obtain maps at high enough resolution to see interesting structures during operando studies of intact devices.

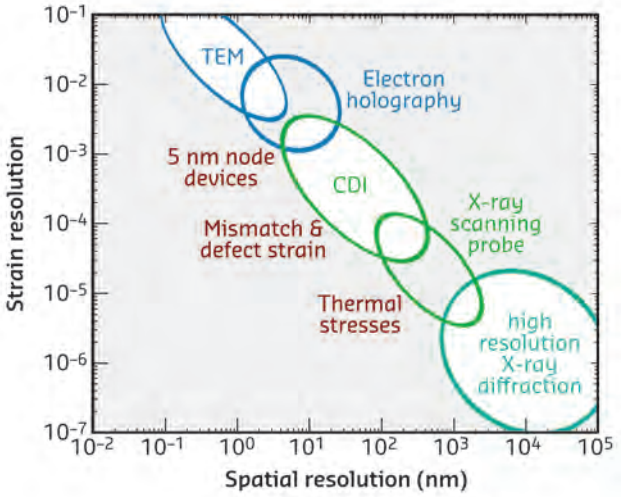

Figure 1.27: Comparison of the resolving power in strain and real space for electron microscopy and X-ray methods. The fields of interest affected typically in microelectronic devices are indicated as red areas.

1.4.4.3. TIME-RESOLVED OPERANDO AND *in situ* STUDIES: COHERENT IMAGING OF GROWTH AND REACTIVITY

BioMEMS devices offer a new analytical tool to measure chemical binding by transmitting mechanical forces which arise from a chemically driven change in stress. Nanomechanical cantilever arrays based on polycrystalline gold films coated with self-assembled monolayers of thiols have been used to study the resistance of superbugs to antibiotics (Ndieyira *et al.*, 2008). By imaging these gold films using coherent X-ray diffraction (Watari *et al.*, 2011), the internal strain fields inside the 300 nm diameter gold nanocrystals could be resolved. The CDI results revealed that the facetted surfaces of the crystals show a contraction on thiol binding while the curved surface regions expand. This change in shape of the nanocrystals couples the chemical behaviour of the bound surface layer to the cantilever bending and depends strongly on the crystalline grain size, morphology and orientation. These results already have broad implications for the design of thiol-on-gold based nanomechanical sensors. A large increase in coherent X-ray flux is needed to extend such studies to systems based on elements lighter than gold. The possibility of carrying out *in situ* studies on a timescale which is relevant for chemically interesting processes also requires a large gain in X-ray flux.

Much of our knowledge about the microscopic world is derived from optical and electron microscopy. Ever since the discovery of X-rays, the idea to exploit extremely short wavelengths of light for microscopy has been confounded by the lack of suitable lenses. Recently, there has been much progress in X-ray optics suited to imaging and full-field X-ray microscopy and a resolution approaching a few hundred atoms can be obtained. Current X-ray imaging optics are unable to exploit the resolution limit offered by the wavelength that could allow us to resolve individual atoms. The proposed upgrade will significantly reduce the X-ray source size in the horizontal plane and provide a large gain in coherent X-ray flux. It is these "coherent" X-rays which are essential for the lensless reconstruction algorithms that have the highest spatial and strain resolution.

The Upgrade Phase II will create a new hard X-ray microscope for the investigation of complex devices. Techniques have been demonstrated at current synchrotron sources on carefully chosen materials.

No currently available source has the capacity to extend these coherent X-ray techniques to real time *in situ* studies or to investigate arbitrarily complex device structures. The brilliance of the X-ray beam is a critical property for such research. Higher brilliance means more X-ray photons can be focused onto a smaller coherent spot, allowing lensless microscopy to be widely used. It will revolutionise imaging by making it possible to map evolving physico-chemical processes. The expertise and infrastructure that already exist at the ESRF will allow us to develop such instrumentation and make it routinely available to a diverse user community. To develop all the different devices that can be imagined in the More-than-Moore framework, we will need to bring together biologists, chemists, physicists, materials scientists and engineers. Building the new source at the ESRF will give these scientists access to a fundamentally new mode of imaging.

References

Béché A., Rouvière J.L., Barnes J.P., Cooper D., Strain measurement at the nanoscale: Comparison between convergent beam electron diffraction, nano-beam electron diffraction, high resolution imaging and dark field electron holography, *Ultramicroscopy* 131, 10 (2013).

Chahine G., Richard M.-I., Homs-Regojo R.A., Tran-Caliste T.N., Carbone D., Vincent J., Grifone R., Boesecke P., Katzer J., Costina I., Djazouli H., Schroeder T., Schülli T., Imaging of strain and lattice orientation by quick scanning X-ray microscopy combined with 3D reciprocal space mapping, *J. Appl. Cryst. accepted* (2014).

Evans P.G., Savage D.E., Prance J.R., Simmons C.B., Lagally M.G., Coppersmith S.N., Eriksson M.A., Schülli T.U., Nanoscale distortions of Si quantum wells in Si/SiGe quantum-electronic heterostructures, *Adv. Mater.* 24, 5217-5221 (2012).

Holler M., Diaz A., Guizar-Sicairos M., Karvinen P., Färm E., Härkönen E., Ritala M., Menzel A., Raabe J., Bunk O., X-ray ptychographic computed tomography at 16 nm isotropic 3D resolution, *Scientific Reports* 4, 3857 (2014).

Hruszkewycz S.O., Highland M.J., Holt M.V., Kim D., Folkman C.M., Thompson C., Tripathi A., Stephenson G.B., Hong S., and Fuoss P.H., Imaging local polarization in ferroelectric thin films by coherent X-ray Bragg projection ptychography, *Phys. Rev. Lett.* 110, 177601 (2013).

Ndieyira J.W., Watari M., Barrera A.D., Zhou D., Vogtli M., Batchelor M., Cooper M.A., Strunz T., Horton M.A., Abell C., Rayment T., Aeppli G., Mckendry R.A., Nanomechanical detection of antibiotic mucopeptide binding in a model for superbug drug resistance, *Nature Nanotechnology* 3, 691-696 (2008).

Paci B., Bailo D., Rossi Albertini V., Wright J., Ferrero C., Spyropoulos G.D., Stratakis E., Kymakis E., Spatially resolved *in situ* structural study of organic electronic devices with nanoscale resolution: the plasmonic photovoltaics case study, *Advanced Materials* 25, 4760–476 (2013).

Salluzzo M., Gariglio S., Torrelles X., Ristic Z., Di Capua R., Drnec J., Sala M.M., Ghiringhelli G., Felici R., Brookes N.B., *Advanced Mater.* 25, 2333 (2013).

Salvatore G.A., Münzenrieder N., Kinkeldei T., Petti L., Zysset C., Strebel I., Büthe L. & Tröster G., Wafer-scale design of lightweight and transparent electronics that wraps around hairs, *Nature Communications* 5, 2982 (2014).

Schroer C.G., Boye P., Feldkamp J.M., Patommel J., Schropp A., Schwab A., Stephan S., Burghammer M., Schöder S., Riekel C., Coherent X-ray diffraction imaging with nanofocused illumination, *Phys. Rev. Lett.* 101, 090801 (2008).

Watari M., McKendry R.A., Vogtli M., Aeppli G., Soh Y.A., Shi X.W., Xiong G., Huang X.J., Harder R., Robinson I.K., Differential stress induced by thiol adsorption on facetted nanocrystals, *Nature Materials* 10, 862 (2011).

Yang W.G., Huang X.J., Harder R., Clark J.N., Robinson I.K., Mao H.K., Coherent diffraction imaging of nanoscale strain evolution in a single crystal under high pressure, *Nature Comm.* 4, 1680 (2013).

1.5. MATTER AT EXTREME PRESSURES AND TEMPERATURES

Opportunities:

- Probing structural complexity and its relation to *e.g.* superconductivity and quantum (critical) phenomena.
- Imaging materials complexity in the TPa regime at the nanoscale.
- Understanding the structure and dynamics of Earth's and Exo-planets deep interiors.

1.5.1. INTRODUCTION

Science at extremes of pressure and temperature is a vibrant field of international research that addresses fundamental questions in domains as diverse as fundamental condensed-matter physics, Earth and planetary science, material synthesis and characterisation, and biology. Pressure strongly alters interatomic distances without changes in thermal energy or chemical environment, and is thus a better thermodynamic variable than temperature and chemical composition to explore free energy landscapes. In the last decade, several major international extreme conditions initiatives have started to tackle some of mankind's most pressing issues, for example, the deep carbon cycle in the Earth (DCO 2009) and the Energy Science project to search for future sources of energy (EFREE 2009, BES 2007). Such projects are also essential if we are to gain a better understanding of the inner structure of the Earth and giant planets in our solar system and beyond, and for the creation of new materials for energy harvesting and storage.

Research at light-based large scale facilities has always been at the leading edge of extreme conditions science, and the recent advent of powerful laser sources (Omega, NIF, ELI, ...), X-ray free electron laser facilities (LCLS, European XFEL, ...), and the exciting perspective of a new generation of diffraction-limited synchrotrons will allow the exploration of material properties at conditions far in excess of those currently achievable. The current third-generation synchrotron facilities have pioneered many of the major breakthroughs in extreme conditions research over the last two decades. Indeed, compared to other large-scale facilities, synchrotron radiation offers a unique diversity of state-of-the-art techniques for characterisation of matter. At the ESRF, the scope of this research field has been constantly expanding and developing (Andrault *et al.*, 2013) such that, remarkably, the structural, dynamical, electronic and magnetic properties of materials at pressures up to 100 GPa can now be determined with the same precision as at ambient conditions.

The proposed X-ray source upgrade will provide significantly higher photon flux density and higher coherence, especially for photon energies above 30 keV, *i.e.* the energy range most relevant for diffraction and imaging at extreme conditions. These improvements will allow studies to be carried out on much smaller sample volumes and on much shorter time scales. The direct impact on studies at extreme conditions is that higher pressure and temperature states that can be generated only in small volumes or in dynamic, transient processes become experimentally accessible. In particular, the

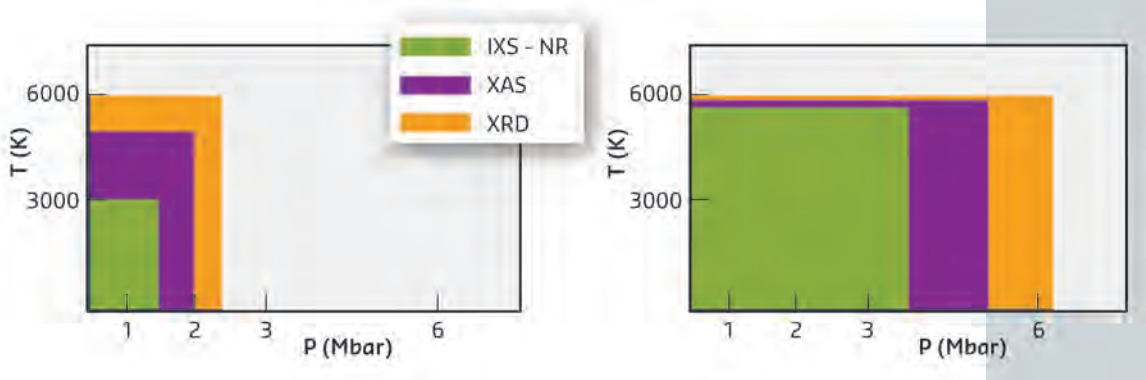

Figure 1.28: ESRF Upgrade Programme Phase II will enable the extension of the accessible P-T range for static high pressure experiments. XRD: X-ray diffraction, XAS: X-ray absorption spectroscopy, IXS: Inelastic X-ray scattering, NR: Nuclear resonance.

detailed characterisation of material structures and properties (up to pressure values of several TPa, *i.e.* tens of Mbars) will become possible (with precision similar to those currently achieved at 100 GPa) by carrying out static compression studies using diamond anvil cells and dynamic compression experiments using lasers with pulse durations in the nanosecond regime. Furthermore, the increased coherence of the X-ray beam at high energies will be exploited to permit techniques such as phase contrast imaging, coherent diffraction imaging, and ptychography imaging to be applied to new areas of research. This will enable studies of nucleation processes, sample morphology and strain state, diffusion of species, and chemical segregation with the highest possible spatial resolution down to a few tens of nanometres. **Figure 1.28** illustrates the domain to which the current P-T limits of the various X-ray techniques will be extended in static compression mode. Breakthroughs can be expected in many scientific areas, these will be introduced below.

1.5.2. NEW OPPORTUNITIES AND CHALLENGES

1.5.2.1. STRUCTURAL COMPLEXITY

The last two decades have shown that unexpected physical and structural behaviour at ultra-high pressures is the rule rather than the exception. Much of this work has been pioneered at the ESRF, particularly studies on low-Z elements, *e.g.* hydrogen, lithium and sodium, where phenomena such as cold melting and quantum effects have striking effects on the phase diagram (Guillaume *et al.*, 2011), as well as on incommensurately-modulated host-guest composite structures. Similarly, complex structures have been predicted by *ab initio* calculations to be commonplace in the TPa range (see **Figure 1.29** for the case of aluminium), as core electrons participate in bonding, leading to complex spatial arrangements of the electronic distribution. X-rays focused down to the sub-micrometre scale will allow single crystal diffraction at much higher pressures than today, and render the structural determination of such complex systems possible.

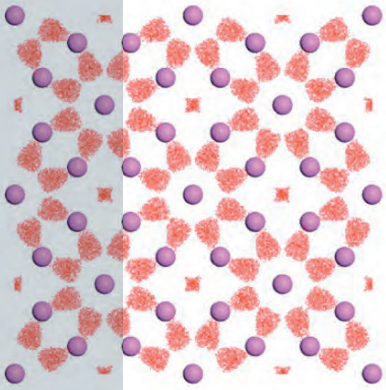

Figure 1.29: Aluminium is predicted to have an incommensurate host-guest structure between 3.2 and 8.8 TPa. Credit: Reprinted by permission from Macmillan Publishers Ltd: *Nature Materials* **9**, 624–627, copyright (2010).

These studies can be extended in the future. By including (pulsed) magnetic fields as an additional variable, the exploration of the interplay between superconductivity and structural order could be explored. The combination of high pressure, low temperature and very high pulsed magnetic fields (destructive coils producing a 1 µs long 100 T pulse are available today) together with the enhanced brilliance of the new source, will provide an ideal test-bench to probe quantum critical phenomena such as the suppression and re-emergence of superconductivity, quantum critical points, new spin structures of anti-ferromagnetically coupled sublattices, magnetic quantum phase transitions, and exotic phenomena including non-Fermi liquid behaviour and unconventional superconductivity. In this context, the polarisation properties of synchrotron radiation will enable techniques such as X-ray magnetic circular dichroism (XMCD) to be used to probe correlations between local structure and electronic and magnetic degrees of freedom simultaneously.

1.5.2.2. DISORDERED MATTER

While the observation of structural complexity in solids at extreme pressures has become commonplace, the appearance of such complexity in the local structure and order of liquid or fluid phases at such extremes remains largely unexplored.

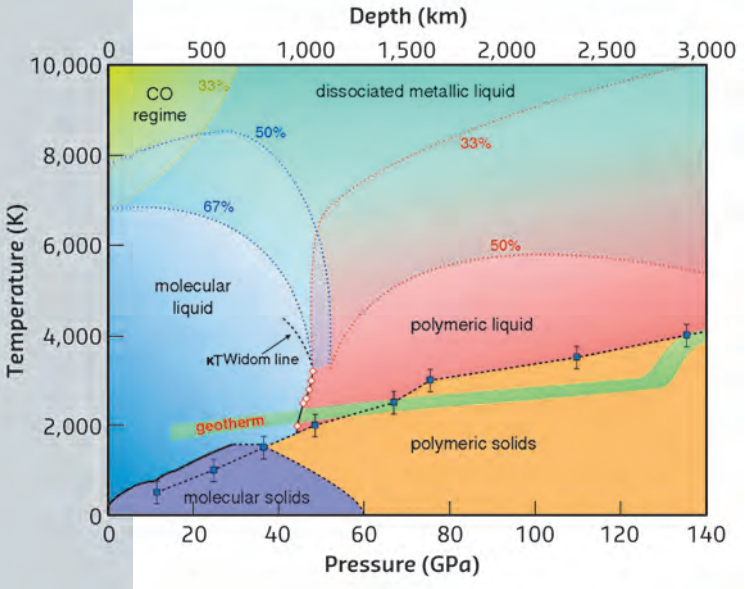

Figure 1.30: The phase diagram of dense liquid CO_2. Credit: Boates *et al.*, 2012.

There is an enormous amount of new physics to be explored, even in simple liquids, at pressures that are not currently accessible to detailed structural studies. For example, the existence of icosahedral order in compressed liquids could be revealed and quantified. Techniques developed at ambient conditions for such purposes can be transposed to extreme conditions, thereby allowing detailed investigations of structural phase transitions in liquids, chemical complexity in molecular systems (see **Figure 1.30** for the example of dense CO_2), supercritical fluids, and the crossover from liquid-like to gas-like behaviour above the critical point (Simeoni *et al.*, 2010). The higher brilliance of the upgraded X-ray source will enable the extraction of the structure factor of low-Z liquids that are out of reach today. Extending the phase diagram of H_2 to reach the fluid - plasma phase transition (expected around 400-500 GPa and 50 K) and being able to measure the structure factor in this fluid phase would be of paramount importance (Babaev 2004).

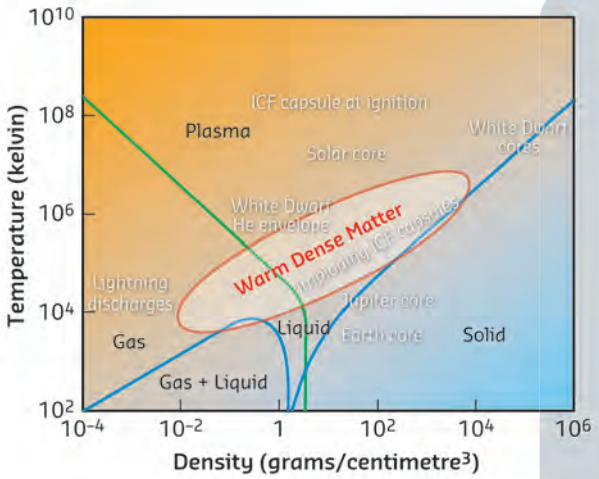

Figure 1.31: Phase diagram comprising the classical three aggregate states, the warm dense matter and plasma state. The temperature-density conditions in stellar objects and inertial confinement fusion (ICF) reactors are indicated. Credit: Michael Desjarlais, Univ. of Florida.

1.5.2.3. WARM DENSE MATTER

To obtain even greater extremes of density and temperature will require moving from the static to the dynamic approach, with the use of compact high-power lasers (~ 100 joule, ns pulse duration). The higher brilliance of the Phase II X-ray source will enable faster measuring times, down to 0.1 ns in single shot mode, and will therefore provide the opportunity for detailed, systematic structural studies at pressures and temperature into the TPa and 10000 K regime. Local equilibrium states as well as phase transition kinetics could be studied with the 100 ps time resolution available at ESRF.

This will be an ideal means to study the warm dense state of matter (WDM) at local thermal equilibrium (*cf.* **Figure 1.31**). Here, where kinetic and potential energies are similar, standard material models break down, and there is no current capability to accurately predict the behaviour of matter under such conditions. One source of motivation to study the warm dense state of matter is to understand stellar and planetary interiors in terms of equation of state (EOS) (see below).

The future Phase II storage ring will complement X-ray free electron laser (XFEL) facilities in the investigation of laser induced extreme states of matter. In this context, the large energy spectrum and the stability of the beam emitted by the Phase II X-ray source would be fully exploited for X-ray absorption spectroscopy (XANES and EXAFS) at extremes of pressure and temperature with a quality similar to that achieved at ambient conditions today. This will allow the detailed, systematic analysis of changes in electronic shielding of atomic inner electron shells due to ionisation, continuum lowering depression, and electron degeneracy. By exploiting the large energy spectrum of synchrotron X-rays, these studies can be extended to different absorption edges to allow binary and even more complex multi-element systems to be studied in the warm dense state. Detailed information on the local structure around each element will become accessible, such as modifications of ion-ion correlation, interactions between different chemical species, formation of compounds, etc. This whole area of research is currently unexplored.

1.5.2.4. NOVEL MATERIALS

The design and synthesis of new materials that can perform reliably under thermomechanical extremes is central to addressing future challenges in fossil fuel, fission, fusion and other technologies. There are increasing demands to extend the lifetime of materials, their efficiency, and develop novel capabilities, while at the same time lowering costs. There is still a significant gap between the theoretical performance of an ideal material and the response of real materials to extremes of radiation, pressure and temperature. This arises from the effects of dislocations, interfaces, grain boundaries, and domain walls on the strength of materials. To further our understanding, studies of dynamical phenomena are needed at length scales ranging from nano- to micrometres. The enhanced P-T range in dynamic compression bridges the gap between mechanical and thermal properties and chemical dynamics and kinetics. Areas of key importance that could be addressed are: synthesis of harder and more resistant materials at even more extreme P,T conditions; tailoring novel materials with unique chemical and physical properties, the prediction and control of their electronic structure; creation of even

higher energy density materials under pressure and investigation of their recovery to ambient conditions; the design of advanced materials resistant to harsh environments such as those in fusion reactors.

The Phase II X-ray source will afford higher spatial resolution from sub-micrometres down to tens of nanometres, by using (scanning) (spectro-) microscopy and tomography techniques. The increased beam coherence at higher energies will allow the study of the morphology and the strain state of samples, via coherent diffraction imaging techniques (Yang *et al.*, 2013), and will also give access to the study of dynamical phenomena such as phase transitions and melting.

1.5.2.5. LIFE SCIENCE

Research in microbiology will also greatly benefit from Phase II of the Upgrade (Picard, 2013). As oceans cover 71% of the Earth's surface and probably more in the early years of the Earth, the present-day high-pressure environment (pressures in excess of 10 MPa and up to 110 MPa) represents the largest habitat for microbial life on Earth. The impact of pressure on microbial activity remains poorly understood and this field of research is still in its infancy although critical to assess the extent of the deep biosphere. An illustrative example is the pressure dependence of the rate and extent of bacterial dissimilatory iron reduction. Furthermore, the food industry has increasingly been using high pressure techniques for inactivating pathogenic microorganisms while preserving the food's nutritional and organoleptic properties (Demazeau, 2011). Due to the higher brilliance of the Phase II X-ray source and the localised nature of the radiation damage, spectroscopy studies such as XANES on systems with realistic metabolite dilutions and cell concentrations will become possible. Under these conditions, radiation damage is no longer an issue since the culture to beam ratio is sufficiently large so that the impact of cell death on the evolution of the biological system is minimised.

1.5.3. EARTH AND PLANETARY SCIENCE

Phase II of the Upgrade Programme will offer new and exciting opportunities for Earth and planetary science. Complex material behaviour is driven by phase transformations that have a significant effect on the density, specific electronic and magnetic properties and redox reactions. The most pertinent questions remaining open concern the nature of the building-blocks for the different planetary systems, the relative sizes between gaseous (or liquid) envelopes, silicate mantle, and metallic cores, the thermal state and internal dynamics of planets in our own and other solar systems (Exoplanets). The vast majority of the planets that have been surveyed have internal pressures and temperatures beyond our actual experimental limitations, with the most abundant constituents being hydrogen and helium. Other major meteoritic bodies in the solar system include comets and planetary ices, which have played a major role in supplying water and volatile elements to the Earth. The internal structure of these bodies include simple molecular compounds such as water, methane, ammonia, adopting a number of structures with interesting properties, such as methane clathrates. Understanding the structure of planets from the surface to the core is fundamental to understanding their evolution and origin, and ultimately their potential for sustaining life or providing resources.

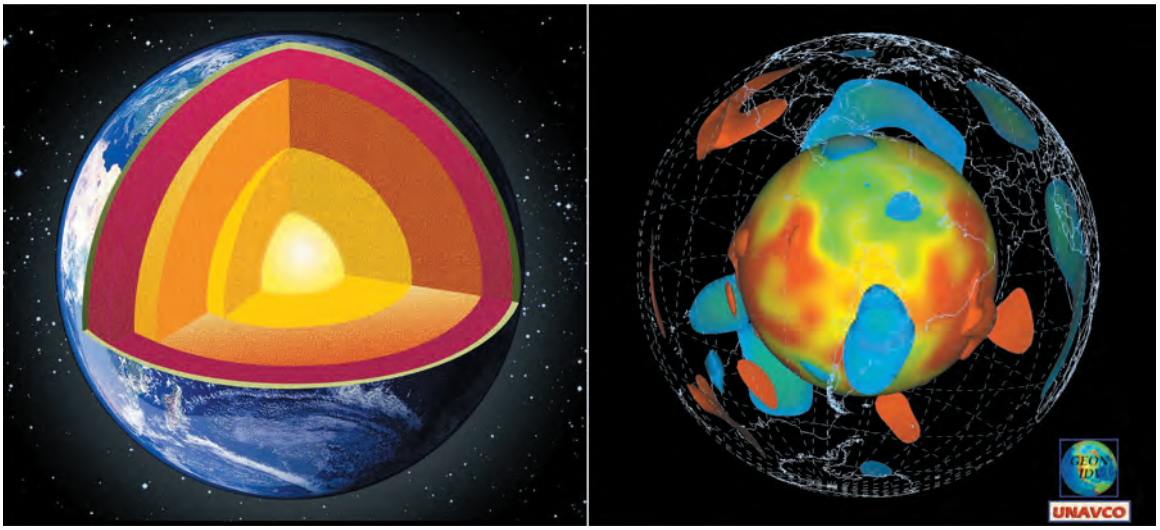

Figure 1.32: Classical representation of the Earth interior (left panel); Earth interior from 3D seismic tomography (right panel, credit: UNAVCO).

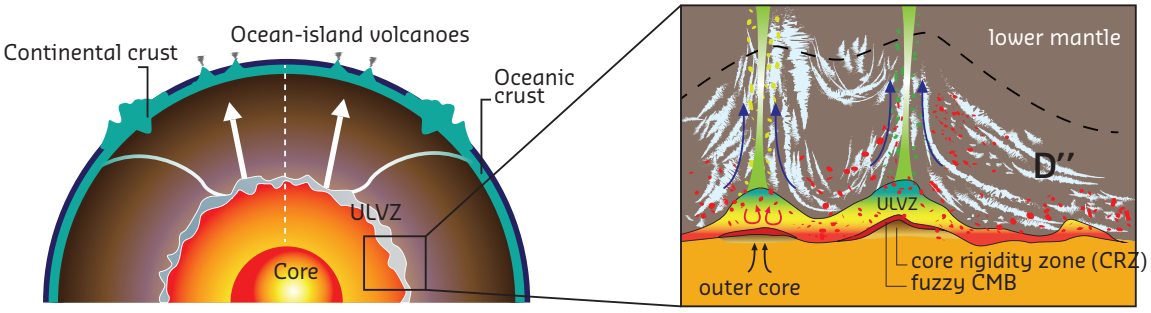

Figure 1.33: Illustration of dynamical processes in Earth's interior with enlargment of a region of the core-mantle boundary (CMB) and the D'' layer.

1.5.3.1. THE INTERIOR OF PLANETS: FROM SIMPLE MODELS TO COMPLEXITY

The Earth's interior is classically depicted as a succession of homogeneous layers comprising minerals in the upper and lower mantle, and liquid and solid iron-alloys for the outer and inner core, respectively. As seismometers spread more evenly over the planet's surface, including the oceans, the seismic imaging of the Earth's interior using three-dimensional tomography has rapidly improved over the last decades (Earth 2009). It now provides a detailed distribution of seismic wave velocities and shows a much more complex internal structure than expected (see **Figure 1.32**). This complexity is intimately linked to the extreme diversity of spatial scales at which Earth's processes take place. While phase transitions, grain deformation, chemical segregation, and partial melting, take place on the atomic scale, these processes directly control large scale phenomena including the Earth's magnetic field, plate tectonics, earthquakes and volcanism.

While seismic and high pressure high temperature X-ray based studies provide increasingly detailed information on the structure of Earth's interior, there remain many fundamental unanswered questions that require new, advanced experimental studies at the pressure-temperature limit of static methods.

The primary scientific goal will be the determination of the exact composition, temperature distribution, and physical properties (structure and mechanical properties) of the solid inner core and liquid outer core. In particular, the nature and the effect of light element impurities, which induce a density reduction of 10% compared to pure iron, are not well understood. This knowledge, however, is essential for refining the bulk composition of the Earth, determining its accretion processes, and identifying the energy sources that sustain the magnetic field which protects life at the Earth's surface. This information is also required to clarify the seismic anisotropy of the inner core.

The chemical interactions that take place at the core-mantle boundary are still unknown. They could affect the state of the mantle, for example by insertion of fusible elements such as hydrogen or sulfur into the lowermost mantle. This could induce partial melting and chemical segregation, and eventually produce deep sources for volcanic oceanic islands (*cf.* **Figure 1.33**. Illustration of dynamical processes in Earth's interior). Chemical exchange at the core-mantle boundary could also help to maintain Earth's geomagnetic field through solutal convection in the liquid outer core. Another key goal is the establishment of a petrogenetic data base, *i.e.* a self-consistent set of thermodynamic data of all relevant minerals as a function of pressure, temperature, and composition. To date, such a data base exists only for the Earth's crust, but to correctly model the large scale phenomena mentioned above, it has to be extended to the Earth's mantle and core.

Addressing these questions is beyond our current experimental capabilities. They require the enhanced brilliance of the Phase II X-ray source and a multi-disciplinary approach. X-ray diffraction will allow phase diagrams and melting curves to be determined at the relevant thermodynamic conditions for silicates and oxides, including [Fe,Mg]O, [Fe,Mg]SiO_4, [Fe,Mg][Si,Al]O_3 and iron alloys (Fe-Ni, Fe-S, Fe-Si, Fe-O, Fe-C), which comprise the Earth mantle and core, respectively.

The combination of inelastic X-ray scattering (IXS) and nuclear inelastic scattering (NIS), with *ab initio* lattice dynamics will provide stringent constraints for elastic and thermodynamic parameters. X-ray absorption spectroscopy with submicrometre resolution at the relevant P,T conditions will probe changes in speciation and partitioning as minerals in the mantle and at the core-mantle boundary undergo chemical reactions, decomposition and diffusion processes. The coherent properties of X-rays will also be exploited to image the anisotropic properties at the nanoscale. Such diversity of analytical methods to investigate the properties of minerals, rocks, and ices in the very wide P-T range of planetary interiors is a unique capability of synchrotron radiation.

The performance of the Phase II X-ray source offers the exciting prospect of extending all such studies

to planets beyond our solar system. One of the most important discoveries in astronomy of the last decade is a myriad of Exoplanets (**Figure 1.34**) with a diversity of size and mass in our galaxy and beyond (Wolszczan 1992). A number of Super-Earth planets were observed with masses up to 10 times that of Earth, and internal conditions that reach several TPa and temperatures up to a few 10000 K. However, crucial experimental data such as phase diagrams and equation of states, required for modelling exoplanet interiors, are currently lacking. Giant planets such as Jupiter are sufficiently massive to influence the dynamics and evolution of entire solar systems. The mechanisms, however, by which such giant planets have formed, are still the subject of debate. To shed light on these mechanisms, a detailed knowledge, for example, of the properties of hydrogen in the warm dense matter regime (P = 7 TPa and T = 17000 K) is a prerequisite.

To advance research in these areas, static measurements of ultra-dense matter properties using diamond anvil cells have to be complemented by dynamic measurements using shocks generated by compact lasers (~100 joules, ns pulse duration). Single shot X-ray diffraction and X-ray absorption spectroscopy (XAFS) will shed new light on phase diagrams, kinetics of chemical reactions/decomposition, and on the local atomic configurations in melts/liquids with chemical selectivity. A strong collaboration with XFELs is desirable, and will lead to a unique and comprehensive view of the behaviour of matter under extreme conditions from the static limit to the extreme dynamic limit.

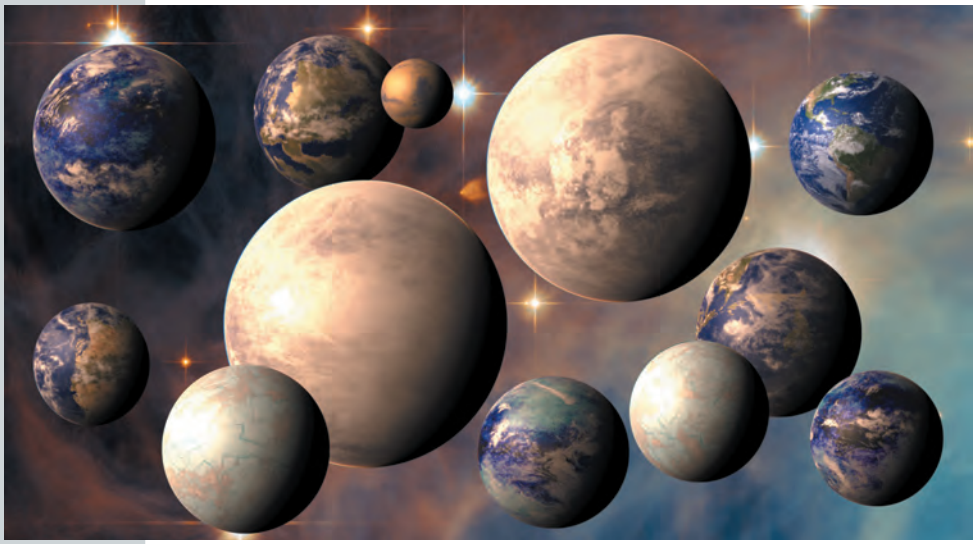

Figure 1.34: Artistic view of a selection of the 1075 exoplanets discovered as of February 2014, including potentially habitable planets. Credit: PHL @ UPR Arecibo (phl.upr.edu), ESA/Hubble, NASA.

References

Andrault D. *et al.*, Science under extreme conditions of pressures and temperatures at the ESRF, *Synchr. Rad. News* **26**, 39-44 (2013).

Babaev E. *et al.*, A superconductor to superfluid phase transition in liquid metallic hydrogen, *Nature* **431**, 666-668 (2004)

Ballentine C.J., Geochemistry: Earth holds its breath, *Nature* **449**, 294-296 (2007).

BES 2007, Basic research needs for materials under extreme environments, Report of the Basic Energy Sciences Workshop on Materials under Extreme Environments (2007).

Boates B. *et al.*, Stability of dense liquid carbon dioide, *Proc. Nat. Acad. Sci. Am.* **109**, 14808–14812 (2012).

DCO 2009, The Deep Carbon Observatory; http://deepcarbon.net/.

Demazeau G. & Rivalain N., The development of high hydrostatic pressure processes as an alternative to other pathogen reduction methods, *J. Appl. Microbiology* **110**, 1359-1369 (2011).

Earth 2009, Physics and chemistry of the Earth's interior: crust, mantle and core, Editors: A.K. Gupta, S. Dasgupta, ISBN: 978-1-4419-0344-0 (2009).

EFREE 2009, Energy Frontier Research in Extreme Environments Center; https://efree.gl.ciw.edu/

Guillaume C.L. *et al.*, Cold melting and solid structures of solid lithium, *Nature Physics* **7**, 211-214 (2011).

Picard A. & Daniel I., Pressure as an environmental parameter for microbial life – A review, *Biophysical Chemistry* **183**, 30-41 (2013).

Pickard C.J. & Needs R.J, Aluminium at terapascal pressures, *Nature Materials* **9**, 624-627 (2010).

Simeoni G.G. *et al.*, The Widom line as the crossover between liquid-like and gas-like behaviour in supercritical fluids, *Nature Physics* **6**, 503-507 (2010).

Wolszczan A & Frail D.A., A planetary system around the millisecond pulsar PSR 1257 + 12 », *Nature*, **353**, 145-147 (1992).

Yang W. *et al*, Coherent diffraction imaging of nanoscale strain evolution in a single crystal under high pressure, *Nature Communications* 4:1680 (2013).

1.6. ENHANCING INDUSTRIAL APPLICATIONS AND EXPLOITATION OF SYNCHROTRON SCIENCE

1.6.1. INTRODUCTION

Creating industrial impact is an important ESRF mission. The Upgrade Programme Phase II is an opportunity from which industry will benefit and from which ESRF will create new, durable industrial relationships, resulting in a more industrially-empowered facility with a greater long-term economic value.

Business is an increasingly important, dynamic and vociferous stakeholder across large-scale central research infrastructures, with specific demands and tailored service needs [1]. Above and beyond the established long-term benefits of curiosity-driven research, European governments desire more direct economic returns from investments made in research infrastructures and are looking to innovation with industry to help provide this. At the European Commission, it is also recognised that research infrastructures have and should have a growing economic impact for the so-called "Innovation Union": *"Ground-breaking research and innovation increasingly require world-class infrastructures. They attract global talent into innovative clusters and are an essential breeding ground for information and communication technologies and key enabling technologies such as micro and nanoelectronics, biotechnologies, new materials and advanced manufacturing."* [2]

The ESRF thus has a strong role to play as a key hub in the knowledge triangle of research, education and innovation for interaction with SMEs and large companies of the European industrial backbone. Industry is already an important client, partner and supplier to the ESRF (**Figure 1.35**) and, to a large extent, the ESRF as the first third-generation light source has set the scene for modern industrial use of synchrotrons. However, and as is described in the earlier science chapters and further below, industry needs ever finer analysis tools for their most demanding proprietary research, as well as when working in partnership with academic experts for upstream pre-competitive R&D. All this needs new high performance tools with extreme stability, which will also drive knowledge and technology transfer opportunities to European industry – for example in the domain of new instrumentation. UP PII will create these new opportunities for European industry to benefit more from the long-term investment made in the ESRF, allowing new, broader and more creative interactions between ESRF and European companies.

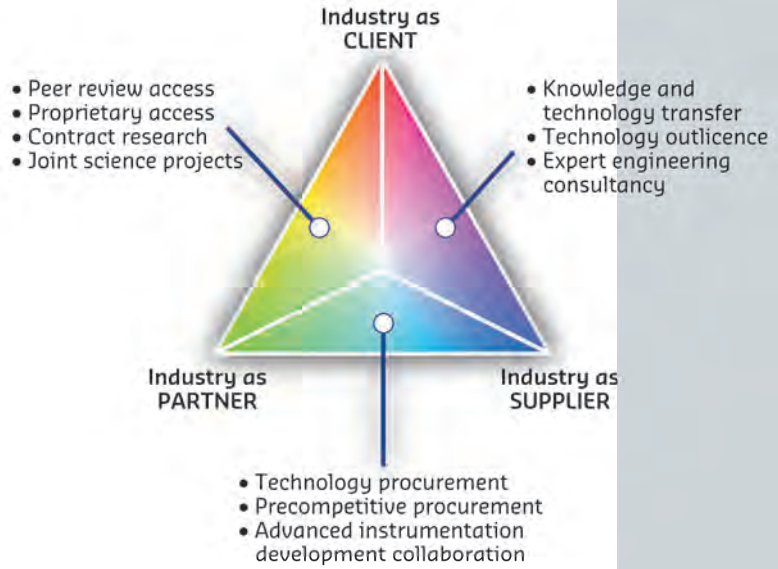

Figure 1.35: ESRF business model via industry as a client, partner and supplier, with the different roles often blending.

1.6.2. INDUSTRY AS AN ESRF CLIENT

Understanding materials, be they smart, nano-structured, bio-degradable, manufactured energy-efficiently or sustainably resourced, are at the heart of industrial R&D&I challenges today. Atomic, nano-, micro- and macro-structure are all critically intertwined with tailored function and properties in the use of these materials in products. To innovate and enhance a competitive edge, European industry needs advanced synchrotron X-ray tools across all levels of end-use inspired science, applied R&D and process optimisation to comprehend the industrial materials that underlie final products, permitting companies to be "smart" integrators and users of modern materials. With UP PII, "nanoscopy" using X-rays to look inside such materials, often under process-relevant conditions, will become the core user strength of the ESRF offering unequalled materials characterisation tools.

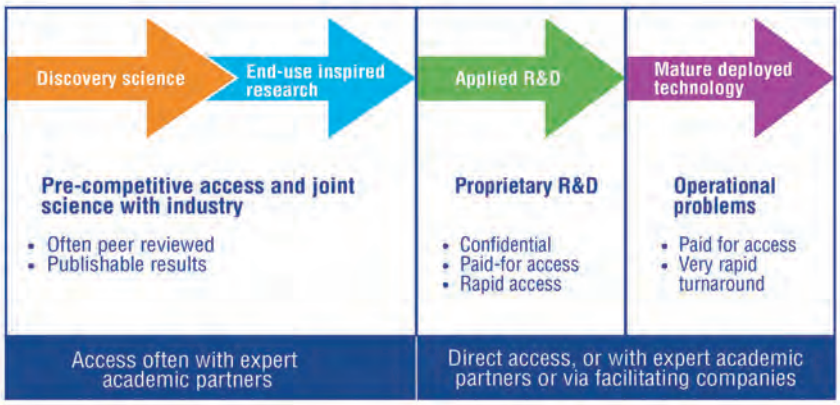

Figure 1.36: Access modes for industry at different levels of technology maturity.

Industry is already a significant user and client (generating 1.5-2.0 MEuros annually) of the ESRF, with the central pillar today being pharma/biotech for drug discovery using protein crystallography. But the UP PII will open the ESRF to more physical science and materials nano-characterisation for industry. The need for industrial research on nanomaterials has already been elegantly identified and described in the GENNESYS white paper (Gennesys., 2009). The entry point for industry to the new nano-techniques at the ESRF will undoubtedly be via academic networks [3] for discovery science and pre-competitive R&D, together with dedicated training opportunities for industry researchers. As companies gain experience and confidence, they will transform towards using the facilities for confidential paid-for work, sometimes still in partnership with academics or via third-party facilitating companies. This follows the model observed at the ESRF and across RI more generally (**Figure 1.36**).

Opening access to such advanced capabilities will not ignore industry's demand for rapid access to robust workhorse techniques providing cost-effective, pre-analysed data ready for industrial consumption. This is an important component of the ESRF's offer to industry and where an important impact is felt by industry for process and product optimisation. As part of the UP PII strategy, ESRF plans to develop streamlined and automated software to provide for high-throughput, robust data pipelines, taking the model developed for structural biology forward to other techniques.

1.6.3. INDUSTRY AS AN ESRF SUPPLIER

Research infrastructures are an important consumer (and creator) of advanced instrumentation, with a market worth estimated at 4-5 billion Euros annually in Europe [4]. Europe has one of the best portfolios of research infrastructures worldwide, with leading companies in the supply of high-end, valuable instrumentation to facilities worldwide. This supply and its linked wealth generation to the European economic area will be an important beneficiary of the investment in the UP PII facilities, where Europe could lead the world in the developments and subsequent supply needed for diffraction-limited storage rings. Instrumentation such as integrated X-ray optics, high precision mechanics, magnet assemblies, vacuum technologies, and sample handling and sample environments will all need development and procurement to make UP PII a reality.

Traditionally, the ESRF has performed much of its own R&D for new instruments in-house building on 20 years of facility and instrument design, commissioning and operation. However, an emerging trend is for research infrastructures to use precompetitive procurement to outsource technology R&D to encourage industry to take on risky developments and to create fresh markets for potentially linked instruments and technologies. Towards this end, Horizon 2020 will pilot aid for pre-competitive procurement actions and from which ESRF and partners could leverage industry R&D for new instruments. A key strategic area for ESRF and other light sources, and where such an approach could be implemented, is advanced detector sub-systems and high speed electronics with spillover to high-end imaging applications.

1.6.4. INDUSTRY AS AN ESRF PARTNER FOR SCIENCE AND TECHNOLOGY INNOVATION

Moving beyond the client and supplier relationships described above is important to perform successful longer-term challenging R&D or joint innovation for synchrotron technologies.

To the benefit of the ESRF in terms of science, both publishable and proprietary industry R&D bring real-world constraints to materials analysis and characterisation, often far beyond the demands of simplified model systems. Industry also demands best practice in experiment reproducibility to ensure that results can be relied upon in process optimisation or materials development programmes. This challenging work will increase with the nanoprobe techniques enabled by UP PII, with more long-term projects established with industrial partners, either via the peer review or industry programmes, allowing a deeper use of the new facilities complementing ad hoc access for "routine" materials analysis. This will naturally benefit the academic programme with new beamline capabilities, novel sample environments and better analytics driven by industry needs (see for example Malbet-Monaco *et al.*, 2013). The longer-term work will include the use of co-funded PhD and post-docs, producing young scientists trained in synchrotron techniques and also industry-and-business savvy. Opening up new techniques to industry is not easy. Towards this industrial representatives will be invited to take part in the development plans of the Phase II beamlines, contributing ideas and views on how the new ESRF facilities can best respond to industry interests. This may further develop into individual companies or industry consortia making financial contributions to specific facilities or to create industry-specific instrumentation on the beamlines – an already successful strategy at other facilities such as SLS, APS and NSLS.

As mentioned earlier, UP PII will require significant leaps in technology to deliver the high performance and advanced instrumentation required for both academic science and industrial R&D to draw the greatest benefits from the UP PII investment. Technology roadmaps for the key areas, such as detector systems, high power magnets, high precision and stable mechanics, and new sample environments are described in **Chapter 4** and will provide opportunities to industry for procurement but also for development in collaboration. European industry, large and small, will be drawn into these instrumentation developments at both tender stage and even, where appropriate, much earlier in the process at conception. By nurturing effective knowledge and technology exchange early on, the ESRF will benefit from industrial competence in design, as well as industry to get a head start on an eventual licence or technology transfer.

References

GENNESYS White Paper. Ed. H. Dosch & M. H. van de Voorde (2009).

Malbet-Monaco S., Leonard G., Mitchell E., Gordon E., How the ESRF helps Industry and how they help the ESRF, Acta Cryst. D. **69**, 128

Notes

1 ERIDWatch, GENNESYS and EIRIISS project reports for further background.

2 Europe 2020 Flagship Initiative, SEC(2010) 546 final, 6.10.2010.

3 An ESRF study carried out in February 2013 to all 7377 scientists having successfully submitted a research proposal to ESRF in the last 5 years received 775 replies. Of those 46% stated that they had collaborations with industrial R&D centres, 39% said their work had industrial applications, and 33% had funding from industry.

4 ERIDWatch: http://ec.europa.eu/research/infrastructures/pdf/bylander_erid.pdf

PART 2
Accelerator and Source Upgrade

2.1. PROJECT OVERVIEW

2.1.1. WORLDWIDE CONTEXT

The last decade has been characterised by a worldwide effort to design and eventually build an ultimate storage ring (Einfeld D. *et al. 1995*). The ultimate storage ring should have an equilibrium emittance of the order of the diffraction limit: about 10 pm·rad for 10 keV X-rays. Smaller emittance does not improve the brilliance significantly, although the transverse coherence still increases from about 0.5 to more than 0.9 for an emittance of about 1 pm·rad. As a general consensus, such a storage ring requires a green-field, since it is very difficult to adapt it to an existing layout. Only SPring-8 (Shimosaki Y. *et al.* 2011), thanks to the larger circumference of its storage ring, has been able to study the possibility of upgrading its source to reach the diffraction limit (Hettel B. *2013*). However, even considering a completely new facility, it is clear that both the design and the required technologies are reaching the limit of current feasibility.

The ESRF has adopted an alternative strategy, aiming to find a solution based on well-proven technologies that would be compatible with the existing infrastructure. This creates a less ambitious project (emittances of the order of 100-150 pm·rad), but one that is readily applicable with a very good cost/benefit ratio (ESRF, White paper, 2012).

This strategy has proven to be very attractive, indeed other facilities have started similar studies for their upgrades, in particular SPring-8 and APS. In the past year, the international community has shifted gears, and it is now strongly focused on defining lattices and engineering solutions consistent with this approach. We can reasonably expect that, in addition to the MAX-IV facility that has pioneered the field (Detailed Design Report on the MAX IV Facility, 2010), the next decade will likely see two to three facilities upgraded in this way. Figure 2.01 compares the new projects with respect to the existing facilities. It should be noted that the emittance figures had to be normalised to standard scaling laws; in general the emittance increases with the square of the beam energy and decreases linearly with the ring circumference.

The ESRF storage ring upgrade will contribute greatly towards maintaining Europe's leadership in synchrotron and accelerator technologies. We also see it as an intermediate and necessary step in the creation of an ultimate storage ring, since many issues related to such an ambitious storage ring will be addressed and understood during the realisation of this project.

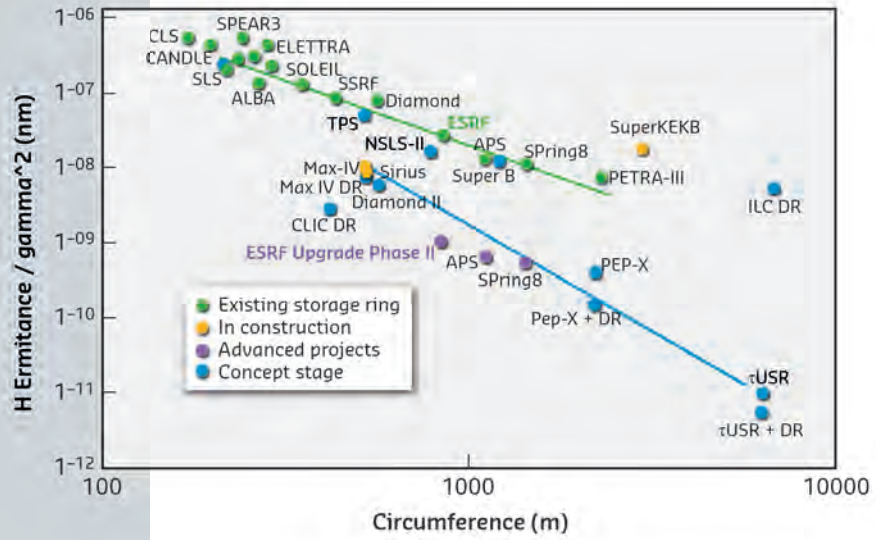

Figure 2.01: Horizontal emittance comparison for storage rings: existing (green), under construction (yellow) and future (purple and blue)

2.1.2. ESRF CONTEXT

The accelerator complex has already undergone many significant upgrades aimed at increasing the brilliance and the reliability of the X-ray source during Phase I of the Upgrade Programme (Revol J.L., 2013). These projects were established by The Purple Book (ESRF, 2007). In addition to these activities, we have also been studying strategies and solutions to further improve the X-ray source for Phase II. The Purple Book underlined the possibility of finding suitable solutions to reduce the storage ring's equilibrium horizontal emittance. The constraints of reusing the tunnel and infrastructure, together with the requirement of maintaining the ESRF's unsurpassed beam quality, have made this problem very challenging.

The project must adhere to the following requirements and constraints:

- Ensure a length of at least 5 m for all the existing insertion device (ID) straight sections.
- Maintain the insertion devices and bending

magnet (BM) beamlines as close as possible to their current location.
- Preserve the time structure operation and a multibunch current of 200 mA.
- Keep the present injection scheme and injection complex.
- Reuse existing hardware as much as possible (power supplies, vacuum components, diagnostics, etc.).
- Minimise the energy lost in synchrotron radiation.
- Minimise hardware power consumption.
- Minimise operation costs.
- Minimise the impact on user operation due to the downtime for installation and commissioning.
- Maintain a budget comparable to what was proposed for Phase II in The White Paper (ESRF, 2012).

2.1.3. HIGHLIGHTS

2.1.3.1. NEW RING LATTICE

We have developed a new hybrid multi-bend achromat (HMBA) lattice design with an equilibrium emittance of about 150 pm·rad (Farvacque L. *et al*, 2013). This should replace the present double-bend achromat design (DBA) lattice, which has an equilibrium emittance of about 4.0 nm·rad (**Figures 2.02** and **2.03**). Installation of the new lattice will require the complete substitution of the 32 arcs of the existing storage ring with 32 new arcs of practically identical length.

The new lattice was designed to fit into the existing facility, maintaining ring circumference, periodicity and beamline positions. The hybrid configuration of the seven bends in the achromat cell takes advantage of a large number of bending magnets to reduce the horizontal emittance (as implemented in the MAX-IV design), and regions with large localised dispersion to allow efficient correction of chromaticity, as already used in the standard double-bend achromat. The lattice produces a small emittance thanks to stronger focusing, lower field dipoles and dipoles with quadrupolar components. Besides the lower emittance, the net result is an energy loss per turn of about 2.6 MeV (compared to 4.9 MeV/turn today), which allows a considerable reduction of operation costs due to decreased RF electricity consumption.

The overall design has been developed taking into account several constraints and criteria:
- Use standard technology as much as possible.
- Adopt solutions already implemented in the existing facilities wherever possible.
- Optimise cost/performance ratio for all subsystems.
- Maintain the overall budget envelope of about 100 M€ as proposed in The White Paper (ESRF, 2012).
- Ensure that the realisation of the project is consistent with the Phase II timescale.
- Ensure the maximum flexibility and tunability of the lattice.

The main parameters of the new source are given in **Table 2.01**.

The design allows for further "adiabatic" improvements, similar to those carried out at the ESRF over the past 20 years such as optics improvements and better undulators. This will ensure a steady improvement of the source throughout the operational life of the new storage ring.

	Present lattice	New lattice
Lattice type	DBA	HMBA
Circumference [m]	844.390	843.979
Beam Energy [GeV]	6.04	6
Beam Current [mA]	200	200
Natural emittance [pm·rad]	4000	147
Energy spread [%]	0.106	0.095

Table 2.01: Main parameters of the present and proposed storage ring sources.

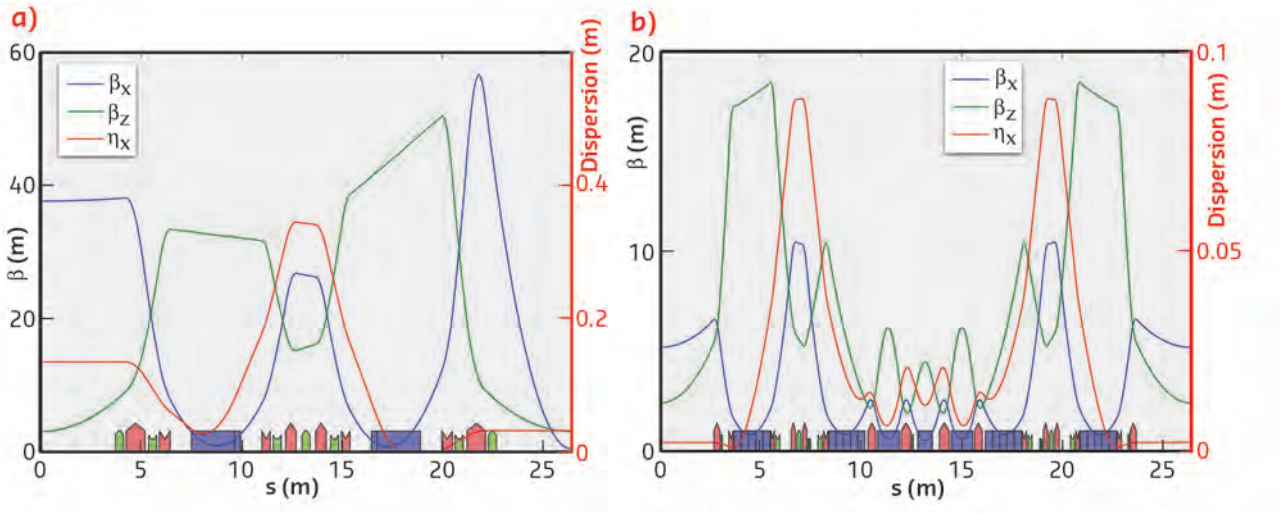

Figure 2.02: DBA lattice functions (a) and new HMBA lattice functions (b). Schematics: dipoles in blue, quadrupoles in red, sextupoles in green.

2.1.3.2. NEW STORAGE RING X-RAY SOURCES

The new lattice will provide an improvement in brightness of the order of 30-100 times for both insertion device and bending magnet beamlines. The coherence fraction on insertion device beamlines will also increase by up to a factor of 30.

Since the X-ray beam will be much narrower, it will be possible to collimate a larger fraction of the white beam component compared to the present. This will result in a reduction of the total power on high-beta beamline optics by more than a factor of 2 and on the low-beta optics by up to a factor of 10. The present beamline optics constraints could then become compatible with a higher stored beam current.

The geometry of the insertion device beamlines will be unchanged; the chosen beam parameters (emittance, beam size and beam divergence) at the source result in tolerable changes in power density on the beamline optics.

Since the dipole fields will have become much weaker, the source for the bending magnet beamlines will be replaced by three-pole wigglers (3PW), resulting in an increase in brightness and flexibility of the X-ray spectra.

2.1.3.3. LATTICE ENGINEERING

The engineering design of all the subsystems matches the criteria listed in section 2.1.3.1 as closely as possible. The magnets have "standard" designs and their stronger gradients are obtained by reducing their apertures. The vacuum chamber system has been designed to have a vacuum chamber size/beam size ratio larger than present and it will be compatible with *in situ* baking. We have adopted anti-chambers and lumped absorbers to ensure a static and dynamic vacuum comparable to the present one. The synchrotron radiation power handling will be similar or better than in the present machine. We have also dimensioned all the systems with large safety margins (power supplies, magnets, supports, vacuum pumps, etc.) to guarantee reliable and extended (at least 20 years) operation.

We also foresee the possibility of increasing the beam current to 300 mA at a later time. All the critical systems will be either dimensioned accordingly (*e.g.* absorbers, vacuum chambers, etc.) or upgradable (such as RF power sources, etc.).

The project will aim to take full advantage of the developments in accelerator technologies that have occurred over the last 20 years at the ESRF and other facilities. This has led to many important results featuring new magnet design, innovative vacuum technology, and extremely accurate beam monitoring and orbit feedback systems. These new capabilities and technologies, which were not available or were in their infancy when the present ESRF storage ring was conceived, today provide a solid basis for the realisation of a considerably more advanced storage ring design.

2.1.3.4. PLANNING

The technical and engineering design is ongoing and will allow the procurement phase to be started from 2015 onwards. The preassembly phase will take place in 2017-2018.

The dismantling of the present storage ring and the installation of the new storage ring is proposed to start on 15 October 2018 for a total duration of nine months, followed by a commissioning period for the new accelerator and the beamlines. The user service mode (USM) is proposed to resume on 1 June 2020.

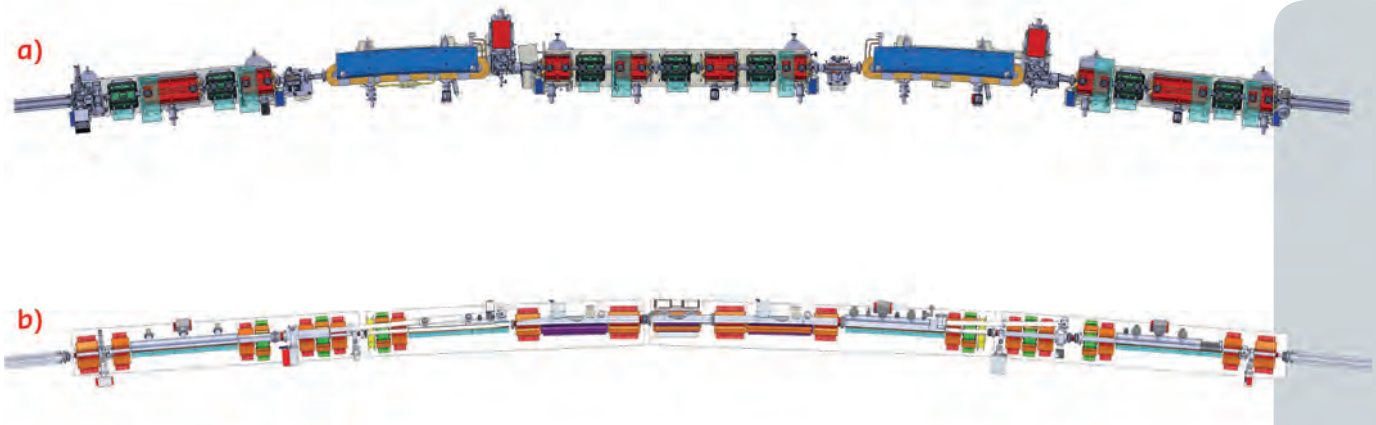

Figure 2.03: Engineering layout of the existing ESRF DBA-ARC-Cell (a) and the new HMBA-ARC-Cell (b).

The installation and commissioning period will affect user operation in the following way:

- 2018: Almost the normal annual amount of beamtime will be delivered to the user programme by a reduction of the machine dedicated time and shutdowns.
- 2019: No user operation.
- 2020: About 50% of the standard annual beam time will be delivered to users.

2.1.3.5. PROJECT MANAGEMENT AND RESOURCES

The accelerator project is organised in ten work packages. An Accelerator Project Office will coordinate all activities. In addition to the existing ESRF staff complement, we plan to recruit 16 extra staff dedicated to the accelerator project for the Accelerator and Source Division and a further 28 for other ESRF Divisions to provide the support required throughout the whole ESRF.

2.1.3.6. BUDGET

The overall budget envelope of the accelerator upgrade is estimated to be 103.5 M€. Both the budget and the cost breakdown are described in a separate document and will be analysed by an *ad-hoc* Cost Review Panel as requested by the ESRF Council.

PART 2
ACCELERATOR AND SOURCE UPGRADE

2.2. PHOTON SOURCE

2.2.1. OVERVIEW

The quality of the photon beam radiated by the various sources installed around the ESRF storage ring will be dramatically improved by the implementation of the new magnet lattice. This improvement will be visible in the brilliance and the transverse coherence, which are two key parameters of X-ray beams. For undulator sources, the increase in brilliance and coherent fraction of the photon flux will be more than a factor of 30 above the photon energy of 10 keV. The brilliance of the bending magnet source will also be considerably improved by more than one order of magnitude. In particular, short three-pole wigglers will be used to provide an improved photon flux for bending magnet beamlines. The length of the free space available for insertion devices will be 5 m in the new lattice. This will require an adjustment of the insertion device layout for sections longer than 5 m. For the bending magnet beamlines, the photon beam delivered at the front end will be different due to the changes in geometrical characteristics of the source points, with a corresponding need to reposition elements of the beamline.

2.2.2. BRILLIANCE

Since the horizontal emittance of the photon beam is largely dominated by that of the electron beam, the brilliance from the different sources will be enhanced by more than one order of magnitude. In the vertical plane, the electron beam emittance will remain comparable to that achieved presently (~5 pm·rad). Figure 2.04 compares the brilliance reached by various sources with the existing (dashed lines) and new lattices (plain lines). The parameters used for the calculation are defined in Table 2.04 of section 2.3.1. The upper part corresponds to a selection of undulators representative of the photon energy range covered by the ESRF. All of these undulators are based on proven technology: conventional devices operated with a minimum gap of 11 mm or short-period, small-gap (5 mm) in-vacuum-type undulators such as the cryogenic permanent magnet undulators (CPMU) that have been used at the ESRF since 2008. At 10 keV, the brilliance is increased by about a factor of 30 and gets progressively higher at higher energies. For lower photon energy, this factor becomes smaller as the photon beam approaches the diffraction limit about 20 at 1 keV).

For bending magnet-type sources, a new approach will be adopted. The present bending magnet sources are based on a main 0.85 T field and a 0.4 T soft end while in the new lattice only 0.54 T and 0.43 T dipole fields are available for these lines. Consequently, beamlines based on these dipole sources would lack in performance in the hard X-ray region above 20 keV. To overcome this limitation, three-pole wigglers will be used to provide improved photon flux in both the soft and the hard X-ray region. These short devices will be installed in a dedicated drift space downstream of the central dipole. For bending magnet sources, the brilliance will also be significantly increased due to the smaller horizontal emittance and the reduced electron beam size in the vertical plane, thanks to the smaller vertical beta function at the source. For long wigglers (W150), the gain in brilliance will be very limited. As the light produced by this type of device is essentially incoherent, the source size is dominated by a depth-of-field effect.

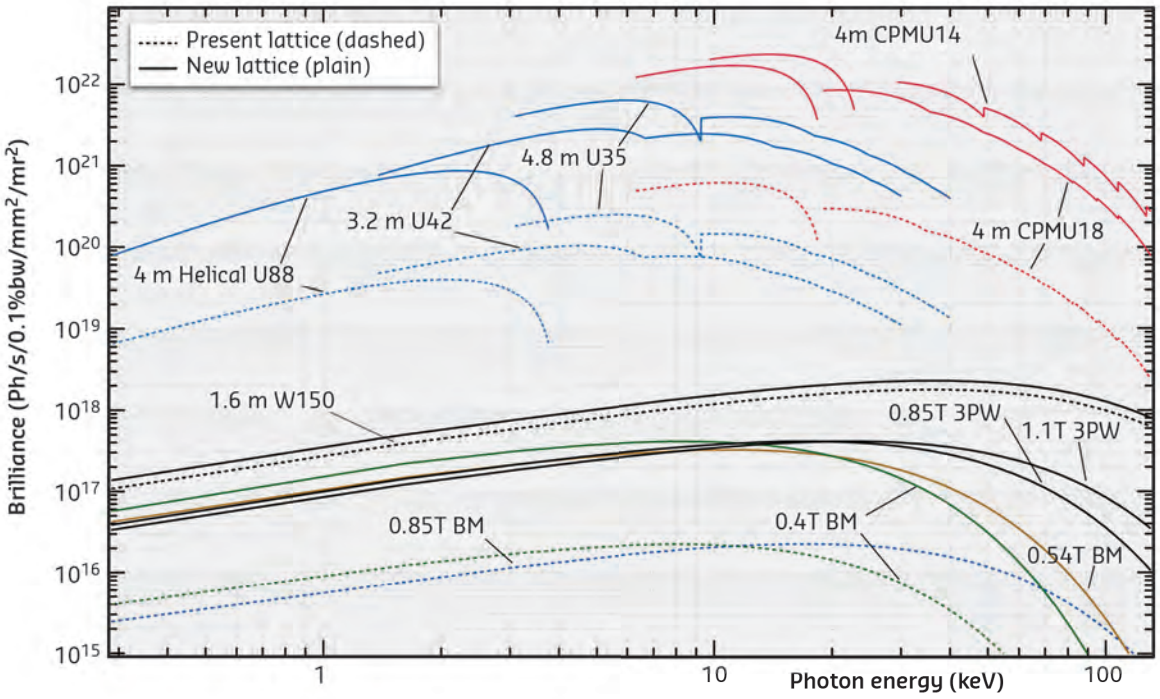

Figure 2.04: Brilliance from various sources for the existing and new lattices.

2.2.3. TRANSVERSE COHERENCE

The reduction of the horizontal electron beam emittance will increase the fraction of transverse coherence in undulator X-ray beams. Table 2.02 compares the performance of the present and new lattices in terms of horizontal and vertical undulator source size and divergence. The undulator under consideration has a length of 4 m and a period of 18 mm (CPMU18). The electron beam parameters are defined in Table 2.04 of section 2.3.1. In this calculation, the impact of the electron beam energy spread on the source size and divergence has been taken into account.

	Lattice	RMS source size [µm]		RMS divergence [µrad]	
		H	V	H	V
10 keV	Present low beta	49.8	6.2	105.6	5.1
	Present high beta	411.6	6.2	11.5	5.1
	New lattice	**28.2**	**6.1**	**7.2**	**5.1**
50 keV	Present low beta	49.6	4.4	105.5	4.5
	Present high beta	411.6	4.4	11.2	4.5
	New lattice	**27.8**	**4.4**	**6.8**	**4.4**

Table 2.02: RMS photon source size and divergence from a 4 m-long undulator (period 18 mm, K = 2) at 10 keV and 50 keV for the present and new lattices.

This example raises a number of interesting points:

- For beamlines using undulators from low-beta straight sections, the gain in coherent fraction with the new lattice will be mostly achieved through the much smaller horizontal divergence.
- Conversely for the high-beta case, the improvement will be mostly achieved with the reduction of the horizontal source size.
- For both low- and high-beta sections, the gain will be similar but slightly higher in the low-beta case due to the effect of the horizontal dispersion.

The expected gain in coherent fraction will be practically the same as that achieved for the brilliance (more than one order of magnitude). Figure 2.05 shows the coherent fraction of the photon flux reached with the existing and new lattices for the same undulators.

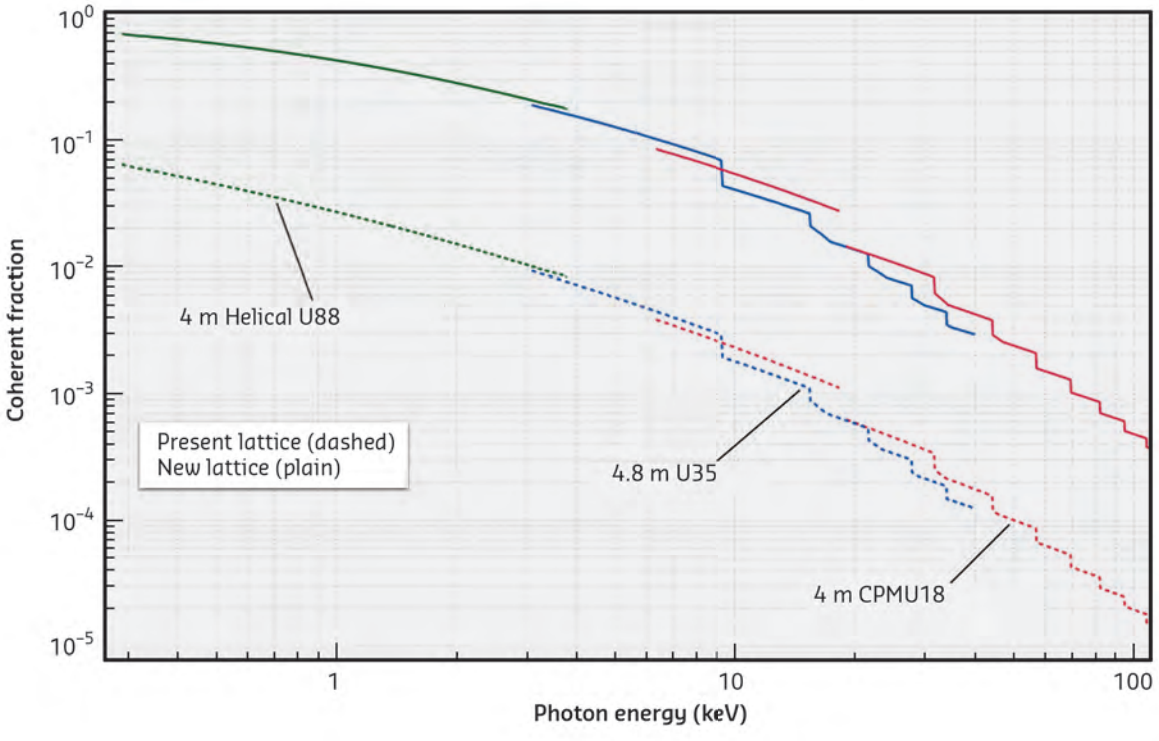

Figure 2.05: Coherent fraction of the photon flux for the existing and new lattices.

2.2.4. PHOTON FLUX AND HEAT LOAD

2.2.4.1. INSERTION DEVICES

The on-axis photon flux density (photon flux per unit surface) reaching the first optical component in a beamline is largely dominated by the divergence of the source. As a result, one can expect a moderate gain in flux for high-beta beamlines (factor of 2) while low-beta beamlines will receive a much higher flux than at present (one order of magnitude). **Figure 2.06** compares the spectral photon flux density at 30 m from the source for a 4 m CPMU18 (gap 6 mm, K=1.68) for the present and new lattices. It shows the improvement of the purity of the undulator harmonics obtained by decreasing the emittance. In particular, in the present low-beta case, a significant part of the photon flux is spread between the harmonics due to the large horizontal divergence of the electron beam. For the present high-beta case, the high harmonics are also affected by both the horizontal divergence and the size of the electron beam.

Heat load is a crucial concern for the optical elements of an undulator beamline, the dominant aspect being the power density of the white beam. Indeed, for a typical beamline, the monochromatic beam extracted from the white beam corresponds to a very small fraction of the total incident power that must be eliminated at the first optical components.

For an undulator beam, the spatial distribution of the power density is primarily driven by the deflection parameter K of the undulator. For a planar vertical field undulator (the vast majority), the horizontal angular distribution of the power density has a typical width (RMS) of K/γ, with γ being the relativistic Lorentz factor. In the vertical direction, this width is $1/\gamma$. Therefore, the spatial distribution of the power density has a weak dependence upon the horizontal electron beam emittance. **Figure 2.07** shows the computed power density at 30 m from an undulator in the vertical mid-plane and as a function of the horizontal position with the present lattice (high beta and low beta) and the new lattice. The undulator is a 2 m-long CPMU18 with a K value of 2.0 (gap 5 mm). The power density reached with the new lattice is practically identical to that produced presently with the same undulator in a high-beta straight section. In the case of low-beta straight sections, the angular divergence of the electron beam (100 µrad) has a visible impact on the horizontal power density, but introduces a modest reduction of less than 20% compared to the high-beta case. Therefore, even in an extreme case, such as the undulator considered above, the power density from the white beam will not change significantly with the reduction of the emittance.

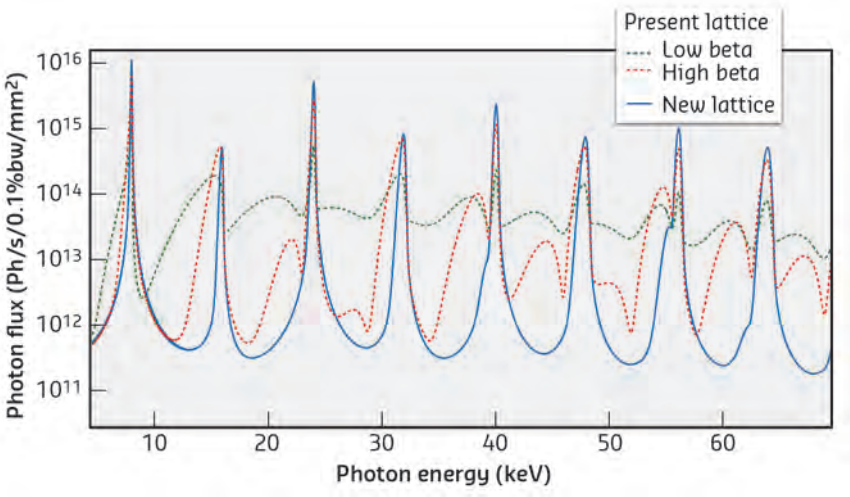

Figure 2.06: Spectral photon flux density (log scale) at 30 m from the source for a 4 m-long CPMU18 (gap 6 mm, K=1.68) for the present and new lattices.

Lattice	RMS photon beam size @ 30 m [mm]		Total power in aperture [W]
	H	V	
Low beta	3.1	0.15	180
High Beta	0.53	0.15	42
New lattice	**0.22**	**0.15**	**17**

Table 2.03: Photon beam size (10 keV) and associated total power in an aperture with the same size. The undulator is identical to that considered in **Table 2.02**.

In general, the incoming beam is collimated with a dedicated aperture in such a way that it is matched to the size of the monochromatic component that is to be used. In many cases the size considered is that of the central cone at a given photon energy and undulator harmonic. **Table 2.03** presents the horizontal and vertical RMS size of the monochromatic beam (10 keV) at 30 m from the undulator (4 m CPMU 18). The right-hand column shows the total power transmitted through a rectangular aperture with the same sizes defined in the two first columns at 200 mA. This table illustrates an important benefit of the reduction of the horizontal emittance: for the same integrated monochromatic photon flux, the total incoming power in the collimated beam is much smaller with the new lattice than presently. For this case, the overall power incident on the high-beta beamline optics will be 2.5 times lower than at present. In the low-beta beamlines, it will be about 10 times lower (provided that the optics has sufficient horizontal acceptance). Similar results can be derived at higher photon energy.

2.2.4.2. BENDING MAGNETS

The bending magnet-type sources need to evolve along a different path than in the past for the reasons discussed in section 2.2.1. The use of three-pole wigglers offers a good alternative to conventional bending magnet sources. One can highlight a number of interesting features of three-pole wigglers:

- Located in a dedicated space and acting as "mini insertion devices".
- Compact permanent magnet devices with less than 150 mm space occupancy.
- Their field can be adapted to suit the beamline's needs (flexibility in terms of field strength, magnet design, etc.).

Figure 2.08 presents the flux integrated over 2 mrad horizontally for the different bending magnet sources of the present and new lattices. The flux does not depend on the emittance of the electron beam and is computed for a 6 GeV electron beam with 0.2 A. One remarkable feature of the graph is that the flux from the three-pole wiggler source is much higher at all energies, and especially in the soft X-ray region, when compared to existing bending magnet sources. This can be explained by the contribution of the two compensating side poles of the magnetic structure.

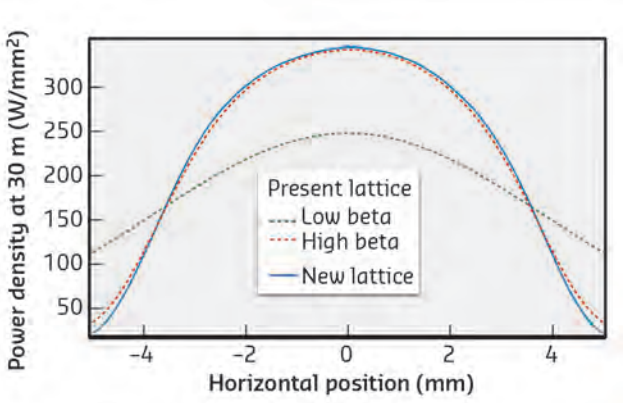

Figure 2.07: Horizontal profile of the power density (white beam) at 30 m from the source (2 m CPMU18) for the present and new lattices. The beam current is 200 mA in all cases.

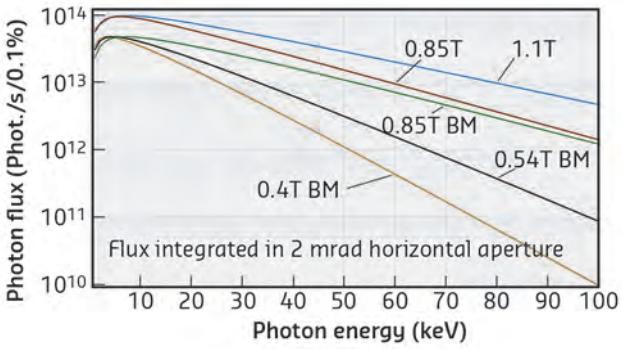

Figure 2.08: Spectral flux integrated over 2 mrad horizontally for bending magnet and three-pole wiggler sources.

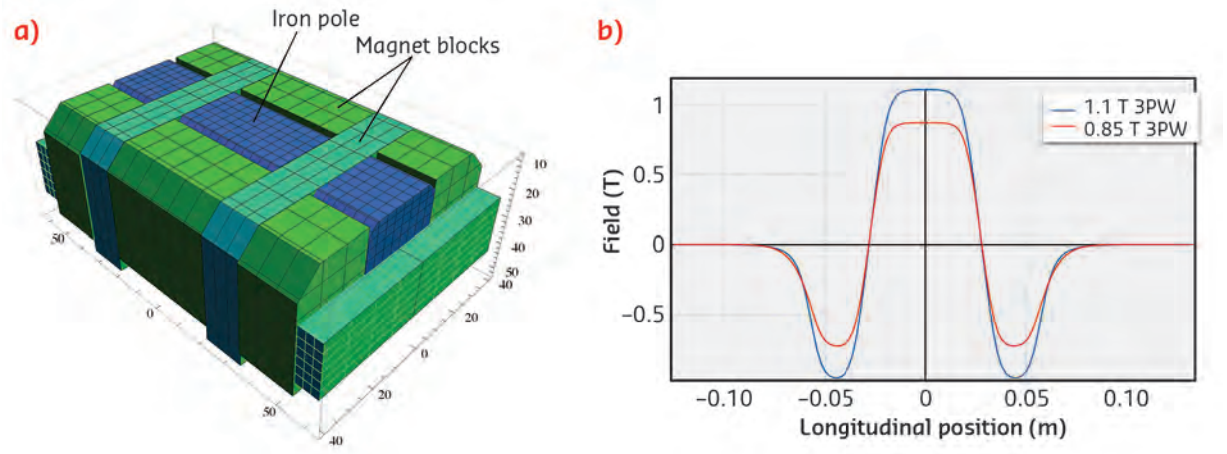

Figure 2.09: a) Magnetic structure of a typical three-pole wiggler (only one half represented for improved clarity) and b): Associated vertical field profile of the three-pole wiggler.

The magnetic structure and field profile of a typical three-pole wiggler is shown in **Figure 2.09**. Only one half of the full assembly is shown for improved clarity (**Figure 2.09** *a*). The field shape on the right includes a flat top portion of the field designed to produce a sufficiently wide radiated fan. Technically, the three-pole wigglers would be simple magnetic structures mounted on a simple removable C-shape structure. To avoid possible magnetic interaction with the neighbouring accelerator magnets, the gap will not be adjustable remotely from the outset. The heat load produced by three-pole wigglers will not be considerably higher than with the existing bending magnet sources. In the worst case (1.1 T 3PW), the beam power density will be about twice that produced by our present 0.85 T bending magnets. Typical values are around 2.5 W/mm^2 at 30 m from the source.

PART 2
ACCELERATOR AND SOURCE UPGRADE

2.3. STORAGE RING LATTICE DESIGN

Overview

The design of the storage ring lattice is responsible for the properties of the electron beam, a critical point in the performance of the new photon source. It is based on the following parameters and constraints:

- A target horizontal emittance around 150 pm·rad.
- The new storage ring must fit within the present tunnel and must keep the insertion device source points at the same location.
- The electron energy remains at 6 GeV, in order to preserve the spectral properties of the existing insertion devices.
- The new ring must be energy-efficient, by minimising the losses due to synchrotron radiation and the electrical consumption of the magnets.
- The present injector complex is to be re-used.

The first-order cell design was governed by the minimisation of the horizontal emittance. The non-linear beam optics were optimised with the goal of maximising the dynamic aperture of the ring, for on-energy and off-energy particles. This is necessary in order to use the present injector complex and to maximise beam lifetime. The tolerances on the field quality of magnets and on their alignment were then defined by a systematic study of their influence on the storage ring's performance. At the end of this section, we have included the results of a preliminary study of the limitations of high bunch current for the operation in few-bunch modes. The lattice design referred to during the whole document is the version labelled S28A.

2.3.1. CELL DESIGN

The equilibrium emittance of an electron storage ring can be minimised by increasing the number of bending magnets. While most of the present lattices are based on two or three bending magnets per cell, recent projects have focused on six or seven bending magnets per cell. The number of bending magnets is limited by the space needed to accommodate the quadrupoles that provide the necessary focusing between the dipoles. However, applying this scheme to large storage rings leads to very small bending angles, and so to a very small maximum dispersion function. As a consequence, the chromaticity correction needs very strong sextupoles. Apart from problems in magnet technology, this makes it

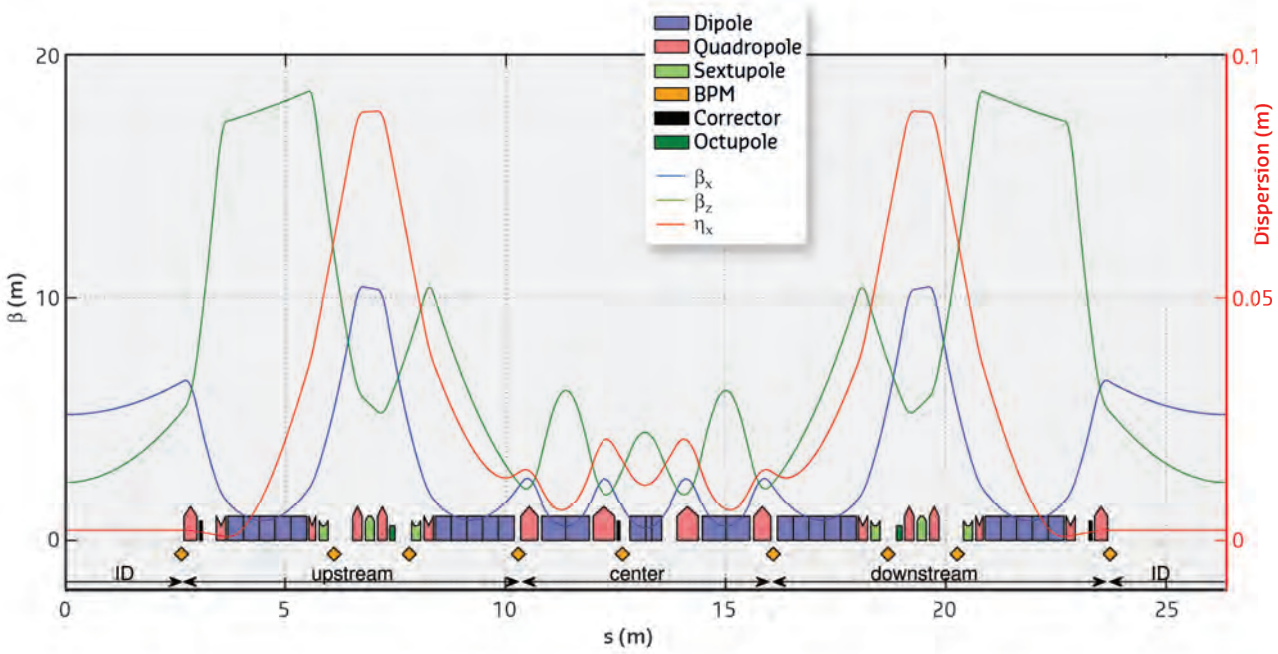

Figure 2.10: Optical functions of a standard cell.

difficult to achieve a large dynamic aperture, needed for efficient injection and acceptable beam lifetime. To mitigate these difficulties, the new lattice is based on a variation of the standard multi-bend achromat: instead of distributing the seven dipoles equally along the arc, more space is left between dipoles 1 and 2, and 6 and 7. In this space, the beta-functions and dispersion are allowed to grow to high values, which makes the sextupoles more efficient. This layout is referred to as the hybrid multi-bend achromat lattice. In the central part four high-gradient horizontally-focusing quadrupoles and three high-gradient bending magnets which also provide vertical focusing are placed alternately. At each end of the cell, two dipoles encompass the regions with large beta-functions and dispersion. Their longitudinally varying bending field helps to reduce the emittance and to increase the dispersion.

The lattice has been optimised to achieve the minimum emittance with the following constraints:

- The straight section must be long enough to accommodate the present low-gap, 5 m-long insertion device vacuum chamber, which leaves 5.56 m between magnets.
- The quadrupole strengths must be compatible with state-of-the-art magnet design and vacuum chamber requirements.

The lattice comprises 30 identical standard cells and two special cells that provide a special straight section for injection. The optical functions are the same in all standard straight sections, thus disposing of the alternating high- and low-beta straight sections found in the present lattice.

Figure 2.10 shows the optical functions of a standard cell. The main parameters are listed in Table 2.04; a more comprehensive list is presented in section 2.3.6.

The insertion device source points will be kept the same as in the present lattice, this implies a reduction of the ring circumference by 411 mm and

	Present lattice	New lattice
Lattice type	DBA	HMBA
Circumference [m]	844.390	843.979
Beam energy [GeV]	6.04	6
Natural emittance [pm·rad]	4000	147
Energy spread [%]	0.106	0.095
Damping times (H/V/L) [ms]	7/7/3.5	8.5/13/8.8
Energy loss per turn [MeV]	4.88	2.60
Tunes (H/V)	36.44/13.39	75.6/27.6
Natural chromaticity (H/V)	-130/-58	-100/-84
Momentum compaction factor	$1.78\ 10^{-4}$	$0.87\ 10^{-4}$

Table 2.04: Lattice parameters.

	Horizontal	Vertical
Cell centre	±8.3 mm	±5.5 mm
Cell upstream and downstream	±15 mm	±10 mm
insertion device straight	±15 mm	±2.0 mm

Table 2.05: Beam stay-clear.

a corresponding increase of the RF frequency by 171 kHz. The booster circumference will have to be reduced, as described in section 2.4.9.2.

The target vertical emittance is set to 5 pm·rad, corresponding to a coupling value of 3.5%, which should be easily obtainable. The equilibrium emittance is 147 pm·rad, but with a set of insertion devices giving an energy loss of 0.47 MeV, which is the present average value, and with 5 pm·rad coupled into the vertical plane, the emittance delivered in user service mode will be below 120 pm·rad.

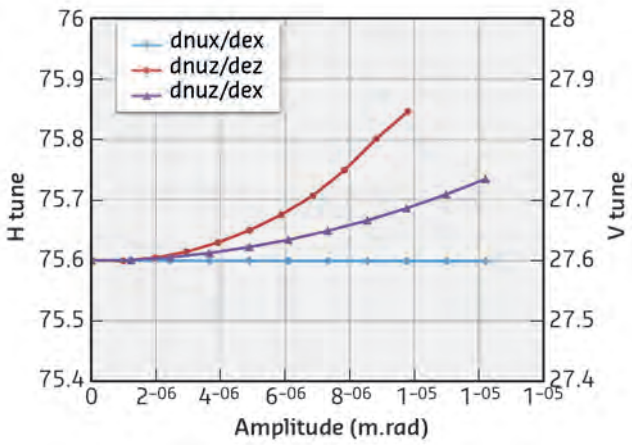

Figure 2.11: Amplitude-dependent tune shifts.

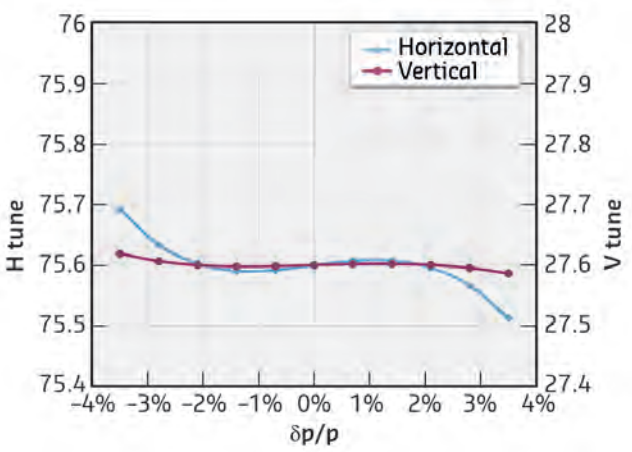

Figure 2.12: Momentum-dependent tune shifts.

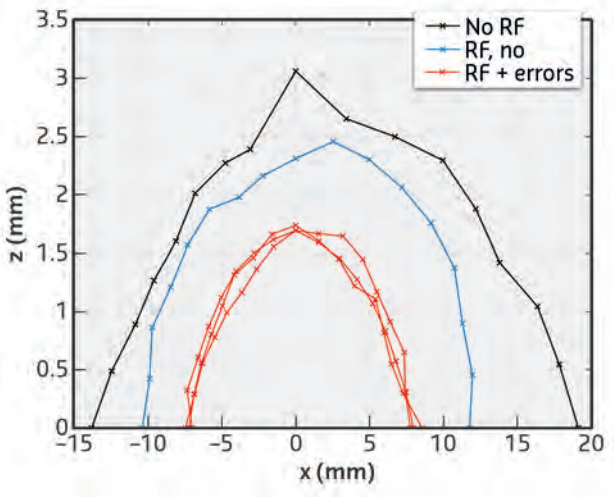

Figure 2.13: Transverse acceptance at injection, β_x = 18.4 m, 512 turns. The red curves show results for three random sets of errors as defined in **Table 2.06**.

The present lattice design already closely matches the engineering requirements. We expect that only minor adjustments will be needed once all of its components have been finalised.

Beam stay-clear

In order to optimise the magnets and the vacuum system engineering, we have defined three beam stay-clear regions (**Table 2.05**). In the central part, the beta functions are small and consequently the beam stay-clear could be reduced making the magnet design easier in order to reach the required high gradients. Similarly in the insertion device region, the vertical beta is compatible with the smallest possible vertical gap of the undulators.

Non-linear dynamics

The basic non-linear optimisation involves two sextupole families per cell (see **Figure 2.10**), located in the high-dispersion regions to correct the horizontal and vertical chromaticities. The phase advances between the sextupoles at both ends of the cell are set to 3π in the horizontal plane and π in the vertical, yielding a -Identity transform between the sextupoles. This property cancels most of the undesirable effects of the sextupoles. This setup provides a satisfying dynamic aperture without any need for additional sextupole families. However, since the horizontal and vertical sextupoles are interleaved, they still generate large amplitude-dependent tune shifts.

These are minimised by a combination of

- a slight deviation from the exact π phase advance and
- the introduction of two families of octupoles spanning two cells.

The linear tune shifts are then cancelled. In a final minimisation of the residual non-linear tune shifts we split the two sextupole families by using different strengths in even and odd cells. The tune shifts with amplitude and momentum are shown **in Figures 2.11** and **Figure 2.12** The resulting dynamic aperture is shown in **Figure 2.13**.

It should be noted that there is a significant path lengthening for large transverse oscillations. Particles thrown on-momentum and phase with large transverse amplitudes will therefore experience a noticeable longitudinal oscillation and this leads to a significant reduction of dynamic aperture when the longitudinal motion is also considered (see **Figure 2.13**).

2.3.1.1. CORRECTION SCHEME

The correction scheme is based on a set of 9 beam position monitors (BPM) and 5 combined function correctors per cell. The 6 sextupoles of each cell are equipped with correction coils and can provide horizontal and vertical steering and skew quadrupole correction. However, only two of these sextupole-correctors will be used (the ones at high horizontal betas); the others will be available and could be powered if needed. Three other dedicated magnets located inside the doublet at each end of the straight section and upstream of the centre bending magnet, respectively, will provide similar horizontal, vertical, skew-quad and sextupole corrections. The correction sequence consists of a closed orbit correction, a correction of β-modulation using the resonance driving terms (RDT) minimisation together with the correction of horizontal dispersion, and a correction of betatron coupling using resonance driving terms again combined with the minimisation of spurious vertical dispersion. Simulations are in progress to determine the minimal set of correctors for each step and to refine the location of beam position monitors.

2.3.2. TOLERANCES

Tolerances on errors are relative to:

- Magnet alignment errors, resulting from the combination of the magnet alignment on its girder and the girder alignment with respect to the theoretical position.
- Field integral errors, resulting from magnet manufacturing errors.
- Field quality errors, systematic, resulting from the magnet design, or random, due to the magnet assembly.

These errors have been studied systematically to define the associated tolerances, taking into account the following figures of merit:

2.3.2.1. ALIGNMENT AND FIELD INTEGRAL ERRORS

To determine the values of alignment and field integral errors, a correction sequence is applied, iterating through a closed orbit correction, a correction of coupling and dispersion, and a correction of the beta-modulation. The resulting model is evaluated in terms of residual closed orbit, corrector strengths, residual beta-modulation, on- and off-momentum dynamic aperture and emittances. Tolerances on each error are deduced by allowing a maximum 4 pm·rad variation on emittances and a maximum reduction of 18% of other parameters such as on- and off-momentum dynamic apertures.

The off-momentum dynamic aperture is the most affected parameter. Table 2.06 shows the resulting tolerances.

2.3.2.2. MAGNETIC FIELD MULTIPOLE TOLERANCES

Multipoles are characterised by their harmonic coefficient according to the field expansion, as described in section 2.4.1, with ρ_0 the normalisation radius depending on the magnet family. The normalisation radius defines the good field region. It is smaller for the magnets in the centre part as for the beam stay-clear.

The effect of magnetic field multipoles is studied by generating sets of multipoles that result in a fixed ΔB/B for dipoles, ΔG/G for quadrupoles and ΔH/H for sextupoles at the normalisation radius. Systematic errors arise from the magnet design, and only allowed multipoles are taken into account. Random harmonic components are mostly generated by a wrong positioning of the poles during the assembly of the different magnet parts, and all multipoles

Error	Tolerance
Quadrupole Δx	50 µm
Quadrupole Δz	50 µm
Quadrupole Δφ	350 µrad
Sextupole Δx	50 µm
Sextupole Δz	75 µm
Dipole Δx	50 µm
Dipole Δz	50 µm
Dipole Δφ	300 µrad
BPM Δx	50 µm
BPM Δz	50 µm
Girder Δx	50 µm
Girder Δz	50 µm
Girder Δφ	200 µrad
Dipole ΔBl/Bl	10^{-3}
Quadrupole ΔGl/Gl	$0.5\ 10^{-3}$
Sextupole ΔHl/Hl	$3.5\ 10^{-3}$

Table 2.06: Alignment and field integral tolerances.

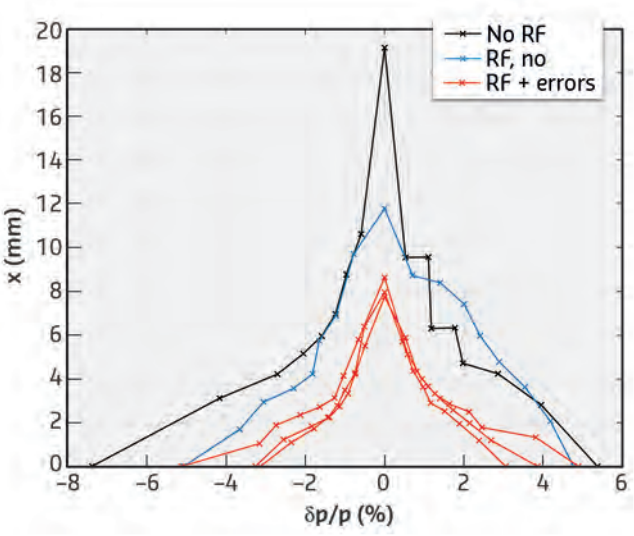

are considered. The tolerances are set to allow a maximum reduction of dynamic aperture by less than 0.5 mm and a maximum tune shift at the limit of the dynamic aperture of less than 0.1. Table 2.07 summarises the tolerances for multipoles together with the values reached for the preliminary magnet design.

The transverse acceptance evaluated at the injection point for the ideal machine and with three random sets of errors as defined in Table 2.06 is shown in Figures 2.13 and 2.14.

Figure 2.14: Momentum acceptance at injection, β_x = 18.4 m, 512 turns. The red curves show results for three random sets of errors as defined in Table 2.06.

	ρ_0 [mm]	Systematic	Magnet design	Random
High-gradient quadrupole [ΔG/G]	7	$5.0\ 10^{-4}$	$2.9\ 10^{-4}$	$5.0\ 10^{-4}$
Moderate-gradient quadrupole [ΔG/G]	13	$5.0\ 10^{-3}$	$<6\ 10^{-4}$	$1.0\ 10^{-3}$
Combined-function dipole [ΔB/B]	7	$5.0\ 10^{-4}$	$4\ 10^{-5}$	$1.0\ 10^{-4}$
Dipoles with long gradient [ΔB/B]	13	$1.0\ 10^{-3}$	N/A	$1.0\ 10^{-4}$
Sextupoles [ΔH/H]	**13**	**0.1**	**0.03**	**0.01**
Octupoles	**13**	**N/A**	**N/A**	**N/A**

Table 2.07: Tolerances of the magnet field quality.

2.3.3. COLLECTIVE EFFECTS

Several parameters will have an effect on the instabilities (transverse and longitudinal) due to collective effects:

- Reduced beam pipe apertures
- HOM damped cavities (beneficial)
- Reduced momentum compaction
- Reduced synchrotron frequency
- Reduced beta functions (beneficial)
- Bunch length (small change with respect to the present machine)

The maximum intensity in few-bunch modes will be limited by coherent instabilities as in the present storage ring.

2.3.3.1. MULTIBUNCH INSTABILITIES

These instabilities arise when bunches couple together through the effect of the impedance of the vacuum chamber or through the effect of ion accumulation.

Longitudinal coupled bunch
This instability, which is observed for the present storage ring, is due to narrow-band impedances, being caused exclusively from the higher order modes of the existing five-cell RF cavities. Though the new storage ring will be more sensitive because of a smaller synchrotron tune and the much longer longitudinal damping time, these modes will be damped with the new cavities, so that this instability will not be a concern (see also section 2.4.6).

Transverse coupled bunch
With the exception of transverse resistive wall instabilities, no instability driven by a transverse higher order cavity mode or any other resonator has ever been observed at the ESRF. Therefore, we do not expect any new transverse narrow-band impedance. As for longitudinal instabilities, bunch-by-bunch feedback is effective.

Transverse resistive wall instability
The threshold for the transverse resistive wall instability is proportional to:

$$\frac{b_{eff}^3}{\beta_z \sqrt{\rho}\, \tau_z}$$

where b_{eff} is the effective radius of the vacuum chamber, ρ the resistivity of the vacuum chamber, β_z the envelope function and τ_z the vertical damping time. Compared to the present storage ring, the new design is better in terms of beta-function and worse in terms of radius and damping time. The overall result depends on the choice of material for the vacuum chamber, and while the current threshold is presently at a value of 20 mA, it would be of the order of 20 mA in the case of copper and 7 mA in the case of stainless steel for the new storage ring. This instability could be resolved by positive chromaticity and/or the existing efficient bunch-by-bunch feedback system.

Ion instability
The slow ion instability is due to the accumulation of ions in the potential well created by the circulating electron beam. Because of the smaller emittances, the critical mass above which ions may be trapped will be higher than at present, so this should not happen. The fast ion instability occurs when ions are trapped within a single bunch train. A bunch-by-bunch feedback system is again efficient for reducing this instability.

2.3.3.2. SINGLE BUNCH INSTABILITIES

Single bunch instabilities occur when a bunch is perturbed by its self-induced wake field. It is a concern for few-bunch operation modes where the bunch current is high and it is due to broadband impedances. Quantitative results depend on the impedance budget of the vacuum chamber, which cannot be estimated yet. Tendencies for the new storage ring may be estimated assuming a longitudinal impedance $Z(\omega)/\omega$ similar to the present one. Transversally, the critical parameter is the product $\beta Z_\perp$. The transverse impedance is linked to the longitudinal impedance by the approximate law:

$$Z_\perp(\omega) \approx \frac{2c}{b^2} \frac{Z_{//}(\omega)}{\omega}$$

where b is the radius of the vacuum chamber.

The beam stay-clear is such that the ratio β/b^2 is approximately preserved, so the net effect of the transverse impedance is also similar to the present one. This of course strongly depends on the design and material of the vacuum chamber. The design of each piece of vacuum chamber will try to minimise the beam coupling impedance.

Bunch lengthening
While the zero-current bunch length is smaller in the new storage ring, the lengthening with current is stronger, so that if we assume the same impedance as for the present storage ring, the bunch length would be smaller by 20% in 7/8 filling pattern, but longer by 15% and 20% in 16-bunch and 4-bunch respectively. A long bunch is beneficial in terms of the Touschek lifetime.

Microwave instability
When increasing the bunch current, the bunch length increases while the energy spread stays constant, as governed by the synchrotron radiation equilibrium, until the microwave instability threshold is reached. Above the threshold (currently at 4.5 mA), turbulent behaviour appears on the longitudinal motion and the energy spread increases. For the same impedance, the threshold decrease due to the storage ring parameters is moderate.

CSR instability
The CSR instability is a single-bunch instability very similar to the microwave instability but the self-induced wake is generated here by coherent synchrotron radiation (CSR). The theoretical single bunch thresholds based on the shielded-CSR model is 35 mA for the present storage ring (never observed) and 21 mA for the new storage ring.

Transverse mode coupling instability
The transverse mode coupling instability is relevant when working at zero chromaticity. The threshold is measured to be at 0.7 mA for the present storage ring. For the same impedance as the current one, the threshold will be lower for the new storage ring because of lower synchrotron tunes and longer damping time. It has been shown experimentally that this can be increased by a factor of up to 5 by transverse feedback, but the operation of few-bunch modes at high positive chromaticity will be required for the new storage ring as it is today.

Head-tail instability
The head-tail instability is reached when operating at higher chromaticity. The current threshold increases with chromaticity and the behaviour of the new storage ring is predicted to be similar to the present one.

Post head-tail instability:
The post head-tail instability is the instability presently limiting the bunch current when operating at high chromaticity. The chromaticity necessary to achieve the desired bunch current (10 mA) will be higher than at present. The new lattice can be operated with chromaticities up to 10.

2.3.4. LIFETIME

Mode	Intensity [mA]	Bunch intensity [mA]	Vertical emittance [pm·rad]	Lifetime [h]
Uniform	200	0.202	5	8.5
7/8+1	200	0.23	5	7.5
16-bunch	90	5.62	60	2.42
4-bunch	40	10	60	1.78

Table 2.08: Lifetime for different operation modes.

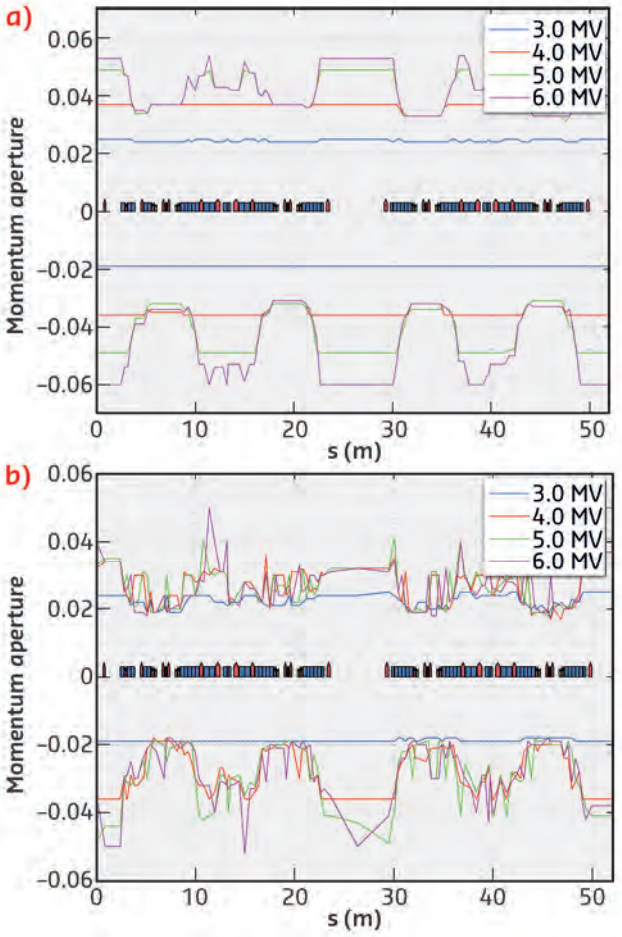

Figure 2.15: Momentum acceptance for a) a perfect machine and b) with all errors included.

Given the low emittances expected for the new storage ring, its lifetime will be dominated in all modes by the Touschek lifetime.

The lifetime is computed for a vertical emittance chosen between 5 and 60 pm·rad. The horizontal emittance includes the growth due to intra-beam scattering, the bunch lengthening is due to an inductive impedance of 0.7 Ω (present value) and the longitudinal motion is taken into account. The scattering rate and the momentum acceptance are computed at each point of the circumference. Figure 2.15 shows the reduction of momentum aperture due to errors and for various RF voltages.

The Touschek lifetime is then computed for the different filling patterns as a function of the RF voltage. Figure 2.16 shows the lifetime behaviour in multibunch as an example. Operation in few-bunch modes is foreseen under the same conditions as now, with a vertical emittance artificially increased to improve the Touschek lifetime. Table 2.08 summarises the values for different modes, with the optimum RF voltage. Top-up operation is mandatory in all cases. The vertical emittance in few-bunch modes can be tuned to any intermediate value between 5 and 60 pm·rad, at the cost of reduced lifetime. A harmonic RF cavity lengthening the bunch could also be envisaged (see RF section: 2.4.7.4).

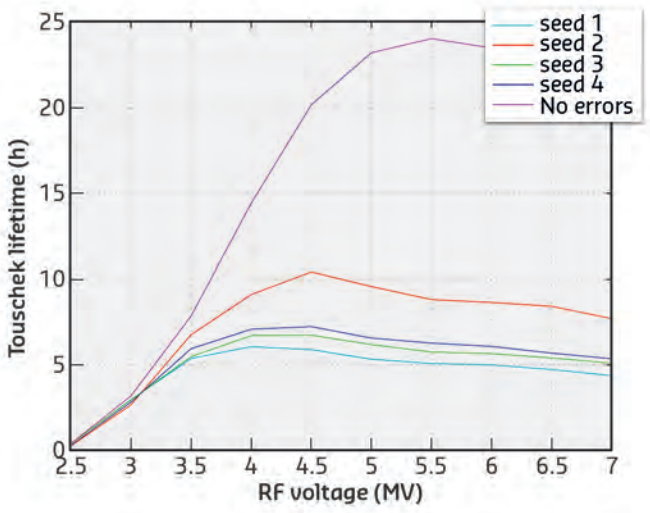

Figure 2.16: Lifetime as a function of RF voltage in multibunch operation. Seed 1 to 4: different sets of errors.

2.3.5. INJECTION SCHEME

As the horizontal beta-function in the standard straight section is only 5.2 m, a special injection section has to be designed. Symmetry breaking is limited by applying the following constraints: the phase advance in each plane is strictly identical to that of a standard cell, and the optical functions are kept identical in most of the cell including the high-beta regions where the sextupoles are located. The only residual modification of the optics is the difference of local chromaticity generated by the quadrupoles in the injection region. This can be corrected by a slightly modified tuning of the sextupoles around the injection section. On both sides of the injection straight section, space is available for 2 kickers, 430 mm long. The horizontal beta at injection reaches 18.4 m. As there is no sextupole within the injection kicker bump, there will be no perturbation of the circulating beam when powering the injection bump, ensuring a stable beam in top-up operation. Figure 2.17 shows the optics of the injection cell.

The injection efficiency has been simulated for two cases:

- Case A corresponds to the beam parameters delivered by the booster as now.
- Case B is obtained by reducing the booster emittance by a factor of 2, either from off-momentum operation or from an increase of the horizontal/vertical coupling. In addition the booster bunch length has been reduced by increasing the RF voltage and the use of a thinner septum blade has been assumed.

Table 2.09 summarises the parameters of both cases.

The injection efficiency was computed by tracking 500 electrons in a storage ring with all presently known errors and corrections, with the RF operating at 6 MV and no damping. The beta-function of the injected beam (**s = 0 in Figure 2.17**) was varied to look for the best match. Figure 2.18 shows the resulting injection efficiency.

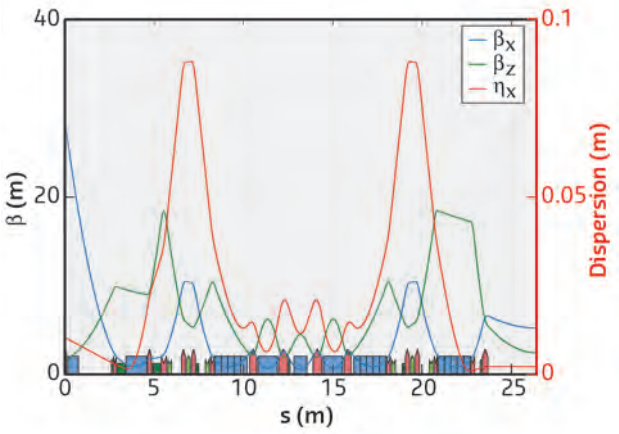

Figure 2.17: Optical functions in the injection cell.

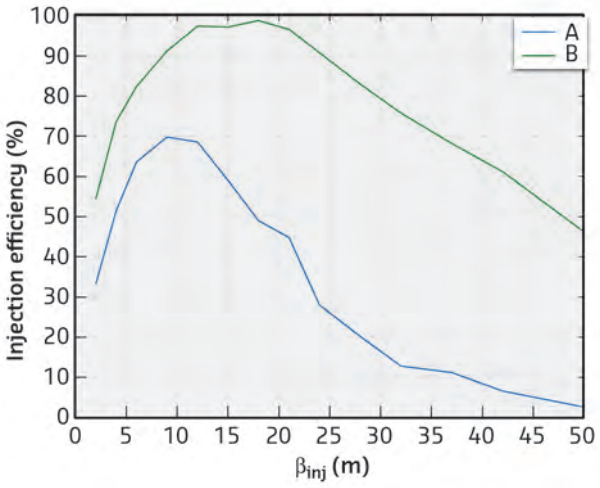

Figure 2.18: Injection efficiency as a function of injected beam β.

	Case A	Case B
Injected beam emittance [nm]	120	60
Booster RF voltage [mV]	7.3	11
Bunch length [mm]	23	17
Septum thickness [mm]	2	1.5
Beam distance from septum [mm]	1	0.5
Max. efficiency [%]	70	95

Table 2.09: Parameters of the injected beam.

2.3.6. PARAMETERS FOR THE PRESENT AND THE NEW LATTICES

The following tables present the parameters for the new lattice in comparison with the existing storage ring: Table 2.10 presents main lattice and RF parameters for the multibunch mode of operation; Table 2.11 presents insertion device and bending magnet source parameters; Table 2.12 presents the parameters specific to the 16 bunch and 4 bunch modes.

	Parameter	S28A	Present high beta	Present low beta	Symbol	Unit
Lattice	Energy	**6.00**	6.04	6.04	**E**	GeV
	Circumference	**843.98**	844.39	844.39	**C**	m
	Number of cells	**32**	32	32		
	Horizontal emittance	**147**	4000	4000		pm·rad
	Energy loss per turn	**2.6**	4.9	4.9	**U0**	MeV
	Energy loss from IDs	**0.5**	0.5	0.5	**U0**	MeV
	Horizontal tune	**75.6**	36.44	36.44	**νx**	
	Vertical tune	**27.6**	13.39	13.39	**νy**	
	Longitudinal tune	**0.00352**	0.00592	0.00592	**νs**	
	Horizontal damping time	**8.51**	7	7	**τx**	ms
	Vertical damping time	**13.02**	7	7	**τy**	ms
	Longitudinal damping time	**8.86**	3.5	3.5	**τs**	ms
	Horizontal natural chromaticity	**-100**	-130	-130	**ξx0**	
	Vertical natural chromaticity	**-84**	-58	-58	**ξy0**	
	Momentum compaction	**8.7E-05**	17.8 E-5	17.8 E-5		
	Energy spread	**0.0009**	0.0011	0.0011	**σδ**	
	Beam current (multibunch)	**200**	200	200	**I**	mA
	Emittance growth	**2.5**	0	0		%
	Vertical emittance	**5**	4	4		pm·rad
	Bunch length	**23**	20	20	**σz**	ps
	Lifetime	**7.5**	45	45	**t**	h
RF	RF voltage	**6**	9	9	**VRF**	MV
	RF energie acceptance (5% for tlife)	**4.9**	4	4	**ΔE/E**	%
	RF frequency	**352.371**	352.200	352.200	**fRF**	MHz
	Harmonic number	**992**	992	992		
	Synchrotron frequency	**1.25**	2.10	2.10	**fs**	kHz
	Number of 5-cell cavities	**0**	6	6		
	Number of mono-cell cavities	**14**	0	0		
	Total RF power (incl. 10% transm. loss)	**0.98**	1.5	1.5		MW
	RF power/cavity	**70**	266	266		kW
	Copper loss per cavity	**19.2**	47	47		kW
	Cavity coupling	**3.2**	4.4	4.4	**β**	

Table 2.10: Lattice and RF parameters for lattice S28A compared to the existing lattice.

	Parameter	S28A	Present high beta	Present low beta	Symbol	Unit
ID source						
	Horizontal beta at ID centre	**5.2**	37.6	0.4	**βx**	m
	Horizontal dispersion at ID centre	**2.0**	134	31	**Dx**	mm
	Vertical beta at ID centre	**2.4**	3.0	3.0	**βy**	m
	Horizontal beam size at ID centre	**27.2**	387.8	37.4	**σx**	μm
	Vertical beam size at ID centre	**3.4**	3.5	3.5	**σy**	μm
	Horizontal beam div. at ID centre	**5.2**	10.3	106.9	**σx'**	μrad
	Vertical beam div. at ID centre	**1.4**	1.2	1.2	**σy'**	μrad
	Relative source point transverse disp.	**0**				mm
	Relative source point longitudinal disp.	**0**				m
BM source						
Hard	Magnetic field	**0.47 to 1.1**	0.86	0.86	**Bz**	T
	Horizontal beta at BM	**1.40**	1.06	1.61	**βx**	m
	Horizontal dispersion	**17**	51	75	**Dx**	mm
	Vertical beta at BM	**2.8**	42.0	32.2	**βy**	m
	Horizontal beam size at BM	**21.3**	77.9	112.1	**σx**	μm
	Vertical beam size at BM	**3.7**	12.9	11.3	**σy**	μm
	Horizontal beam div. at BM	**24.2**	110.9	98.5	**σx'**	μrad
	Vertical beam div. at BM	**3.0**	0.5	0.4	**σy'**	μrad
	Source point transverse disp.	**-25.1**				mm
	Source point longitudinal disp.	**-2.9**				m
Soft	Magnetic field	**0.43**	0.4	0.4	**Bz**	T
	Horizontal beta at BM	**0.6**	1.3	2.1	**βx**	m
	Horizontal dispersion	**11**	62	89	**Dx**	mm
	Vertical beta at BM	**4.3**	41.7	32.1	**βy**	m
	Horizontal beam size at BM	**14.4**	98.3	131.7	**σx**	μm
	Vertical beam size at BM	**4.6**	12.8	11.3	**σy**	μm
	Horizontal beam div. at BM	**17.8**	115.5	103.1	**σx'**	μrad
	Vertical beam div. at BM	**1.5**	0.5	0.4	**σy'**	μrad
	Source point transverse disp.	**-6.4**	0			mm
	Source point longitudinal disp.	**-3.3**				m

Table 2.11: Insertion device and bending magnet source parameters for lattice S28A compared to the existing lattice.

	Parameter	S28A	Present high beta	Present low beta	Symbol	Unit
16 Bunch	Beam current	**90**	90	90	**I**	mA
	Emittance growth	**15**	0	0		%
	Vertical emittance	**60**	4	4		pm·rad
	Bunch length	**64**	48	48	**σz**	ps
	Lifetime	**2.42**	16	16	**t**	h
	Energy spread	**0.0012**	0.0012	0.0012	**σδ**	
4 Bunch	Beam current	**40**	40	40	**I**	mA
	Emittance growth	**20**	0	0		%
	Vertical emittance	**60**	4	4		pm·rad
	Bunch length	**77**	55	55	**σz**	ps
	Lifetime	**1.78**	9	9	**t**	h
	Energy spread	**0.0015**	0.0016	0.0016	**σδ**	

Table 2.12: 16 bunch and 4 bunch parameters for S28A compared to the existing lattice.

2.3.7. MAGNET SPECIFICATION LIST FOR THE S28A LATTICE

The following list summarises the longitudinal dimensions and fields/gradients for all the new lattice magnets (**Figure 2.19**).

For all the quadrupoles, sextupoles, combined dipole-quadrupoles and electromagnetic dipoles the coils take about 31 mm on each side of the iron poles.

QF1	**Quadrupole**
Iron length:	295 mm
Estimated magnetic length:	13 mm
Nominal integrated gradient:	16.0 T
Gradient (assuming 313 mm magnetic length):	51.1 T/m

QD3I (x2 magnets in the injection section) same as QF1 but operating at 53.9 T/m.

QD2, QF4, QD5	**Quadrupole**
Iron length:	212 mm
Estimated magnetic length:	230 mm
Nominal integrated gradients:	11.0 T (lowest) 12.0 T (highest)
Highest gradient (assuming 230 mm magnetic length):	52.2 T/m

QF1I, QF2I (x4 magnets in the injection section) same length (212 mm) and operating at integrated gradients between 9.0 T and 11.5 T.

QD3	**Quadrupole**
Iron length:	162 mm
Estimated magnetic length:	180 mm
Nominal integrated gradients:	8.9 T
Gradient (assuming 180 mm magnetic length):	49.3 T/m

QD2I (quadrupoles in the injection section) same as QD3 but operating at 31.5 T/m.

QF6	**Quadrupole**
Iron length:	388 mm
Estimated magnetic length:	401 mm
Nominal integrated gradient:	34.3 T
Gradient (assuming 401 mm magnetic length):	85.5 T/m

QF8	**Quadrupole**
Iron length:	484 mm
Estimated magnetic length:	497 mm
Nominal integrated gradient:	42.47 T
Gradient (assuming 497 mm magnetic length):	85.5 T/m

The moderate gradient quads must work comfortably from 28 T/m to 57 T/m. The power supply and the cooling will be able to guarantee operations at +20% more current than is necessary for 52 T/m.

The high-gradient quads must work comfortably from 81 T/m to 90 T/m. The power supply and the cooling will be able to guarantee operations at +20% more current than is necessary for 85.5 T/m.

DQ1	**Combined Dipole-Quadrupole**
Iron length:	1078 mm
Estimated magnetic length:	1094 mm
Nominal integrated gradient:	37.1 T
Gradient (assuming 1094 mm magnetic length):	33.9 T/m
Nominal integrated field:	0.584 Tm
Average field (assuming 1094 mm magnetic length):	0.538 T

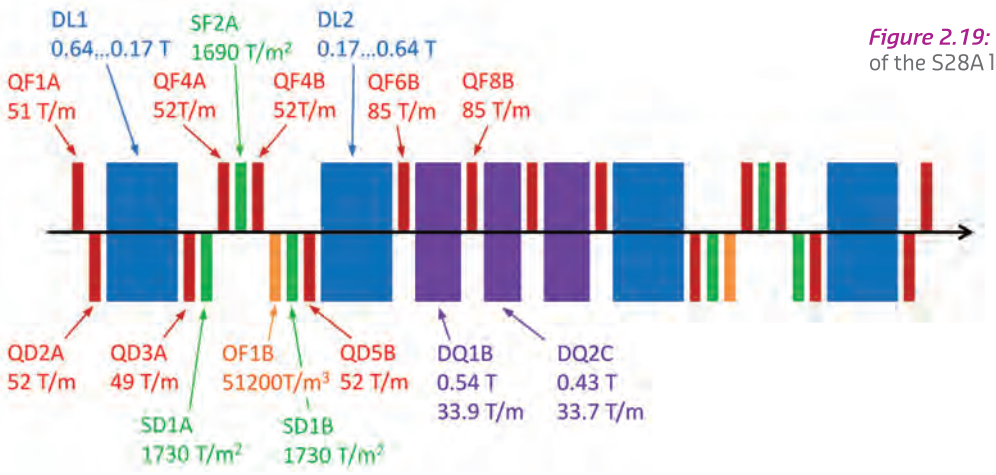

Figure 2.19: Positions and strengths of the S28A lattice magnets.

DQ2	Combined Dipole-Quadrupole
Iron length:	720 mm
Estimated magnetic length:	736 mm
Nominal integrated gradient:	24.8 T

Gradient (assuming 1094 mm magnetic length: 33.7 T/m
Nominal integrated field: 0.314 Tm

Average field (assuming 736 mm magnetic length): 0.427 T

DQ1 and DQ2 have the same pole profile. The difference in the vertical, *i.e.* dipole field (B_y) is provided by offsetting it horizontally by roughly -3.3 mm (towards the ring centre).

The optimisation of the good field region is compromised between DQ1 and DQ2 requirements.

Coils added to the outer poles will allow a tunability of the gradient of at least +/-2% while leaving B_y constant, regardless of the effect on the good field region. The induced multipoles (mostly sextupoles) due to the change in gradient are compensated by the main sextupoles and the "corrector" sextupoles SH1-6.

DQ1 and vacuum chamber design should allow the possibility of offsetting it horizontally (manually) by +/-1 mm.

DQ2 and vacuum chamber design should allow the possibility of offsetting it horizontally (manually) by +4 mm (outward) and -1 mm.

DQ2 and DQ1 should work comfortably in the range +/-5% of the design value, assuming that both gradient and B_y vary together. The power supply and the cooling should be able to guarantee operation at +20% more current than the design current.

DL1A_1-2-3-4-5, DL1E_1-2-3-4-5
Longitudinal Gradient Dipoles (5 slides)

Iron length:	0.3576 m
Deflection angles:	3.1 – 4.2 – 5.35 – 7.05 – 12.0123852 mrad

DL2B_1-2-3-4-5, DL2D_1-2-3-4-5
Longitudinal Gradient Dipoles (5 slides)

Iron length:	0.3576 m
Deflection angles:	3.1 – 4.2 – 5.35 – 7.05 – 9.7123852 mrad

The dimensions are assumed valid for the permanent magnet (PM) solution. In this case, it is assumed that the steerers on both sides of the dipoles will provide about 1-2% adjustment capabilities.

For the electromagnet (EM) case, the length of each module has to be shortened to make provision for the additional space taken by the coils. Supposing that the coils take about 35 mm on each side, all the modules have to be shortened by 14 mm. The deflection angles for each module could be compromised (up to +/-5%) with the best coil arrangement.

The geometry of the dipoles (the relative angles between the modules) should be optimised considering the trajectories in the DL2s. This will cause a less than 1 mm deviation of the beam trajectory in DL1A_5/DL1E_5.

SD1-SF2-SD3-SF4	Sextupole
Iron length:	204 mm
Estimated magnetic length:	216 mm
Nominal integrated gradients:	346.0 T/m (lowest)-707.1 T/m (highest)
B" (assuming 216 mm magnetic length):	3274 T/m² (highest)

The sextupoles must work comfortably from 650 T/m² to 4300 T/m² (corresponding to a chromaticity of about +10 and an additional 20% margin for optics changes). The power supply and the cooling will be able to guarantee operations at +10% more current than that necessary for 4300 T/m².

OF1B/D, OF2B/D	Octupole
Iron length:	120 mm
Total magnet length:	150 mm (not exceeding)
Estimated magnetic length:	125 mm
Nominal integrated gradient (maximum):	6400 T/m²

The octupoles must work comfortably from 100 T/m² to 9300 T/m² (corresponding to a chromaticity of about +10 and an additional 20% margin for optics changes). The power supply and the cooling will be able to guarantee operations at +10% more current than the one necessary for 9300 T/m².

SH1 to SH6 Corrector: H-steerer, V-steerer, Skew Quadrupole, Sextupole

Magnet total length (coils included):	120 mm
Maximum horizontal deflection angle:	0.5 mrad
Maximum vertical deflection angle:	0.4 mrad
Maximum skew-quad integrated gradient:	0.2 T
Maximum sextupole integrated gradient:	35.0 T/m
B"(assuming 110 mm magnetic length):	318 T/m²

The power supplies and the cooling should be able to guarantee operations at +20% more current than that necessary for the maxima.

2.4. ENGINEERING DESIGN

Overview

The engineering design conforms to the lattice and photon source requirements. The design benefits as much as possible from standard technology and expertise gained at the ESRF and similar facilities. Innovative technology or solutions are used when it is the only way to match the requirements or when they simplify the design. The necessary prototyping is fully compatible with the project timescale and their validation process.

Together with the design of the new storage ring, we are also implementing three Phase I Upgrade Projects that are relevant to the new lattice upgrade:

- Injector upgrade
- RF upgrade
- Controls upgrade

These projects are mostly financed by the Phase I budget. They do need some adaptation to fulfil the new requirements.

The engineering is mainly focused on the design of:

- Magnets
- Vacuum chambers
- Girders and supports
- Power supplies
- Diagnostics
- Full integration of all the hardware

These activities started with the launching of the technical design study (TDS) phase by the ESRF Council in November 2012. Now, the design and prototyping are already well advanced and in line for the procurement phase to begin in 2015 (see section 2.5.1.1 master schedule 2012-2020).

The design of magnets, vacuum chambers and mechanical systems complies with the lattice specifications and assembly constraints. Upon integration of all components and in order to solve mechanical conflicts, improve the overall coherency and optimise the performance of all of the subsystems, several iterations had to be made (as shown in **Figure 2.20**).

The design presented in the following chapters is related to the S28A lattice, we foresee that only minor adjustments will still be needed upon completion of the TDR.

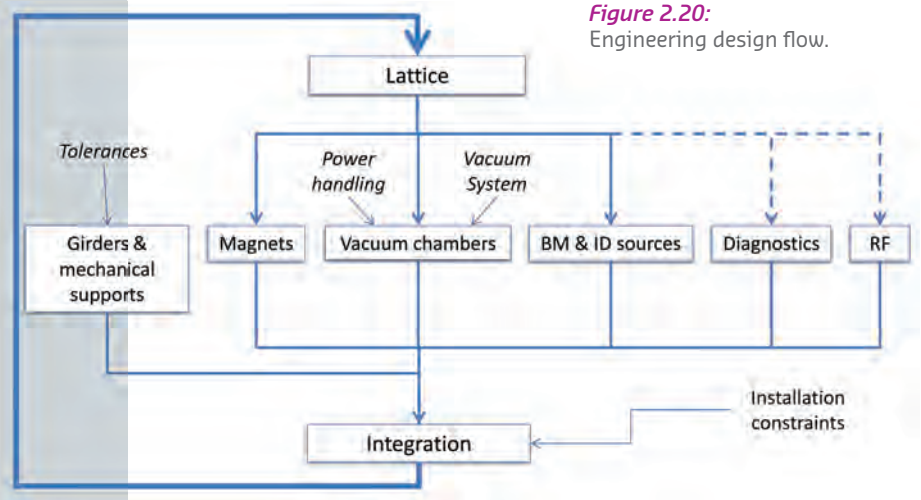

Figure 2.20:
Engineering design flow.

2.4.1. MAGNETS

The design of the magnets of the new storage ring is a challenge because the magnets must reach magnetic specifications that are significantly higher than those of the present third generation light sources. In addition, they must be compact and have low power consumption. More than 1000 magnets, including new concepts such as dipoles with longitudinal gradients, must be ready for installation in 2018, consequently permitting only a short time for R&D. The magnet designs are relatively conventional for quadrupoles and sextupoles, but the large gradients required has led to a magnet design with the bore radii reduced by a factor of three, when compared to the magnets of the present storage ring. This has

had an impact on the field quality, on the tolerances, and finally on the mechanical design. Dipoles with a longitudinal field gradient are new magnets, and various designs have been envisaged including permanent magnet dipoles. An unconventional single sided concept has been developed for the combined dipole quadrupoles in order to ease the vacuum chamber design. Moreover, an effort has been made to reduce the power consumption of all the magnets.

2.4.1.1. DEFINITION AND SPECIFICATIONS

The integrated magnetic field is described by the complex field

$$B = B_Y + i\,B_X$$

where B_Y is the vertical component of the integrated field and B_X is the radial component. The multipole components are defined as follows:

$$B = B_N \sum_{n=1}^{\infty} (b_n + i\,a_n) \left(\frac{z}{\rho_0}\right)^{n-1}$$

where $z = x + i\,y$, ρ_0 is the normalisation radius (see **section 2.3.2.2**), and $b_N = 1$ for the main multipole. The multipole strength is b_N/ρ_0^{N-1}, *i.e.* $1/2\ d^2B_z/dx^2$ for sextupoles and $1/6\ d^3B_z/dx^3$ for octupoles. For dipole magnets, the field errors are defined as

$$\Delta B/B = \sum_{n=2}^{\infty} (b_n + i\,a_n) \left(\frac{z}{\rho_0}\right)^{n-1}$$

and for quadrupoles, gradients errors are given by

$$\Delta G/G = \sum_{n=3}^{\infty} (n-1)(b_n + i\,a_n) \left(\frac{z}{\rho_0}\right)^{n-2}$$

Figure 2.19 summarises the strength and the location of the different magnets in one cell. The number of magnets of each type is given in the Table 2.13.

The minimum vertical gap between magnet poles has been set to 11 mm because of the requirements from the vacuum system and synchrotron radiation handling.

2.4.1.2. DESIGN METHOD

Magnet designs rely on 3D magnetic simulations. The Radia software (Chubar O. *et al.*, 1998), developed at the ESRF, was used for the computations. The magnets are described with fully parameterised 3D models. Initially, the main parameters are tuned manually to reach approximately the required field strength with reasonable magnet dimensions and power consumption. The required field quality is then obtained using a pole shape optimisation algorithm. The pole shape optimisation is treated as a non-linear, constrained, ill-posed problem.

2.4.1.3. DIPOLES WITH LONGITUDINAL GRADIENT

In the S28A lattice, there is only one design for the dipoles with longitudinal gradient (DL), DL1 and DL2. The field ranges from 0.17 T up to 0.67 T along the 1.79 m length of the magnets. As dipole magnets work at fixed magnetic field, a permanent magnet solution has been envisaged. A more conventional resistive design has also been studied. At the present time, we have yet to choose between PM and resistive DL.

Permanent magnet dipole

The permanent magnet (PM) design of the dipoles with longitudinal gradient magnets is based on five permanent magnet modules (**Figure 2.21 and 2.22**). All of the modules have the same magnetic

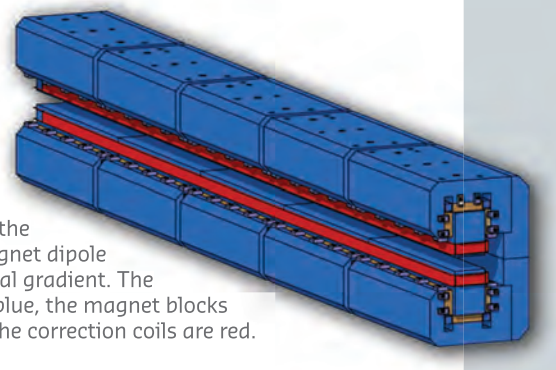

Figure 2.21: Design view of the permanent magnet dipole with longitudinal gradient. The iron yoke is in blue, the magnet blocks are ochre and the correction coils are red.

Table 2.13: Multipole strengths and number of magnets for each type (includes provision for chromaticity on sextupoles).

Magnet type	Abbreviation	Qty	Strength	Iron length
Dipoles with longitudinal gradient	DL	128	0.17–0.67 T	1788 mm
Dipole quadrupoles	DQ	96	0.43–0.54 T	1078 mm
			34 T/m	
Moderate gradient quadrupoles	Q	384	52 T/m	162–295 mm
High gradient quadrupoles	Q	128	85 T/m	388–484 mm
Sextupoles	S	192	900–2200 T/m^2	204 mm
Octupoles	O	64	51.2 10^3 T/m^3	120 mm
Correctors H(V)	C	96	0.08 T	120 mm

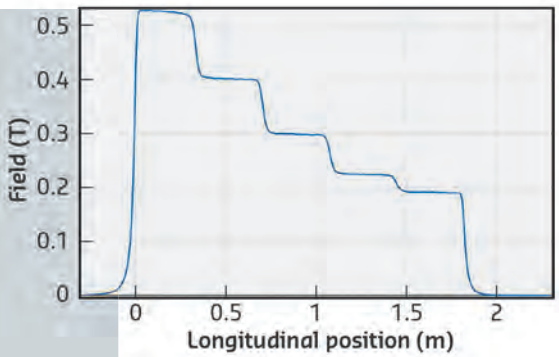

Figure 2.22: DL2 Dipole longitudinal field profile.

	DL1	DL2	
Dipole maximum field	0.67	0.54	T
Dipole minimum field	0.17	0.17	T
Integrated field	0.638	0.591	T/m
$\Delta B/B$ required @ 13 mm	10^{-3}	10^{-3}	
$\Delta B/B$ obtained @ 13 mm	10^{-4}	10^{-4}	
Iron length	1788	1788	mm
Vertical gap	26	26	mm
Pole width	60	60	mm
Permanent magnet material	Sm_2Co_{17}	Sm_2Co_{17}	
Pole material	pure iron	pure iron	
Iron mass	510	510	Kg
Permanent magnet mass	40	40	Kg
Total mass	550	550	Kg

Table 2.14: Main parameters of the permanent magnet dipole with longitudinal gradient for the S28A lattice.

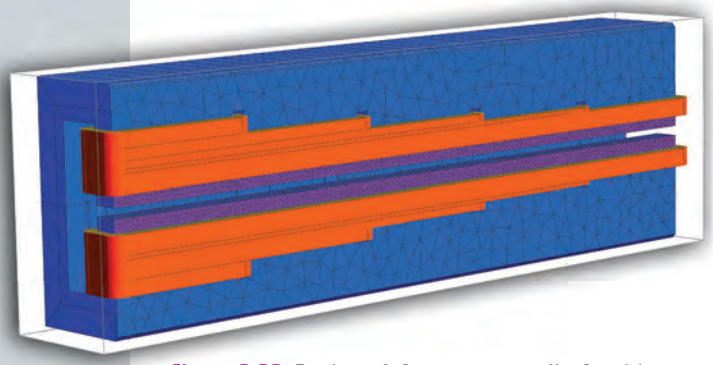

Figure 2.23: Design of electromagnet dipole with longitudinal gradient.

gap, but are magnetised by a different amount of magnet material. The yoke is made of bulk soft iron (Armco iron or XC10 steel). The best choice for the PM material is Sm_2Co_{17} and strontium ferrite due to its proven resistance to radiation damage and its temperature stability. As such a magnet is iron dominated, the tolerances on the magnet block quality (inhomogeneities, north-south asymmetries) are less strict than for undulator magnets, leading to cheaper prices. The main parameters of the permanent magnet dipole are given in **Table 2.14**.

The design's sensitivity to mechanical tolerances has been estimated by generating a large number of dipole models with errors on the pole shape. The required field error $\Delta B/B < 10^{-4}$ was obtained with ±20 µm tolerances for a 20 mm gap. The magnetic field will be stabilised against temperature fluctuation using dedicated nickel-iron shims.

The field will be tuned finely to the desired value using flux shunt schemes. An optional small coil could also be used.

Electromagnet dipole

There are various solutions for resistive dipoles with longitudinal gradient. Homogeneous gap designs are preferred, as they allow easier shimming of the field quality. The design under study is shown in **Figure 2.23**: it is the resistive counterpart of the permanent magnet design described above. The number of coils varies along the magnet, leading to a stair like field profile.

Permanet magnet dipole prototyping

A first prototype permanent magnet dipole module has been built (**Figure 2.24.a**). The following points have been checked on the prototype:

- Mechanical tolerances (machining and assembly)
- Tools for permanent magnet assembly
- Magnetic measurements and comparison with magnetic simulations
- Test of the shimming system

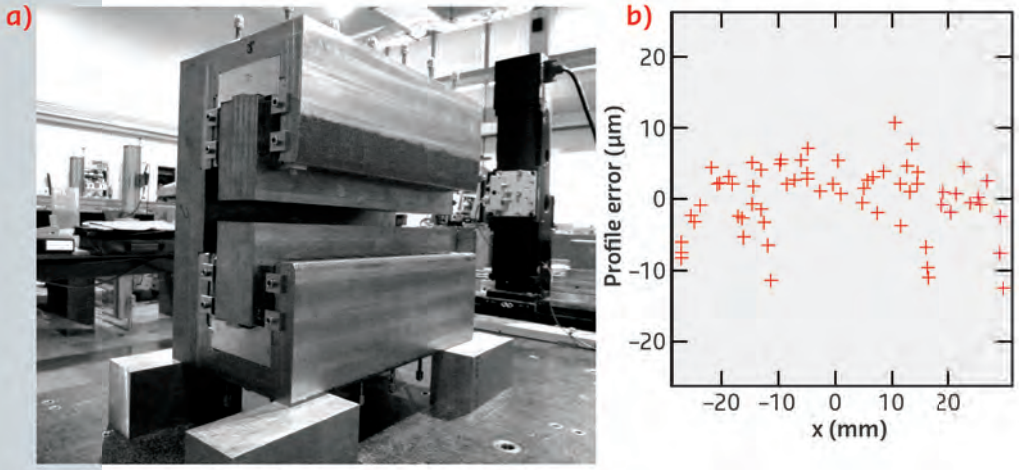

Figure 2.24: a) Prototype permanent magnet dipole installed on a moving stretched wire measurement bench. b) Mechanical errors measured on one pole in profile.

	QF1	QD2, QF4 QD5	QD3	QF6	QF8	
Quadrupole gradient	51.1	52.2	49.3	85.9	85.5	T/m
Magnetic length	0.313	0.230	0.180	0.399	0.497	m
b_6 requested	$5\ 10^{-4}$				$1\ 10^{-4}$	
b_{10} requested	$10\ 10^{-4}$				$0.5\ 10^{-4}$	
b_6 obtained	$0.03\ 10^{-4}$				$-0.44\ 10^{-4}$	
b_{10} obtained	$0.01\ 10^{-4}$				$0.40\ 10^{-4}$	
Bore radius	15.9	15.9	15.9	12.8	12.8	mm
Vertical gap	11.0	11.0	11.0	11.2	11.2	mm
Iron length	0.295	0.212	0.162	0.388	0.484	m
Magnet length	0.349	0.266	0.216	0.442	0.538	m
Magnet width	0.660	0.660	0.660	0.605	0.605	m
Magnet mass	570	400	300	690	870	kg
Current	87.5	87.5	87.5	90.4	89.0	A
Voltage	12.1	9.8	8.4	16.0	18.6	V
Power	1.06	0.86	0.73	1.45	1.65	kW
Number of turns	65	65	65	69	69	turns
Magnet resistance	140	110	95	175	210	mΩ
Magnet inductance	120	90	70	150	185	mH
Temperature rise	9.3	6.6	5.2	9.7	12.2	K

Table 2.15: Main parameters of the quadrupole magnets. Multipole errors are given at 13 mm for the QF1 magnet and at 7 mm for the QF8 magnet.

Electric discharge machining and spherical end milling has been tested for the machining of the pole profile. The machining errors measured on the pole profile are shown in Figure 2.24b.

2.4.1.4. QUADRUPOLES

The S28A lattice includes two main types of quadrupole magnets: moderate gradient quadrupoles, with a gradient of approximately 50 T/m, and high gradient quadrupoles with gradients of the order of 85 T/m. The main parameters of the quadrupoles are given in Table 2.15. The bore radii are 12.5 mm for the high gradient quadrupoles and 15.5 mm for the moderate gradient quadrupoles. The use of bulk yokes simplifies the mechanical design; it is expected that the mechanical assembly will be more accurate with bulk iron than with a laminated yoke. The yokes will be machined from pure iron blocks.

The moderate gradient quadrupoles should work with gradients ranging from 28 T/m up to 57 T/m in order to allow tuning of the lattice and flexibility of the optics. The magnetic design of one of the moderate gradient quadrupoles is shown in Figure 2.25a. The high gradient quadrupoles (Figure 2.25b) has been optimised for a gradient range limited from 81 T/m to 90 T/m.

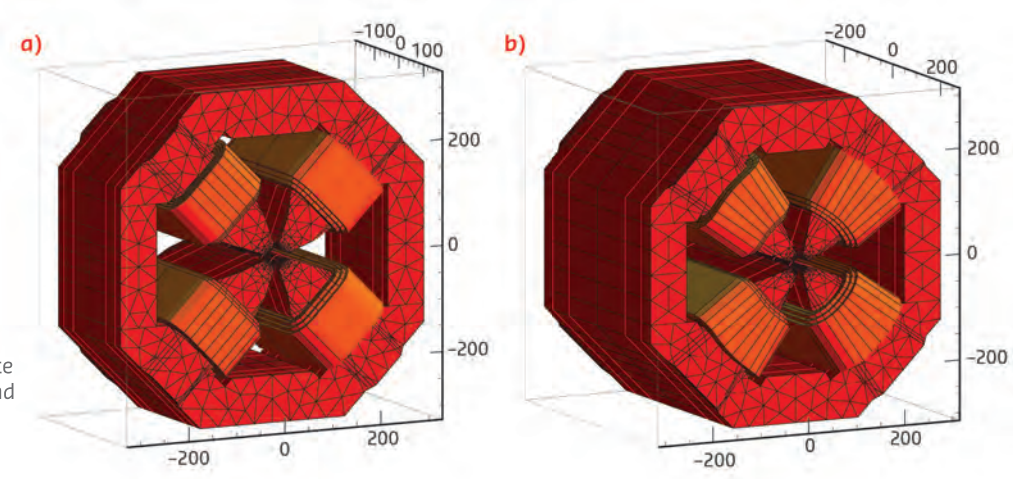

Figure 2.25: Design view of a) QF1 moderate gradient quadrupole and b) QF8 high gradient quadrupole.

The excitation curves of the QF1 (moderate gradient) and QF8 (high gradient) magnets are given in Figure 2.26. The higher gradient is mostly obtained by decreasing the bore radius. The QF1 magnet works below saturation. Its field quality is almost independent of the current throughout its whole excitation range. The QF8 magnet is closer to saturation: the field quality has been optimised at this working point.

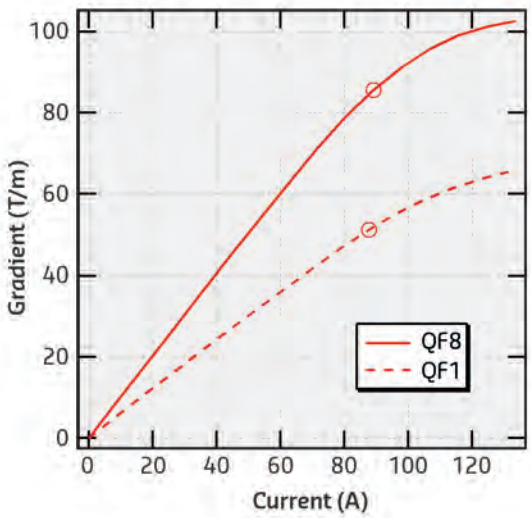

Figure 2.26: Excitation curves for the moderate gradient quadrupole (QF1) and the high gradient quadrupole (QF8). The circles indicate the nominal working point.

The sensitivity of the field quality to the mechanical tolerances is shown in Figure 2.27. The values for the sensitivity appear to be different for the two magnets, but this can be explained by the difference in the ratio of good field region to bore radius, which is 0.81 for the QF1 and 0.54 for the QF8. For both magnets, it appears that the field quality is dominated by pole displacements for lower order multipoles and by shape errors for higher order multipoles.

A high gradient quadrupole prototype has been ordered. Delivery of the prototype was planned for October 2014. This magnet will be used to check the mechanical tolerances, the mechanical assembly, and the accuracy of the simulations. The reproducibility of the magnetic field with increasing number of opening and closures of the assembly is an important point to be checked with magnetic measurements.

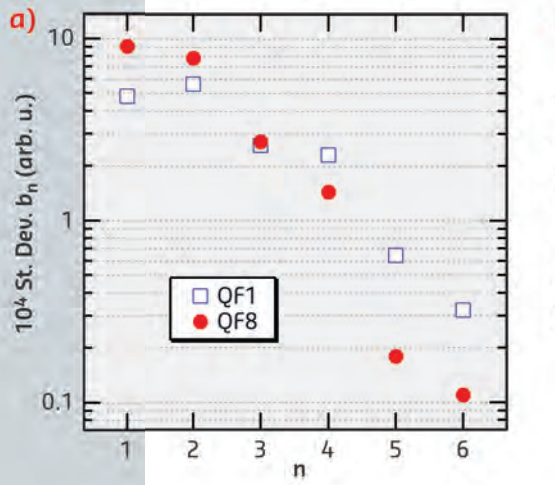

Figure 2.27: Quadrupole harmonics sensitivity to mechanical tolerances. a) Impact of pole displacements. The positions of the poles are normally distributed with a standard deviation σ = 20 µm. b) Impact of pole shape errors with standard deviation σ = 10 µm. The sensitivities have been computed with a set of 200 samples. For comparison, the systematic 12-pole component for QF1 is b_6 = 5 10^{-4} and for QF8 is b_6 = 10^{-4}.

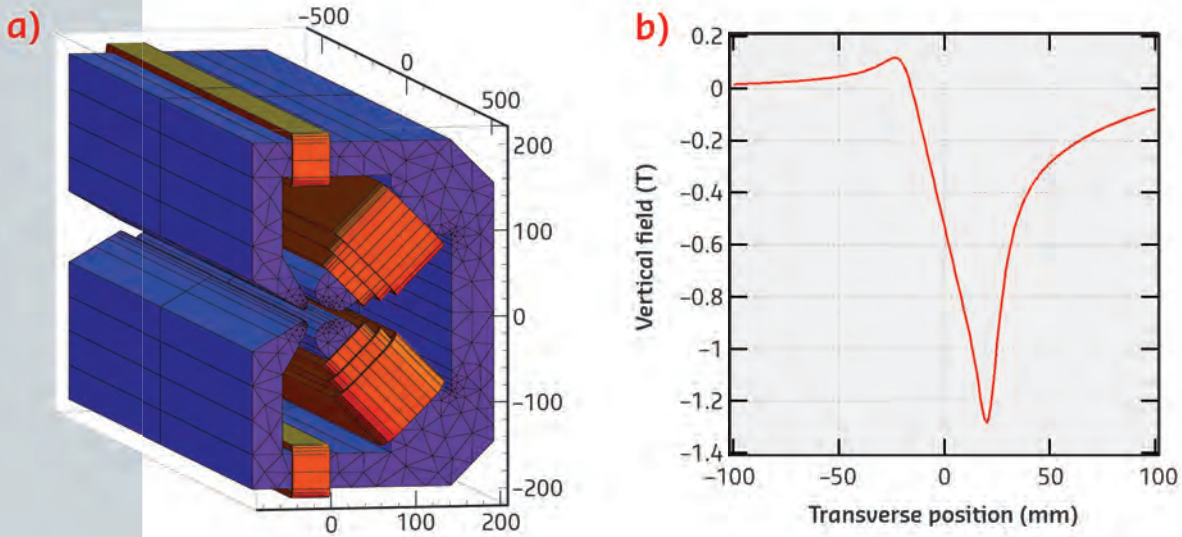

Figure 2.28: Single sided dipole quadrupole. a) Design view of the DQ1 magnet. b) Vertical field vs. transverse position.

2.4.1.5. COMBINED DIPOLE QUADRUPOLE MAGNETS

The combined dipole quadrupoles (DQ) have a large gradient that cannot be obtained with a tapered dipole design. Two designs have been studied: an offset quadrupole and a single-sided (septum like) magnet. The single-sided design (**Figure 2.28**) has been selected because it simplifies the design of the vacuum chamber. Moreover, it is more compact, lighter, and has a lower power consumption.

The specified field quality is $\Delta G/G < 10^{-2}$ at a 7 mm radius. This forgiving tolerance and the fact that the gradient is the same for the DQ1 and DQ2 magnet makes it possible to design only one magnet and to move it transversally to obtain the required dipole field.

The DQ excitation curve is shown in **Figure 2.29**. The working point of the DQ is fixed due to its dipole component. However, it is possible to tune the gradient by ±2% while keeping the field constant, by modifying the ratio of the currents in the main and auxiliary coils.

The DQs will be built with bulk pure iron yokes. The main parameters of these magnets are given in **Table 2.16**. The engineering design of a DQ1 prototype is underway.

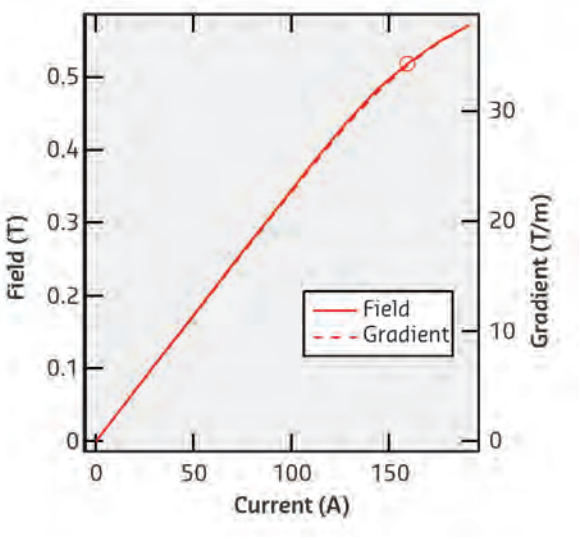

Figure 2.29: Excitation curve of the DQ1 magnet. The circle indicates the nominal working point.

Table 2.16: Main parameters of the combined dipole quadrupole magnets.

	DQ1	DQ2	
Dipole field	0.529	0.427	T
Magnetic length (field)	1.112	0.735	m
Quadrupole gradient	34.6	33.7	T/m
Magnetic length (gradient)	1.098	0.735	m
$\Delta G/G$ requested @ 7 mm	$< 10^{-2}$	$< 10^{-2}$	
$\Delta G/G$ obtained @ 7 mm	$3\ 10^{-3}$		
Bore radius	18	18	mm
Vertical gap (open side)	12.7	12.7	mm
Iron length	1.078	0.720	m
Magnet length	1.136	0.720	m
Magnet width	0.285	0.285	m
Magnet height	0.425	0.425	m
Magnet mass	695	465	Kg
Current	159	159	A
Voltage	9.9	6.8	V
Power	1.57	1.08	kW
Number of turns (main)	33	33	turns
Number of turns (aux.)	5	5	turns
Magnet resistance	30	21	mΩ
Temperature rise	9.5	6	K

2.4.1.6. SEXTUPOLE MAGNETS

The sextupoles have a nominal strength ranging from 900 T/m² up to 1600 T/m² (the maximum strength is 2200 T/m²). They will be used as dipole and skew quadrupole correctors: corrector coils have been added and the yoke is laminated in order to be compatible with the fast orbit feedback requirements. Figure 2.30 shows the magnetic design of a sextupole magnet. The main parameters of this magnet are given in Table 2.17. The excitation curve is given in Figure 2.31: the magnet is linear at its nominal strength.

Figure 2.32 shows the sensitivity of the sextupole field quality to pole displacement errors, for two ranges of errors. It appears that a mechanical tolerance of ±50 µm is acceptable for the sextupoles.

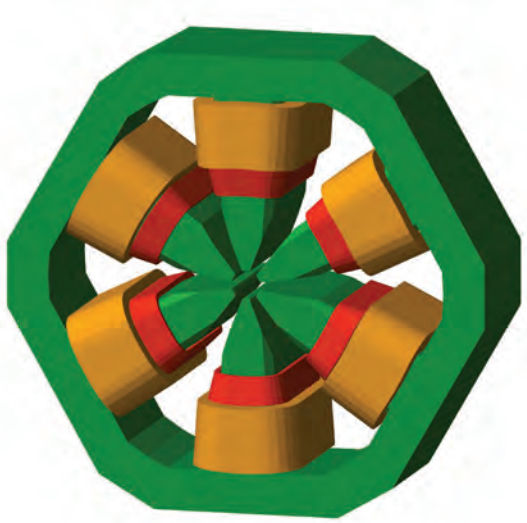

Figure 2.30: Design view of a sextupole magnet. The red coils are the corrector coils.

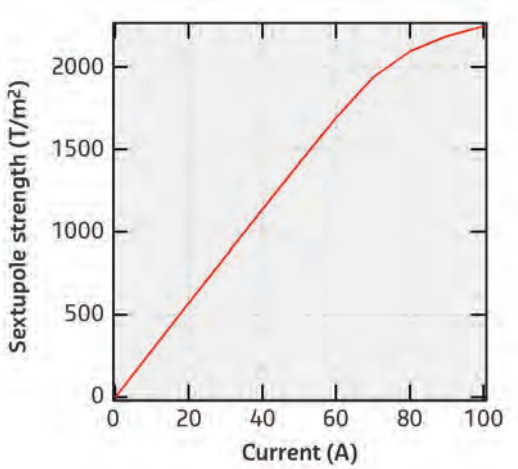

Figure 2.31: Sextupole excitation curve (the sextupole strength is half of the second derivative of the field).

	SD1 - SF2 - SD3 - SF4	
Sextupole strength	900 - 2200	T/m^2
Magnetic length	0.212	m
b_9 requested	$< 5\ 10^{-2}$	
b_{15} requested	$< 5\ 10^{-2}$	
b_9 obtained	$42\ 10^{-4}$	
b_{15} obtained	$-16\ 10^{-4}$	
Bore radius	19.2	mm
Vertical gap	11.2	mm
Iron length	204	mm
Magnet length	262	mm
Magnet width	660	mm
Magnet mass	450	kg
Current	31.5 - 90	A
Voltage	4.1 - 12.2	V
Power	0.13 - 1.10	kW
Number of turns	51	Turns
Resistance	136	mΩ
Temperature rise	1.1 - 9.4	K
Vertical corrector angle	0.5	m rad
Horizontal corrector angle	0.4	m rad
Integrated skew quad corrector	0.28	T

Table 2.17: Main parameters of the sextupole magnets. Multipole errors are given at 13 mm.

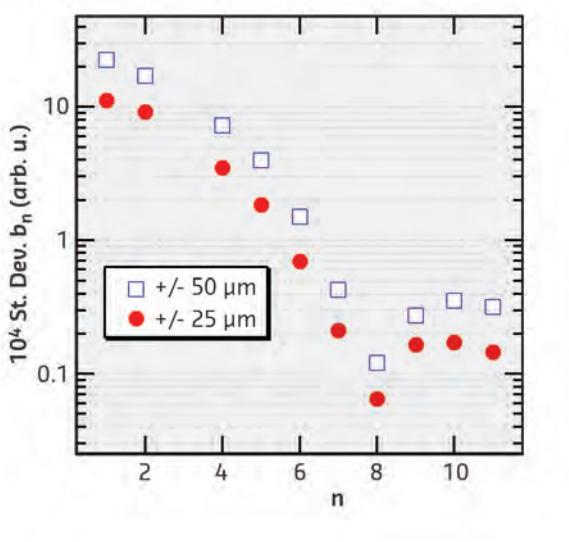

Figure 2.32: Sextupole harmonic sensitivity to pole displacement tolerances, obtained with 100 samples. Pole displacements are uniformly distributed in the range ±25 µm (standard deviation σ = 15 µm) and ±50 µm (standard deviation σ = 29 µm). For comparison, the systematic errors are b_9 = 41 10^{-4} and b_{15} = –16 10^{-4}.

2.4.1.7. OCTUPOLE MAGNETS

Figure 2.33 shows the design of the octupole magnet. The main parameters of this magnet are given in the Table 2.18. This design reaches the strength specifications with sufficient margin to run with positive chromaticity and for eventual modifications to the optics. The octupole excitation curve is shown in Figure 2.34.

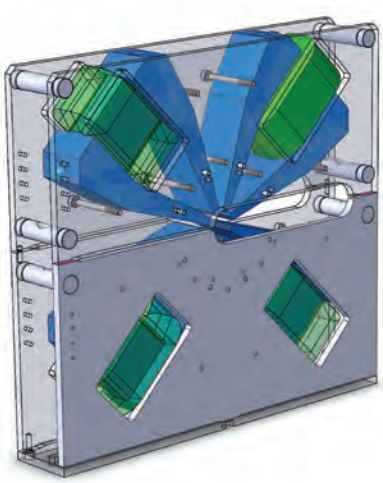

Figure 2.33: Design view of the octupole magnet prototype.

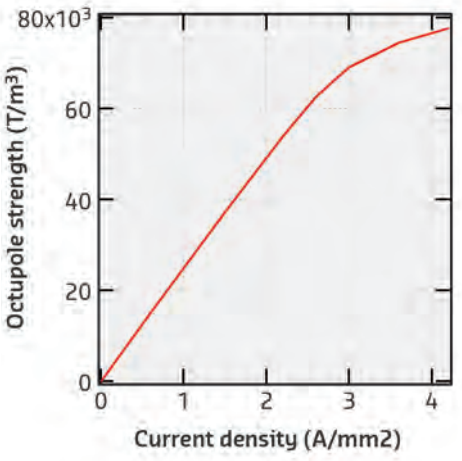

Figure 2.34: Excitation curve of the octupole magnet.

	OF1 – OF2	
Octupole strength	40 000 - 52 000	T/m^3
Maximum strength	78 000	T/m^3
Magnetic length	125	mm
b_{12} requested	5	%
b_{12} obtained	1.7	%
Bore radius	18.6	mm
Vertical gap	11	mm
Iron length	120	mm
Magnet length	144	mm
Magnet width	425	mm
Magnet mass	120	kg
Current	72-94	A
Voltage	2.4-3.2	V
Number of turns	30	turns
Resistance	38	mΩ

Table 2.18: Parameters and specifications of the octupole magnets for the S28A lattice.

2.4.1.8. CORRECTOR MAGNETS

Figure 2.35 shows a possible design for corrector magnets. This C-type structure is compatible with the stay-clear as imposed by the vacuum chamber. This magnet has an iron length of 100 mm and a gap of 25 mm. It can be simultaneously used as horizontal and vertical steerer, skew quadrupole corrector and sextupole corrector. Integrated fields of 11.9 T mm (vertical field) and 4.9 T mm (horizontal) are obtained with a 1 A/mm^2 current density. This magnet design is at an early stage: the parameters and shapes have yet to be optimised. The main parameters of the C-type steerer are given in the Table 2.19.

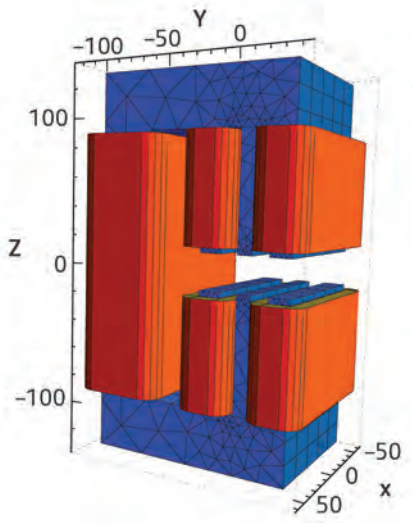

Figure 2.35: Magnetic design of a corrector magnet.

2.4.1.9. MAGNETIC MEASUREMENTS

A stretched wire measurement bench has been developed at the ESRF for the Upgrade Phase I (Le Bec G. *et al.*, 2012). It has been used for the measurements and the alignment of new magnet girders for the ID23 beamline (Figure 2.36). This bench is used routinely and has already been transferred to one magnet manufacturer. It is particularly suitable for small bore radius magnets, which is the case for the S28A magnets. This bench is multipurpose: it can be used for fiducialisation, strength measurements, and harmonic measurements. An update of this bench is underway, to add vibrating wire functionalities. The rigidity of the linear stage support structures has been improved, new wire supports have been designed, and the necessary electronics is under development for monitoring the wire's vibrations. Better sensitivity to magnet pitch and yaw angles is expected with the upgraded measurement bench.

	SH 1 – SH6	
Corrector length	120	mm
Integrated vertical field @ 1A/mm^2	11.9	T mm
Integrated horizontal field @ 1A/mm^2	4.9	T mm
Integrated skew quadrupole @ 1A/mm^2	0.43	T
Integrated sextupole @ 1A/mm^2	51	T/m

Table 2.19: C-type corrector parameters.

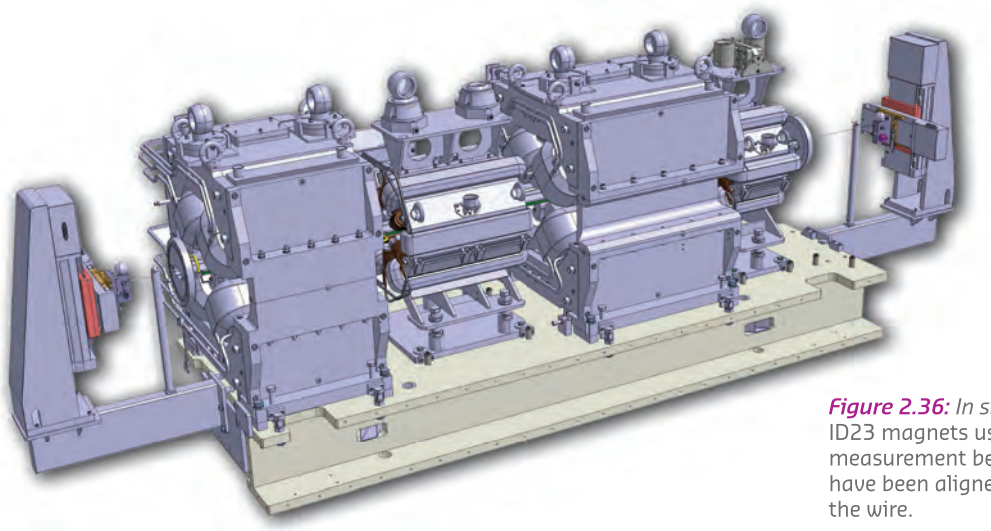

Figure 2.36: In situ measurements of ID23 magnets using the stretched wire measurement bench. All of the magnets have been aligned on an axis defined by the wire.

2.4.2. VACUUM

2.4.2.1. VACUUM SYSTEM

A conservative approach has been chosen for the vacuum system layout. Vacuum chambers with antechamber will provide space and access for discrete ultra-high vacuum (UHV) pumps and lumped absorbers. The main gas source is desorption of the photon absorbers receiving the synchrotron radiation produced by the seven bending magnets per cell.

The photodesorption yields will be very large during the start-up phase but are going to decrease gradually with beam conditioning. The vacuum systems need to be dimensioned to cope with high gas load to allow reasonably fast current ramping during the initial start-up.

Pumping concept

The existing storage ring pumps will be reused wherever possible. This will comprise triode sputtering ion pumps (SIP) as well as cartridge based non-evaporable getter (NEG) pumps. Even though limited to the pumping of getterable gases, NEG pumps provide some operational advantages as well as reducing the budget required for controllers. For in-vacuum undulators, it is also foreseen to completely reuse their vacuum pumps including the titanium sublimators.

Vacuum devices

Prepumping valves, residual gas analysers (RGA) and discrete vacuum pumps have to access the vacuum chamber from the limited space in between the magnets or otherwise they will be mounted on the antechambers. The schema in Figure 2.37 shows the different vacuum devices (UHV pumps and vacuum measurement) as a function of the anticipated arrangement of magnets and absorbers.

Pressure simulation

The specific vacuum conductance values of the various vacuum chambers is used to create a simulation model of the sectors and a conductance based vacuum simulation is used to calculate the pressure distribution. The validity of the assumption on which the model is based has been checked by applying it to the existing storage ring vacuum system and comparing the calculated pressures to gauge readings (Figure 2.38). For the pressure simulation

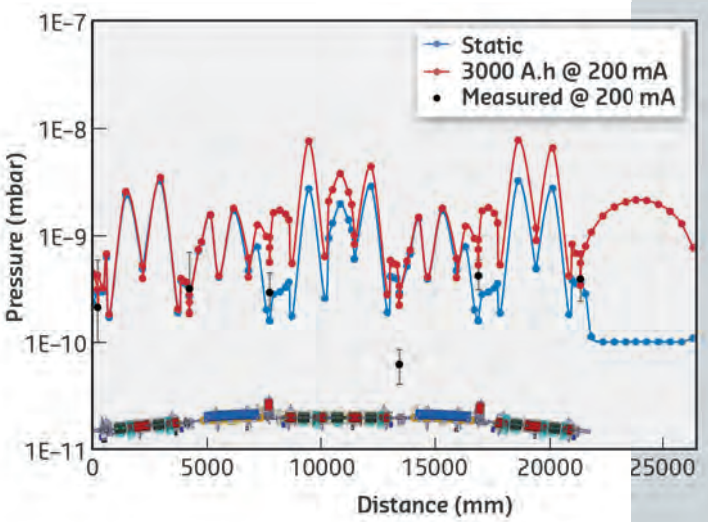

Figure 2.38: Existing lattice vacuum profile - Static and dynamic pressure distribution simulation of the existing storage ring compared to measured values.

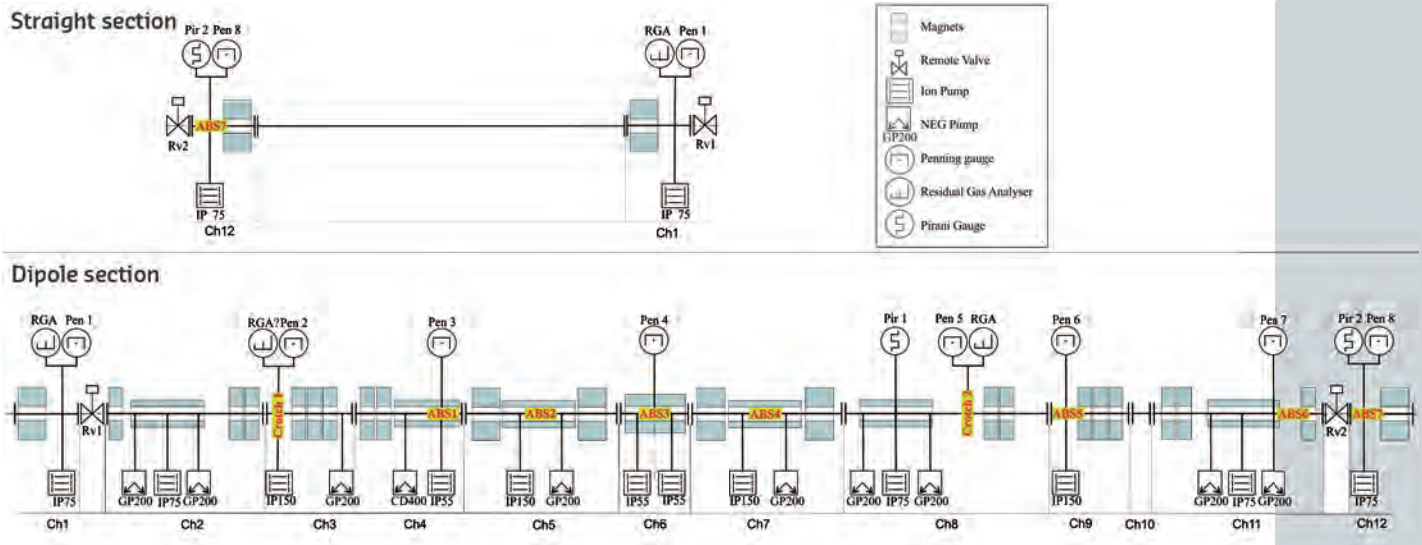

Figure 2.37: UHV device arrangement in a standard vacuum cell.

of the NEG-coated chambers, the photodesorption (PD) yield as measured at location D31 of the current storage ring has been used. The same method has been applied to the new layout and the results are shown in Figure 2.39.

The simulated pressures are on average a factor two higher for the new storage ring than those of the present machine at 200 mA for a given amount of conditioning. Nevertheless, this will ensure a vacuum lifetime of the order of 400 hours at 200 mA beam current, adequate for our needs since it will be more than one order of magnitude higher than the Touscheck lifetime.

Figure 2.39 shows the simulation of the vacuum profile relative to the latest vacuum system design.

The highest pressure expected in the insertion device chamber is about a factor of 3 higher than the present lattice. Nevertheless, the overall radiation due to gas-bremsstrahlung in the beamlines will be about a factor of 2 lower because the total length of the straight section (from dipole to dipole) is reduced by about a factor 2, and the average pressure across the straight section will be similar to the present one (Figure 2.38 and Figure 2.39).

Furthermore we will reuse the existing storage ring insertion device chambers which are presently very well conditioned.

We expect further improvement of the vacuum system performance as the design optimisation is finalised.

NEG coating

Non-evaporable getter coatings provide reduced thermal desorption and photo-desorption. They are a very elegant way to limit the gas loads in conductance-limited vacuum chambers. NEG coating has been in use for the last 15 years at the ESRF and has proved invaluable for the production and operation of small gap insertion device chambers.

The existing 5 m long undulator chambers that are already NEG coated and well conditioned will be reused in the new storage ring.

To further decrease the average vacuum pressure and the gas-bremsstrahlung in the straight section, CH1 and CH12 chambers will be NEG coated as well.

Other synchrotron light sources such as MAX-IV (MAX-IV, 2010) further exploit NEG technology by realising a fully coated storage ring. The new ESRF vacuum system will be more conventional, and although the extensive use of coating is not envisaged, the vacuum chambers will be designed taking into account the constraints required by the coating process so that the technology can be adopted at a later time if deemed necessary.

Baking system

The potential need to regenerate the vacuum system in the initial operation phase and the probability of venting requires the operation of a permanent *in situ* baking system. After the initial bake which is mainly to remove water vapour, the baking system is needed to avoid gas condensing on the chamber walls during activation of the vacuum pumps. After a programmed intervention or a vacuum incident the baking system allows the vacuum system to be

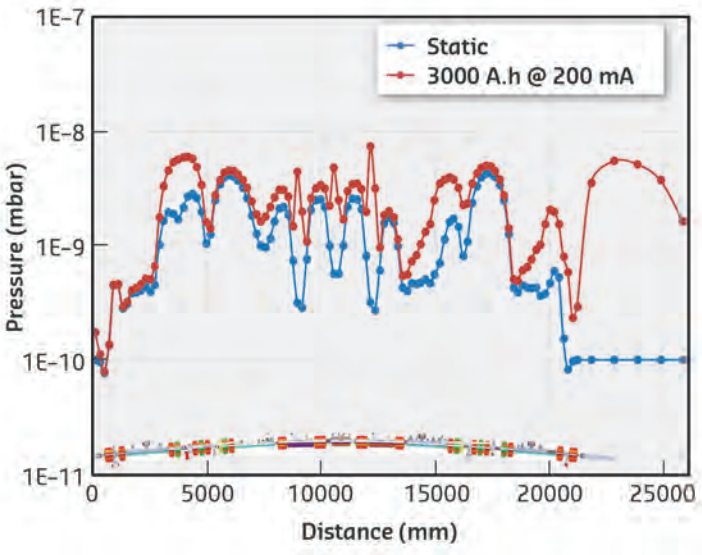

Figure 2.39: Lattice S28A vacuum profile - Pressure distribution simulation at 200 mA after 3 kAh conditioning with NEG coated vacuum chambers CH1 and CH12, compared to the static vacuum.

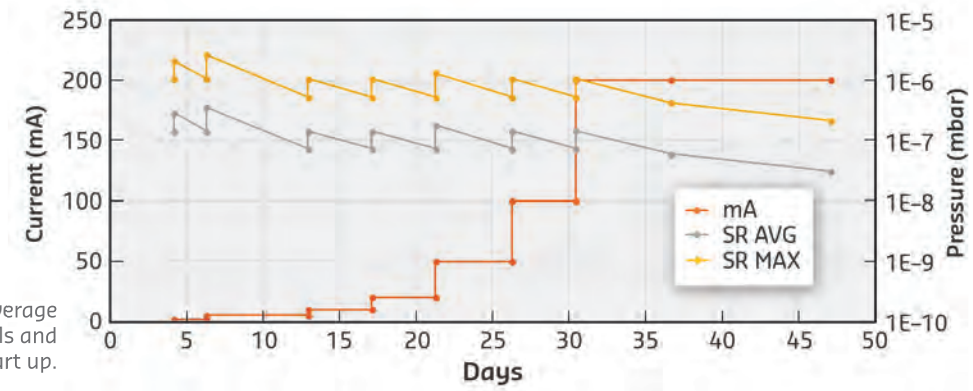

Figure 2.40: Simulated average and peak vacuum levels and beam current at start up.

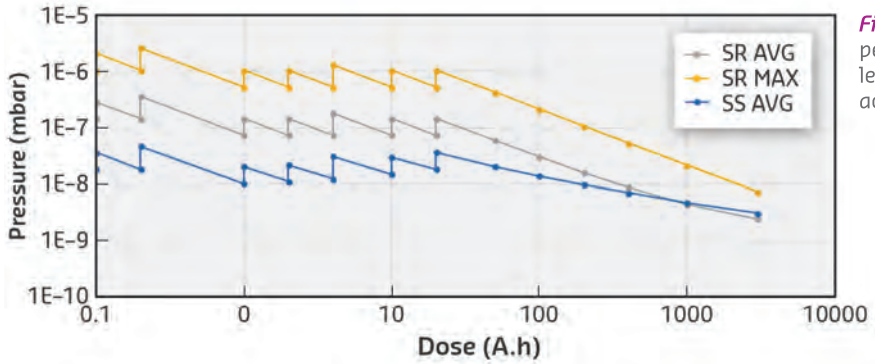

Figure 2.41: Simulated average, peak and straight section vacuum levels as a function of the accumulated dose.

regenerated without the need to open or dismount magnets. The place available for heating elements is limited, therefore an appropriate solution has to be found for each chamber segment. The fixed wiring of the power electronics in the technical zone will minimise the risk of broken equipment due to assembly and disassembly cycles and will further minimise the downtime of the accelerator due to a vacuum intervention.

Instrumentation and control

The 64 vacuum sectors delimited by the valves will be equipped with total pressure gauges of the inverted magnetron type (IMG), residual gas analysers (RGA) as partial pressure gauge and heat loss measurement based vacuum gauges of the Pirani type. With the increased number of dipole magnets and lumped absorbers on one hand and a smaller conductance of the vacuum chamber on the other, a considerable variation of the pressure along the beam path is expected. As a consequence, more vacuum measurement than today is required. Each insertion device sector will be equipped with two IMG, one RGA and one Pirani gauge. The dipole sectors will be equipped with 6 IMG, one RGA and one Pirani gauge.

Pressure information from ion pumps will also be used for vacuum measurement. The main vacuum interlock system, which ensures the remote valve closure in case of critical pressure increase, will be based on IMG's signals, as for the existing storage ring.

For redundancy we will take into account the possibility to integrate the ion pump signal within the interlock system when necessary. Indirect vacuum control equipment based on beamloss detectors, as described in chapter 1.4.8.4, and bremsstrahlung measurement will be used.

Initial start-up

During the initial start of operation, high vacuum pressures are expected, resulting from outgassing of the unconditioned copper absorbers.

With the aim of keeping the average pressure in the 10^{-7} mbar range, the stored current can gradually be increased while conditioning progresses. Start-up simulations (**Figure 2.40** and **Figure 2.41**) show the expected behaviour, 200 mA could be reached after thirty days of continuous beam conditioning. The conditioning estimation is based on the current status of the design and with conservative parameters for the simulation. Further work will be performed to improve the vacuum system. An average pressure of 10^{-8} mbar in a straight section will be reached after 100 Ah additional accumulated dose, which corresponds to 20 days of conditioning at 200 mA. This vacuum level will be compatible with the operation of the beamlines with acceptable gas-bremsstrahlung levels.

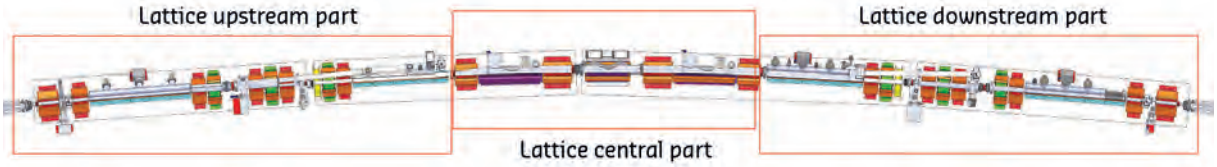

Figure 2.42: Lattice S28A cell layout.

Figure 2.43: Cell upstream part.

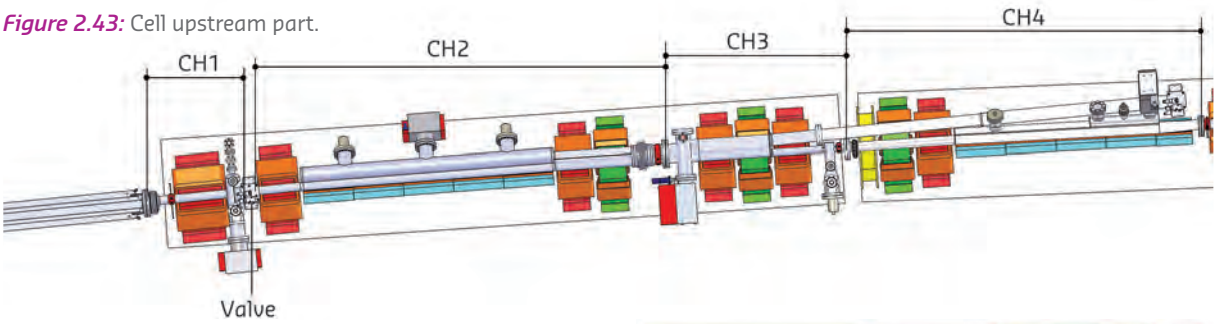

2.4.2.2. VACUUM CHAMBERS

The vacuum chamber design must comply with the beam stay-clear requirements, overall ring impedance budget, acceptable vacuum levels and synchrotron radiation handling. This is directly translated into a design which includes a chamber that is as large as possible within the magnets, anti-chambers almost everywhere and lump absorbers to collect the synchrotron radiation.

The limited available space restricts the locations where vacuum chamber hardware such as flanges, bellows, pumps and the diagnostic equipment can be installed. The design and distribution of vacuum chambers is therefore more complex than in the present storage ring. In addition, the vacuum chamber distribution should facilitate the preparation of pre-assembled girders with magnets, vacuum chambers and vacuum equipment.

A first layout of a cell, with 12 chambers, following these constraints is presented in Figure 2.42.

The circumference of the synchrotron ring is segmented into 32 cells. Each cell type requires identical vacuum chambers, with the exception of the injection section. The insertion device chambers consist of a 5 m long aluminium extruded profile vacuum chamber already installed and conditioned in the existing storage ring.

Lattice upstream part

The upstream part (Figure 2.43) is composed of elliptical shape straight vacuum chambers with variable dimension antechambers to provide the path for photon extraction, depending of the distance between the electron beam and the photon beam. Figure 2.44 shows typical chamber profiles with

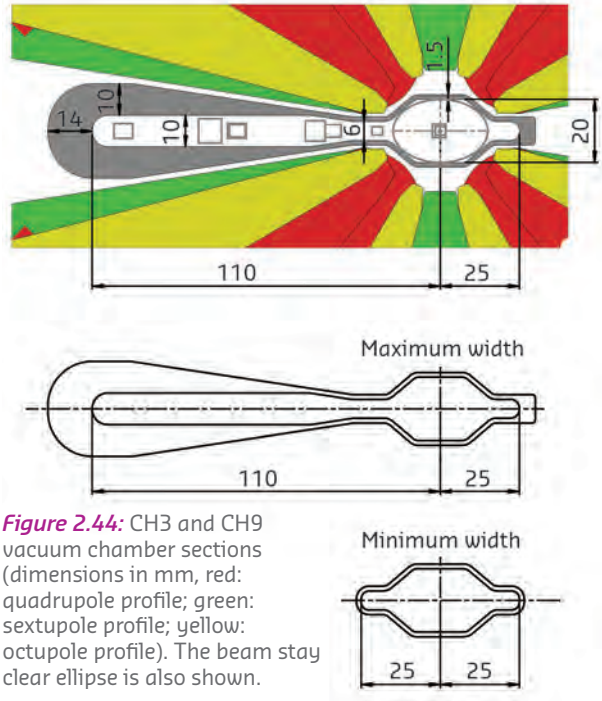

Figure 2.44: CH3 and CH9 vacuum chamber sections (dimensions in mm, red: quadrupole profile; green: sextupole profile; yellow: octupole profile). The beam stay clear ellipse is also shown.

two extreme cases where the electron and photon beam axes are at minimum and maximum distance from each other. The wall thickness is 1.5 mm with reinforcement at the location of the antechambers. The vacuum chambers pass through the inside of the lattice magnets (quadrupoles, sextupoles, octupoles) with a minimum clearance of 1 mm everywhere, necessary in particular at the pole restriction. The long dipole vacuum chamber wall thickness is 2 mm with reinforcement at the location of the antechamber (Figure 2.48).

Lattice central part

The central part vacuum chamber (Figure 2.45) construction is an elliptical shape with a large antechamber to provide optimal geometry for

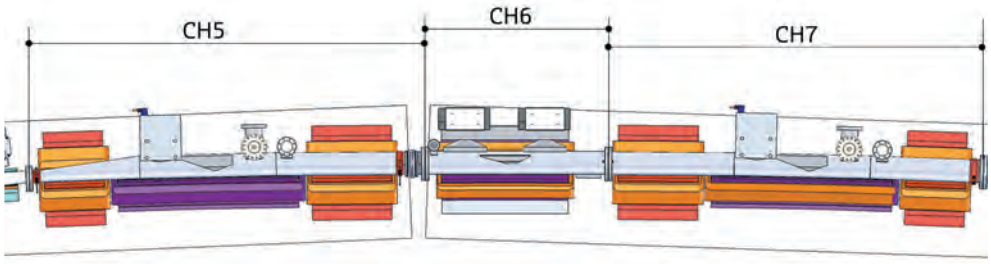

Figure 2.45: Cell central part.

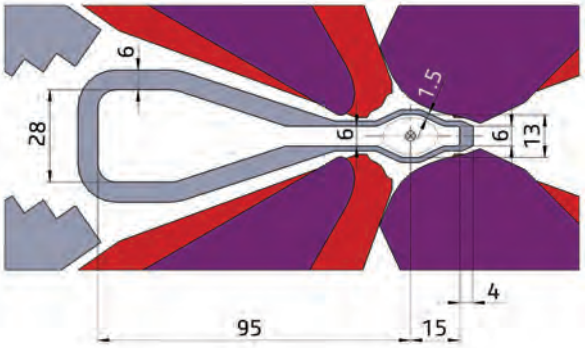

Figure 2.46: Central part vacuum chamber section (dimension in mm, magenta: dipole & quadrupole; red: quadrupole). The beam stay clear ellipse is also shown.

dipole photon beam extraction and to optimise the distribution of absorbers (Figure 2.46).

Lattice downstream part

The downstream part (Figure 2.47) is similar to the upstream part, composed of elliptical shape vacuum chambers with antechambers to provide optimal geometry for photon extraction. The wall thickness is 1.5 mm with reinforcement at the location of the antechambers, except for the long dipole vacuum chamber where the wall thickness is 2 mm. Figure 2.48 shows a typical profile of a dipole chamber.

The 5.073 m existing vacuum chambers in the insertion device straight sections will be reused, no modifications are needed (see Figure 2.49).

Power distribution

There are 32 cells containing 7 dipole bending magnets. The total power generated by the 7 dipoles in a cell is ~16.6 kW for a standard cell and 17.2 kW for the injection cell due to the different dipole configuration. The total dipole bending magnet synchrotron radiation power is then 534 kW for an electron beam of 6 GeV energy and 200 mA current intensity.

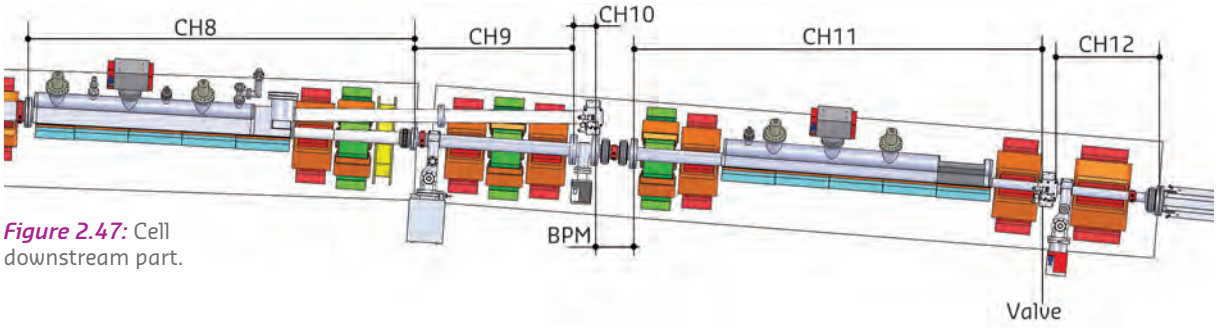

Figure 2.47: Cell downstream part.

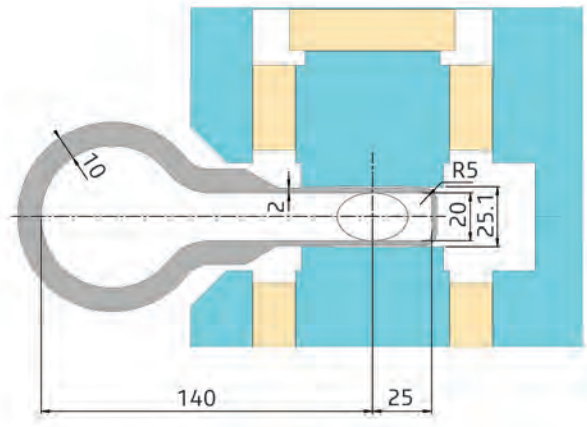

Figure 2.48: Dipole chambers section – dimensions in mm. The beam stay clear ellipse is also shown.
Insertion device straight section part.

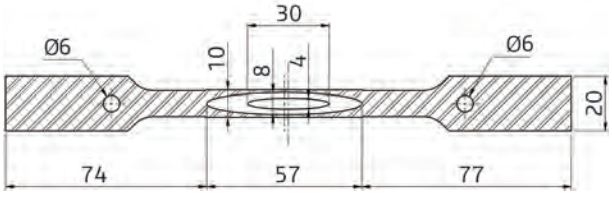

Figure 2.49: Insertion device chambers section – dimensions in mm. The beam stay clear ellipse is also shown.

Absorbers and crotches

The thermal absorbers used to protect the vacuum chambers can be classified as two major types and some particular absorbers for the special regions: lumped absorbers, crotch absorber, and special absorbers. All these absorbers will be partially or totally made of oxygen-free high thermal conductivity (OFHC) copper, water-cooled, and designed such that there is no water-to-vacuum joint. The aim at the design stage is to reduce the maximum temperature and stress on the absorbers to avoid the use of special dispersion strengthened copper (Glidcop™) material which is difficult to braze.

The design optimisation of a low thermal-stress absorber (Lotsabs) is progressing well. The objective is to have the thermal stress in the absorbers and crotches compatible with the material properties of OFHC copper. If this Lotsabs (in OFHC) cannot be used in some particular area, for reasons such as limited space in vacuum chambers, Glidcop™ made absorbers like those used in the present storage ring or similar will be the fallback solution.

A NEG coating on the absorbers could also be beneficial. Prototypes are presently being made and tests will be performed in the present storage ring.

RF fingers

The bellows/RF finger module bridges the gap between fixed parts of vacuum chambers. It serves several distinct functions:

- Accommodates the thermal expansion of the vacuum chambers during the 200°C *in situ* bake out.
- Provides flexibility during installation. Flexibility is also needed for alignments and to compensate fabrication tolerances.
- Ensures continuity of the RF system.

To minimise instabilities and impedances, the module should present a continuous chamber geometry and electrical conduction path. Dedicated RF fingers will bridge the gap between the neighbouring chambers inside the convoluted bellows.

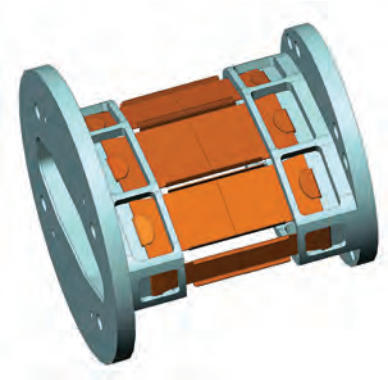

Figure 2.50: RF finger prototype for present ESRF.

A preliminary design based on a design from the Soleil Synchrotron has been produced (Figure 2.50). Due to the demanding functionalities, a full prototype of the entire bellows/RF fingers module is in preparation for mechanical acceptance and later for test under beam on the present machine.

Ref	Length mm	Bellow	Absorber	Crotch	BPM	Pumps SIP / NEG	Pre pumping	RGA/ Pirani	Penning
CH1	785	1	0	0	1	1x75ls^{-1} / -	1	1/1	1
CH2	2811	1	0	0	1	1x75l.s^{-1} / 2x200l.s^{-1}	0	0	0
CH3	1572	1	0	1	0	1x150l.s^{-1} / 1x200l.s^{-1}	1	0	1
CH4	2501	0	1	0	1	55l.s^{-1}/-	0	0	1
CH5	2346	1	1	0	1	1x150l.s^{-1} / 1x200l.s^{-1}	1	0	0
CH6	1220	0	1	0	0	2x55l.s^{-1} / -	0	0	1
CH7	2247	0	1	0	0	1x150l.s^{-1} / 1x200l.s^{-1}	1	0	0
CH8	2490	1	0	1	1	1x150l.s^{-1} / 2x200l.s^{-1}	0	1/1	1
CH9	1235	0	1	0	1	150l.s^{-1}/-	1	0	0
CH10	279	0	0	0	1	55l.s^{-1}/-	0	0	0
BPM	158	2	0	0	1	- / -	0	0	0
CH11	2711	0	1	0	0	1x75l.s^{-1} / 2x200l.s^{-1}	1	0	1
CH12	775	1	1	0	1	75l.s^{-1} / -	0	0	1
Valves	2x85								
Total	21300	8	7	2	9	23	6	2	7

Table 2.20: Standard cell vacuum chambers components.

Valves and flanges

Full metal gate valves are used to separate the 32 vacuum cells and to isolate the insertion device sector from other sectors. Due to the change in section of the vacuum chamber, the existing valves cannot be reused and need to be replaced. The valves are connected to the chambers by means of stainless steel flanges following the Conflat standard flange with a custom modification to assure a good RF conductance. These flanges are also used to connect the vacuum chambers and all other vacuum devices.

Material considerations

The vacuum chamber cross section has to be as thin as possible. Stainless steel (316LN) is suitable for this, and would also provide the required stiffness. The existing storage ring is made of this same material, so experience is available for all aspects of a stainless steel vacuum system.

Impedance consideration

The vacuum chamber design must take into account various items such as bellows, flanges, pumping ports and tapers for changes of the chamber cross section. To evaluate their contribution to the storage ring impedance, each item needs to be considered separately.

List of vacuum system components

The list of vacuum components is given in Table 2.20 for a standard cell.

Prototypes for vacuum chambers

Several prototypes are planned for procurement in 2014 in order to optimise and validate the vacuum design before manufacture (Table 2.21).

Table 2.21: Vacuum chambers prototypes.

Prototype	Objective
BPM block	Validate mechanical feasibility Validate performance under beam
Bellow/RF finger	Validate mechanical design and needed stoke
	Tests under beam
Dummy vacuum chambers profiles	Validate mechanical profile and manufacturing process Vacuum test & bakeout preparation
Complete vacuum chambers	Validate manufacturing process Validate NEG coating feasibility Validate new suppliers
Absorbers	Validate mechanical profile and manufacturing process
Crotch	Validate mechanical profile and manufacturing process Validate brazing process

2.4.3. MECHANICAL ENGINEERING

2.4.3.1. ALIGNMENT

The alignment tolerances for the new girders are given in Table 2.22. The overall alignment envelope is the maximum positional deviation that the magnets, BPMs and girders of the storage ring can have with respect to their nominal position. Also see Table 2.06 for more details on alignment tolerances for magnets, BPMs and girders.

As an example, the measured alignment envelope of the existing machine is shown in Figure 2.51. This gradual deviation from the nominal position does not affect the beam performance, similar behaviour is expected for the new lattice.

Typically alignment progresses in three steps: fiducialisation (creating the link between the

Table 2.22: Alignment tolerances for new girders.

Alignment tolerances	Tolerance X (µm)	Tolerance Z (µm)
Intra-girder	50	50
Inter-girder	50	50
Alignment envelope	1000	1000

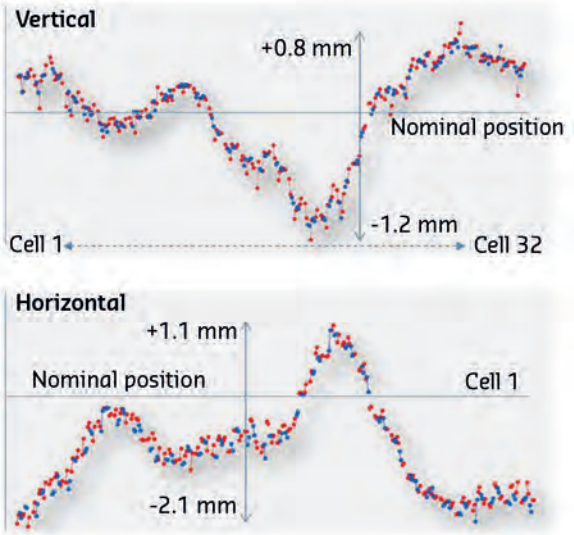

Figure 2.51: Alignment envelope of the present storage ring along the circumference of the ring (from cell 01 to cell 32). Blue: dipole girders, red: quadrupole girders.

Alignment uncertainties	U(X) and U(Z) (µm)
Fiducialisation	20
Magnet alignment on the girder	22
Inter-girder alignment	41

Table 2.23: Fiducialisation, magnet and girder alignment uncertainties derived from recent experience at the ESRF.

Alignment envelope uncertainties	U(X) (µm)	U(Z) (µm)
Estimated	345	330

Table 2.24: Alignment envelope uncertainties derived from ESRF instrument measurements and calculations.

magnetic axis and survey reference marks on the magnet); the alignment of the magnets on the girders; and, the alignment of the girders in the tunnel. The magnet manufacturer will provide fiducialised survey references with an uncertainty of 20 µm. The magnets will be pre-aligned on the girders and then transported into the storage ring tunnel. The final alignment of the magnets on the girders will be made in the tunnel. After all of the magnets have been aligned on their girders, a full survey of the machine will be made and the girders will be moved to an optimal curve designed to minimise the overall alignment envelope and inter-girder alignment errors. Estimated uncertainties for these steps are presented in Table 2.23 and Table 2.24.

Although challenging, we expect to be able to meet the required alignment tolerances.

Recent measurements show that the uncertainties in the measured beamline positions with respect to their expected positions are in the order of 0.7 mm. This means that if the new storage ring is aligned in the same position as the existing one, the photon beam will not necessarily be in its expected position. Therefore, the new storage ring could instead be aligned in its nominal position. In this case, combining the beamline position uncertainties with the machine alignment errors yields maximum beamline alignment uncertainties in the range of -4.2 mm to + 3.2 mm. They will be recovered by an orbit correction in the few ID straights where such a considerable displacement will be observed (statistically 10% of the straights are expected to be concerned, *i.e.* around three ID beamlines).

Site stability

There are several movements specific to the ESRF site. Long term movements are driven by geomorphological and geological phenomena. The local Vercors and Chartreuse mountain ranges

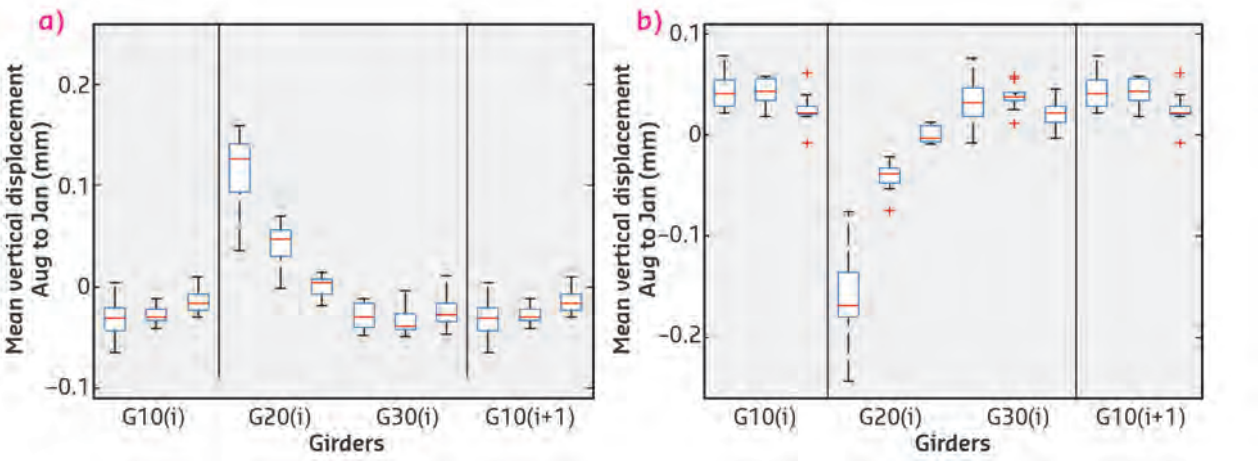

Figure 2.52: Slab curling effects on the three families of girders G10, G20 and G30 between January and August a) and between August and January b) of the existing storage ring. Maximum movement is at the first G20 girder jack support which is very close (< 0.5 m) to the slab construction joint. Joints are between G10 and G20 and cracks are between G30 and G10.

Figure 2.53:
Girder repartition.

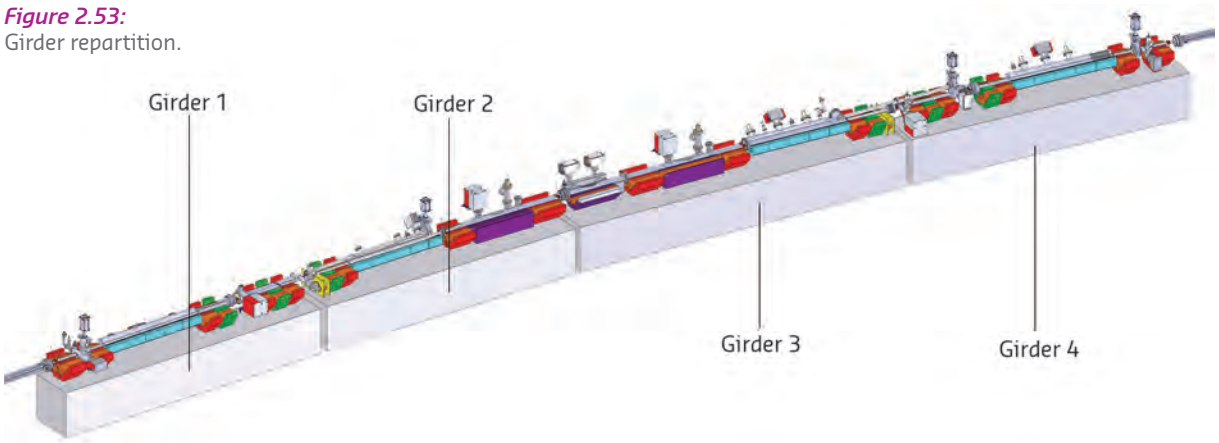

are slowly moving apart. This has two effects: the Grenoble basin and specifically the ESRF site are tilting downwards; and, deforming along the Isere river valley. Locally, vertical site deformation is caused mainly by the adjacent Drac and Isère rivers and their influence on the ground water level.

Overall, these medium and long term effects cause a systematic horizontal deformation in the order of 100 µm per year. This will require realignment once every year. Mean long term vertical movements are 360 µm per year. Realignment to correct these movements is required on average every six months.

Tunnel motion (cracks, joints, etc.)

Concrete slabs curl because of variations in the thermal gradient through them. Maximum curling occurs at the slab edge where the construction joints are. Over 24 to 48 hours, the temperature of the ground underlying the slab is stable. The tunnel has a diurnal temperature cycle (< 0.5°C) which drives the gradient variations and movements. Over a year, the tunnel is relatively stable but the ground temperature has a sinusoidal variation of a few degrees. In this case, the ground temperature drives the gradient variations. The effect on the slab is the same in both cases, but the magnitude is much larger for the seasonal variations.

Figure 2.52 shows the characteristic effects of slab curling on the three quadrupole girder families in the existing storage ring. There is upward movement during the spring and downward movement in autumn. There is additionally a net long term downward movement.

In addition to the joint, there is a crack in the slab in the insertion device straight section between the G30 and G10 girders of the present storage ring. Movements between the G30 and G10 appear to be much smaller than at the slab joint. However, because measurements are made far from the crack, the magnitude of the effect at the crack is not necessarily well illustrated or represented in the results shown Figure 2.52.

When the ESRF was built, problems related to ground movements and slab curling were not well understood. In anticipation of future movements, the ESRF installed motorised jacks under all of the quadrupole girders. Synchrotrons built after the ESRF had the benefit of our experience and were designed to accommodate ground movements.

Modifications to the existing slabs to reduce the thermal curling effect have been considered. However, this would require extensive civil engineering work. It has been decided to adopt the more conservative and economical solution that has been employed successfully at the ESRF for over 20 years: all the girders will have motorised jacks and will be realigned approximately every 6 months. Alignment with beam in the storage ring using motorised jacks and the hydrostatic levelling system has proven fast and effective.

2.4.3.2. GIRDERS AND STABILITY

Girder layout and dimensions

The support of the storage ring magnets and vacuum chambers will rely on 128 girders, 4 girders for each of the 32 storage ring cells (Figure 2.53). Each girder supports 7 to 9 magnets with a layout which copes with the space constraints and the necessity to have flanges and bellows between vacuum chambers supported by adjacent girders. The girders will have a length between 4.9 and 5.9 m and will support 4 to 5.3 tons of hardware.

Required alignment motions

As explained in section 2.4.3.1, the intra-girder and inter-girders alignment requirements are 50 micrometres, both in the vertical and transverse directions and, in order to respect the inter-girders alignment tolerances, a re-alignment of the girders in the vertical direction will be necessary every six months because of the medium term displacements of the floor. As mentioned above, the possibility to

improve the slab rigidity has been abandoned. For this purpose, each girder should be equipped with a ± 5 mm motorised vertical adjustment and a ± 5 mm manual transverse adjustment with 5 micrometres resolution.

Stability requirements

In order to estimate the sensitivity of the lattice to magnet differential displacements from vibrations or other effects, the electron beam displacement induced by random magnet motions has been calculated. Table 2.25 indicates the calculated RMS magnet random motion acceptable to generate an electron beam displacement smaller than 10% of the beam size. The results show that the S28A lattice stability requirements or required efficiency of fast orbit correction is 2.2 times higher in the vertical direction than the present storage ring. In the horizontal plane the stability requirements are 6.3 times higher but still ten times less than in the vertical direction.

As general strategy we will implement solutions that maximise the stability of the source to guarantee the highest possible performance over the medium and long term. Experience gained at other synchrotron facilities shows that the best results in term of vibrational stability are obtained with manually adjustable girder systems, which support and rigidly clamp the girder in multiple points as opposed to motorised girders systems.

Efforts will be made in the first place to develop a motorised girder system with optimum stability for the new girder systems:

- Vibration amplification factor (over 1-100 Hz) < 1.1.
- First natural frequency f1 > 35 Hz

The design of the girder must also comply with the installation. The installation procedure is detailed in section 2.5.7.

Girder and support system

The girder assembly must meet the conflicting requirements of easy alignment and high stability. A survey of the storage ring girder systems developed for synchrotron facilities during the last fifteen years shows that several projects have chosen high-stiffness manually-adjustable girder systems associated with a slab optimised for ultra high stability (SOLEIL, NSLS II, MAX IV).

Lattice		Average beam size [µm]	RMS magnet motion [nm]
S28A	H	26	84
	V	4	8
Present	H	310	526
	V	9	18

Table 2.25: Calculated magnet motion producing a beam displacement equal to 10% of beam size without orbit feedback.

These high-stiffness manually-adjustable girder systems are not suitable for the new ESRF storage ring because of the need for motorised vertical adjustments imposed by the existing slab motion and associated frequent re-alignment. Most motorised girder systems developed for synchrotron storage ring light sources (SLS, Diamond, TPS, Petra III) are based on cam systems, a concept providing good positioning in 5-6 motorised degrees of freedom.

However, the cam system has several drawbacks: the stiffness at the support points is limited due to small contact areas at the cams contacts and the first natural frequency obtained was lower than 20 Hz (except at TPS where clamping systems and dampers have been added). Six motors per girder are required, driven by a complex algorithm with a strict definition of the home position.

Alternative concepts have been explored for the girders of the new ESRF storage ring aiming at increasing the stiffness of the supports and at reducing the numbers of motors. The orthogonal hexapod concept described below offers promising characteristics which need to be confirmed by some validation tests.

The girder is supported by 6 legs of adjustable lengths (see Figure 2.54): Three vertical Z legs (red), two horizontal Y legs (blue) and one horizontal X leg (green). Each leg is equipped with a ball joint at each end, one ball joint linked to the girder, the other one to the floor or to a fixed bracket.

The Z legs are motorised, the X and Y legs are manually adjustable, enabling the vertical and tilt positions to be controlled by only three motors per girder. The coupling between Z and Y motions is negligible for small motion ranges.

The legs and ball joints must be designed to maximise their axial stiffness. To provide the adjustment, commercial type levelling wedges can be integrated in each leg and will be motorised for the vertical adjustment. The cross section of the girders is based on the optimisation of their mechanical characteristics, with the intention of minimising the cross sectional area (which is directly proportional to the mass and the cost of the structure), while concurrently maximising the stiffness of the girders.

Calculations by a finite element analysis method have been made to assess the influence of the stiffness of the girder, of the X, Y and Z legs and of the floor on the first natural frequency of the assembly. The longer girder has been used in mechanical analyses since the stability problems associated with larger length are more severe. With the model

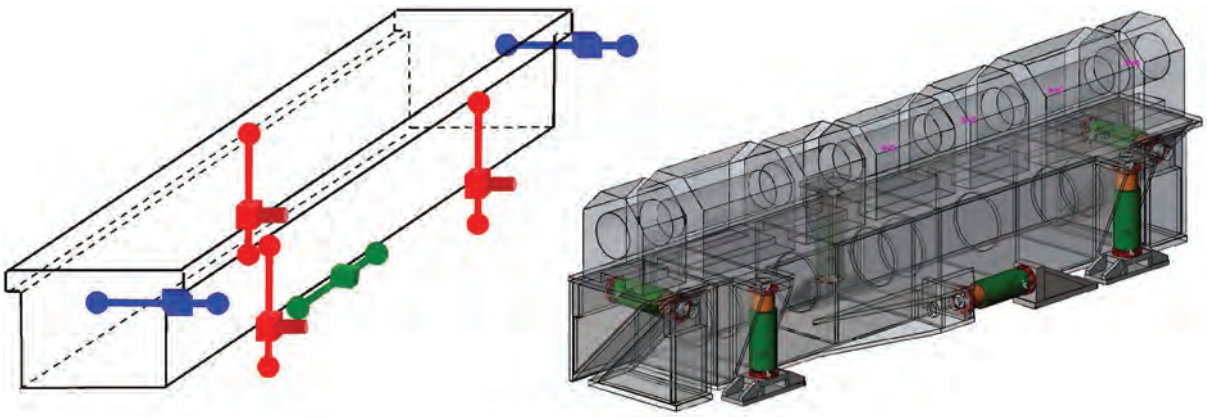

Figure 2.54: Girder orthogonal hexapod concept.

shown in Figure 2.55, the results of the calculations give a range for the first natural frequency between 32 and 47 Hz, depending on the assumed stiffness for the legs and the adjusting devices. The stiffness of the adjusting devices and ball joints cannot be precisely estimated by calculations and therefore tests on prototype components will be made in order to optimise the stiffness of these crucial components.

Support system of magnets on girder

Girders are used to support the magnets and BPMs with high precision positioning. The interface between each magnet and the girder must be stiff in order to avoid amplification of vibration and must provide adjustment capabilities for the alignment of the magnetic centre of each magnet within the required tolerance of 50 micrometres. To reach this positioning precision, each magnet will be aligned and adjusted on the girder. The horizontal adjustment will be done with a mobile adjustment system which will be removed after adjustment. The vertical adjustment will rely on fine adjustment systems associated with stiff shims on which the magnet will be clamped after adjustment.

Prototypes for the girders assembly

Several prototypes are planned for launch in 2014 in order to optimise and validate the girder concept before the manufacture of the complete batch of girders (Table 2.26).

Prototype	Objective
Adjustable leg and ball joint	Validate the adjusting system and ball joint stiffness Validate the adjustment resolution
Dummy girder and 3 dummy magnets	Validate the adjustment systems between girder and magnets: resolution, stiffness, ease of use
Complete prototype girder assembly and dummy magnets	Validate first natural frequency of the assembly Evaluate uncontrolled permanent deformations

Table 2.26: Mechanical prototypes.

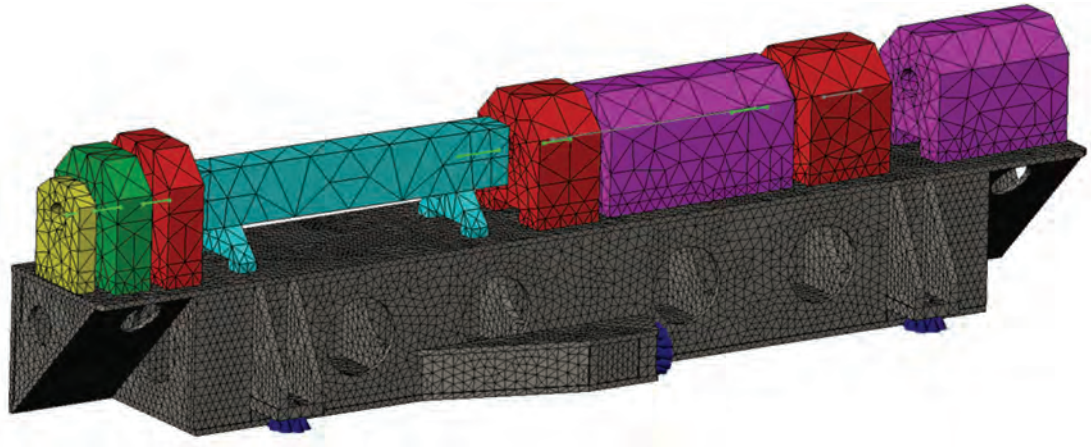

Figure 2.55: Finite element analysis model of the orthogonal hexapod girder system.

2.4.4. FRONT END

2.4.4.1. INSERTION DEVICE BEAMLINES

Insertion device front ends at the ESRF are of two types: undulator (in air, in vacuum, helical) and wiggler (multi-pole). Insertion devices can produce powerful synchrotron radiation with a power density of about 400 kW mrad^{-2} and a total power up to 25 kW. The modular design of the front end in its high power configuration allows horizontal apertures from ±0.08 mrad to ±0.24 mrad. Insertion device front ends are further subdivided into single insertion device and canted insertion device types. Canting allows two insertion devices in one straight section to produce two beams. For existing beamlines the beams are separated by ±0.75 mrad for ID23, ±2.3 mrad for ID30 and ±2.7 mrad for ID16. All insertion device front ends will be kept and adapted to the new lattice. All sources including those in the canted configuration have been taken into account in the design of the storage ring vacuum chambers.

The front end can be split into three parts. Module 1 refers to the first part of the front end nearest to the storage ring and to the second part composed of a series of connecting chambers, called the transition module. Module 2 refers to the third part, upstream of the port end wall that separates the storage ring from the corresponding beamline optics hutch.

The main components of front end module 1 are:
- Photon XBPM: photon beam position monitor.
- Dipole absorber: this absorber protects the vacuum chambers from parasitical photons produced in upstream dipoles.
- Horizontal slit: defines the horizontal aperture of the photon beam.
- Photon shutter: a water-cooled Glidcop™ copper shutter that stops the X-ray beam from reaching the optics hutch when in the closed position, or enables the beam to enter the optics hutch when in the open position.
- Pneumatic valve: this is an all-metal gate valve that serves to isolate the front end from the storage ring.
- Fast shutter: the fast shutter is a rapid closing valve that stops an air inrush in case of a fast vacuum-to-air leak.

The transition module consists of several vacuum chambers including one acoustic delay line (ADL). The ADL is a segmented vacuum chamber. The different segments are divided by baffles that let the synchrotron radiation pass through. In the event of a vacuum incident on the beamline, the pressure wave coming from the beamline is damped and the level of vacuum inside the storage ring is protected.

The main components of front end module 2 are:
- Vertical slit: the vertical slit defines the vertical aperture of the photon beam. It is made from water cooled OFHC – Cu (oxygen free high conductivity copper).
- Trigger gauges: two vacuum sensor gauges close the fast shutter of module 1 in just a few milliseconds to protect the vacuum of the storage ring in the event of a vacuum accident on the beamline. These gauges work in association with the acoustic delay line in the transition module.
- Pneumatic valve: this ultra-high vacuum valve isolates the front end from the beamline on windowless front ends.
- Diamond window: this window filters the X-rays and separates the storage ring vacuum from the vacuum of the optics hutch.
- Radiation shutter: this shutter is a block of lead that stops the radiation from the storage ring from entering the optics hutch when in the closed position.

All insertion device beamline front end module 1s will have to be refurbished due to the compactness of the S28A lattice:

- The XBPM will be removed.
- The dipole absorbers will have to be designed for the new lattice.

Nevertheless, most individual components will be re-used. The horizontal slit and photon shutter will have to be moved downstream by approximately 1.6 m to allow the installation of the storage ring DQ2 vacuum chambers and their associated girder. We plan to motorise the horizontal slit and photon shutter for fine adjustment of their position. Downstream, the photon shutter dedicated space will be reserved for the installation of new equipment such as compound refractive lenses.

The present front end power and power density configurations are compatible with the new lattice.

2.4.2.2. BENDING MAGNET BEAMLINES

Similarly to insertion devices, bending magnet front ends can be split into three parts grouped in two modules.

All bending magnet beamline front end module 1s will need to be refurbished due to the compactness of the new lattice and the change in source parameters. Further calculations will be necessary to verify that the beryllium window can operate in safe conditions regarding the increased heat-load. The front ends will need to be re-aligned. The water cooled horizontal aperture will be modified to better match the new radiation fan.

2.4.5. INSERTION DEVICES AND BENDING MAGNETS SOURCES

2.4.5.1. INSERTION DEVICES

Most of the installed insertion devices in the present storage ring (more than 70 ID segments) will be reused. The position of the insertion device source points will remain identical, both longitudinally and transversally. Refurbishment/update of the insertion devices will continue to be pursued to improve the performance of beamlines by using new insertion device technology. Some consequences following installation of the new lattice will need to be addressed for the insertion devices:

Field quality

One important point for insertion devices is the consistency of the field quality presently achievable with the requirements set by the new lattice. This includes the residual interaction with the stored beam and the spectrum quality of undulators. The interaction with the stored beam is primarily seen through residual closed orbit distortions induced by ID gap changes.

The induced electron beam displacements are usually scaled to the size of the electron beam and specified to some maximum percentage (generally 10%). For the large majority of installed insertion devices (90%), no specific improvement will be needed thanks to the proven field correction methods in use today. For the remaining devices, active correction by means of small resistive dipoles (feed forward correction) will continue to be used. In addition, the fast orbit feedback will complement the stabilisation.

A second visible class of magnetic error is the gap dependent residual skew quadrupole field left in some insertion devices. This affects the coupling in the beam and consequently induces visible changes of the vertical emittance for operation modes with very small vertical emittance (~ 5 pm.rad). Stabilisation of the vertical emittance becomes difficult in the existing lattice without introducing dedicated skew correctors operated in feed forward mode with the perturbing insertion device gaps. The new lattice will be quite different: with similar vertical emittance and insertion device error as presently, the impact of insertion device gap on the vertical emittance will be at least one order of magnitude smaller due to the smaller horizontal emittance and beta function at the insertion device straight section. As a benefit, the stability of the vertical emittance should be considerably improved for the new lattice. The lower values of both horizontal beta and dispersion will also make the beam orbit and beam energy less sensitive to first integral field errors.

Concerning the spectral quality of undulators, the currently achieved phase error correction will also be compatible with the new high quality photon beam. Indeed, because of the low residual phase error remaining on undulators (~2 degrees RMS), the quality of the undulator harmonics will still be dominated by the electron beam emittance and energy spread.

Canted beamlines

Canted beamlines will be preserved in the new lattice. It will even be possible to create new ones should the need arise. In the present storage ring, the necessary canting angles are provided by a permanent magnet dipole in the middle of the insertion device straight section and two others on each side of the straight section. In the new storage ring, such angles will be provided by keeping the permanent magnet dipole in the middle of the insertion device straight section and by reducing the bend angles of the last modules of the two dipoles immediately upstream and downstream of the straight section. This will be slightly beneficial with respect to the present solution, since there will be less space taken by the canting dipoles and less synchrotron radiation generated by the canting.

Length of insertion device straight sections

In the new lattice, the length of the insertion device straight sections will be 5 m to ensure compatibility with the majority of the existing insertion device layouts. However, since 2008, through Phase I of the ESRF Upgrade, nine straight sections were modified to provide lengths of 6 m and 7 m. Of these, eight have been equipped with insertion devices, three included canting. As a consequence, the straight sections will need to be reconfigured back to a length of 5 m, while keeping optimal performance and canting angle for the corresponding beamlines. Each case will be summarised below:

ID24 and ID20

Both straight sections are presently equipped with four insertion device segments including revolver type undulators. The new scheme will simply consist of removing one short segment (ID20) or merging two undulators on a revolver support (ID24). In both cases the total undulator length will be reduced to 4.8 m.

ID16 and ID30

These two beamlines depend on the canting scheme that was implemented during Phase 1 of the ESRF Upgrade. The canting scheme including its canting angle will have to be kept identical in the new lattice.

		Present lattice	New lattice
Hard X-ray source	Magnetic field [T]	0.86	0.86
	Angle [mrad]	9	7.85
	Aperture [mrad]	±3	±1.5
	Longitudinal displacement [m]		-2.93
	Transverse displacement at the source point [mm]		-25
	Transverse displacement at 30 m [mm]		+9.5
Soft X-ray source	Magnetic field [T]	0.40	0.44
	Angle [mrad]	3	3
	Aperture [mrad]	±3	±3
	Longitudinal displacement [m]		-3.26
	Transverse displacement at the source point [mm]		-6.4
	Transverse displacement at 30 m [mm]		-6.4

Table 2.27: Bending magnet source points.

The technical solution will consist of replacing the existing undulator combinations with shorter single piece devices. For ID16, the 2.5 m long in-vacuum undulator will be replaced with a 2 m long version in the first branch while the second branch, presently equipped with a tandem of two 1.4 m long revolver undulators, will be replaced by a single revolver with a length of 2.3 m. For ID30, a similar approach will be used for the existing tandem undulators that will be replaced by a 2.3 m long undulator for each branch. In all cases, the existing magnetic assemblies will be used for the new undulators.

ID23, ID32 and ID01

The ID23 straight section was updated from 5 to 7 m to accommodate RF cavities in the middle. The two canted undulators were not modified but only translated. Backward migration will not pose any problem since we expect to remove the RF cavities in the context of the accelerator upgrade. The canting of the undulators will be preserved without any specific difficulty. For ID01 and ID32, the last straight sections scheduled to be updated to 6 m, their insertion devices are presently under construction and we have restricted their layout to 5 m, without additional consequences.

Two other straight sections (ID31 and ID15) were initially expected to be lengthened, but these projects are now based on 5 m free space and high performance insertion devices.

The most effective technical solutions will require the design and construction of new support structures of 2.3 m or the use of the existing design for combining undulators together. The magnetic assemblies will be recovered from the existing segments and installed on the new supports during the long shutdown. It should be noted that the new support structures will have improved mechanically performance over present devices and could serve as a basis for further refurbishment of insertion devices in the new accelerator.

2.4.5.2. BENDING MAGNETS

The main geometric parameters of the present and new hard and soft X-ray sources are presented in Table 2.27.

The displacements are given relative to the present X-ray beam paths. For the double branched beamlines (soft and hard), if the present beamline optic is kept, the absolute separation at 60 m will decrease by about 50 mm.

The bending magnet source point will be kept as close as possible to the existing ones, but, since the cell geometry is completely different, their position and angle may vary. The soft X-ray source will be provided by the centre magnet, while the hard X-ray source will be provided by the short three-pole wiggler located immediately downstream.

It has to be noted that:

- The new source points will be further away from the beamline. The longitudinal displacement is 3.26 m for the low field bending magnet source and 2.93 m for the three-pole wiggler source point.
- The angular aperture of the X-ray fan delivered by the low field magnet will be identical to that of the

present soft end source but the source point will be translated in the horizontal transverse direction by 6.4 mm toward the ring tunnel.
- The new hard X-ray source point from the three-pole wiggler will be centred at -7.85 mrad while the present axis from the high bending magnet field is at -9 mrad. Horizontally, the X-ray beam will be shifted by 25 mm toward the ring at the source and 9 mm outward at the front end (30 m from the source). Moreover, the X-ray fan delivered by three-pole wigglers will have a maximum angular aperture of 3 mrad instead of the actual 6 mrad.

The transport of the photon beam from the different bending magnet source points of the new lattice to the front end will require vacuum chambers with narrow vertical aperture and large horizontal aperture. Moreover, some magnets of the new lattice (quadrupoles and sextupoles) need to be adapted to allow the photon beam transport to the port end.

The impact on the different bending magnet beamlines is currently being investigated. The longitudinal displacement of the source points will have an impact on the optical components used for focusing the photon beam. The transverse displacement of the source points may also require re-alignment of beamline components.

We will finalise the best configuration on a case-by-case basis; we do not foresee any unsolvable technical issues that will prevent the bending magnet beamlines from being reconfigured for the new layout. Finally, we should also consider that many other bending magnets ports are still available for the beamlines for both hard and soft X-rays sources.

2.4.6. ELECTRICAL SUPPLY ENGINEERING

For the present lattice, the magnets are powered in families. There are 14 power supplies located in a central room to power the 14 families of magnets. Within each family, magnets are powered in series. For the new lattice, all magnets will be powered individually. The required number of power supplies will be larger than one thousand. We already have some experience with the use of individual power supplies for magnets following the lengthening of the ID23 straight section to 7 metres. The magnets of the two cells around this straight section are powered individually.

Table 2.28 presents a summary of the power supplies for the new lattice. The specifications are based on the maximum power required by each group of magnets. Further optimisation of the ratio cost/performance is necessary as a function of final requirements. The present power supplies will be reused for the correctors. As the number is not sufficient, new power supplies will be ordered in complement.

2.4.6.1. MAGNET POWER SUPPLY SYSTEM

Powering all magnets individually is more expensive than the series-connected magnet solution. In addition, special attention must be paid to related issues such as the reliability of the power supply

Magnet type	Abrev.	Quantity	Current [A]	Voltage [V]	Maximum power [kW]
Dipole (PM solution)	DL	0			
Dipole (EM solution)	DL	2	Reused existing PS		
Dipole quads	DQ	96	190	12	2.3
Quadrupoles mod grad	Q1-5	384	105	15	1.6
Quadrupoles high grad	QF6-QF8	128	107	23	2.5
Sextupoles	S	192	130	18	2.4
Octupoles	O	64	150	6	0.9
Correctors	Horizontal	160	2	14	28
Correctors	Vertical	160	2	7	14
Correctors	Skew quad	160	2	21	42
Correctors	Sextupole	96	TBD	TBD	TBD

Table 2.28: Power supply quantities and specifications.

systems and the power quality of the local mains network.

The final system to be put into place to power the magnets is still under investigation. Two technical solutions are currently under evaluation and will be studied in parallel until the final version of the lattice is chosen. The first solution is based on an AC distribution of power all along the technical gallery; the second is based on DC distribution. We will adopt and finalise one solution by the end of 2014, based on technical grounds, cost, procurement schedule and long term availability of components.

AC Distribution design

Powering the technical gallery via an AC distribution is the most straightforward as it entails a power converter being connected to the 50 Hz mains supply for each electromagnet. This solution is simple in terms of procurement and its architecture is linear. However, this would lead to a substantial change in the electrical power distribution. Several additional drawbacks would be introduced:

The electrical harmonic pollution needs re-evaluation, with a modification of the filter configuration for at least 3rd, 5th and 7th harmonics.

1. The reliability of the power supply system will be poorer than the DC case because the most critical component of such power supplies is the input rectifier that in the DC case is centralised.
2. This solution is the more space-consuming choice due to the need for individual rectifiers.

The mean time between failures (MTBF) calculation for specific power supply equipment is being carefully evaluated. The mean time to repair (MTTR) failures will depend on the diversity of spare parts stocked by the chosen converter supplier. The stand-by support will be more complicated. The variety of spare parts will have to be limited as much as possible in order to simplify interventions.

DC Distribution design

The second option being studied looks at the possibility of centralised DC voltage distribution and local distributed conversion for current fine-regulation (Figure 2.56).

Using this solution, the harmonic pollution would be better suited to our present 20 kV harmonic filter system. The present four-rank filtering on the 20 kV supply, plus the two active filters on ranks 2, 3, and 13, is sufficient and could be reused without major changes for this level of power.

The individual low power size of each power supply (from 500 W to 1.7 kW) means that no ready-made 12-pulse rectifying system is available on the market and even a triphase connection is usually reserved for power levels above 3 kW. This means that the centralised rectifying solution, by reusing the present quadrupole rectifiers, would be more efficient in terms of harmonic treatment and the compensation of the reactive power would be corrected by the high quality power supply with the rotating alternators, as is today the case.

Within this solution, the matrix switchboard system could easily be reused to allow fast intervention and could also be exchanged with a modified spare unit, even if the electromagnet design for the longitudinal gradient dipole is chosen. The redundancy is only on the DC distribution supply, the DC/DC converters being independent. There would also be better MTBF or MTTR due to easy replacement and/or switchover via the matrix switchboard.

This option also requires much less space allocation and fewer modifications to the presently running 50 Hz electrical distribution. The mains AC transformers and distribution switchboard would be kept. The reused power supplies would need some refurbishment such as the triggering system.

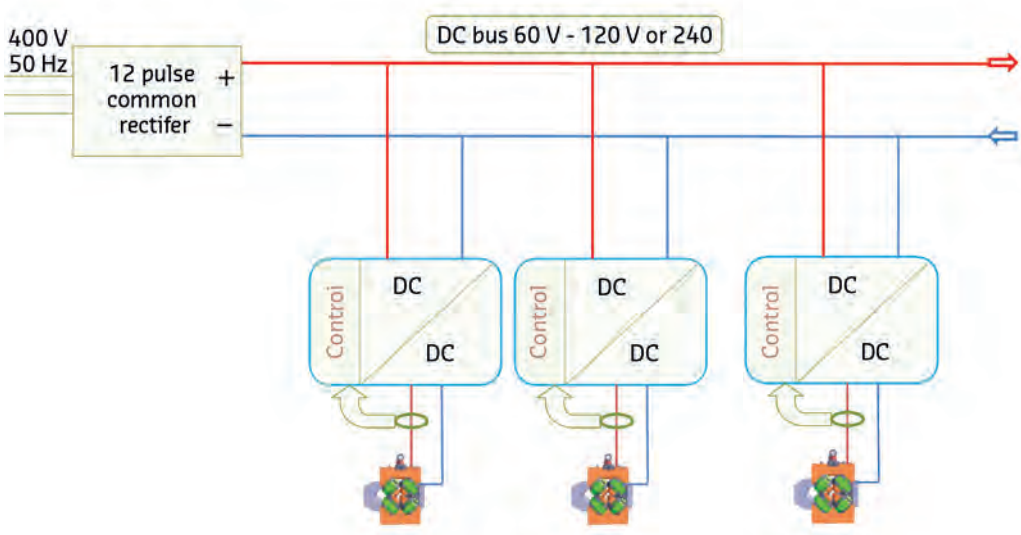

Figure 2.56: DC voltage distribution using a DC bus at 60, 120 or 240 V.

The cabling cost implication is still under evaluation. The DC voltage transport has already been quoted for 200 V distribution (the 60 V and 240 V solutions are still under evaluation) for the old quadrupole power supplies. This option has an efficient path and an innovative structure, with less thermal release in air and more in water. This philosophy has been adopted at other institutes including DESY and Elettra.

2.4.6.2. CABLING ISSUES

- The individual power supply solution will require a full redistribution of the AC 50 Hz feed and associated changes to the homopolar filters. The cable path to the tunnel is not an issue due to the low current used (max 160 A), which requires cables of smaller diameter, minimising the cost of cables, the tunnel space needed and the logistics. This means that the same number of trenches is required as today, except in particular zones, such as the injection and cavity zones, where more space will be necessary. The estimated value is 3 dm^2 for power cables, not including control cables.

- The routing of the DC buses feeding local multichannel high-precision converters is foreseen inside the technical gallery from the main SRDC room. The 400 V 50 Hz distribution of the first solution would also be routed inside the technical gallery, and only the size of the cables would introduce a differential cost, which would be compensated by higher investment in power electronics using built-in AC/DC conversion.

2.4.6.3. RELIABILITY, MTBF AND FALLBACK POSITION

- To provide the ESRF with a reliable solution, all efforts will be put into creating a simple design with enhanced debugged engineering.
- Due to the standard use of a single copper cross-section for the magnets, it will be possible to have one single design for all the power supplies below 100 A, which equates to around 800 units.
- For power supplies of more than 100 A, of which there is only one type, we would benefit from the experience acquired from the present high-precision current power supplies.
- The custom design of the choppers in the power supplies will include a water-cooled solution to avoid having to modify the ventilation and air cooling of the experimental hall. This design could be similar to the one made for the existing corrector power supplies. We will reuse the present air handling units in the experimental hall, completely in line with the major constraint of not changing the general infrastructure for air treatment.
- The 60 hours average MTBF at the ESRF is driving the specification of the power supplies design which should be much higher.
- To keep the repair time short, the matrix connection system will be reused in the DC bus solution, which has already proven itself keeping the replacement time below half an hour.
- The level of the DC bus voltage should be determined by the compromise between acceptable resolution, stability, ripple, efficiency, minimum current and protection and the use of standard DC circuit breakers.
- The number of cells to be powered by one AC/DC rectifier at 560 A is still to be determined.
- The power supply control system will need to be modified in order to simplify it and to increase reliability (OS9 together with the triggering and active filtering will have to be abandoned for obsolescence). The switching matrix will be integrated within the controller of the eight renewed power supplies.
- The power supplies for series connected magnets will be dismantled if the AC distribution is chosen.

From a technical point of view, the DC solution is of advantage, however, its delivery would take longer than the AC solution.

The cost of each solution is similar. The final choice will be determined by budgetary constraints. The consequences of the different choices are still being assessed to determine the best solution.

2.4.7. RADIO FREQUENCY SYSTEM UPGRADE

Upgrading the storage ring RF system by replacing the existing 5-cell cavities with HOM damped cavities was foreseen for Phase I of the ESRF Upgrade Programme. However, given the sizable cost of the project, we plan to partly finance this project with Phase II funds or by the regular operation capital budget available in the period 2015-2019. This upgrade will allow:

- Operation with higher current (up to 300 mA)
- An increase is the reliability of the system
- The possibility of replacing the klystrons with solid state amplifiers (SSA)

Since the approval of Phase I, the idea to run at higher current has been abandoned because it required major changes in the beamline optics to cope with the increased beam power. Therefore, the RF project has been readjusted to fit these new requirements and also to optimise it for operation with the new storage ring. In particular, the RF voltage and

the power requirements have been substantially reduced, so that now only 11 HOM damped cavities (plus one spare) will be needed in addition to the 3 prototypes in operation on the ring (instead of the 18 initially foreseen). The 12 cavities have already been ordered and are financed from the Phase I budget. Only auxiliary equipment such as tuners, couplers, field probes and instrumentation remain to be financed by Phase II. The SSAs will have to be moved, the RF power distribution will have to be re-designed and some refurbishment of the low level RF and the control system will be necessary. However, no substantial investment is required for new RF power generators, as the existing klystron transmitters and SSAs can be re-used with some adaptations to match the needs of the new lattice. In-house development of the next generation of SSAs, which is already making good progress, will be pursued to prepare for the after-klystron era.

To increase the Touschek lifetime, the study of a harmonic RF system will be continued as a post Phase II project.

2.4.7.1. RF REQUIREMENTS

For the new storage ring the beam energy loss will be about 3.1 MeV/turn. Of this, 2.6 MeV/turn is due to synchrotron radiation from dipoles and up to 0.5 MeV/turn from insertion device and short wiggler radiation. The RF system is dimensioned to provide the total power radiated at the design current of 200 mA, with some reasonable margin, a comfortable RF-energy acceptance and a proper synchrotron tune for optimal longitudinal stability. Table 2.29 compares the relevant storage ring parameters and the derived RF parameters for the existing storage ring and for the new lattice.

The new storage ring will be operated at nearly the same RF frequency as the existing one, which will allow much of the hardware for the RF and the beam diagnostics systems to be reused. While the harmonic number is kept unchanged, a 171 kHz increase of the RF frequency will account for the reduction of the circumference as discussed in section 2.3.1.

RF parameters		Present lattice	S28A
Electron energy in the storage ring	E	6.04 GeV	6 GeV
Maximum stored current	I_{bmax}	200 mA	200 mA
Energy loss (incl 0.5 MeV/turn for IDs)	U	5.4 MeV/turn	3.1 MeV/turn
Longitudinal damping time	τ_s	3.5 ms	8.86 ms
Momentum compaction factor	α	$17.8\ 10^{-5}$	$8.72\ 10^{-5}$
Energy spread (low bunch current)	σ_E/E	$10.60\ 10^{-4}$	$9.48\ 10^{-4}$
RF frequency	f_{rf}	352.200 MHz	352.371 MHz
Harmonic number	h	992	992
Nominal RF voltage	V_{acc}	8 MV	6 MV
Resulting RF energy acceptance (incl. IDs)	σ_E/E	2.9%	4.9%
Synchrotron frequency	f_s	1.86 kHz	1.22 kHz
Compared Instability thresholds for HOM driven instabilities (LCBI), for one given HOM	ratio	1.9 to 1.0	
Number of cavities	N_{cav}	5 five-cell cav's (≈ 25 cells)	14 mono-cells, HOM damped
Shunt resistance of the accelerating mode	R_s	26.8 MΩ/cavity	4.8 MΩ/cavity
Unloaded quality factor of the accelerating mode	Q_0	38500	33000
Cavity coupling	β	4.4	3.2
Copper losses per cavity	P_{Cu}/N_{cav}	47 kW	19 kW
RF power per cavity at I_{nom} = 200 mA (incl. 10% transmission losses)	P_{tot}/N_{cav}	292 kW	70 kW (75 kW @ 5.7 MV with 1 cavity off)
Total RF power at 200 mA (incl. 10% transmission losses)	P_{tot} at 200 mA	1460 kW	980 kW

Table 2.29: Main storage ring parameters for the dimensioning of the RF system.

During the last few years, the storage ring was operated with five instead of nominally six five-cell cavities and an accelerating voltage of 8 MV instead of the former 9 MV.

Figures 2.57 and 2.58 show the three HOM damped cavities recently installed in cell 23 (Jacob J. *et al.,* 2011) and the three 150 kW solid state amplifiers (Jacob J. *et al.,* 2013), that power them. With these systems, the ring is again being operated at between 9 and 9.5 MV, yet the figures for 8 MV were chosen for the comparison of **Table 2.29**.

With an RF voltage of 8 MV in the existing storage ring, depending on the filling pattern and the particular chromaticity setting, the RF energy acceptance of 2.9% is in the range of the dynamic energy acceptance and doesn't substantially limit the lifetime. The computed energy acceptance of the new S28A lattice is below 3%, however, further optimisation is under way to enhance this value and to maximise the Touschek lifetime which is still rather short. The new RF system is dimensioned for 6 MV providing 4.9% of RF energy acceptance in anticipation of expected lattice improvements.

Selection of cavities

The threshold for a longitudinal coupled bunch instability (LCBI) driven by a higher order monopole resonance of a cavity with the shunt resistance R_{HOM} at the frequency f_{HOM} is:

$$I_{threshold} = \frac{2 f_s E/e}{\alpha f_{HOM} R_{HOM} f_0 \tau_s}$$

(see **Table 2.29** for definition of symbols)

The new storage ring has the same energy and about the same circumference, so for given HOMs, the LCBI thresholds scale according to:

$$I_{threshold} \sim \frac{f_s}{\alpha \tau_s}$$

and are thus lower by a factor 1.9 for the new S28A lattice than for the existing storage ring. A careful HOM tuning by controlling the temperature of the cooling water for each of the existing five-cell cavities to less than ± 0.05 deg C allowed the instability thresholds to be pushed from 60 mA to more than 200 mA. However, 300 mA could only be reached during accelerator development shifts by using a longitudinal bunch-by-bunch feedback system. To prepare for safe operation at higher currents without a permanently active feedback system, the development of single cell HOM damped cavities was launched ten years ago. As the new S28A lattice will be twice as sensitive to LCBI's, only HOM damped cavities will allow the design current of 200 mA to be stored. With 15 such cavities in the ring, the current thresholds for HOM driven LCBI's will be well above 1 A.

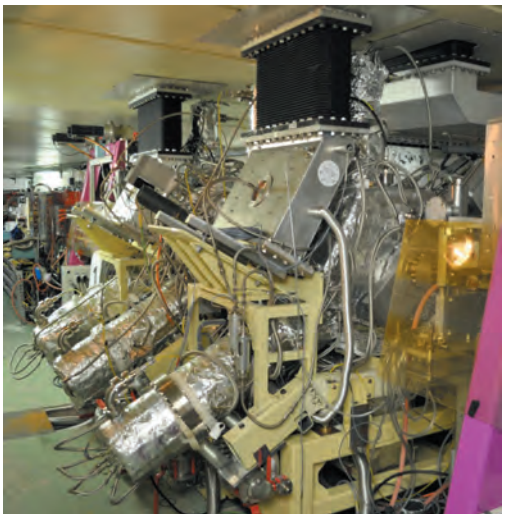

Figure 2.57: Three HOM damped cavities developed within Upgrade Phase I, now in operation on the 7 m long cell 23 of the storage ring.

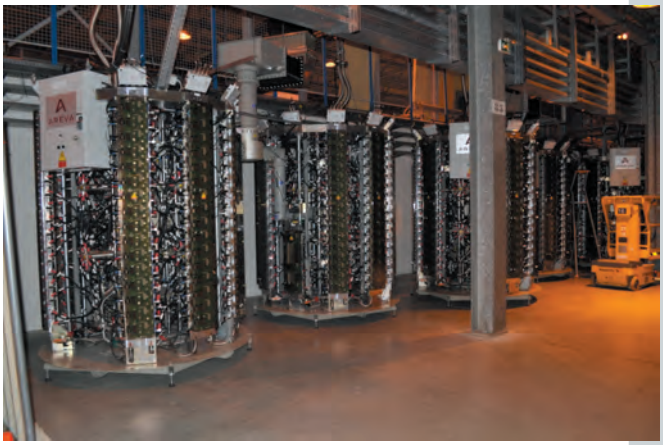

Figure 2.58: 150 kW Solid state amplifiers delivered by ELTA/AREVA, powering three HOM damped cavities in cell 23 – each SSA combines the power from two 75 kW towers.

The nominal RF voltage being 0.5 MV per single cell HOM damped cavity, the baseline RF design foresees the installation of 14 or 15 cavities, thereby providing a reasonable operational margin for voltage and power per unit, even in case one or two units should fail. To complement the 3 fully operational prototypes of cell 23, another 12 HOM damped cavities were ordered in December 2013 with a delivery scheduled for end of February 2016. For the time being, it is planned to install the new cavities during the installation shutdown in 2018.

RF power requirements

The beam loading diagram in **Figure 2.59** shows that, with a coupling of 3.2, the RF system will be perfectly matched at 200 mA with 14 cavities in operation at a total of 6 MV accelerating voltage. This will require 890 kW of power to be fed to the cavities. A total generator power of 980 kW will

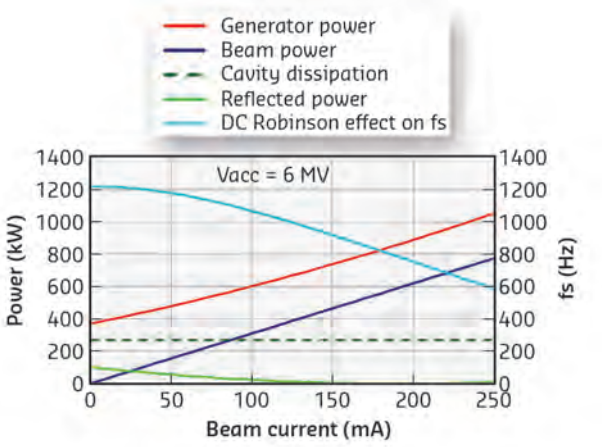

Figure 2.59: Beam loading diagram for 14 single cell HOM damped cavities in the new storage ring with a S28 lattice, coupling b = 3.2, transmission losses not included.

have to be provided at 200 mA if one includes 10% RF transmission losses (see also Table 2.29), corresponding to a reduction by 900 kW of the required wall-plug power (assuming 50% efficiency of the RF system), compared to the RF system of the existing storage ring.

2.4.7.2. RF TRANSMITTERS

The existing storage ring has been operated for 16 years with three 1.1 MW klystron transmitters (TRA1, TRA2 and TRA3). Three 150 kW SSAs are now powering the first three HOM damped cavities. To limit the cost, it is planned to start the new storage ring by re-using the existing RF power sources. Figure 2.60 shows the RF layout that will allow powering 14 or 15 cavities installed in the existing RF sections in cells 5, 7 and 25.

Re-use existing klystron transmitters

Today, the klystron transmitters TRA1 and TRA2 can be switched to the 4 five-cell cavities in cells 5 and 7: their power is then split into 8 to power two couplers per cavity. In the upgrade scenario, a similar splitting will allow 8 out of the 10 single cell cavities of cells 5 and 7 to be fed, thereby also keeping the TRA1/TRA2 redundancy. Note that these klystrons will be operated at about 550 kW, *i.e.* about half of today's value of 1 to 1.1 MW.

Re-use existing solid state amplifiers

As shown in Table 2.29, a single cavity will require at maximum 75 kW transmitter power including transmission losses when only 13 cavities are in operation at 5.7 MV total RF voltage, *i.e.* when one or two cavities are switched off. This is half

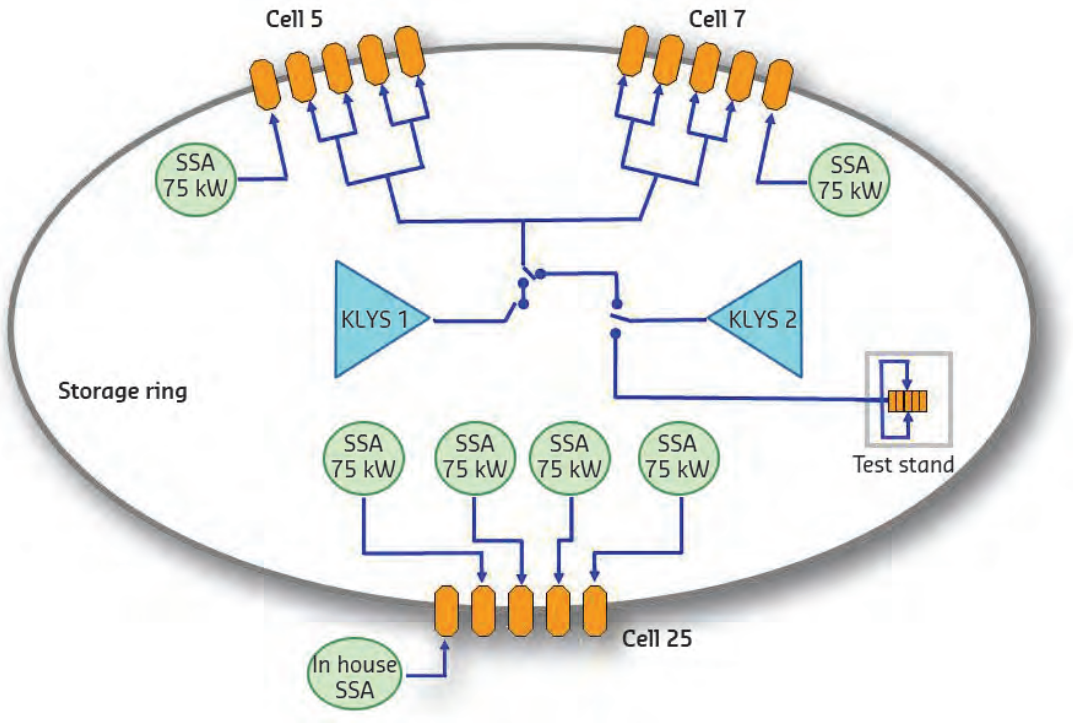

Figure 2.60: RF layout for the new lattice with 14 to 15 single cell HOM damped cavities installed in the old RF sections of cells 5, 7 and 25, and powered by existing klystron and solid state transmitters.

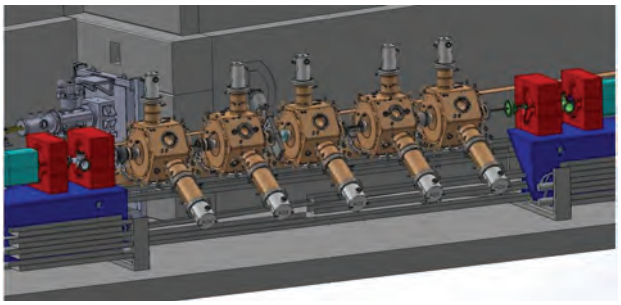

Figure 2.61:
Installation of five cavities in one straight section.

the nominal power of the three 150 kW SSAs in Figure 2.57, which presently feed the new cavities in cell 23. For the new storage ring it is thus foreseen to separate the two towers of each SSA to obtain 6 SSAs delivering 75 kW each. Thanks to the modular design of the SSAs, splitting them will be straightforward – and this will be tested on cell 23 in the coming year. The 75 kW SSAs will be removed from their present location on cell 23 to be connected to one cavity in each of cells 5 and 7 and to 4 cavities in cell 25. In parallel, a further 75 to 90 kW SSA using a cavity combiner is currently under development (Jacob J. *et al.,* 2013). This could be used to power a fifteenth cavity that would be installed in cell 25 to provide additional modularity and redundancy and to further increase the reliability of the system. Note that it is foreseen to dismantle the existing klystron transmitter TRA3 in cell 25 as that klystron will be replaced by SSAs.

Power circulators for the SSAs

Each of the hundreds of individual transistor modules of the SSAs is protected against reverse power by means of a small circulator and a load. Nevertheless, the high power output of each SSA needs to be protected against excessive reverse power, which can, for instance, be generated in the cavity by the beam. Today, this protection requires tripping the beam if a single SSA is in fault. In order to fully benefit from the modularity and redundancy of the SSAs, it is planned to add 100 kW circulators at their output, which will drain excessive reverse power to a dummy load. If then a single SSA trips, it will no longer be necessary to kill the beam and interrupt the service to users.

2.4.7.3. RF STRAIGHT SECTION LAYOUT

As shown in Figure 2.61, a straight section of the new lattice S28A provides enough space for 5 HOM damped cavities, the necessary tapers, bellows and photon absorbers; it will also contain a vacuum valve to allow separation of the cavities into two groups containing 2 and 3 cavities in order to limit the number of units to be vented in case of intervention involving the vacuum system.

2.4.7.4. HARMONIC CAVITY

To increase the Touschek lifetime, in particular for high currents per bunch, a lengthening of the bunches by means of a harmonic cavity could be envisioned. A harmonic to fundamental frequency ratio of 3 constitutes a good compromise between a large bunch elongation factor and a reasonable harmonic voltage. For the RF parameters in Table 2.29, this would be the case with a third harmonic voltage of 1.7 MV with a phase advance of 86° with respect to the bunch position. This could be obtained with a passive harmonic superconducting cavity with a strong inductive detuning, driven by the beam. With a single Super3HC type cavity (Bosland P. *et al.,* 2003), a scaling in frequency of the harmonic cavities at SLS and Elettra, the optimum voltage could easily be adjusted by controlling the inductive detuning between 89.93° for 40 mA up to 89.99° for 200 mA stored current. These angles are close to the optimum 86° to provide substantial bunch lengthening. Simulations carried out for the existing ESRF storage ring (Serrière V. *et al.,* 2002) indicate that the bunch elongation factor from a harmonic system would also be applicable to bunches that are already lengthened due to their interaction with the longitudinal broadband impedance of the ring. It is expected that this could lead to an overall increase in the lifetime by at least a factor 2. However, with gaps in the filling pattern such as for the 7/8 filling mode, the bunch lengthening would be affected by RF phase transients.

The design of a harmonic RF system for the new lattice deserves further investigation, which should include an update of beam simulations with a check of RF stability issues. The cost of a Super3HC type cavity can be estimated to be around 1 M€ for the superconducting cavity together with its cryostat and about 1 M€ for the required cryogenic plant. The implementation of a harmonic cavity will be considered after the construction of the new ring (2020), to be financed by the operation capital budget. Space will be reserved in the new storage ring for the later installation of a superconducting harmonic cavity.

2.4.8. DIAGNOSTIC AND FEEDBACK SYSTEMS

The diagnostic instruments will cover all the needs and requirements of beam measurements and characterisation, for all possible beam modes and currents of normal operation as well as during commissioning and detailed beam physics studies. Existing instruments will be re-used wherever possible. New or additional components and systems will aim at simplicity, cost-effectiveness and high reliability.

2.4.8.1. BEAM POSITION MONITORS

A total of 9 BPMs per cell will be needed, which is 2 more than the present storage ring, as specified in section 2.3.1.1. Also, the cross-section of the BPM chamber at the given locations will have different dimensions and geometry. This means that each BPM will have different mapping and calibration factors to calculate the beam position from its four pick-up button signals.

Each of the 288 BPMs will have the same functionality and performance characteristics as those of the present BPMs. They will have a measurement rate up to the turn-by-turn frequency, with the highest possible resolution and with high reproducibility (or stability) with time and low drift or dependence on the beam parameters such as filling pattern and current. The typical target values are a position resolution of 3 nm and the stability with varying currents and filling patterns of 1 µm. This includes all drifts and movements including thermo-mechanical motions of the BPM block and vacuum chamber.

All the BPMs will be installed close to a bellows in order to allow the chamber to move (because of thermal dilation etc.), while keeping the BPMs themselves fixed in position to the adjacent quadrupole or to the girder. Stainless steel material will be used for the BPM blocks.

Button feed through design

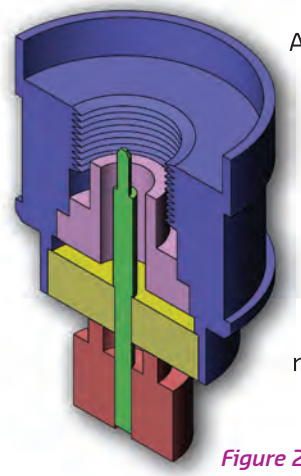

Figure 2.62: BPM block.

As in the present storage ring, a self-contained weldable BPM button & UHV feed through design has been adopted. The vacuum chamber design is compatible with a 6 mm button diameter for all the BPMs. The button design, the material choices inside that button and feed-through, and the geometry of the BPM chamber are optimised to minimise heating issues linked with trapped RF modes. The external body of the feed-through is of stainless steel and will be welded reliably and precisely to the (steel) BPM block. Prototype buttons have been designed in house and then fabricated to our specifications by two external companies. The Figure 2.62 shows a drawing of a button and its feed through.

A few BPM blocks will be built based on these buttons and installed in a straight-section of the storage ring in 2014. We will test their beam position monitoring performance and look for any over-heating problems.

Electronics for RF signal measurement

The present BPM electronics use Libera Brilliance units (from Instrumentation Technologies). Currently, 224 units are active in the present BPM system and the ESRF has an additional 30 spares. The failure rate of these units appears low and we expect in 2019 to still have 224 units in working order with a sufficient number of spares. This would provide 7 of the 9 BPMs required per cell. However, an additional 64 units (32 x 2) will be needed in complement.

As the Libera Brilliance is now commercially obsolete, the most logical choice would be to adopt its successor, the Libera Brilliance Plus from the same company. However, the Brilliance+ is distinctively different in its hardware structure (or platform) and also for its computer interface for control and data read-out. A Brilliance+ unit has been procured to test its performance and to implement a control interface for it. However, other alternatives for these 64 additional BPM electronics will be studied in the coming years as the final choice is not needed before 2017.

The BPM system will therefore be a hybrid system consisting of two main elements:

1. The existing Libera system for 224 BPMs, all integrated within a dedicated 10 kHz network for the Fast Orbit Control (FOC).
2. A new BPM system for the 64 additional BPMs. This system will aim to provide the same performance and functionality (resolution, reproducibility, turn-by-turn functionality, etc.) as the existing system.

The final choice for the new electronics will be largely determined by the ease of integration of the 64 additional BPMs into the existing network, which may prove to be very difficult.

2.4.8.2. FAST ORBIT CONTROL

The orbit correction for the new storage ring will use 288 BPMs and 160 horizontal and 160 vertical correctors, as specified in section 2.3.1.1. However, due to the probable hybrid structure of the BPM system, the suppression of fast orbit deviations, in the 0.01 Hz to 120 Hz range, will rely on the 224 BPMs using the present Libera electronics, and 128 fast correctors (compared to 96 correctors in the present system). The components of this system are interconnected through a dedicated 10 kHz data broadcast network. With this scheme we can easily reuse the present fast orbit correction system, thereby avoiding any new development for a fast orbit control for the new ring.

The number and position of correctors and BPMs has been optimised for optimal compensation of orbit perturbations caused by the insertion devices and by vibrations and drifts of the magnets.

2.4.8.3. EMITTANCE DIAGNOSTICS

Horizontal and vertical emittance measurements will be made mainly using the well established method of the X-ray pinhole camera. These devices will use X-rays from the 3-pole wigglers, serving as source for the so-called bending magnet beam ports. The spectral flux from these wigglers is perfectly suitable for the electron beam size measurement and very similar to the present pinhole configuration. The lattice functions as well as the pinhole magnification of roughly M = 2.2 (given by the distances between source, pinhole and detector) are such that the electron beamsize can be fully resolved in both planes without needing complex or expensive X-ray imaging systems.

A considerably large number of pinhole cameras may be installed around the storage ring, since very likely not all of the 32 available 3-pole wiggler ports will serve beamlines. The beamports will be equipped with a specially adapted absorber and a water cooled Al-window (vacuum-air interface).

The same pinhole camera systems can be temporarily adapted or re-configured to also measure, during the initial and possibly delicate commissioning phase, the large beam sizes when the stored beam at that time is still very far from the ultimate targeted values of coupling and beamsize.

Possibilities of installing X-ray projection monitors measuring only the vertical beamsize at various locations around the storage ring are under investigation. These devices would not be dedicated to precision measurements but allow the survey and comparison with the accelerator model of the coupling around the storage ring.

Beamline ID14 is already dedicated to beam diagnostics and other accelerator and source activities. More exotic emittance diagnostics (*e.g.* using undulator radiation) may be installed at this beamline at a later time.

2.4.8.4. BEAM LOSS MONITORS

The existing 64 beam loss monitors (2 per cell) can be re-used and will be complemented by an additional 64 units of similar functionality but with a number of improvements such as reduction of overall size, speed of measurement, linearity and measurement range, and they will also use modern components for radiation scintillators, photon detectors and acquisition electronics.

The present set of available beam loss monitors (BLM) use heavy and cumbersome lead shielding to prevent the scintillator material used from reacting to scattered X-ray photons. The need for shielding of the new additional BLMs could be avoided by using Cherenkov radiation monitors, insensitive to X-rays, detecting only electrons and positrons in the electro-magnetic shower produced by the loss of the primary 6 GeV electrons. A typical scintillator material for this purpose would be pure quartz or silica. Another improvement could be on the visible light detector component: the photo-multiplier tubes presently used have drawbacks such as limitations in their linearity and measurement range, and even their dependence on magnetic fields. Modern semi-conductor components may offer improvements but their robustness in a hostile radiation environment needs to be verified.

The development of prototypes first for this set of 64 additional monitors will benefit from the possibility to test and assess their functionality and performance but also their robustness in the present ring and in direct comparison with the existing BLMs.

2.4.8.5. BUNCH-BY-BUNCH FEEDBACK SYSTEM

Both vertical and horizontal bunch by bunch feedback systems will be implemented by reusing the electronics of the systems in the present ring. They allow damping of coupled bunch modes of oscillations with a damping time as low as 20 turns. The noise contribution of the electronics is negligible compared to an overall apparent emittance reaching as low as 3 pm.rad, which is the lowest vertical emittance achieved so far with the present ring. The combined operation of the feedback system with hybrid filling of a highly charged single bunch and uniform filling of the 7/8 part of the 992 buckets is also possible.

We will need to add a set of BPM pickups at high beta locations to provide the input signals to the feedback systems and a set of stripline kickers to apply the damping kicks to the beam.

Due to the use of HOM damped cavities, no longitudinal feedback system should be necessary; however we will most likely reinstall the longitudinal feedback system of the present ring which can be useful for diagnostic purposes.

2.4.8.6. OTHER IN-VACUUM DIAGNOSTIC ELEMENTS

A dedicated space of 250 mm to 300 mm, located in the downstream part of the cell (Drift tube right downstream CH10, see **Figure 2.47**), has been reserved in each cell to implement specific diagnostics.

A first set of horizontal scrapers (with internal and external jaws) will be implemented in the injection cell, close to the septum magnet. A second set of horizontal scrapers will be installed at a high dispersive section of the storage ring. The main function of these horizontal scrapers is to concentrate as much as possible the electron beam losses into one section only and thereby avoiding losses and the subsequent radiation dose related issues elsewhere in the ring. This should be true for losses due to insertion devices and for those from the natural beam current decay.

The exact design of the horizontal scrapers is still to be elaborated; it should take into account the compatibility of this device with the radiation dose that it will accumulate over time.

In addition, one or two pairs of vertical scrapers will be implemented.

The beam current measurement will be made using the existing current transformers: parametrical current transformers (PCT) for the DC current and integrated current transformers (ICT) for the single bunch current. Ceramic gap vacuum chambers and their associated RF shielding and cooling components will be designed to fit into the available space for diagnostics equipment in the storage ring. If the space constraints allow, one PCT and one ICT will be grouped together, thereby only needing one ceramic gap chamber per group. However, if space is insufficient, PCTs and ICTs can be installed independently at different points in the ring, but in this case each of the current transformers needs its own ceramic gap chamber. For reasons of redundancy, a total of two PCTs and two ICTs will be installed in the ring.

Two kinds of striplines will be implemented: pick-up striplines that will be used as wide bandwidth, high sensitivity, general purpose beam signal pickups, and kicker striplines that will be used to act upon the beam as instability dampers in the bunch by bunch transverse instability feedback systems.

For the latter, the design parameters aim at achieving a good transverse shunt impedance up to 200 MHz while minimising the impedance at frequencies above 200 MHz. We also need to implement them in locations with sufficiently high vertical or horizontal beta values for the respective kickers.

The design of these new kickers will in principle be similar to those already used in the present ring. However, with the reduced vacuum pipe diameter, we intend to develop a prototype at dimensions very close to that for the new ring, and test it with beam in a straight-section of the existing storage ring in 2015 to verify its satisfactory functioning.

A number of specific detectors will be dedicated to interlock systems that should protect the components in the ring from damage, notably the vacuum chambers from heat load damage, in case of abnormal beam conditions such as excessive position offsets or beam size. A specific system for emergency protection (the so-called beam killer) needs to be re-installed. It consists of an obstacle that is rapidly inserted into the electron beam path in case all other means of dumping the electron beam (switching off RF transmitters or dipole magnets) are ineffective, for whatever reason.

The use of visible synchrotron light in diagnostics serves many different purposes.

For instance, for determination of bunch length with a streak camera, a precise bunch population (or bunch purity) measurement with a time-correlated photon counter system, together with a beamsize measurement through classical optical imaging methods. The latter has the advantage of being highly sensitive and capable of easily measuring large electron beam dimensions. However, due to diffraction at these visible light wavelengths, it cannot resolve the ultimately small electron beam sizes. However, different systems that use the interference properties of visible light can overcome this limitation and could also be implemented.

All these systems need to be installed in a dedicated laboratory space and to be provided with visible synchrotron light through a light extraction system that starts, still within the UHV region, with a mirror behind the dipole magnet serving as the source of the light. In the present ring a small laboratory space of about 20 m^2 in the experimental hall accommodates the aforementioned instruments. The visible light is guided into this laboratory through a 10 cm wide hole in the tunnel wall and through additional radiation shielding structures for compatibility with radiation safety.

To reuse the same optical laboratory with the new light extraction system is planned, arranged so that the visible light will be guided through the existing passages. Nevertheless, this may require substantial reinforcement of the radiation shielding. The new light extraction system will be more complex since the dipole magnet to be used for the source will be at a completely different position than it is today. This complexity concerns both the first mirror that is inside vacuum and has to deal with the heat load of the X-rays, as well as a set of up to 2 or 3 further mirrors that need to be controlled remotely for position and orientation.

2.4.9. INJECTOR UPGRADE

Upgrading the injector was foreseen for top-up operation within Phase I of the Upgrade, scheduled by the end of 2015. This upgrade is mandatory for the implementation of Phase II as the new storage ring will require top-up operation. The actual injector, which consists of a 180 MeV linac and a 6 GeV booster synchrotron, is now ageing and was not designed for top-up operation. The most critical devices will therefore be upgraded to optimise redundancy and to prepare the hardware for a higher injection frequency. Finally, a few topics are described for the new storage ring as part of the Phase II of the Upgrade.

2.4.9.1. TOP-UP IMPLEMENTATION

Power supplies upgrade

The booster magnet power supplies based on a 10 Hz resonant circuit will be replaced by ramped power supplies. Their design has been inspired by the power supplies implemented at SOLEIL and ALBA and relies on IGBT technology (insulated-gate bipolar transistor).

To avoid French regulation concerning high voltage, the maximum voltage should stay below 1500 volt DC limiting the maximum repetition rate to 4 Hz. The optimised waveforms for the dipole power supplies are plotted on Figure 2.63 as well as the block diagram of the hardware Figure 2.64. The 5 kV distribution hardware has already been implemented and will allow switching between the old resonant power supply and the new one within an hour, ensuring redundancy of the power supplies. Magnet current measurement with a dynamic range of 10^6 has been implemented and will allow a regulation of the tunes with a precision better than 0.01 units or 10 kHz. The power supplies should be operational by 2016.

Additional RF cavities

Two RF cavities ensure the RF voltage of 7 MV required to accelerate the beam at 6 GeV. If one fails, the booster cannot be operated and no injection is possible. Each cavity is fed by 2 SSA RF amplifiers. The limits of the system are defined by the maximum voltage achievable in a cavity and the power supply of the SSA amplifiers. Therefore, we plan to complement the existing system with two more cavities. Some space is available close to the present cavities for their installation. The 4 cavities will be individually fed by the SSA amplifiers (which will be rearranged). The overall RF cavity shunt impedance will double, thus resulting in cutting in half the total RF power for a given voltage. The maximum achievable voltage will increase by 40%, which could help in reducing the bunch length for better injection efficiency. This solution will also provide redundancy, as 7 MV will be achievable with only 3 (out of 4) cavities in operation: thus increasing the reliability for top-up operation. Their installation is foreseen for the end of 2015.

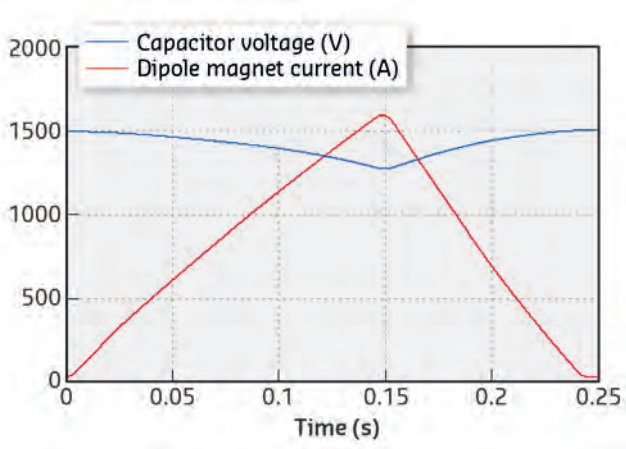

Figure 2.63: Current and voltage waveform.

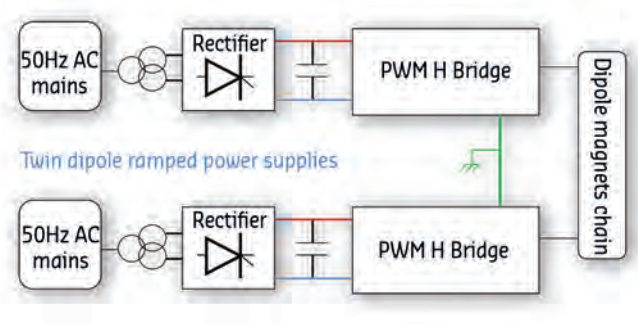

Figure 2.64: Block diagram of the dipole power supplies.

Linac upgrade

An upgrade of the actual linac to improve its reliability for top-up operation began a few years ago and includes:

- Replacement of the buncher, keeping the old one as spare. This will be completed by the end of 2014.
- Installation of a third modulator that could replace either of the two modulators used to operate the linac. This modulator will be operated via simple wave guide and cable switching and it will be commissioned in 2014.
- Replacement of all ageing power supplies for beam focalisation and steering.

Bunch cleaning in the booster

Top-up operation for time structure modes will require bunch cleaning in the injector. A system already exists that uses a strip-line kicker for resonant excitation of the impurities. The excitation drops to zero at the passage of the main bunches via a phase inversion of the excitation signal. This system did not give satisfactory results as the shot to shot reproducibility of the tunes was not stable enough, while the excitation frequency was fixed. A feedback system will be implemented based on a precise measurement of the booster magnet current to properly drive the excitation frequency.

In parallel, a scheme for bunch selection at booster injection has also been foreseen. The impurities are known to originate from the linac accelerating structures. Using a fast kicker as injection kicker in the booster will enable only the main bunches to be injected while eliminating the impurities. The existing kicker is a magnet kicker with a 1 µs flat top that fills the whole circumference of the booster. Below 25% of the nominal kick, the injection efficiency in the booster goes to zero (**Figure 2.65**) in order to selectively inject individual bunches. We plan to keep the present kicker in place, operating at reduced amplitude, and add next to it a 50 cm strip-line kicker powered by a 2·15 kV pulse generator which provides a pulse width of 2-3 ns. The feed-through, strip-line, and their implementation in the ring have now been designed, the pulse generator has been ordered, and we expect first tests to be performed in 2014 for a full installation and test by the end of 2015. The first set up will provide proof of principle and can later be extended for further needs in terms of number of pulses, effective pulse width and amplitude.

2.4.9.2. INJECTOR ADAPTATION FOR THE NEW LATTICE

Emittance decrease of the injected beam

As described in section 2.3.5 the injection efficiency increases with a lower emittance from the booster. This can be achieved by increasing the RF frequency with respect to the nominal frequency. **Figure 2.66** shows the horizontal emittance and bunch length versus the RF frequency offset. Also shown in this figure is the induced RMS horizontal orbit, which limits the maximum frequency shift achievable. An increase of the RF frequency by 40 kHz has already been successfully tested.

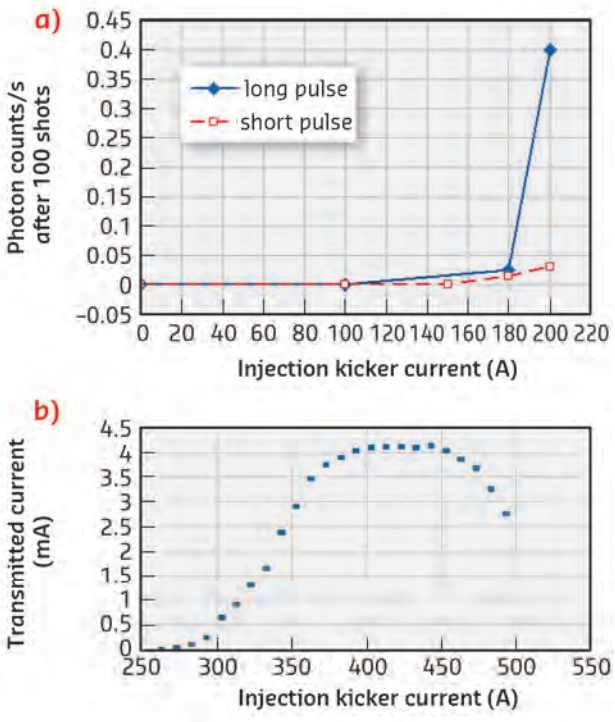

Figure 2.65: a) No trace of beam injected after 100 injected pulses, for injection kicker current below 100 A while optimised injection (b) is reached for a current range from 400 to 440 A.

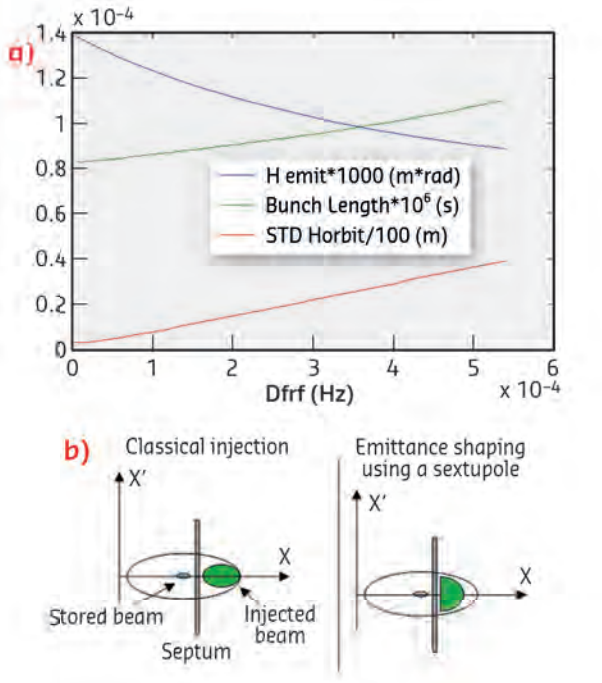

Figure 2.66: (a) H emittance bunch length and horizontal RMS orbit versus RF frequency mismatch. (b) Principle of emittance shaping using a sextupole to reduce beam offset at injection.

Reducing horizontal emittance can also be achieved by fully coupling horizontal and vertical motion via equal tunes. However, its benefit on the injection efficiency will depend on the vertical acceptance.

Phase space manipulation

A sextupole could be installed in the TL2 transfer line at a proper location, separated by a 90 degree horizontal phase advance with respect to the septum. This will shape the beam phase space as shown in Figure 2.66, so that the beam centre of mass gets closer to the septum. Implementation will require the exchange of a quadrupole by a sextupole (one of the existing ESRF sextupoles can be used) in the TL2 transfer line.

Orbit control in the injector

A full refurbishment of the BPM electronics has been scheduled for 2015. This will be coupled with the implementation of an orbit correction scheme based on quadrupole displacement in the booster. Sixteen quadrupoles will be equipped with moving supports enabling orbit correction at any energy of the cycle while the present DC correctors only work at injection energy. Four motor axes have already been installed and they have allowed the RMS horizontal orbit to be reduced from 1.7 mm to 1.2 mm. The TL2 transfer line will be equipped with single pass BPM's, allowing a full control and possibly some orbit feed-back.

Circumference reduction and new injection layout

Since the RF frequency has to be increased by 171 kHz due to the new storage ring being shorter, the RF cavities have to be retuned by adjusting the piston tuners. We also have to reduce the booster radius by about 1.9 cm. In fact, it will only need to be decreased by 1.3 cm in order to reduce the equilibrium horizontal emittance as described above.

Most of the girders have sufficient adjustment margin, however special sections such as injection and extraction will have to be modified. The TL2 transfer line will also have to be modified because of the different booster extraction and storage ring injection positions. The injection layout changes will also involve the redesign of storage ring septum magnets and their power supplies.

2.4.10. CONTROL SYSTEM

The accelerator control system controls the entire accelerator complex in a precise and timely fashion. The most important roles of the system are interfacing with, configuring and controlling the equipment, reading and archiving the parameters and interacting with a database for online and offline analysis. The on-going programme of modernisation of the control system will be pursued during Phase II to ensure it stays state-of-the-art and serves the users in the best possible way.

The upgraded control system will provide smart diagnostic and analysis tools. It will sample data at the highest possible rate, manage archiving and provide powerful tools for analysis.

Phase II of the Upgrade of the control system will focus on the following points:

- Increase the sampling rate and long-term archiving of the control data.
- Provide new tools for analysing control data for online and offline analysis.
- Replace the timing system and improve the accuracy of time stamping.
- Provide better synchronisation of the beamlines with the source for data acquisition and insertion device control.
- Develop device servers for the many new types of equipment.
- Continue modernising the TANGO control system and the infrastructure.

2.4.10.1. THE TANGO CONTROL SYSTEM

The TANGO control system was initiated at the ESRF for the accelerator and beamlines in 2000 (ref: www.tango-controls.org). The project was joined soon after by the Soleil Synchrotron, then, later by the majority of the other light sources in Europe. TANGO has continued to be improved, its development was carried out collaboratively. Now it has become the *de-facto* standard control system for accelerator based light sources in Europe. The large community of users guarantees the long term continuity of the system and allows fruitful exchange between the different synchrotron facilities and industrial partners sharing the same technology. Thanks to its continuous development, the present system is ready to tackle the control of the Phase II accelerator complex with no critical challenges foreseen in terms of software characteristics. TANGO is based on the concept of distributed objects which is still considered state-of-the art.

TANGO has been benchmarked as the fastest control system for sending binary data via events. Future improvements will accelerate TANGO such that it will be possible to make use of feedback loops in real time, which is required for the upgrade Phase II. Other extensions are foreseen such as the opening to new embedded platforms, mobile devices or the web interface.

The accelerator upgrade is also an opportunity to finish the modernisation of the existing control system and eliminate obsolete parts such as the ageing RF klystron control system.

2.4.10.2. A HIGH PERFORMANCE HISTORY DATABASE

The present accelerator history database (HDB) was designed 20 years ago to archive a limited number of signals at a rate that was much lower than that needed for the future storage ring. The system had since been interfaced to TANGO so that the majority of data is now obtained from TANGO device servers. Both the hardware and the software need to be redesigned to match new specifications (**Table 2.30**).

We need to increase the data rate by an order of magnitude and multiply by 4 the number of archived signals. Requirements are therefore for 40 times more disk space and data throughput.

Through the TANGO collaboration, we have started a new history database project in collaboration with the Elettra facility. We are redesigning the TANGO archiver to increase the bandwidth, the volume of data and the time resolution from a second to a millisecond. Furthermore, we intend to profit from the new big data oriented databases that have recently appeared and are being used in big data cloud applications. The data will be replicated on multiple servers and therefore the system is, by design, fault tolerant without compromising performance.

The new historical database will be operational before the shutdown of the current accelerator to validate its performance. In addition, it will allow the storage of reference data to be used for the start-up.

Fast temporary history buffers

We will enhance the use of local polling buffers to build a massively distributed temporary circular history buffer for the last few days of acquisition. This data will be accessible with a software oscilloscope tool (see **Figure 2.67**) which will enable users to diagnose and delete problems by carrying out common analyses such as spectral, FFT and digital correlation. A similar tool has already been developed for the vacuum and insertion devices during Phase I. This will be very useful during the equipment commissioning period and for the first tests of the new lattice. It will allow a wide variety of signals to be monitored and cross-correlated while using a frequency of up 1 kHz. This temporary buffer will fill the gap between the history database sampling storage and the BPM fast data logger (10 kHz).

2.4.10.3. TIME STAMPING

The time resolution of the archiving system and the temporary buffer has been increased. However, time stamping is still not accurate enough. The control system is distributed over hundreds of computers separated by hundred of metres of Ethernet cable. To keep a correct time stamp, we have to work on 2 different aspects:

1. System clock synchronisation: to ensure that the clock of each host is synchronised; detect de-synchronisation and issue an alarm in such a case. Develop enhanced diagnostic tools for monitoring the correct timing of each host; Replace the network time protocol (NTP) with the precision time protocol (PTP) for distributing the time with sub-microsecond precision.
2. Conserve timestamp: to keep track of the initial time stamp while processing the data in high level software.

	Present HDB	Future HDB
Time precision	1 second	1 millisecond
Total number of Insertions/hour	120 k	6 M
Filling mode	Polling/events	Events
No. Signals total	6 k actives/14 k total	24 k/56 k
Beamline signals	2 k	10 k
Extraction tools	C GUI	Java/python/matlab/web
Database size	0.5 TB/y	20 TB/y
Online capacity	9 months online 5 years archive Older data on tape	Unlimited online
Database	Oracle	MySql/NoSql

Table 2.30: Characteristics of present versus future history database.

2.4.10.4. SYNCHRONISATION SYSTEM

The synchronisation and clock distribution system of the accelerator system is based on a 25 years old design. It works well but is difficult to extend and it is not flexible enough to allow rapid modification and enhancement. The current system is made up of three separate systems:

1. The bunch clock or fast timing, distributing timing based on the RF frequency period of 2.8 ns and the storage ring revolution frequency of 2.5 microseconds. This system manages the filling pattern and triggers acquisition based on the beam bunches.
2. The slow timing is based on VME programmable delay units (VPDU) and is in charge of distributing delays of a few milliseconds with nanosecond resolution to all the Injection elements. This slow timing is synchronised with the 10 Hz injection clock.
3. The computing network time protocol is used to synchronise the clocks of all the computers.

The accelerator upgrade is the opportunity to design a new synchronisation system to replace both the fast and slow timing systems with a resolution from nanoseconds to seconds. The new system will be easily extendable and reconfigurable. We also aim to distribute the radio-frequency, the revolution frequency trigger and the injection triggers to all beamlines to enable synchronous acquisition.

Several systems used in other accelerator complexes are available today. The first study we have made shows the White-Rabbit system developed and used at CERN for the LHC to have advantages. This synchronisation system has excellent characteristics in terms of low jitter and has benefits in its configurability and flexibility. Furthermore, since it is based on an open standard, it allows products from different suppliers to be integrated.

This system is an extension of the standard precision time protocol (PTP) that will be used to distribute the computer clock over our entire computing infrastructure. It will allow the triggering of the data acquisition system and the time stamping of the data.

2.4.10.5. HIGH LEVEL SOFTWARE

The update of graphical user interfaces and high-level interfaces written with obsolete toolkits are on-going and will be completed during Phase II. The TANGO sequencing tool will be used to automate standard operation actions and increase the efficiency of diagnostic tools. The interactive command line (Itango) will be implemented and used during commissioning of equipment to build flexible test sequences. The high-level interface of TANGO with commercial tools such as Matlab or Labview will greatly ease the commissioning, allowing fast and flexible development of applications.

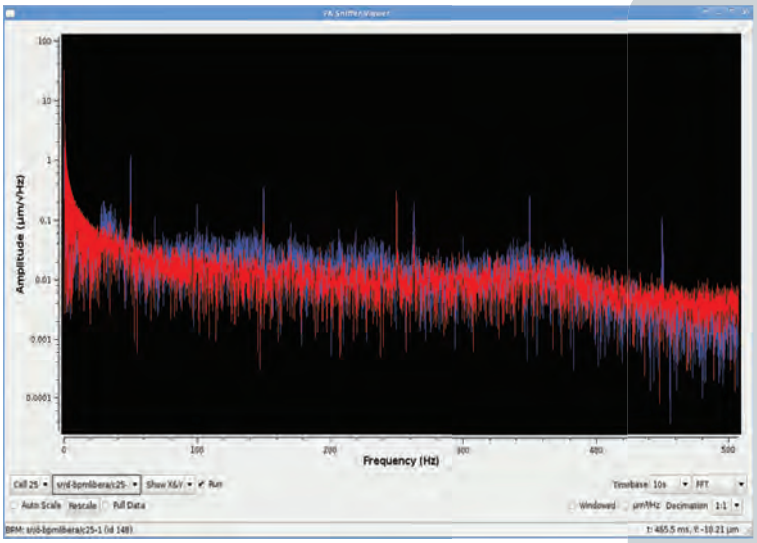

Figure 2.67: Software oscilloscope application for fast temporary history buffers.

2.4.10.6. IMPROVE SERVICE TO BEAMLINES

All beam parameters including beam position signals, tune, and emittance will be made available to the beamlines with accurate time stamping.

The new timing system will be distributed to the beamlines allowing for the synchronisation of data-acquisition with the revolution frequency, the bunch clock or the topping up signal. The use of the precise time protocol (PTP) on both the accelerator and beamlines means that control data and software processes will be synchronised with higher precision (microsecond).

2.4.10.7. SPECIFIC REQUIREMENTS FOR THE ACCELERATOR PROJECT

Network and computing infrastructure

The accelerator upgrade foresees thousands of new Ethernet connected devices for the new individual magnet power supplies, BPMs, various diagnostics, gigabit Ethernet cameras, etc.

An evaluation of the needs has to be made in order to forecast the necessary infrastructure. Due to the large number of new connections required for Phase II, the option of low cost private network connections based on commodity hardware (copper cables to multi-port network cards mounted in PCs) will be studied in order to lower the budget.

The computing infrastructure will follow the current development trends, *i.e.* virtualisation, SSD, multi-core architecture.

Electronic equipment interfaces

The upgrade of the accelerator will lead to the design of various new acquisition systems (injector, power-supplies, radio-frequency, beam diagnostics, vacuum, etc.). This could result in a large number of different hardware interfaces and may become difficult to manage and maintain in the long term. Furthermore, multiplying the hardware interface types will have a high impact on software workload. To be efficient, the electronic hardware choices need to be limited and standardised. Dedicated solutions should be used for specific functionalities and requirements.

Device server software

Many software interfaces and device servers will have to be developed.

Software should be ready and adapted to the different phases of the equipment (test, commissioning and operation). The control requirements and consequent workload should be identified as early as possible to adapt resources and planning.

The specification for the control software will be possible only after the final design of the hardware of each sub-system. Therefore, the control group will face high peak load in the year 2016-2017 at the same time in many different fields. Consequently, one or two peak-load engineers will be recruited. The large TANGO community will facilitate setting up collaboration with other European institutes for development of new elements of the accelerator control system. In addition, this workload can also be absorbed by subcontracting to companies with TANGO expertise.

PART 2
ACCELERATOR AND SOURCE UPGRADE

2.5. PROJECT IMPLEMENTATION

Overview

The accelerator project has to be carried on while maintaining operational performances of the facility. Its implementation within the existing tunnel is also a complex and a manpower intensive task. Many aspects have to be considered and good coordination between the different activities will be essential. A proper organisation of the resources and tasks involved has to be ensured.

A risk management process will be necessary. The project organisation will guarantee that risk assessment will be carried out periodically and in a timely manner for all the activities. It will also ensure that, where necessary, effective mitigation actions will be taken.

The Upgrade Phase II project will be managed using the present resources, procedures, support and organisation. Flexibility will be required to ensure the execution of such a large project while maintaining an operational facility.

Radiation safety is a key issue, since it has to deal with the proper disposal of the removed equipment and with the operation of the new accelerator according to French regulations and ESRF policies.

The timescale for procurement, assembly, installation and commissioning had already been defined in the white paper (ESRF, 2012) and has since been updated as the project has progressed. The overall time-envelope of the project is well defined and we will try to adopt all the solutions necessary to avoid significant changes to this.

Solutions have been found to provide the necessary space for storage and preassembly. A few modifications to the conventional facilities will be necessary for construction, but also for subsequent operations. The compatibility of the activities with the standard user mode operation of the facility up to the shutdown for installation has also been ensured.

2.5.1. ACCELERATOR PROJECT IMPLEMENTATION SCHEDULE

2.5.1.1. PROJECT SCHEDULE

The project timeline is based on a best knowledge estimation at the time of writing. The timeline will be validated by the middle of 2015.

Initiated in 2012, the overall accelerator project schedule extends over 8.5 years and will end on 31 December 2020. The main activities and their time-span is shown in **Figure 2.68**.

Design: Assuming launching of the project on the 1st January 2015, the engineering design of the new machine will be completed by mid 2017, although the level of detail of different parts will be finalised already during the procurement phase starting in 2015.

Prototyping: The design does not require new technologies to be validated, so no R&D is foreseen. However, prototypes will be needed to validate the design, finalise the engineering design of the fully assembled elements (*e.g.* magnets with supports on girders), and verify that the required tolerances can be achieved at industrial level.

The magnet prototyping has started in fall 2013. All prototypes will be ordered by the end of 2014 and will be validated by summer 2015. The prototypes will also allow the detailed engineering to be completed by the end of 2015 for all items related to the magnets (supports, cooling, etc.).

The prototype of a chamber with 3 new BPMs will be tested in the storage ring with beam by mid 2014.

The prototyping will allow the final design of all the components, including bellow shields, absorbers etc., to be validated and make possible the solving of related problems such as identifying the setup for baking.

Given the complexity of the system and the amount and variety of components, it is foreseen to complete the design of all components by the end of 2016.

Procurement and preassembly (Spring 2015 – Spring 2018): The calls for tender, selection of suppliers, follow-up of contracts and the manufacture and reception of equipment will take place in this period. The schedule will be determined according to the advancement level of the design and prototypes. Standard measures will be taken to avoid delays, such as the pre-qualification of companies. Off-the-shelf equipment such as some power supplies, vacuum instrumentation and diagnostics components will be ordered as soon as possible, spending profile permitting.

The logistics activities which also include some building modifications will start in mid 2015 in order to be ready for reception of the equipment in 2017.

The preassembly of the girders with all their hardware will start in fall 2017 and will continue until the end of 2018.

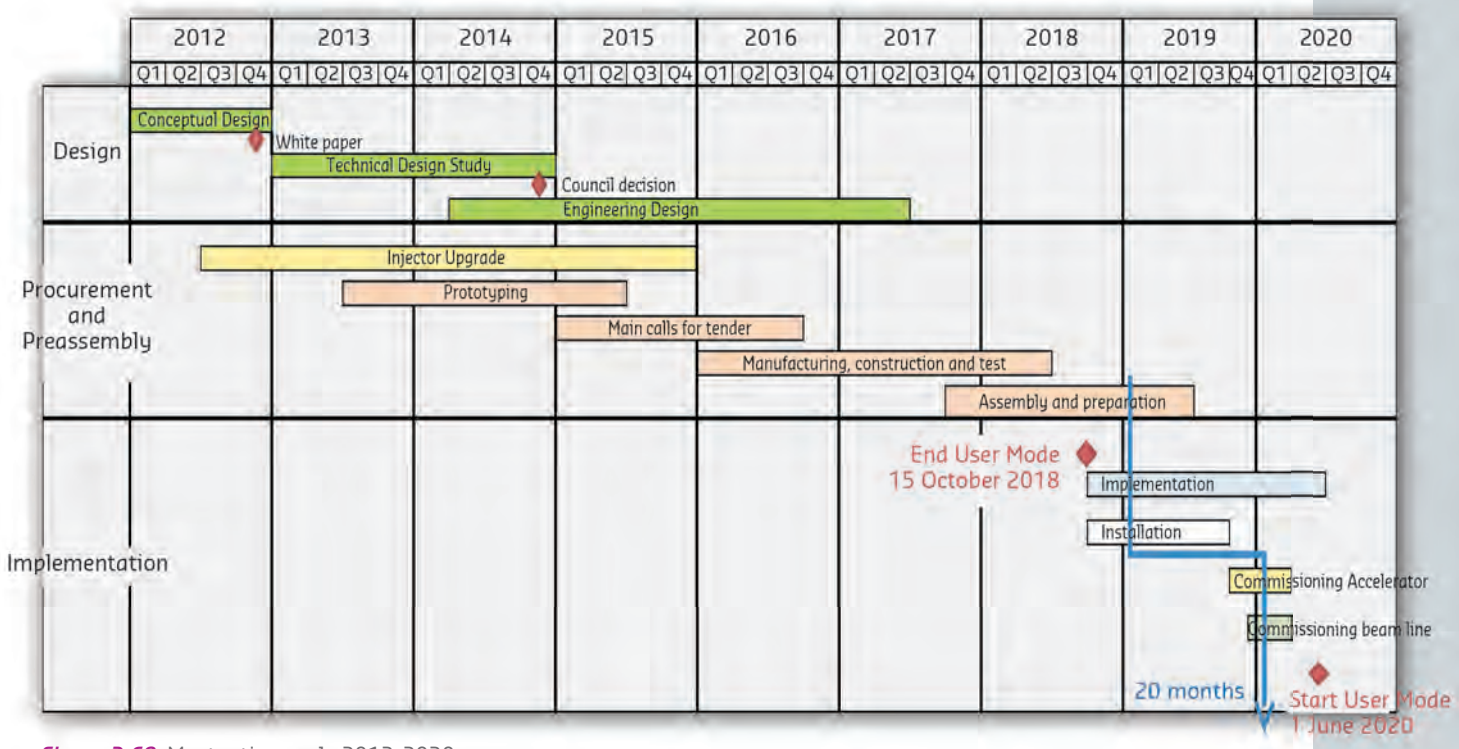

Figure 2.68: Master timescale 2012-2020.

Implementation: 15 October 2018 – until June 2020.

User operation will end on 14 October 2018 and will restart on 1 June 2020 after 19.5 months of shut-down. The implementation stage is composed of:

- Nine months for dismantling the present storage ring arcs and for the installation of the new hardware.
- Six months for commissioning of both the new storage ring and the beamlines.
- Four and a half months reserved for contingency.

2.5.2. PERSONNEL RESOURCES

Staff resources must be shared between the upgrade project and the operation of the facility. The ongoing Phase I projects (injector upgrade, RF, control) will occupy a large number of the Accelerator and Source Division (ASD) staff until 2015. Additionally, the beamline Phase I upgrade projects have to be completed before the engineering resources are fully available for the accelerator project. In 2014, about 28 full-time equivalent staff members have worked on the Technical Design Study. The ASD manpower is complemented by dedicated staff from the Instrumentation Service and Development Division (ISDD) covering control requirements, mechanical engineering and drafting. The Technical Infrastructure Division (TID) provides support for vacuum, alignment, building and infrastructure facilities. It is also in charge of the logistics for the implementation of the new lattice. The allocation of staff between the different tasks has to be managed very carefully and thoughtfully. From 2016 until full commissioning by June 2020, the accelerator upgrade will be the only project that the ASD will carry out. A detailed project management structure will be implemented, charged with the coordination of the necessary human resources. Temporary staff transfer from the other ESRF Divisions is envisaged, as well as the recruitment of peak load engineers and technicians. A detailed breakdown of the manpower requirement is being made and will be finalised by the beginning of 2015.

At the present stage of the project, we can draw up the following guidelines.

Design (28 FTE as per 2014)
The design will be mostly completed using ESRF expertise and resources. The work breakdown has been clarified and the engineering design is ongoing. The additional resources required have been identified and are under allocation. Collaborations with other institutes are also being considered and implemented.

2.5.3. PROCUREMENT AND MAIN CALLS FOR TENDER

Manufacturing, construction and test
Upon the finalisation of the design, the call for tender process will start. The associated resources for the specifications, the purchasing and the technical follow-up of the contracts is currently under preparation and assessment.

Implementation and installation
The installation phase will be developed and supervised internally with the support of external companies. The related cost has either been included in the overall implementation budget or in the individual tasks costing (cabling, piping, etc.). The final assembly will be executed and supervised by ESRF technical staff specialised in each field of activities. In order to limit the need of external support, we will identify all the ESRF staff that will be available to support the installation.

Test and commissioning
Equipment tests and commissioning of the new storage ring will be carried out by internal personnel.

2.5.4. SAFETY

2.5.4.1. GENERAL SAFETY ISSUES

The dismantling of the existing storage ring and the installation of the new one will present a number of safety issues, such as the manual and mechanical handling of many components, the safe coordination of contractors, etc. All of these potential hazards however are well within the remit of normal ESRF operations and will be managed accordingly using existing safety rules and procedures.

2.5.4.2. RADIATION PROTECTION ISSUES RELATED TO THE DISMANTLING

The operation of the ESRF is subject to an authorisation delivered by the French Nuclear Safety Authority (ASN). The upgrade of the accelerator facility, through Phase II of the Upgrade Programme, will require a new ASN authorisation. During preliminary discussions, ASN has indicated that the ESRF will have to submit successively two distinct authorisation requests, the first one concerning the dismantling of the existing storage ring and the second one concerning the installation and operation of the new storage ring. Both documents must include an impact study in terms of ionising radiation hazards for the workers, the public and the environment. The dismantling of the existing storage ring, in particular the evacuation of the accelerator components, could become particularly complicated due to the fact that the French radiation protection legislation does not foresee clearance levels for radioactive materials, as defined in the corresponding European Basic Safety Standards (Council Directive 96/29/Euratom, 1996). As a consequence of this, all accelerator components taken out of the storage ring tunnel should be considered as activated and, if no recycling is foreseen, should be treated as radioactive waste. The absence of clearance levels in the French legislation will also complicate trans-boundary movement of such components. Discussions with ASN on these issues are ongoing. In particular, the ESRF has asked the ASN to provide clear guidance concerning the radiation zoning in terms of waste classification to be adopted for the activation calculations to be included in the impact study. Preliminary activation calculations show that the activation of the large majority of the storage ring components is well below the 96/29/Euratom clearance levels. This will still hold with respect to the more stringent clearance levels defined in the recent Council Directive (Council Directive 2013/59/Euratom, 2014), which should be transposed by the Member States into their national laws before 6 February 2018.

2.5.4.3. INSTALLATION AND OPERATION RADIATION PROTECTION ISSUES

The second authorisation request to be submitted to the ASN concerns the installation and the operation of the new storage ring. Here the corresponding impact study must in particular include a detailed radiation shielding study for the new lattice. Since one of the boundary conditions of the Phase II Upgrade is to use existing infrastructures as much as possible, the shielding study must demonstrate that it will indeed be possible to operate the new facility without major upgrades of the existing shielding. One of the basic radiation protection requirements is the ALARA principle (as low as reasonably achievable). The impact study must clearly demonstrate how the ESRF applies the ALARA principle to minimise radiation hazards for workers, for the public and for the environment. In this context, the operation

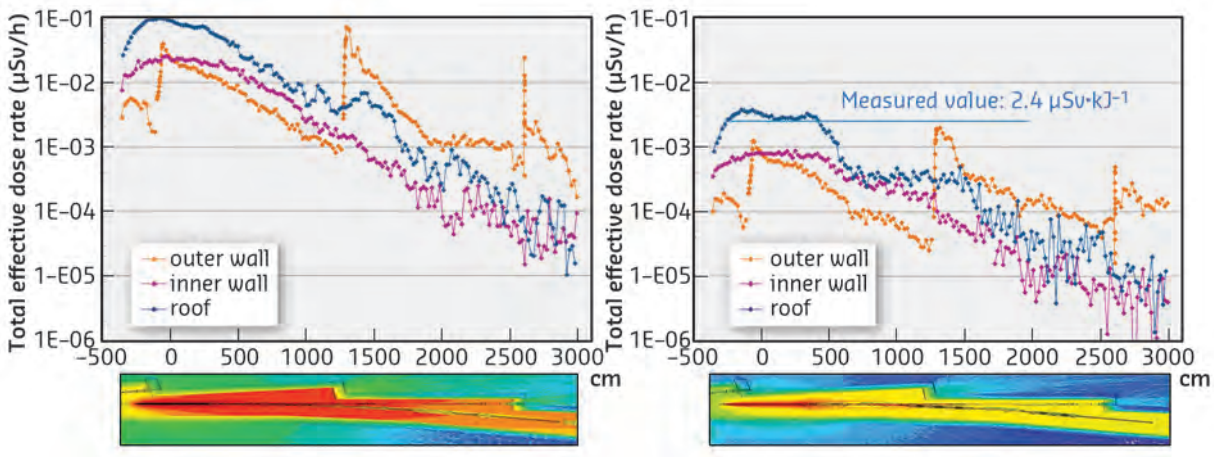

Figure 2.69: Total (photon + neutron) dose rates behind the outer wall, the inner wall and above the roof. Left: new lattice, 90 mA, 0.7 h lifetime, continuous top up, 1% local loss; Right: existing lattice, 90 mA, 16 h lifetime, average dose over 4 h decay, 1% local loss.; right: existing lattice.

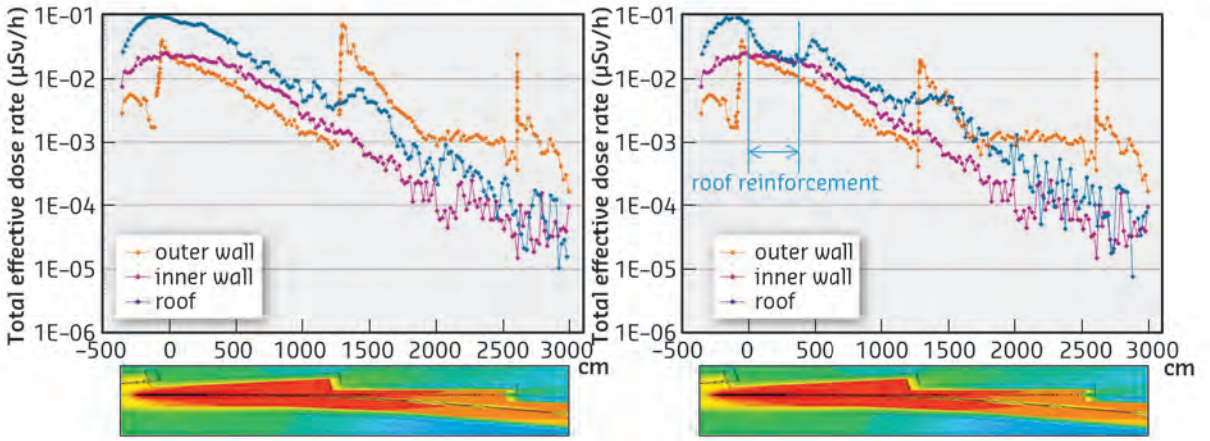

Figure 2.70: Total (photon + neutron) dose rates behind the outer wall, the inner wall and above the roof. Left: no local shielding reinforcement; right: heavy concrete roof under footbridge and bending magnet portend lead reinforcement. Beam loss conditions: New lattice 90 mA, 0.7 h lifetime, continuous top up, 1% local loss; Existing lattice, 90 mA, 16 h lifetime, average dose over 4 h decay, 1% local loss.

of the new facility without major reinforcement of the existing shielding can only be justified if one can show that the present ESRF radiation protection policy, which guarantees the non-exposure of all people working at the ESRF, can be maintained.

Preliminary shielding calculations have been carried out, comparing the existing lattice with the new lattice. FLUKA simulations were therefore made for the existing lattice and for the new lattice. In the standard cells of the existing lattice, primary electron losses are essentially concentrated at the entrance of the insertion device vessels. For the new lattice, in a first conservative approach, we have assumed that the electron losses are concentrated at the same locations.

Due to the small lifetime, the expected dose rates outside the storage ring tunnel shielding are much higher with the new lattice. **Figure 2.69** shows that local beam losses of only a few percent will result in dose rates on the roof exceeding the 0.5 μSv/h limit. We therefore foresee to forbid access to the storage ring tunnel roof during operation and to move the interlocked radiation monitors to the technical zone, next to the tunnel inner wall. This strategy will require local shielding reinforcements around the (at present 3) footbridges on the storage ring roof to allow access between the experimental hall and the technical zone as well as a reinforcement of the bending magnet port end walls. **Figure 2.70** shows the corresponding results when replacing the roof beam over 4 metres with heavy concrete roof beams (3.8 g/cm^3 haematite concrete as presently on the outer wall) and when adding 5 cm of lead on the bending magnet port end walls. One sees that in this case the maximum dose rates are indeed obtained in the technical zone. With this configuration, we can now accept local losses up to about 10%, including the necessary margin for non-optimal injection efficiency. These shielding reinforcements are included in the Phase II budget.

In conclusion, the results of the preliminary shielding calculations show that, if the beam losses around the storage ring are more or less uniformly distributed over the different unit cells, with maximum local losses up to 10% for a given cell, the operation of the new storage ring with beam lifetimes of the order of 0.7 h in 16 bunch mode will be possible while maintaining the present ESRF radiation protection policy, requiring only minor shielding reinforcements.

2.5.4.6. BEAMLINE RADIATION PROTECTION ISSUES

Contrary to the storage ring, the shielding requirements for the beamlines will not change with the new lattice. The shielding requirements for the optics hutches of the insertion device beamlines are completely determined by scattered gas-bremsstrahlung. Since the gas-bremsstrahlung power for the new storage ring should not increase and possibly decrease by up to a factor of two, compared to the present situation, no shielding reinforcement of the insertion device beamline hutches will be required.

In the case of the bending magnet beamlines, shield wall thicknesses are completely determined by scattered synchrotron radiation. The use of 3-pole wigglers as sources of synchrotron radiation for the existing bending magnet beamlines is foreseen and possible consequences for the shielding of the corresponding hutches must be evaluated. From a radiation shielding point of view, the present optics hutches can accept a 6 mrad$_H$ radiation fan produced at B = 0.86 T. The results of **Figure 2.71** show that, when using a 3-pole wiggler as synchrotron radiation source, the shielding of the optics hutches will require reinforcement for values of the maximum magnetic field of the wiggler B_0 above 1 T.

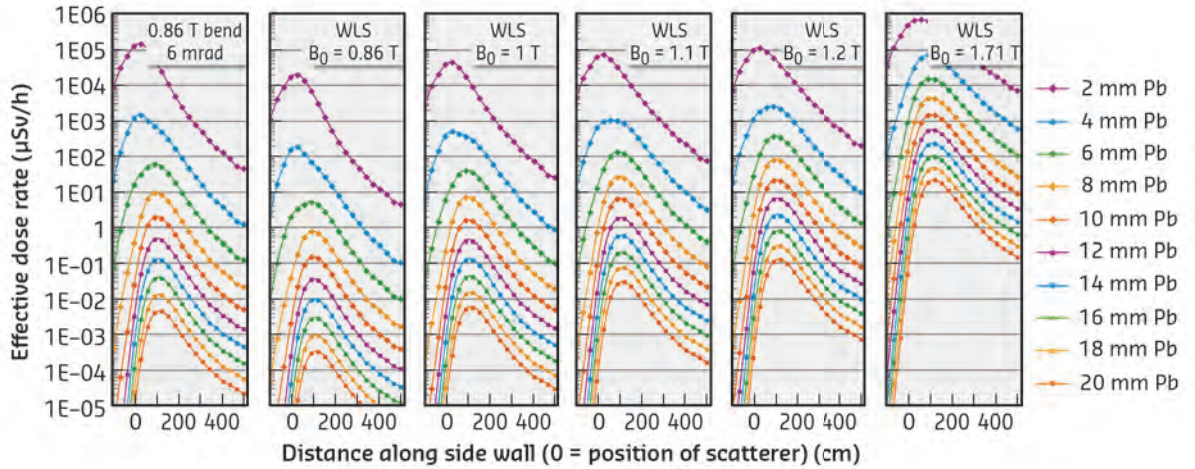

Figure 2.71: Radiation dose rates outside an optics hutch side wall, as a function of the distance along the side wall, for different values of the lead wall thickness, for a 6 $mrad_H$, 0.86 T bending magnet source and for five 3-pole wigglers with maximum magnetic fields between 0.86 and 1.71 T (scattering source: Si grazing incidence scatterer; distance scatterer to wall = 1 m).

2.5.5. SUPPORT BUILDINGS FOR STORAGE AND PREPARATION

2.5.5.1. STORAGE AND PREPARATION AREAS, EXTERNAL STORAGE

A site dedicated to primary storage will be set up; this logistics base will receive equipment after transport from manufacturing points and will enable equipment to be stored correctly by type, module, and reference and to prepare it for final transport to pre-assembly areas.

The main elements to be stored are:
- Magnets and power supplies
- Electronic equipment
- Mechanical supports
- High-precision mechanical parts

Parts will be between 0.5 m and 6 m long and a maximum of 1.1 m high, unit's weight ranges from 20 kg to 5 t.

Storage will be organised to be able to best deal with deliveries to pre-assembly areas. To achieve this, a preparation platform for modules must be set up to constitute packages. The minimum surface is 40 m^2 and will be equipped with a plastic wrap machine for dust protection and re-packing for transport.

The area will be equipped with industrial type shelving for heavy and very heavy loads (1 t to 2 t/m). Stacked storage will be prohibited for modules or cases protecting the modules.

The characteristics of the storage building are:

- Effective storage capacity: 1000 m^2.
- Weight bearing slab: ground resistance > 3 t/m^2, dust protection coating.
- Class A building with a height of 7.5 m (no requirement to store large parts).
- Air temperature control: + or - 5°C, min/max temperature 18°C/35°C.
- Air processing unit with high quality filters to avoid dust on stored equipment.
- No regulation of the humidity level.

The building will also provide manoeuvring areas for heavy transport machines and light vehicles. The building must be secured and guarantee safety and protection conditions. This storage unit will be located in an area at less than 20 km from the site. A team charged with preparation and delivery of the modules is foreseen depending on the pre-assembly needs.

Chartreuse area

The Chartreuse building has 1,170 m^2 available for pre-assembly and workshops.

All the conditions, in terms of safety and availability have been set out (ready access for delivery vans, access control, and fire detection, circulation of forklifts, overhead crane, lighting and air processing).

It is planned to install four 75 m^2 areas for the pre-assembly of elements; each area will be equipped with the utilities necessary for the assembly (electricity and compressed air) and will have laminar air flow (clean room laboratory type).

In addition an area of 100 m^2 will be dedicated to the initial control of magnets.

A 50 m^2 area will be dedicated to vacuum tests.

A 50 m² area will be dedicated to power supply tests.

A 75 m² area will be dedicated to the assembly of a full prototype cell.

A 100 m² secured storage area is foreseen for various mounting accessories.

The Chartreuse building is connected to EXPH and transfer zones to the storage ring tunnel:

- via the Belledonne building and the freeway for access to BM07.
- Directly to EXPH and the freeway for access to BM24.

ID14, ID08, BM07 BM24 areas (Figure 2.73)
Several transit and intermediary storage areas have been identified before final transfer to the storage ring tunnel:

ID14: Currently used as an ASD development beamline: full dismantling of ID14 is foreseen; the resulting surface will be 440 m². This surface will be used as buffer storage for elements awaiting final assembly. After the accelerator project implementation, it is planned to build an optics hutch for radiation protection and machine development activities (not within the scope of the Phase II budget).

ID08: Currently not used by a beamline: full dismantling of ID08 is planned, the resulting surface will be 300 m². This surface will enable buffer storage for elements awaiting final assembly. After Phase II, this area could be made available for the construction of a beamline.

BM07: Currently used for storage of equipment: full dismantling of this area is planned. The resulting available surface would be 175 m². This area will be used as one of the two entry points to the tunnel after removal of the port end. After the accelerator project, this area will be rehabilitated for storage of equipment or for a new bending magnet beamline.

BM24: Currently used by a beamline: It is planned to proceed with the removal of all storage elements in this area, the resulting surface will be 147 m² (essentially dedicated to circulation). This area will be used as the second entry point to the tunnel after removal of the port end. It is foreseen to partially

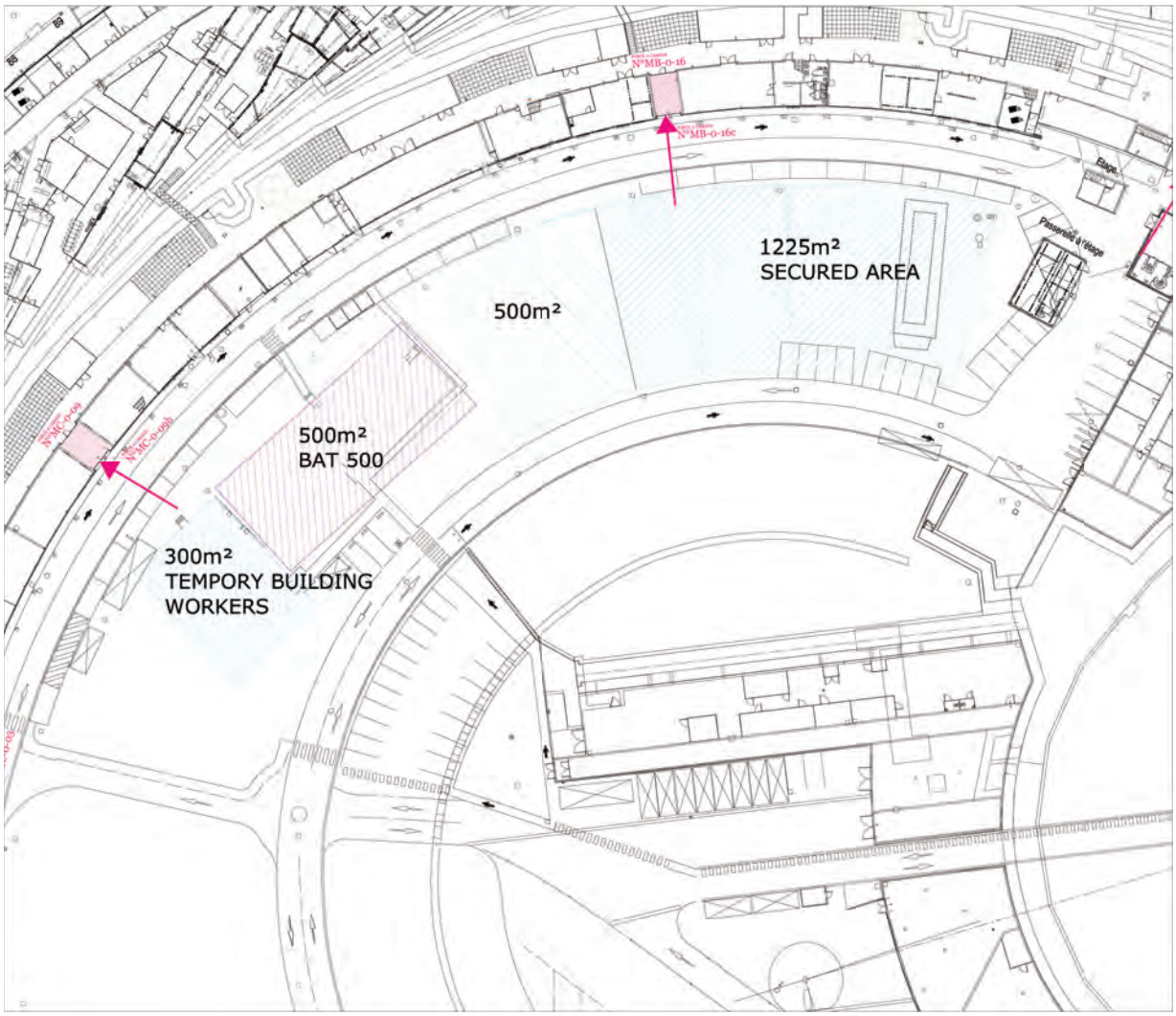

Figure 2.72: Storage in the centre of the ring.

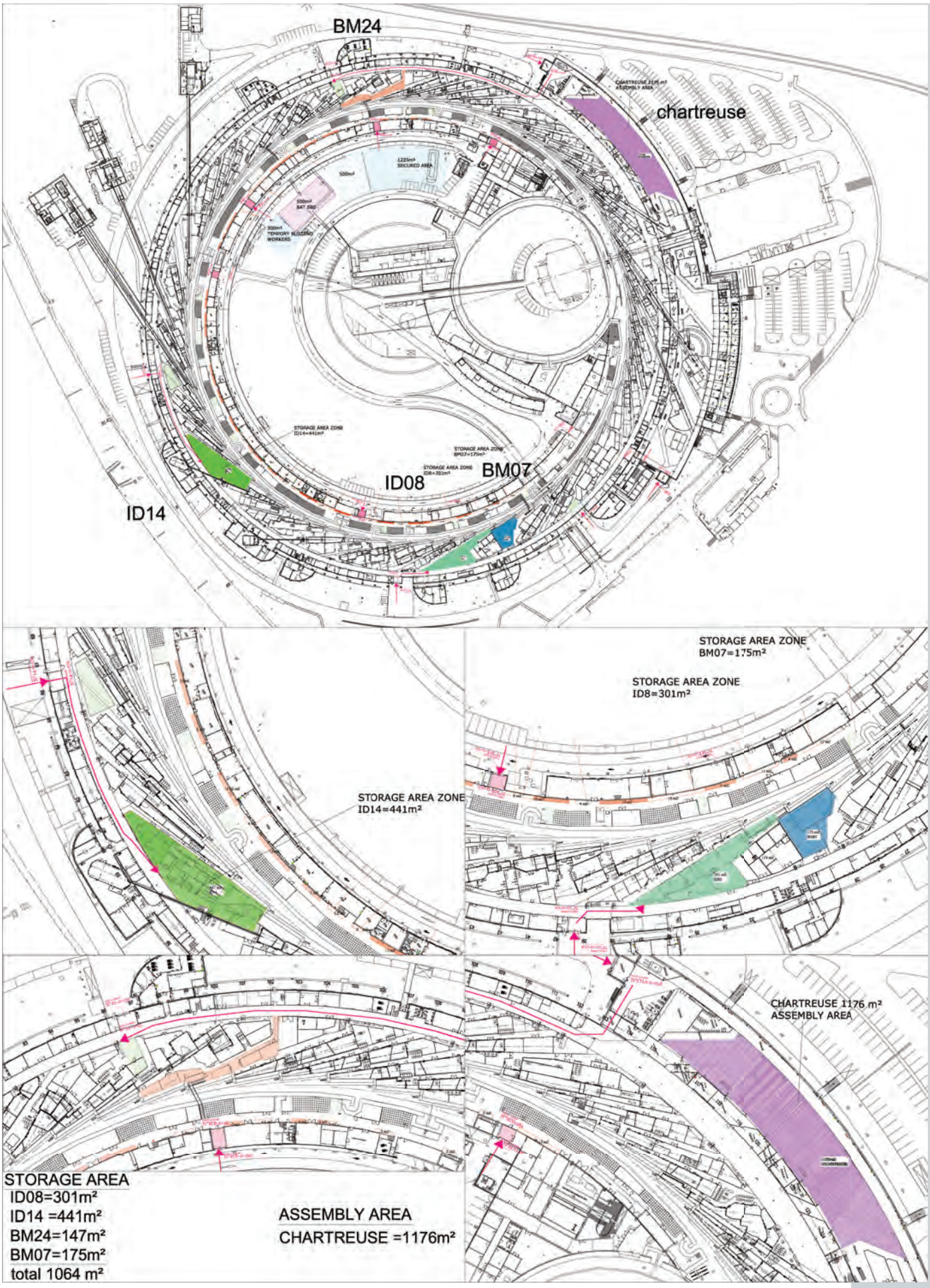

Figure 2.73: Logistics EXPH.

use the EXPH freeway as a buffer storage area. After Phase II, this area will be restored to its initial state.

New specific building (BAT500), (see Figure 2.72): After dismantling, the equipment from the old accelerator must be inspected for eventual activation. A building in the centre of the ring will be built to store and carry out the activation measurement of the dismantled storage ring components, prior to the activation measurements. After the construction of the new storage ring, this building will remain available for storage purposes.

The characteristics of this storage building are:

- Effective storage surface: 500 m^2.
- Weight bearing slab: ground resistance 3 t/m^2, dust protection coating.
- The storage area must be easy to access and secure for equipment, it will be equipped with two high sectional doors (> 4m height).
- The building will be at ground level with no loading/unloading bays.

Secured storage area for the old storage ring (Figure 2.72): After the activation measurements, the storage ring components will be stored in a secured area until their disposal, which will depend on the final decision of the ASN. Some parts of equipment must be stored under watertight and airtight conditions. To accomplish this it is foreseen to use part of building BAT500, and in addition a light structure for a temporary storage surface of 500 m^2. An additional 1 225 m^2 of secured surface will be set aside to store cables, piping and other small equipment.

2.5.5.2. LOGISTICS (see Figure 2.73)

Several logistics teams will be required for:

- Transfer of the primary stock to the pre-assembly area in the Chartreuse hall.
- Transfer from the pre-assembly area in the Chartreuse hall to the buffer areas ID14, ID08 and close to BM24.
- Transfer from the buffer areas to the entrance of the tunnel at BM07 and BM24.
- Handling of loads with the three EXPH cranes (opening and closing or roofs, removal of old equipment and introduction of new front end and insertion device equipment).
- Removal of equipment to the centre of the ring for BAT500 or secured areas, transfer to measurement points, transfer to final storage areas.

These teams will be composed of sub-contractors for intense activity periods and by ESRF staff who have the qualifications and expertise.

2.5.6. INFRASTRUCTURE ADAPTATION

2.5.6.1. COOLING SYSTEM

Cooling network/deionised water

The main cooling network of the accelerators will remain as it is, with an adaptation of the flow as a function of the reduced needs for the new storage ring elements. As discussed later, the distribution network inside the tunnel will be re-constructed. We plan to add an extra filter unit for each of the cell supplies.

Cooling water for aluminium cells

The main cooling network for the aluminium vacuum chambers will remain unchanged; the distribution network inside the tunnel will be re-constructed and adapted to the new configuration.

Air treatment in the storage ring tunnel

The air in the storage ring tunnel is currently processed by four central air handling units. Each unit operates with air taken from the previous zone with a limited introduction of pre-treated fresh air. The control system maintains a temperature stability of ± 2°C, however it has an irregular diffusion profile.

It is not possible to modify the distribution of these four air processing units; however it is planned to improve the control systems on each unit to optimise the overall temperature stability.

Other fluids

Liquid nitrogen and compressed air networks will be dismantled and reconstructed to satisfy the needs of the new equipment. The capacity of the production and storage is sufficient and no modifications are required.

2.5.6.2. AC ELECTRICAL SUPPLY

Selection of the electricity distribution network system will be made by mid 2015 from the two solutions under consideration.

Electrical network distribution design for an AC/DC distribution

The present electricity distribution network in the technical zones is powered by a 1000 kVA transformer, which is insufficient for the future power requirements. To supply electricity to many more locations and devices, the main branches will have to be reinforced. Existing secondary branches will be sufficient to meet the power upgrade requirements.

The present electrical arborescence has to be split into four parts. One of the electrical substations close to the RF station 3 has to be extended to supply power to half of the technical zones, two new transformers and a new mains distribution board have to be installed in the electrical substation. The current cabling infrastructure can be kept and used for the facilities power backup.

Electrical network distribution design for a DC/DC distribution

For this scenario (*cf.* section 2.4.6.), the power distributed in the technical zones is supplied by 16 of the present storage ring magnet AC/DC converters. The power will be distributed to 16 points all around the storage ring.

2.5.6.3. CABLING

Control cabling
The control/command power cables in the cells will be removed and replaced with new ones, some connectors will be re-used.

Cable trays
The existing cable trays will be dismantled. New cable trays will be installed following the guidelines for the mechanical assembly of the girders.

Additional trench requirements
Existing trenches will be re-used. A few additional trenches will be created.

2.5.6.4. CRANES AND HANDLING TOOLS

Following the strategy adopted for the assembly of equipment and the use of the port end as entry point to the tunnel, three overhead cranes (6.3 t capacity) will be sufficient to open the roof, for dismantling and partial reinstallation of equipment (front end modules, insertion devices and straight section of chambers).

Special tools will be required, notably for the transfer of equipment in the tunnel and for dismantling:

- Lifting platforms between EXPH and the tunnel
- Trolleys to transport girders

2.5.7. PREASSEMBLY AND INSTALLATION

2.5.7.1. EXPERTISE

The installation is a complex task but most of the procedures are well known to the ESRF due to the expertise gained during the numerous interventions during past years and notably in the context of the UP PI. (see **Figure 2.74**) Such past projects involved dismantling and installing a large variety of hardware in the storage ring tunnel.

2.5.7.2. GIRDER ASSEMBLY

The installation plan requires that at least all the girders for 6 cells have to be fully assembled prior to the start of the installation. A large part of the existing Chartreuse hall extension will be used for this pre-assembly.

Upon arrival, the hardware will be stored on rented storage areas and then transferred into the Chartreuse hall for preassembly. The detailed logistics and storage policy are given in section 2.5.5.

The preassembly process has to be started in time in order to optimise the procedure and train the teams in charge of the preassembly. The preassembly is planned to begin in the fall of 2017.

The magnets will be characterised and accepted at the factory. Their alignment will rely on mechanical references, and no magnetic measurements are envisaged once the magnets are mounted on the girder. However, we will carry out random quality control measurements for some magnets using a dedicated laboratory test stand. The alignment of the magnets on the girders will be carried out during the assembly phase.

Figure 2.74: Lengthening the straight section in Cell 23 during the 2012 winter shut down.

Vacuum chambers will also be qualified at the factory. An area in the Chartreuse hall will be reserved for random quality tests and other preparation activities. Vacuum chambers, diagnostics and most of the instrumentation will also be installed on the girders. The vacuum chambers on each girder will then be placed under vacuum and baked.

On a routine basis, it should be possible to prepare one full cell per week. The assembled girders will then be stored at the specific dedicated areas near ID14, ID08 and BM07 (section 2.5.5.1).

2.5.7.3. HARDWARE DISMANTLING AND REMOVAL

We plan to empty three cells per week. The existing three 6.3 ton cranes will allow three cells to be dismantled in parallel. The roof of each cell will be removed and stored on the adjacent cell for the duration of the hardware removal. Cables, pipes and most of the instrumentation will be disconnected. Upon completion of the preparatory work, the five girders of each cell will be removed using the existing cranes with magnets, vacuum chambers and most of the instrumentation in place (only cell 7 and cell 1 are not fully accessible by crane due to bridges).

According to the present strategy, it is planned that, together with the removal of the hardware from the arcs, all straight sections will also be dismantled to facilitate installation of the new lattice.

All hardware removed from the tunnel must be inspected for activation. Storage areas will be foreseen to house equipment awaiting radiation tests, which will take place in a dedicated area (see section 2.5.4.2). After these checks, the dismantled accelerator components will be stored prior to proper disposal.

2.5.7.4. PREPARATION OF THE TUNNEL PRIOR TO INSTALLATION

The weight of each assembled girder (girder, supports, magnets, chambers) will be heavier than the capacity of each crane, and the experimental hall's metallic structure does not allow an upgrade of the cranes' capacity. Consequently, the new girders will be rolled in through the openings in the tunnel walls made at the most convenient and available front end locations. Since the port end walls are made of removable concrete blocks, their removal will be very simple.

The two entrance points BM07 (completely free), and BM24 (where some beamline control cubicles need to be dismantled), are diametrically opposed. They have been chosen because they will permit equipment to be installed around the RF cells first, allowing the installation and connection of cavities to start as soon as possible.

Transport rails will be installed in order to roll in the new girders. All the straight section hardware will be re-installed using the cranes.

The new girders will take up more space in the tunnel than those in the current configuration (**Figure 2.75**). To accommodate the new arrangement, the inside cable tray for family power supply cables will be removed (these cables no longer being needed due to magnets being cabled individually). The inner cable tray will be rebuilt and will house the control cables as well as the individual magnet power supply cables (**Figure 2.76**).

At present, two trenches per cell accommodate pipes and cables. Most pipe trenches have the space to hold extra cables, but five additional trenches will be built in cells where trenches are already full. All piping inside the tunnel will be removed and replaced by new piping to fit the new requirements in terms of girder location and distribution of magnet cooling.

The pillars used in the past for alignment will be removed, since alignment will be performed with a laser tracker.

The tunnel refitting includes refurbishment of the floor, painting of the walls and the alignment of the reference plates for the girders.

In addition to this, 30 bending magnet port ends will be reinforced with lead panels, and the standard concrete roof beams under the four footbridges will be replaced with more radiation resistent concrete roof beams.

2.5.7.5. INSTALLATION OF THE NEW HARDWARE

The vacuum chambers will be kept under vacuum while their girders are moved to their final location. A pre-alignment of the girders will be performed prior to vacuum chamber connection.

Four weeks are allocated for the installation of:
- cable trays
- cooling pipes
- cabling and piping
- the new front end module 1
- the insertion device chambers, installed using the crane via the part of the roof that has been left open

Once all equipment has been connected, the vacuum chambers will be baked. It will be done with all magnets in position except the dipoles, which shall be retracted during this operation. After installation of the straight section equipment, the roof will be closed. Only final equipment connections and tests could then be performed.

Each cell of the tunnel will take around twelve weeks from beginning of the dismantling to full mounting and roof closure.

The installation schedule has been drawn up considering normal day activities. Depending of the availability of ESRF supervisory staff, it might be possible to carry out exceptional shift work if necessary during the week (in particular for cabling, piping and alignment activities). No work is foreseen during the weekends, except for the baking of vacuum chambers.

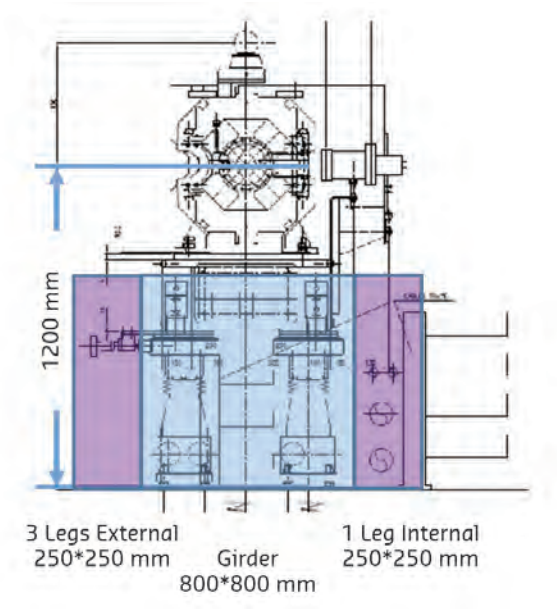

Figure 2.75: Girder bulk in super position to the existing girder and magnet system. Blue: new girder, magenta: legs.

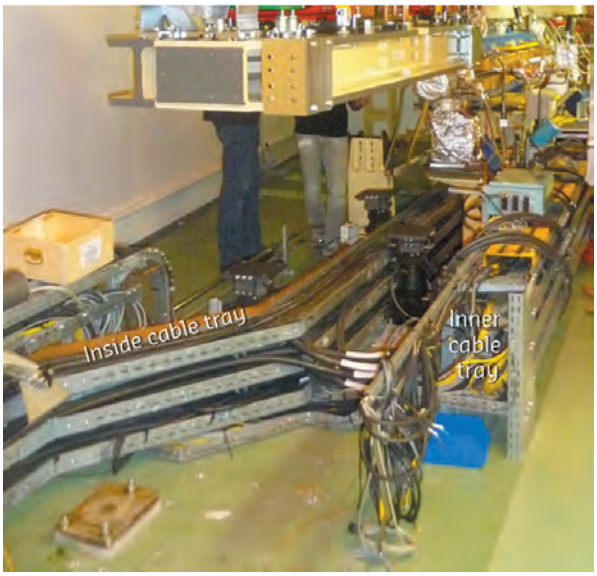

Figure 2.76: Present cable tray layout.

2.5.8. STORAGE RING COMMISSIONING

The injector complex will be re-commissioned at the end of the installation during the equipment test when the tunnel roof is closed.

The commissioning of the new storage ring is planned to start in summer 2019.

The protection systems must be in place and operational before restarting. Time will also be allocated to fully commission the interlock systems.

At this date, all equipment will have been checked beforehand and will be ready for the first injection

attempts. The initial objective is to store a beam current of only a few mA, in order to be able to optimise the lattice and commission all of the new hardware and software. Depending on the progress, a large amount of time will then be devoted to the vacuum conditioning to reach a good vacuum level at high current. As discussed in section 2.4.2.1, reaching 200 mA will need at least 30 days of continuous beam conditioning.

The restart of the new storage ring will rely heavily on existing ESRF expertise and tools (*e.g.* our First Turn system). All hardware and software will be fully integrated into the control system so that procedures can be tested well in advance of the restart.

Shutdown periods are planned to be scheduled for any necessary intervention, repair or modification. We expect to be able to start beam delivery to the beamlines after about 2 months of commissioning. This preliminary delivery will be reserved for radiation tests and subsequently to the beamlines alignment. Depending on the vacuum and radiation levels, the beam might be delivered at reduced current for a few weeks.

A buffer period of 3 months is foreseen in spring 2020 to further optimise the ring performance, for hardware interventions and to reach user service mode conditions.

References

Bauer J., Bharadwaj V., Brogonia H., Brugger M., Kerimbaev M., Liu J., Mallows S., Prinz A., Roesler S., Rokni S., Sanami T., Santana M., Sheppard J., Vollaire J., Vincke H., Benchmark study of induced radioactivity at a high energy electron accelerator, Part I: Specific activities, ARIA 2008, 1st Workshop on Accelerator Radiation Induced Activation, Paul Scherrer Institut, Switzerland, October 13-17 (2008).

Bosland P., Brédy P., Chel S., Devanz G., Luong M., Craievich P., Penco G., Svandrlik M., Pedrozzi M., Gloor W., Anghe A., Chiaveri E., Losito R., Aberle O., Calatroni S., Marchand P., Third Harmonic Superconducting Passive Cavities in Elettra and SLS, Proceedings of the 11th Workshop on RF Superconductivity, SRF 2003, Lübeck/Travemünde, 239-243 (2003).

Chubar O. *et al.*, A three-dimensional magnetostatics computer code for insertion devices, *Journal of Synchrotron Radiation* 5, 481-484 (1998).

Cooper D. *et al.*, Managing risk in large scale projects and complex procurements (2004).

Council Directive 2013/59/Euratom, Commission of the European Communities, Official Journal of EC, Series L, No 13 (2014).

Council Directive 96/29/Euratom, Commission of the European Communities, Official Journal of EC, Series L, No 159 (1996).

Einfeld D. *et al.*, Design of a Diffraction Limited Light Source (DIFL), Particle Accelerator Conference, PAC, Dallas, USA, 1995.

ESRF, Science and Technology Programme 2008-2017, "The Purple Book" (2007); http://www.esrf.eu/about/upgrade/documentation/purple-book.

ESRF, ESRF Upgrade Programme Phase II (2015 - 2019) White Paper, "The White Paper" (2012); http://www.esrf.eu/files/live/sites/www/files/about/upgrade/documentation/whitepaper-upgrade-phaseII.pdf.

Farvacque L., *et al.*, A low emittance lattice for the ESRF, International Particle Accelerator Conference, Shanghai, China (2013).

Ferrari A., Sala P.R., Fasso A., and Ranft J., FLUKA: a multi-particle transport code, CERN-2005-10, INFN/TC_05/11, SLAC-R-773 (2005).

Hettel B., Perspectives and challenges for diffraction-limited storage ring light sources, SLAC, Particle Accelerator Conference, PAC2013, Pasadena, USA, (2013).

Jacob J., Farvacque L., Gautier G., Langlois M., Mercier J.M., Commissioning of first 352.2 MHz – 150 kW solid state amplifiers at the ESRF and status of R&D, Proceedings of IPAC-2013, Shanghai, 2708-2710 (2013).

Jacob J., Serrière V., Ogier B., Goirand L., Triantafyllou A., Bandyopadhyay A.K., Boilot D., 352.2 MHz HOM damped normal conducting ESRF cavity: design and fabrication, *Proceedings of IPAC 2011*, San Sebastian, 68-70 (2011).

Le Bec G. *et al., Phys. Rev. ST Accel. Beams* **15**, 022401 (2012).

MAX IV, Detailed Design Report on the MAX IV Facility, (2010); https://www.maxlab.lu.se/node/1136.

Revol J.L., *et al*, ESRF operation and upgrade status: International Particle Accelerator Conference, Shanghai, China, 2013.

Sanze P., Internat Audit Service (IAS). Audit 12-10-2002 – Memo on the risk management process (2002).

Serrière V., Jacob J., Expected lifetime improvement with a superconducting harmonic RF system at the ESRF, Proceedings of EPAC-2002, Paris, 748-750 (2002).

Shimosaki Y. *et al.,* Lattice design of a very low-emittance storage ring for Spring-8-II, International Particle Accelerator Conference, San Sebastian, Spain (2011).

PART 3
Beamlines

Pages

INTRODUCTION

The installation of a new storage ring with drastically reduced horizontal emittance, and therefore improved brilliance and coherence, will have a profound impact on the beamlines.

During Phase I of the Upgrade Programme, about 60% of the ESRF's beamline portfolio (19 beamlines / end stations) have already undergone a complete upgrade or in-depth refurbishment. A pre-requisite of the proposal for a new lattice was to ensure that a majority of the beamlines upgraded or refurbished during Upgrade Programme Phase I could be adapted to the anticipated new source performance.

The proposal for UP PII includes the construction of a set of four new beamlines that are specifically tailored to profit to a maximum extent from the unique properties of the new source. The construction of the four new beamlines will take place towards the end of UP PII (2020 - 2022), and the selection and technical design of the four beamlines will be carried out starting in 2017 in order to consider the most recent developments in X-ray science in the decision making process.

In this chapter we describe first briefly the process for the selection of the four new beamlines. We then provide details on the impact of the proposed new source on the existing public insertion device beamlines, and how we plan to prepare the beamlines in order to make best use of the new source characteristics. To this effect, a survey of all public beamlines has been conducted in order to determine

- the evolution of key performance figures (beam size at sample, flux, speed of experiments, etc.) with the advent of the upgraded source should the beamlines remain unmodified,
- the required investment to best adapt the beamlines to the proposed new source, and
- the key performance figures of the beamlines after the aforementioned upgrade.

More details on the scientific instrumentation programme that is the basis for the adaptation of the existing beamline portfolio to the new source are provided in **Chapter 4**. The planned investments shall be undertaken during the period from 2016 to 2020 (inclusive) as an upfront measure to best prepare the ESRF beamline portfolio for the proposed new source. The planned investments in the existing beamline portfolio are funded in the context of the regular Operation budget of the ESRF.

The last part of the chapter deals with the restart of the beamlines and the return to user operation after the shutdown in 2018/2019.

3.1. NEW BEAMLINES

In order to take full advantage of the upgrade of the source, a set of four new beamlines (UPBLs) featuring cutting-edge technology is included in the proposal for Phase II of the Upgrade Programme. The science case outlined in **Chapter 1** and the new source performance discussed in **Chapter 2** demonstrate the tremendous potential the new source will offer for new science and scientific applications. This revolutionary approach calls for the construction of new beamlines to realize new X-ray techniques and applications that are not available today. The following two examples may serve here as an illustration:

- On beamline ID29, the best structural biology beamline we offer today, the structural biology community will benefit from an increase in flux density at the sample position by more than 5 orders of magnitude, assuming that the beamline will be extended into the new Chartreuse Hall as a long beamline and upgraded with state-of-the-art beam transport X-ray optics, new sample delivery systems, and a high performance X-ray detector. It is clear that such an increase in performance will open new avenues, for instance in synchrotron serial crystallography, that are far beyond anything possible today.
- New developments in compact X-ray optics and the strong increase in source brightness offered by the new lattice, in combination with new short-period small-gap insertion devices such as the U14 cryo-undulator developed in UP PI, will enable a new type of highly efficient full-field microscopy in complement to traditional transmission electron microscopy. A fully optimized new instrument would indeed push the spatial resolution by several orders of magnitude to the level of a few nanometres or better, while still exploiting the large penetration power of the hard X-rays. Such an instrument would constitute a new tool for *in situ* and *in operando* studies of device-like structures that would be fully complementary to traditional transmission electron microscopy.

Despite the late start of the beamline construction, foreseen in 2021, the prospect of a new high brightness photon source at the ESRF has already triggered the process for the identification of potential new beamlines in the user community and the first ideas have started to emerge from these reflections. The discussions so far have resulted in suggestions for possible new beamlines such as:

- a long beamline dedicated to Hard X-ray Diffraction Microscopy (HXDM – dark-field microscopy, bright field microscopy)
- a long beamline for serial and dynamic nano/micro-crystallography
- a multi-technique beamline for materials chemistry
- a long X-ray cinematography beamline for time-resolved full-field hard X-ray imaging
- a long beamline for photoelectron spectroscopy (HAXPES/HAXPEEM) in spectroscopic and/or imaging mode
- a long beamline for dynamic compression studies.

Some of the proposals have already led to Conceptual Design Reports (CDRs) that will be further updated in the coming years to include the most recent technology for optimised performance. In all these proposals, the potential for not only evolutionary but revolutionary improvement is high. The increase in total photon flux, photon flux density at the sample position, and coherence will push space and time resolution by several orders of magnitude, in particular for imaging and/or diffraction applications. The identification of more candidate upgrade beamlines is a continuous process and we expect new proposals to emerge in the coming years.

The construction of the new beamlines will commence in 2020 after the restart of the new accelerator and source complex and the return to user operation in June 2020. The selection of the new beamlines will follow the same procedure that has been successfully applied in the preparation of Phase I of the UP. A series of workshops will be held in 2017/2018 to identify the most promising scientific areas calling for the construction of new beamlines. Broad participation of the user community and the Science Advisory Committee (SAC) will be essential to ensure full transparency of the process for the selection of the new beamlines. The workshops will produce a set of CDRs for potential new beamlines that will serve as a pool for the final selection. The final four candidate beamlines will be identified in discussions with the ESRF SAC and recommended to Council for realisation in its autumn meeting 2018. Once the final decision on the four beamline projects is taken, detailed Technical Design Reports (TDRs) will be developed in 2019 by the teams in charge of the construction of the four new beamlines. The last step before the actual start of the construction will be a full review of the TDRs within the well established beamline review process of the ESRF with participation of external experts and members of the ESRF SAC.

From a more technical point of view, the construction of two new beamlines is required in any case to replace the two beamlines that were closed and dismantled after the adoption of the Council resolution in November 2010. This will re-establish the full beamline portfolio of 30 public beamlines and mark the return to full user operation.

3.2. IMPACT ON EXISTING PUBLIC BEAMLINES: OVERVIEW

The study of the impact of the new source on the beamlines follows the procedure applied to determine the overall beamline improvement in Phase I of the Upgrade Programme. Table 3.01 summarises, in a global and thus cursory manner, the result of this survey by listing, for each beamline:

- the beam line characteristics (columns 1 to 3),
- the evolution of the key performance figures in case the beamline remains "as is" (columns 4 to 8),
- the modifications and refurbishment measures required to tap into the potential of the new source, differentiated by investment in i) the source device, ii) the beam transport equipment (optical elements from the front end down to the sample stage), iii) the end station, and, finally, iv) the detector (columns 10 to 13), and
- the expected improvement of the key performance parameters, assuming the proposed improvements have been carried out (columns 14 to 18).

Table 3.01 also lists, in column 9, beamline equipment becoming obsolete if the source is upgraded.
In total, the investment foreseen for the period 2016 – 2020 amounts to:

The investment in the existing beamline portfolio will be financed from the regular operation budget. Upgrade Programme Phase II funding for beamlines is required for the construction of four new Upgrade beamlines.

We emphasise that for some investments (such as certain sample environments or detectors), we are currently not in a position to establish concrete budget needs. Furthermore, the investments towards detectors would only cover commercially available detectors and planned detector refurbishment programmes. Detectors tailored for the needs of some beamlines will be obtained through a dedicated detector programme (see section 4.3), mostly financed by Phase II funds.

Source upgrades	Investment in beam transport	Investment in end stations	Detectors
3,250 k€	6,400 k€	400 k€	6,350 k€

(01)	(02)	(03)	(04)	(05)	(06)	(07)	(08)	(09)
Beamline	**Source device**	**Length of straight section**	**Performance of unchanged beamline (*Dynamics end Extreme Conditions* Group)**					**Equipment becoming obsolete**
			Beamsize at sample		**Flux**	**Speed of experiments**	**New type of experiments**	
			(h)	**(v)**				
ID06 LVP	U18	5 m	nc	nc	nc	nc		None
ID 15B	U22, U20, W67	5 m	x 1/2	nc	x 10	nc, (q)	use of coherence	flat panel area detectors
ID 18	3 x U20/U27	6 m	x 1/5	nc	x 2	x 1.4	evolutionary	none
ID 20	3 x U32/U26 + U26	6 m	x 1/20	nc	nc	nc	evolutionary, extreme conditions and mapping	none
ID 27	U23 (6mm)	5 m	x 1/2	nc	x 30	x 2, (q)	coherent imaging under high pressure	none
ID 28	3 x U32/U17.6	5 m	x 1/2	nc	nc	x 2, (q)	evolutionary, high pressure heating possible	none
ID 28 Side Branch	3 x U32/U17.6	5 m	x 1/2	nc	nc	x 2, (q)		none

Table 3.01a: "Performance of the unchanged beamline with the new lattice" (column (01) to column (09)) for the beamlines of the ESRF's *Dynamics and Extreme Conditions* Group ("nc" = no change, "(q)" = trade in higher speed due to improved flux for better data quality).

(1)	(10)	(11)	(12)	(13)
Anticipated beamline modification (*Dynamics and Extreme Conditions* Group)				
Beamline	**Source**	**Beam transport**	**End stations**	**Detectors**
ID 06 LVP	tailored for high energy, possibly CRL in FE	CCM for high energies	redesign to give larger sample-to-detector distance	pixellated high energy detector
ID 15B	new ID for 30 keV			fast area detector, high energy, photon counting
ID 18	CRL in FE	horizontal deflecting heat load monochromator	new KB	
ID 20	6 m → 5 m straight section compensated by shorter period undulators	inversion KB optics		2D hybrid pixel (25 x 25 μm^2, high Z sensor
ID 27	tailored U14 (single line 30 keV)	shorter ML mirror		high energy detector (CdTe)
ID 28				
ID 28 side branch		CRG Be lens upgrade		

Table 3.01b: "Anticipated beamline modifications" (column (10) to column (13)) for the beamlines of the ESRF's *Dynamics and Extreme Conditions* Group.

(01)	(14)	(15)	(16)	(17)	(18)
Performance of upgraded beamline (*Dynamics and Extreme Conditions* Group)					
Beamline	**Beamsize at sample**		**Flux**	**Speed of experiments**	**New type of experiments**
	(h)	**(v)**			
ID06 LVP	nc	nc	up to x 10	mapping up to x 5	
ID 15B	x 1/2	nc	x 50	nc, (q)	use of coherence
ID 18	x 1/20	x 1/10	x 4	x 2	spin/valance/oxidations state selectivity, surface nanostructure mapping
ID 20	x 1/7	x 1/3	x 2	x 40	evolutional extreme conditions experiments and mapping
ID27	x 1.2	nc	x 100	x 10, (q)	nanosecond time resolved laser shock experiments
ID 28	x 1/2	nc	nc	x 2, (q)	
ID 28 side branch	x 1/4	nc	nc	x 8	efficient measurements above 50 GPa

Table 3.01c: "Performance of the upgraded beamline with the new lattice" (column (14) to column (18)) for the beamlines of the ESRF's *Dynamic and Extreme Conditions* Group ("nc = no change, "(q)" = trade in higher speed due to improved flux for better data quality).

(01)	(02)	(03)	(04)	(05)	(06)	(07)	(08)	(09)
Beamline	**Source device**	**Length of straight section**	Performance of unchanged beamline (*Electronic Structure and Magnetism* Group)					**Equipment becoming obsolete**
			Beamsize at sample		**Flux**	**Speed of experiments**	**New type of experiments**	
			(h)	**(v)**				
ID 12	HU52 HELIOS,HU35 APPLE	5 m	x 1/15	nc	x 2	nc, (q)	evolutionary	none
BM 23	BM, -9 mrad	n/a					evolutionary	none
ID 24	3 x U27/U32, U27	6 m	nc	nc	x 2.5	nc	evolutionary	FReLoN, Laser heating equipment
ID 26	U35, U35, U35/U27	5 m	x 1/7	nc	nc	nc	evolutionary	none
ID 32	APPLE II (2 x 1.6 m, 1 x 2.5 m)	6 m	x 2/3	nc	nc	nc	no change	none

Table 3.01d: "Performance of the unchanged beamline with the new lattice" (column (01) to column (09)) for the beamlines of the ESRF's *Electronic Structure and Magnetism* Group ("nc" = no change, "(q)" = trade in higher speed due to improved flux for better data quality).

(1)	(10)	(11)	(12)	(13)
Anticipated beamline modification (*Electronic Structure and Magnetism* Group)				
Beamline	**Source**	**Beam transport**	**End stations**	**Detectors**
ID 12	HELIOS revolver 3 periods (2015/06)	spectroscopy-DCM BE CRL	50 mK under high field, dilution cryostat with magnet; infrastructure: modify space around magnet	natural modulation lock-in detector for time structure
BM23	3-pole wiggler	spectroscopy DCM	portable analyser crystal for fluo detection	more elements, more solid angle thicker Si vortex detector (2mm)
ID 24	harmonics free helical undulator	pink beam on sample	analyser behind sample	
ID 26	3 revolvers, lower gap, CRL in FE	spectroscopy-*DCM* white beam collimating mirror		continued development of more efficient analyser crystals
ID 32	maximise straight section for 2 x 2.5 m APPLE II	replace 2nd collimating mirror with cylinder and modify final RIXS cylinder		

Table 3.01e: "Anticipated beamline modifications" (column (10) to column (13)) for the beamlines of the ESRF's *Electronic Structure and Magnetism* Group.

(01)	(14)	(15)	(16)	(17)	(18)
Performance of upgraded beamline (*Electronic Structure and Magnetism* Group)					
Beamline	**Beamsize at sample**		**Flux**	**Speed of experiments**	**New type of experiments**
	(h)	**(v)**			
ID 12	x 1/15	nc	up to x 100	n/a	ultra low, ultra high p with high field combined with XMCD, sub monolayer investigations on substrates, polarisation dependent spectroscopy
ID 24	x 1/10	nc	x 2.5	x 2 - 3	laser shock dynamical high pressure, high temperature, photocatalysis, solution chemistry (industrial)
ID 26	x 1/7	nc	nc	x 5	Photosynthesis
ID 32	x 1/4	x 1	nc	nc	

Table 3.01f: "Performance of the upgraded beamline with the new lattice" (column (14) to column (18)) for the beamlines of the ESRF's *Electronic Structure and Magnetism* Group ("nc = no change, "(q)" = trade in higher speed due to improved flux for better data quality).

(01)	(02)	(03)	(04)	(05)	(06)	(07)	(08)	(09)
Beamline	**Source device**	**Length of straight section**	**Performance of unchanged beamline (*Structure of Materials* Group)**					**Equipment becoming obsolete**
			Beamsize at sample		**Flux**	**Speed of experiments**	**New type of experiments**	
			(h)	**(v)**				
ID 01	U27/U35	6 m	x 1/2	nc	x 50	x 2, (q)	time resolved annealing, ageing of devices	none
ID 03	2 x U35, 1 x U42	5 m	nc	nc	up to x 20	nc, (q)	CDI for *in-situ* surface processes, heterogeneous catalysis, electrochemically controlled growth or corrosion	none
ID 11	CMP18, U22	5 m	nc	nc	x 10	up to x 10	evolutionary	none
ID 15	U22, U20, W76	5 m canted	x 1/2	nc	x 10	x 2, (q)	evolutionary	none
ID 22	IVU23, U35	5 m	x 2/3	nc	x 2.5	x 2	evolutionary	none
ID 31	IVU14	5 m	x 1/4	nc	x 11	x 1.5, (q)	nc	none

Table 3.01g: "Performance of the unchanged beamline with the new lattice" (column (01) to column (09)) for the beamlines of the ESRF's *Structure of Materials* Group ("nc" = no change, "(q)" = trade in higher speed due to improved flux for better data quality).

(1)	(10)	(11)	(12)	(13)
Anticipated beamline modification (*Structure of Materials* Group)				
Beamline	**Source**	**Beam transport**	**End stations**	**Detectors**
ID 01	U14 @ 4mm, possibly CRL in FE	shorter white beam mirrors, mirror to replace MLMC		10 MPixel detector
ID 03	tailored (revolver) undulator, CRL in FE	MLMC	improvement of data acquisition speed to mSec range	increase of max. count rate dynamical range of current 2D detectors
ID 11	U14, CRL in FE	upgrade MC cooling		faster shutterless detector
ID 15				
ID 22				
ID 31	IVU with even shorter period, superconducting undulator			large area CdTe detector

Table 3.01h: "Anticipated beamline modifications" (column (10) to column (13)) for the beamlines of the ESRF's *Structure of Materials* Group.

(01)	(14)	(15)	(16)	(17)	(18)
Performance of upgraded beamline (*Structure of Materials* Group)					
Beamline	**Beamsize at sample**		**Flux**	**Speed of experiments**	**New type of experiments**
	(h)	**(v)**			
ID 01	x 1/2	nc	x 50 - 2000	x2, "unseen" experiments	combination of coherent diffraction with in-operando chemistry, electronic devices, ageing
ID 03	nc	nc	up to x 100	nc, (q)	CDI for in situ surface processes (ms), heterogeneous catalysis, electrochemically controlled growth or corrosion
ID 11	nc	nc	x 20	up to x 50	3D diffraction tomography (point scanning)
ID 15	x 1/2	nc	x 100	x 2, (q)	5D diffraction imaging
ID 22	x 2/3	nc	x 5	x 2	
ID 31	x 1/4	nc	x 11	x 10	CTRs on the facets of nanoparticles

Table 3.01i: "Performance of the upgraded beamline with the new lattice" (column (14) to column (18)) for the beamlines of the ESRF's *Structure of Materials* Group ("nc = no change, "(q)" = trade in higher speed due to improved flux for better data quality).

(01)	(02)	(03)	(04)	(05)	(06)	(07)	(08)	(09)
Beamline	**Source device**	**Length of straight section**	Performance of unchanged beamline (*Structure of Soft Matter* Group)					**Equipment becoming obsolete**
			Beamsize at sample		**Flux**	**Speed of experiments**	**New type of experiments**	
			(h)	**(v)**				
ID 02	2 x U21.4	5 m	x 1/3	nc	x 3	nc, (q)	reduced horizontal beam size is an advantage for many sample environments, especially for rapid switching of biochemical milieu with cardiac muscles	none
ID 09	IVU17, 5 m	5 m	x 1/1.4	nc	x 2	x 1.4	emission spectroscopy, laser induced T and p jumps. New dynamics	none
ID 10 CS	U27/U35, U35, U27	5 m	nc	nc	x 10	CDI: x 10	high pressure XPCS with 10 nm resolution on 1 μm objects with CDI	none
ID10 LSIS	U27/U35, U35, U27	5 m	x 1/80	x 1/2.5	x 2.5	x 2.5	Evolutionary	none
ID 13	IVU18, U35	5 m	nc	nc	x 3	up to x 5	Evolutionary	FReLoN 4M (too slow)

Table 3.01k: "Performance of the unchanged beamline with the new lattice" (column (01) to column (09)) for the beamlines of the ESRF's *Structure of Soft Matter* Group ("nc" = no change, "(q)" = trade in higher speed due to improved flux for better data quality).

(1)	(10)	(11)	(12)	(13)
Anticipated beamline modification (*Structure of Soft Matter* Group)				
Beamline	**Source**	**Beam transport**	**End stations**	**Detectors**
ID 02	tailored shorter period undulator, possibly CRL in FE	toroidal mirror for clean harmonic rejection		size 150 - 200 mm, small pixel (25 – 30 µm), high resolution area detector
ID 09	low-k undulator, top up of single bunch in 7/8+1 mode CRL in FE	spectroscopy-DCM	KB multilayer for 5 ?m focusing	XES detection with MAXIPIX
ID 10 CS	tailored U20 (2x)	liq. N2 cooling of monochromator, shorter white beam mirrors	Cryo/vacuum sample environment, sample changer	Eiger 4M
ID 10 LSIS				
ID 13	U15 CPMU	MC stability improvement	ML final stage focusing fast scanning system	

Table 3.01l: "Anticipated beamline modifications" (column (10) to column (13)) for the beamlines of the ESRF's *Structure of Soft Matter* Group.

(01)	(18)	(19)	(20)	(21)	(22)
Performance of upgraded beamline (*Structure of Soft Matter* Group)					
Beamline	**Beamsize at sample**		**Flux**	**Speed of experiments**	**New type of experiments**
	(h)	**(v)**			
ID 02	x 1/6	nc	x 3	up to x 2	phase retrieval in small angle diffraction, dynamics by exploiting the high degree of coherence and resolution
ID 09	x 1/20	x 1/10	x 20	x 5 - 10	laser shocks in Mbar range, EOS in warm dense matter and planetary research
ID 10 CS	nc	nc	x 60 - 100	CDI: x 50	high pressure XPCS with 10 nm resolution on 1 mm objects with CDI
ID 10 LSIS	x 1/80	x ½.5	x 5	(q)	
ID 13	x 1/4	x 1/2.5	x 10	up to x 500	time and space resolution 20 nm and 400 ms for spacially resolved *in operando* experiments

Table 3.01m: "Performance of the upgraded beamline with the new lattice" (column (14) to column (18)) for the beamlines of the ESRF's *Structure of Soft Matter* Group ("nc = no change, "(q)" = trade in higher speed due to improved flux for better data quality).

(01)	(02)	(03)	(04)	(05)	(06)	(07)	(08)	(09)
Beamline	**Source device**	**Length of straight section**	Performance of unchanged beamline (*X-ray Imaging* Group)					**Equipment becoming obsolete**
			Beamsize at sample		**Flux**	**Speed of experiments**	**New type of experiments**	
			(h)	**(v)**				
ID 16A	U18.3, U22.4 (1.4m)	6 m canted	nc	nc	x 20	nc, (q)	Evolutionary	FReLoN
ID 16B	IVU26	6 m canted	nc	nc	x2	only (q)	evolutionary	horizontal focusing mirror
ID 17	W150, W125	5 m	nc	nc	nc	nc	nc	none
ID 19	U32/U13, W150, U32/17.6	5 m	up to x 1/8	up to x 1/5	up to x 100	x 10 - 10000	rapid low dose *in vivo* coherent phase contrast imaging on small animals; sub micron tomography on dense materials; single bunch cardioscopy	none
ID 21	U42, U42, U32	5 m	nc	nc	x 10	nc, (q)	evolutionary	none

Table 3.01n: "Performance of the unchanged beamline with the new lattice" (column (01) to column (09)) for the beamlines of the ESRF's *X-ray Imaging* Group ("nc" = no change, "(q)" = trade in higher speed due to improved flux for better data quality).

(1)	(10)	(11)	(12)	(13)
Anticipated beamline modification (*X-ray Imaging* Group)				
Beamline	**Source**	**Beam transport**	**End stations**	**Detectors**
ID 16A	tailored short period undulator in vacuum	shorter ML mirror	ultra fast NI + *in-situ* stations	fluo microscopy: high throughput energy dispersive detector, phase nano-tomography: ultra-fast image sensors FReLoN CMOS
ID 16B	Tailored IVU26	shorter first mirror, upgrade cooling	permanent LN2 cryo sample environment	fluorescence detector
ID 17	tailored U14, CRL in FE	Transfocator in EH1		fast 2D detector to cover enlarged footprint
ID 19	4 position revolver, IVU + shorter wiggler, CRL in FE	new Be CRLs	new sample environment for rapid tomography, cinematography	high speed FReLoN developments
ID 21	revolver U27/U32	LN2 cooled spectroscopy DCM	full field optimised mechanics KB refurbishment	fluorecence multi-element detector, independent modules

Table 3.01o: "Anticipated beamline modifications" (column (10) to column (13)) for the beamlines of the ESRF's *X-ray Imaging* Group.

(01)	(14)	(15)	(16)	(17)	(18)
Performance of upgraded beamline (*X-ray Imaging* Group)					
Beamline	**Beamsize at sample**		**Flux**	**Speed of experiments**	**New type of experiments**
	(h)	**(v)**			
ID 16A	nc	nc	x 20	up to x 25	fast / ultra-fast X-ray fluorescence and nano-tomography, *in-situ* experiments
ID 16B	nc	nc	x 50	x 2, (q)	
ID 17	150 mm	150 mm	up to x 100	up to x 100	fast 2D/3D *in-vivo* imaging of whole animal/organ, high resolution CT of large objects (industrial), improved complementarity with ID19
ID 19	up to x 1/8	up to x 1/5	up to x 100	x 10 – 10000	detection in the 10 ps range, suitable to follow crack propagation in semiconductor materials or fuel injection processes in engines
ID 21	x 1/6	x 1/2	x 15	x 10	multi dimensional full field spectroscopy (3D, 4D); time resolved spectroscopy, micrometric emission spectroscopy based on CDI

Table 3.01p: "Performance of the upgraded beamline with the new lattice" (column (14) to column (18)) for the beamlines of the ESRF's *X-ray Imaging* Group ("nc = no change, "(q)" = trade in higher speed due to improved flux for better data quality).

(01)	(02)	(03)	(04)	(05)	(06)	(07)	(08)	(09)
Beamline	**Source device**	**Length of straight section**	Performance of unchanged beamline (*Structural Biology* Group)					**Equipment becoming obsolete**
			Beamsize at sample		**Flux**	**Speed of experiments**	**New type of experiments**	
			(h)	**(v)**				
ID 23-1	U35	7 m canted with cavities	x 1/1.2	nc	x 10	nc	evolutionary	none
ID 23-2	U20.2	7 m canted with cavities	no change	nc	x 10	x 3	evolutionary, serial crystallography	none
ID 29	IVU21, U35	5 m	small reduc-tion	small reduc-tion	x 10	no change, detector limited	evolutionary	sample mounter, detector
ID 30A	U21, U21	6 m canted	no change	nc	nc	nc	evolutionary	none
ID 30B	U35, U35	6 m canted	no change	nc	x 2	nc	evolutionary	horizontal focusing mirror

Table 3.01q: "Performance of the unchanged beamline with the new lattice" (column (01) to column (09)) for the beamlines of the ESRF's *Structural Biology* Group ("nc = no change, "(q)" = trade in higher speed due to improved flux for better data quality).

(1)	(10)	(11)	(12)	(13)
Anticipated beamline modification (*Structural Biology* Group)				
Beamline	**Source**	**Beam transport**	**End stations**	**Detectors**
ID 23-1	remove cavities possibly CRLs in FE	replace toroidal mirror with CRL for variable focusing	new sample changer and goniometer	High frame rate large field pixel detector
ID 23-2	remove cavities	monochromator refurbishment	new optical configuration and experimental table for 1 µm x 1 µm beam New robotics and sample changer	
ID 29	windowless FE	optics for microfocus MAD, transfocators, new monochromator	new robotic sample changer/goniometer	state of the art 2D detector (integrating hybrid pixel?)
ID 30A	CRL in FE	simplify optics for CRL and transfocator only		
ID 30B		vertically and horizontally focusing CRLs; pink beam for SMX		

Table 3.01r: "Anticipated beamline modifications" (column (10) to column (13)) for the beamlines of the ESRF's *Structural Biology* Group.

(01)	(14)	(15)	(16)	(17)	(18)
Performance of upgraded beamline (*Structural Biology* Group)					
Beamline	**Beamsize at sample**		**Flux**	**Speed of experiments**	**New type of experiments**
	(h)	**(v)**			
ID 23-1	up to x 1/30	up to x 1/30	x 10	x 20	multi-crystal datasets, ultra-fast RT data collection; serial crystallography; propagation-based phase contrast imaging.
ID 23-2	x 1/7	x 1/7	x 10	x 20	ultra fast room temperature data collection
ID 29	x 1/10	x 1/5	x 10	x 50	serial crystallography, ultra-fast room temperature data collection
ID 30A	x 1/10	nc	nc	nc	serial crystallography, multiple crystal analysis, optically adapting beam to crystal (CRL, focusing)
ID 30B	nc	nc	x 2	nc	serial crystallography, room temperature measurements

Table 3.01s: "Performance of the upgraded beamline with the new lattice" (column (14) to column (18)) for the beamlines of the ESRF's *Structural Biology* Group ("nc = no change, "(q)" = trade in higher speed due to improved flux for better data quality).

PART 3
BEAMLINES

3.3. IMPACT ON EXISTING INSERTION DEVICE AND BENDING MAGNET BEAMLINES: DETAILS

The new accelerator complex has clear improvements as far as photon flux, flux density, and coherence at the sample are concerned. However, these improvements can only be exploited by beamlines specifically tailored to these source properties. Some of the existing beamlines may have problems coping with photon flux and flux density due to heat load problems or general obsolescence of beamline instrumentation. In this section, the principle areas of concern are addressed together with an assessment of the investment needed for existing beamlines to fully benefit from the enormous potential of the new source.

This applies also to bending magnet beamlines where the opportunity to finally exploit the new

3-pole wiggler source will increase substantially the photon flux. However, the increased flexibility in tailoring the total wavelength range will provide the opportunity to exploit new scientific applications.

The new source properties render the ESRF bending magnet ports among the brightest bending magnet based sources worldwide.

3.3.1. SOURCE CHARACTERISTICS

The expected beam characteristics are shown in **Section 2.3** and in **Chapter 4** in terms of flux on the sample at a specific energy. To determine the compatibility of existing beamline instrumentation, the effective heat load on components that are in contact with the white beam needs to be considered. Figure 3.01. shows the beam profile transmitted through the primary slits at a maximum opening of 4 mm x 4 mm.

The figure illustrates that for beamlines on high beta straight sections (even numbers) the effective heat load is unchanged. For low beta straight sections (odd numbers) the beam will be less divergent horizontally, thus increasing the central power density significantly to similar values as in the existing high beta sections. As the beamlines located on present-day high beta straight sections are readily coping with the heat load we expect no technical challenges for basic absorbers, slits, attenuators etc. An audit of beamlines currently located on low beta straight sections may be needed to ensure that they feature the correct instrumentation to withstand the modestly increased heat load.

Bending magnet sources, in accordance with **Section 2.4.5.2.**, will maintain the flexibility of a hard and a soft X-ray branch, although this may require some

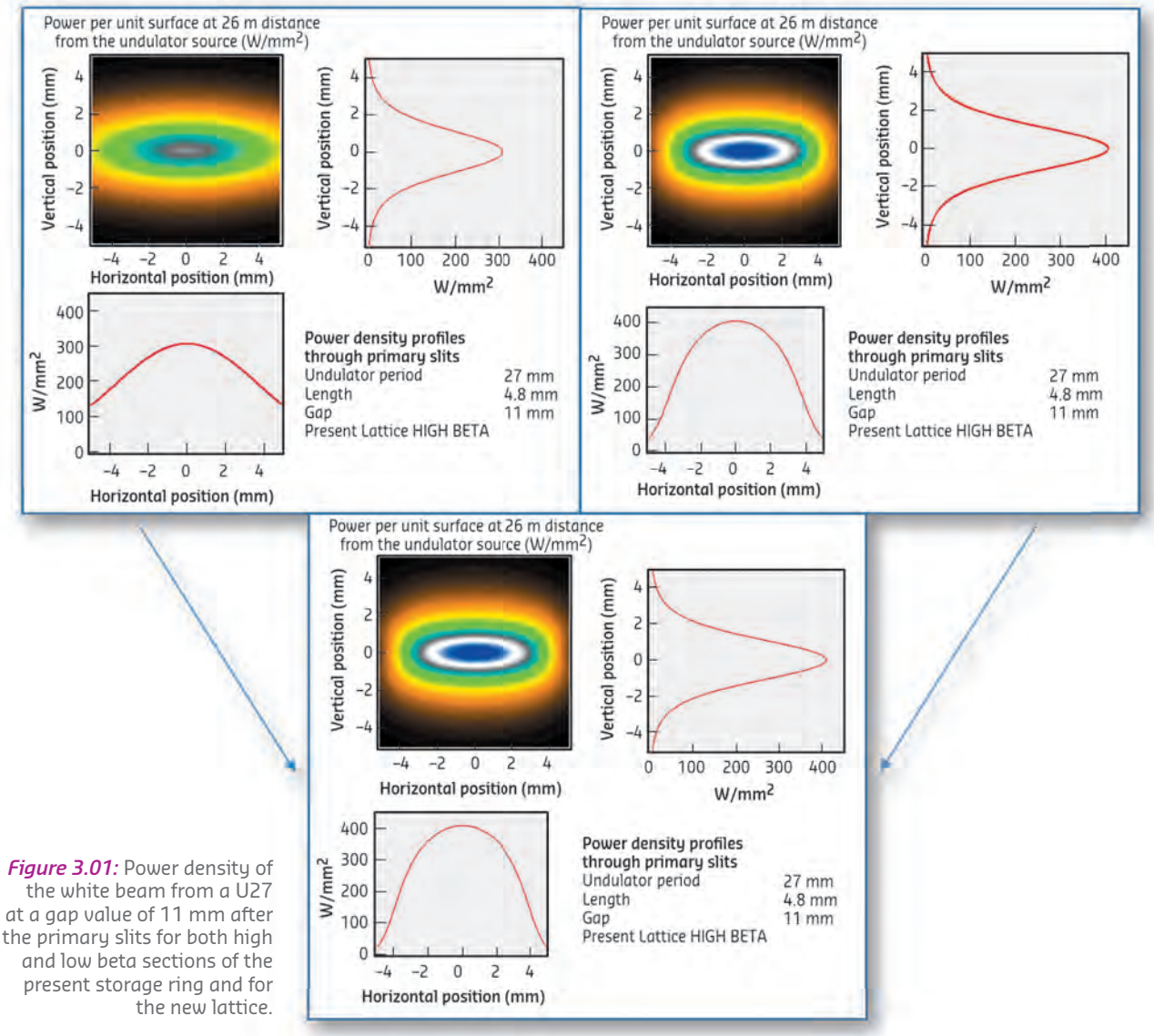

Figure 3.01: Power density of the white beam from a U27 at a gap value of 11 mm after the primary slits for both high and low beta sections of the present storage ring and for the new lattice.

important re-alignment and re-engineering of some beamline components as the two branches will be approximately 50 mm closer at 60 m distance from the source point. In terms of heat load and performance, the soft energy branch will be similar to today but will benefit from a brightness increased by a factor of 10. The hard X-ray branch (3-pole wiggler source) can be up to a factor of 50 brighter than today with a flux increase up to a factor of 5, depending on the chosen strength of the magnetic field of the 3-pole wiggler.

3.3.2. BEAM TAILORING

3.3.2.1. WHITE BEAM MIRRORS

During Upgrade Programme Phase I, significant efforts were made to tailor the optical components to the beam in order to optimise the performance.

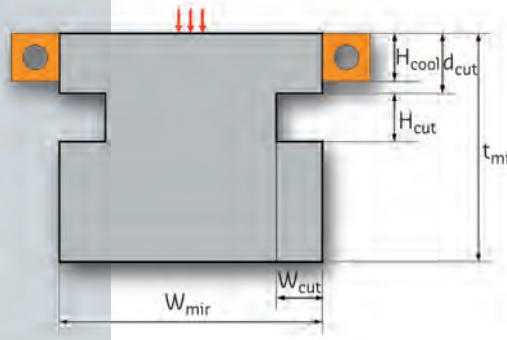

Figure 3.02: An example of the cross section of a "Smart" profiled white beam mirror, Credit: Lin Zhang, ESRF.

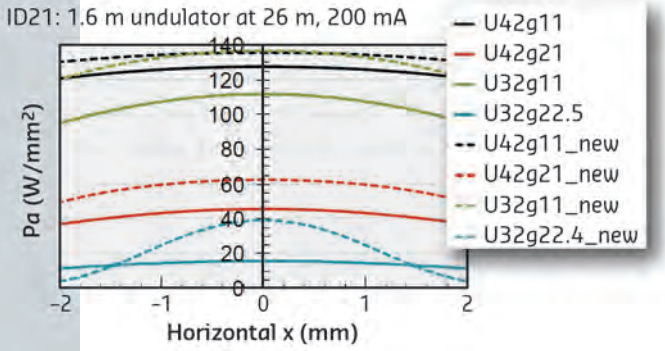

Figure 3.03: Power density incident on a white beam mirror for varying undulator gap values at an existing low beta section and in the new lattice. Credit: Lin Zhang, ESRF.

For white beam mirrors, this entails overfilling by (i) matching the mirror length to the horizontal size of the white beam and (ii) optimising the horizontal cross section, the so called "Smart profile", to the specific characteristics of the undulator radiation. The undercut W_{cut} (**Figure 3.02.**), is optimised in order to reach slope errors as small as 20 nrad for one specific undulator setting.

Figure 3.01 shows that the power profile for high beta section beamlines hardly changes with the new lattice. Consequently, the efforts to optimise white beam mirrors on these beamlines have been well invested. For mirrors installed on beamlines at low beta straight sections the optimisation carried out in Upgrade Programme Phase I was performed in the horizontal direction, exploiting the relatively flat profile. Most of these mirrors are long enough to capture all the available photons.

The horizontal power profile for beamlines on low beta straight sections will change considerably. This is illustrated in **Figure 3.03** for beamline ID21 where a refurbishment of the first horizontally reflecting white beam mirror is in planning. The new mirror must be adapted to the increased power density as well as to the change in the beam profile.

While it is still possible to optimise a mirror for one particular undulator period and gap, it may not be possible in every case to find a value for W_{cut} that is optimised for all undulator periods and gap values. **Figure 3.04.** shows that for a mirror that has been optimised for a current low beta beamline, the mirror slope errors may increase to a value as high as 400 nrad with the new lattice.

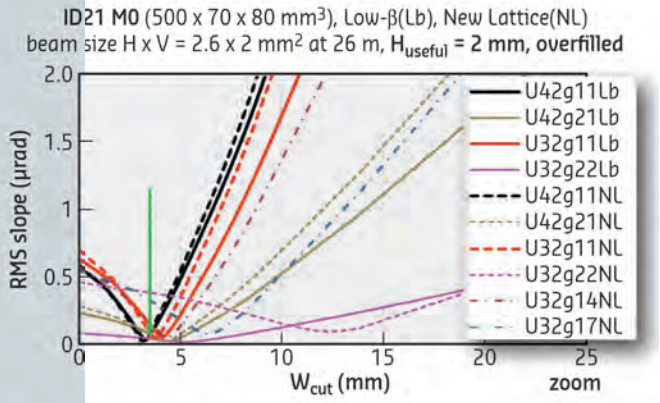

Figure 3.04: Relation between residual slope error and the undercut dimension W_{cut} for varying undulator gap values at an existing low beta section and in the new lattice. Credit: Lin Zhang, ESRF.

3.3.2.2. MONOCHROMATORS

Tailoring of monochromator crystals for specific undulator conditions is currently not beneficial as the beam footprint is always relatively small and the angle of grazing incidence is relatively high.

The maximum power density on monochromator crystals for beamlines currently located on low-beta sections is expected to increase by approximately 35%. However, these beamlines will also benefit from a reduced beam divergence and consequently they will operate with smaller openings of the primary slits. Globally, this will result in a higher power density but lower total power absorbed on the first crystal of the monochromator. Experience has shown that monochromators on high beta sections generally perform as well as, if not better than, the ones located on low beta sections. Consequently, we do not expect any additional performance issues with monochromators due to the change in the lattice.

3.3.2.3. SPECTROSCOPY MONOCHROMATORS

The reduced size of the source and expected improvement in beam stability requires beamline optics to be more stable than in the past. This is particularly important for spectroscopy beamlines that require true fixed exit characteristics, very high energy resolution and beam stability compatible with beam focussing to the nanometric level. A transverse working group with ExpD and ISDD experts has already started to investigate the replacement of spectroscopy monochromators mostly for ageing but also in anticipation of the improved source.

3.3.3. CANTED BEAMLINES

The number of canted beamlines at the ESRF has modestly increased during Upgrade Programme Phase I. ID23, which was installed in 2003 as the first canted beamline, has since been joined by ID16, ID30 and ID15 (the latter still to be modified at the end of Upgrade Programme Phase I). As indicated in section 2.2.4, it is possible to maintain the canting angles for these beamlines. This ensures the compatibility of the beamline layout with the accelerator design. Each beamline may have to move laterally by ±1 mm to compensate for a slight change in the position of the canting magnets, but this is within the range of a standard alignment.

3.3.3.1. 6 METRE AND 7 METRE STRAIGHT SECTIONS

All canted beamlines are currently located on either 6 metre or 7 metre straight sections. As the new accelerator can only accommodate 5 metre straight sections, the suite of undulators installed on these modified straight sections will be adapted by installing either shorter devices or revolving devices. Included in these canted beamlines are ID24 and ID20 that feature 6 metre straight sections, installed during Upgrade Programme Phase I.

3.3.4. OPPORTUNITIES OFFERED BY THE NEW LATTICE WITH MINIMAL INVESTMENT

While it is clear that a beamline specifically designed for the new lattice would feature optical elements for beam transport and conditioning quite different from current day instrumentation (for ref. see **Section 4.2**), substantial improvements can be achieved on existing beamlines by either adding new devices or removing existing ones.

Two generic cases are evident from the survey of existing beamlines shown in **Table 3.1**.

3.3.4.1. WHITE BEAM CRL

Due to the lower horizontal divergence of the beam, in particular for odd harmonics and at high energy, it becomes easier to capture the entire undulator beam by refractive lenses of reasonable dimensions. The ideal location for such a device is in the front end downstream of the photon absorbers and fast valve. In such a scenario, the beamline layout would not change. A suitable lens assembly has to (i) sustain a very high power density, (ii) provide alignment capabilities and (iii) feature exceptional reliability. A detailed study of the advantage of such a system is currently underway.

3.3.4.2. USE OF PINK BEAM

The proposed source will produce very sharp undulator harmonics with reduced energy bandwidth. Isolating a single undulator line will allow certain experiments to achieve sufficient energy resolution without the use of a monochromator. This might be realised by a suitable combination of high band and low band filters such as refractive lenses or mirrors. The resulting gain in photon flux is very high and has been calculated for some beamlines (**Table 3.1**). Such a modification of the primary beamline optics has a profound effect on radiation protection installations and calls for a careful analysis of hutch shielding and their eventual strengthening.

3.3.5. USE OF THE LONG SHUTDOWN

3.3.5.1. NEW INSTALLATIONS

The installation of a new storage ring requires the existing lifting facilities mainly for the removal of the existing storage ring during a short period of time at the beginning of the long shutdown. Major modifications of beamlines are therefore possible during the long shutdown.

3.3.5.2. ALIGNMENT

The reliability of alignment systems implemented at the ESRF and their meticulous maintenance has shown that it is possible to predict where the photon beams are located in reference to the quadrupole magnets and electron beam monitors inside the storage ring tunnel. However, the uncertainties involved in aligning the new source together with ground movements during the long shutdown lead us to predict that each insertion device beamline will have to be realigned at the end of the shutdown, within a typical range not exceeding ±2 mm, and in most cases ±1 mm. This is possible, but requires a typical alignment time of several days per beamline. Therefore, a sufficiently large number of alignment teams working in parallel is required. The existing alignment and survey staff should be reinforced with external resources.

3.3.5.3. BEAMLINE CONTROL SYSTEM UPGRADE

The long shutdown is a unique opportunity to update the beamline control system from the old SPEC based architecture to a new, more versatile system on all beamlines in the ESRF's portfolio, and to strengthen our capacity in online data analysis to be best prepared for the beamline's increased data rate after the machine upgrade (see **Section 4.4**).

3.3.6. SAMPLE ENVIRONMENT

With the strongly increased flux (and flux density) at some beamlines, we will encounter problems with the beam perturbing the sample (modification of its structure, photo-electron charging of the sample surface, radiation damage destroying the sample, etc.). Methods to mitigate these adverse effects are the application of sample scanning (for larger solid samples), the introduction of either cryogenically cooled or vacuum sample environments, and sample replacement at appropriate rates (flow in the case of liquid samples). In particular the latter represents a technological challenge when a high throughput of samples is required. This requires further developments that should benefit from experience gained within Upgrade Programme Phase I in projects such as MASSIF for structural biology.

By way of example we address, in the following, three classes of experiments.

3.3.6.1. HIGH PRESSURE EXPERIMENTS

The ever decreasing beam spot size routinely enables experiments at multi-megabar pressures that are increasingly demanding in terms of loading of diamond anvil cells. Laser cutting such small samples without destroying their structure will require femto-laser cutting systems. Due to its complexity, the manipulation of high pressure samples will be carried out more and more at the ESRF instead of at the user's home laboratories.

3.3.6.2. HIGH TEMPERATURE EXPERIMENTS

In situ studies such as tomographic studies of annealing or quenching processes in materials will require the development of a new generation of tomography furnaces that are rotatable, while featuring a high spatial stability in a sample volume of a few mm^3 and for high heating and cooling rates of several tens of degrees per second.

3.3.6.3. HIGH MAGNETIC FIELD EXPERIMENTS

The strongly increased brightness of the new source will enable imaging, diffraction, and spectroscopy down to the time scale of a single bunch. This calls for the development of self-destructing coils supplying a single high field pulse up to 100 T.

3.3.7. BEAMLINES NOT COMPATIBLE WITH THE NEW SOURCE

3.3.7.1. ID24

ID24 has been identified as the only insertion device beamline which could suffer significant adverse effects from the new lattice. ID24 exploits the horizontal divergence of the undulator beam in order to create a secondary source which is then tightly focused to give a polychromatic beam of 2-3 µm size at the sample. In order to supply an energy band sufficiently wide for EXAFS, the focussed beam should cover an energy range of 1000 eV at the Fe K-edge of 7.112 keV.

As shown in **Figure 3.01**, the beam size at the primary slits for a beamline on a high-beta section does not change. However, as the undulator harmonics are more collimated into the central cone of the emitted beam and as the undulator lines are narrower with the new lattice, the energy content of the off-axis radiation changes. First calculations show that these changes, in addition to the increase in coherence, are not necessarily beneficial to the operation of ID24. If the beamline proves to be incompatible with the new lattice and in order to fully exploit the new machine parameters without a complete redesign of the beamline, we would propose the following strategy:

- Maintain one branch (EDXAS_L) as it is today, and restrict it to high energy applications (11-28 keV). EXAFS will still be possible in an extended k-range, with an increase in photon flux up to a factor of 3. The X-ray spot size at the sample position remains unchanged.
- Modify the EDXAS-S branch to exploit the reduction in horizontal source size while maintaining the extended k-range for EXAFS in the full energy range (5-28 keV) and achieving an increase in flux up to a factor of 3. A reduction in spot size by a factor of 10 can be achieved (focal spot size of 0.3 x 0.3 µm^2 FWHM). This leads to an increase in brilliance of up to a factor of 30.

PART 3
BEAMLINES

3.4. RESTART OF THE BEAMLINES

The commissioning of the beamlines with the new source will start with radiation tests of all radiation safety enclosures in the Experimental Halls and satellite buildings (optics hutches, experimental hutches, beam transfer pipes, etc.). It is obvious that useful tests can only be performed once the ring current has reached a sufficiently high level. We expect to be able to deliver 50mA ring current by end of October 2019 for a first four weeks commissioning period with beamlines. A necessary condition for the opening of the beam shutters is a sufficiently low pressure in the straight sections in order to keep on-axis bremsstrahlung at an acceptable level. The X-ray beam will be available during the two day shifts, while the night shift will be used for further vacuum conditioning of the storage ring. But, if ever possible, the beamline start-up should be done at a storage ring current of 200 mA as this will represent significant savings in time for radiation tests which need to be performed at each intermediate step in beam current.

The initial commissioning of the beamlines requires significantly different efforts for public beamlines located on insertion device ports and beamlines located on former bending magnet ports. Due to the fact that the source point and angle will not change for insertion device beamlines, it should be straightforward to bring these beamlines back into operation. Since the source point and angle will change for all bending magnet beamlines with the introduction of 3-pole wigglers as the standard radiation source for these beamlines, the former "Bending Magnet" beamlines will require a much more in-depth commissioning. We will therefore treat both cases separately.

ID beamlines

In most cases the ID source configuration will be identical to the present configuration. The total power emitted on ID beamlines will be equivalent to the levels presently supplied by the individual sources. We expect therefore no particular problems in terms of radiation protection, provided that vacuum in the straight sections is comparable to the level achieved today.

Based on the plans to deliver the X-ray beam at the sample position within 2 mm of the current position, we do not expect major difficulties with alignment on insertion device beamlines. Due to continuous ground motions also during the shutdown period, we plan, nevertheless, to check the alignment of the beamline components in dedicated campaigns at each beamline.

For a total number of 29 public beamlines we expect the radiation tests to be performed within two weeks. Two teams will work in parallel. We expect a period of two full working days to be sufficient for the preliminary alignment of all beamline components of each beamline in this first commissioning campaign. This requires the parallel work of up to four alignment teams in order to finish this preliminary alignment within the allocated three weeks.

BM beamlines

The spectrum of the emitted radiation will change significantly for many BM beamlines, mostly due to the opportunity to increase magnetic field strength in the 3-pole wigglers. In this case the spectrum of the emitted radiation could be extended to higher energies with higher intensity. The beamlines may therefore have to cope with significantly increased radiation levels, in particular in the optics hutches which may have to be reinforced in radiation hardness. A particularly careful survey will therefore be required to ensure the safe operation on these beamlines.

The source position and angle will change for all former BM beamlines. BM ports that are currently hosting a single beamline should be able to accommodate the required re-arrangement of all the beamline components within the existing hutches.

BM ports that are hosting two beamlines may have to be re-aligned and some optical equipment may have to be re-engineered. This concerns beamlines BM01A/B, BM25A/B, BM26A/B, and BM30A/B.

The commissioning of all beamlines for full user operation is expected to start in February 2020. The ASD has committed to deliver full beam current for this phase. A final survey of all beamlines concerning radiation protection is required before the actual commissioning can start. We anticipate another period of three weeks for this period before the beamlines can start commissioning under conditions requiring the full performance of all components.

The milestones for the shutdown, the restart of the accelerator complex, and the restart of the beamlines for full user operation in June 2020 is summarised in Figure 3.05.

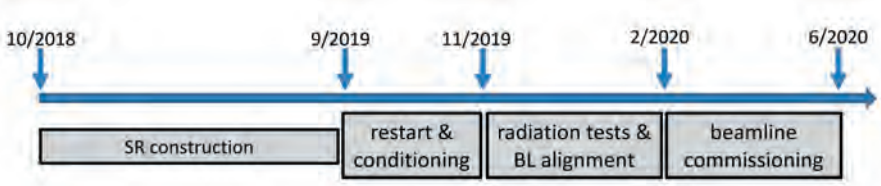

Figure 3.05: Timeline from construction of the new source to restart of the beamlines.

PART 4
Scientific Instrumentation

INTRODUCTION

While the new source will offer dramatic improvements for beam coherence and brightness, only the right scientific instrumentation can truly unleash the scientific potential of the Phase II synchrotron beam. Beamline instrumentation will have to be developed accordingly to keep pace with the quantitative and qualitative improvements of the X-ray source. The majority of the ESRF beamlines should reap immediate performance benefits from the improved source, principally through increased brightness and/or a reduction in the horizontal beam size at the sample. In many cases, novel instrumentation will be needed and this chapter aims to provide a comprehensive overview of the ESRF's strategy for the development of future beamline instrumentation, driven by the new storage ring's capacities. This plan is built upon two challenging objectives:

The first objective is the development of new instrumentation, which will be crucial in exploiting the new source properties to the full and thus opening the way for new scientific breakthroughs. These new instrumentation development programmes will be reliant on new funding of 20 million euros, as included in the Phase II financial plan.

The second objective is the consolidation of ongoing instrumentation programmes, capitalising on advances already made on the most recent beamlines. Initially foreseen within the scope of Phase I, these instrumentation developments suffered severe setbacks due to budget cuts. It is crucial to scale these programmes back up to full capacity. They are expected to provide solutions for the entire beamline portfolio, strengthening existing technological expertise and developing new engineering areas that are currently underdeveloped at the ESRF and identified as critical for the future of the facility. These actions will be funded mainly by the regular ESRF Operation budget.

An additional challenge to conducting these two instrumentation programmes concomitantly is ensuring the appropriate allocation of resources. Advanced project management will be critical for accurate monitoring and astute distribution of resources between projects, including the construction of the new accelerator. Project management will also enable an optimum use of the shutdown period – an important strategic element of Phase II, as it provides a unique opportunity to implement a large-scale beamline modernisation programme that would otherwise be detrimental to the regular User programme, causing delays or down time.

The proposed scientific instrumentation programme to be financed in the context of Phase II includes, by order of importance:

- The launch of a robust detector programme, which is mandatory to make best use of the new source properties.
- Beamline control and data analysis are becoming instrumental for more efficient use of ESRF instruments. Phase II will provide crucial extra resources to complete an ambitious modernisation programme, of which the benefit will go far beyond Phase II.
- Information technology and computing infrastructure has to be developed to the best level in order to be able to manage and process large volumes of data. Phase II will provide resources to upgrade network bandwidth and storage solutions.
- Development of advanced metrology tools and methods for X-ray optics in order to anticipate the very challenging characteristics of the new optical components needed to preserve the new source properties.
- Development of new expertise in mechatronics and online metrology to enhance the performance of the new end stations in terms of stability, accuracy, speed, automation and user-friendliness.

- **Phase II deliverables and associated budget (20 M€)**
  - Detector programme with consolidation of ongoing projects on enabling technologies and development of two new 2D detector systems (8.9 M€)
  - Modernisation of beamline control and data analysis platforms (3.4 M€)
  - IT and computing infrastructure (4.5 M€)
  - Development of advanced metrology tools and methods for X-ray optics (1.7 M€)
  - Development of new expertise in mechatronics and online metrology (1.5 M€)

Therefore, rather than focusing on the Phase II-specific development programmes, this chapter aims to provide an overview of the instrumentation roadmap for the next decade, including both regular activities and Phase II-specific projects. To facilitate the reading of this roadmap, the chapter structure reflects the typical instrumentation sequence of a beamline rather than focusing on Phase II deliverables. It includes:

- Beam transport and conditioning
- End station integration
- X-ray detectors
- Beamline control
- Data analysis
- Computing infrastructure

For each of the above sub-sections, Phase II deliverables will be highlighted and put into the perspective of the overall instrumentation roadmap.

4.1. BEAM TRANSPORT AND CONDITIONING

Phase II deliverables

- New metrology instruments for reflective optics
- Advanced surface processing tools and methods

The fundamental role of the beam transport and conditioning systems is to transfer the photon beam from the front-end to the experimental hutch and to tailor the properties of the X-ray beams from the storage ring source prior to delivery to the end stations. In this respect, the systems may be required to act upon the beam size, beam divergence, photon flux, temporal coherence, spatial coherence and/or polarisation. An important and related role of the systems is to modulate the unwanted power developed by the source in order to alleviate thermal deformation or radiation damage of downstream components or samples.

4.1.1. OBJECTIVES AND DELIVERABLES

Several programmes are foreseen, as detailed in Table 4.01. The latter provides an overview of the roadmap, the elements of which may be specific to Phase II or integral to the standard beamline refurbishment process.

The following sub-sections detail the development programmes listed in Table 4.01, which again follows the logic of a beamline design rather than project priorities. The reference ID (column 2) is used to identify each development programme within the different sub-sections.

	#	Technology	Development objectives	Type	Phase II
Engineering	BT1	Power management	Cooling schemes to minimise wavefront perturbation	G	
	BT2	Photon beam diagnostics	Online tools for measuring and optimising performance of optical systems	A	
	BT3	Vacuum technologies and related phenomena	Improved optics longevity	G	
	BT4	Choppers and shutters for controlling time structure and sample dose	Control of X-ray pulse time structure and exposure.	A	✓
X-ray optics	BO1	Optical modelling	Unified tools for modelling of incoherently, partially-coherently and coherently illuminated X-ray optical systems	G	
	BO2	Coherence/brightness/wave-front preservation	Reduction of phase error to optical imperfections	A	✓
	BO3	Mirror technologies	Opto-mechanical mounting methods Corrective figuring Surface metrology	G	✓
	BO4	Multilayer technologies	Optimisation of deposition methods for high-energy applications Precise deposition control for short optics and alternative focusing technologies	G	✓
	BO5	Refractive lens technologies	Optics in front-end Lens manufacture	G	✓
	BO6	Crystal monochromator systems	High performance fixed-exit double crystal monochromator for fast energy scanning applications	G	

Table 4.01: Overview of development programmes in the beam transport (BT) and beamline optics (BO) instrumentation programme. # = R&D programme reference ID. Type: G = General purpose technologies; A = Application-specific development. Projects dependent on Phase II are marked in the last column.

4.1.2. DEVELOPMENT STRATEGY FOR BEAM TRANSPORT SYSTEMS

With the new lattice, the most marked improvement in the source quality will be due to the considerable reduction of the horizontal emittance. Due to a consequent narrowing (~1.5 x) of the undulator peaks, more flux will be accepted into the bandpass of a typical monochromator. Furthermore, the divergence and source size of the photon emission will be reduced such that it will become possible to focus almost the full ESRF beam into a sub-micrometre spot. As a direct consequence, many techniques that are currently operating with moderately focused beams (~10 x 5 µm) due to the requirement of maximal flux will have the potential to benefit from an improvement factor of 10-20 of the spatial resolution. Other techniques already being applied in the sub-micrometre range will reap benefits either through improved brightness or reduced focal spot size. The emission will remain partially coherent over the entire range of routinely used X-ray energies. However, the reduction in horizontal source size will also give rise to a considerable increase in the transversely coherent fraction of the photon flux (**Figure 4.01**), which will be particularly beneficial for applications exploiting diffraction limited focusing, ptychographic methods and coherent scattering.

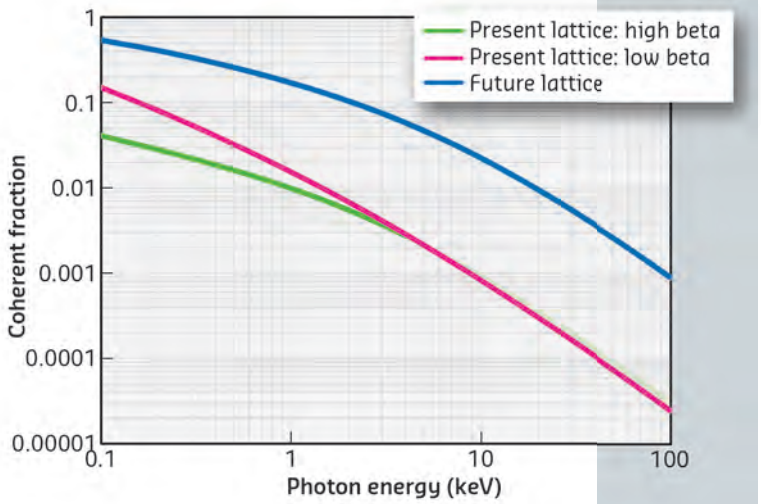

Figure 4.01: Comparison of the variation of the coherent fraction of X-ray emission with energy for the current insertion devices (low-β and high-β source points) and the proposed source.

Such profound modifications in the photon beam characteristics may incite the use of innovative beamline designs employing more sophisticated optical schemes (see for example **Section 4.2**). Considerations might include the implementation of zoom configurations offering flexible and fast capabilities to continuously vary the X-ray beam size and divergence at a given experimental station while preserving the focused beam condition. Beamline designs might also benefit from the possibility to include active moveable optical elements such as lenses or apertures within the front-end modules. In the latter case, power management issues as well as the risk to beamline operation due to component failure will need careful assessment.

The implementation of 'top-up' will maintain the power load on the optical systems during beam delivery. This will help reduce thermal drifts of optical components in standard operation. However it will be necessary to remain vigilant to potential negative effects during the top-up process such as emittance 'blow-up' and other disturbances of the photon source characteristics.

4.1.3. MAIN AREAS FOR DEVELOPMENT

Power management (BT1): For an equivalent storage ring current, the total power generated by insertion devices in the new lattice will be identical to the equivalent devices in the current storage ring and power densities will be comparable with those currently experienced on the high-β source points. Consequently, through careful optical design and component optimisation, power management aspects should not be a limit to the ability to exploit the source to its full potential. A detailed assessment of the impact of the new source on the heat load experienced by optical components is underway, however initial calculations indicate that the thermal management solutions that are currently deployed should remain applicable in their present or slightly adapted form in most cases. For 'passive' components (windows, slits, filters, apertures, choppers, etc.), on the basis of cooling considerations alone, the current designs should be appropriate for use with the new source. In the case of 'active' components (mirrors, monochromators, lenses, etc.) more stringent requirements for preservation of the wavefront quality and the application of radically new optical design paradigms may reveal the need for revised cooling approaches. For the particular case of monochromators, any significant increase in the absorbed power (*e.g.* due to increased storage ring current) might not be sustainable with present

cooling strategies. The capacity for refractive components to operate satisfactorily when exposed to the extremely high flux densities in the front-end module may prove a limiting factor in their deployment in this zone. Nevertheless, apart from silicon crystal monochromator optics, the use of cryogenic cooling for components is not expected to be routine. Power management remains a critical aspect of the beamline optical design that will require continued study both for modelling and experimental validation.

Power management for the revised dipole sources have not been assessed here.

Optical modelling (BO1): Modelling, simulation and optimisation tools will be paramount for the optimal exploitation of the source. Whilst established tools exist, the integration of some optical elements and cross compatibility between codes is either incomplete or absent. As an ultimate aim, the tools to be developed for optical design should permit flexible choice of the optical interactions to be modelled via a common interface using, according to the specific requirements, fully incoherent, partially coherent or fully coherent illumination. The implementation of freeform optical surfaces and the straightforward consideration of manufacturing errors in the tools is essential. Global optimisation methods and codes, *e.g.* for the optimisation of refractive lens-based systems and bent crystal optics, should be incorporated into the toolboxes. Straightforward transfer of results from mechanical, dynamic and thermal modelling and metrology measurements to optical simulation codes is a prerequisite.

Coherence/brightness preservation (BO2): All optical imperfections have the potential to degrade the coherence and source brightness. Such imperfections can originate from either manufacturing errors of the optical component, static deformations due to mounting, thermal distortions due to the incident X-ray beam, or dynamic instabilities from vibrations of the system. The very low vertical emittance of the existing source meant that these aspects were already of capital importance for beamline designs, and engineering solutions for their control have already been developed. For tolerancing purposes, experience has shown that the error margin for the cumulated effect of these imperfections should not result in an increase of the effective source size (over the typical acquisition time of the considered experiment) of more than 10%. This remains, however, a simplification and the tolerancing of the optical quality for components, particularly for imaging applications, using phase contrast or holographic techniques, will rely strongly on advanced modelling methods. Some of the optical design practices adopted for the existing source with larger horizontal emittance, for example, the use of reflective optics in horizontal deflection to relax the slope and figure error requirements, may no longer be valid. This may result in either more stringent optical specifications for mirror and multilayer optics or, in some applications, their replacement by refractive optics, for which the apertures will be able to accept most or all of the horizontal beam. In a more general context, new methods for flexible matching of the spatial coherence of the beam to the experimental requirements (*e.g.* providing incoherent illumination for full-field microscopy techniques) may need further development.

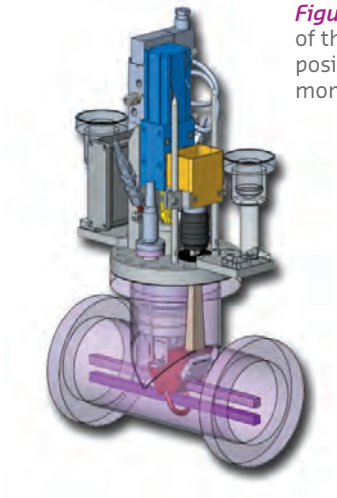

Figure 4.02: Schematic of the white-beam beam position and intensity monitoring system.

Photon beam diagnostics (BT2): During the Upgrade Programme Phase I, considerable development work was carried out for standard integrated tools for X-ray beam position and intensity monitoring for both monochromatic and white beams. Figure 4.02 shows the module developed for white-beam diagnostics, which can operate in a semi-transparent mode allowing it to be used dynamically during beamline alignment processes or during data acquisition. The monochromatic version is a non-transmissive beam viewer which will require the development of semi-transmissive converter screens for Phase II.

The core of the systems should remain compatible with the requirements of the upgraded source and only limited developments are envisaged. The implementation of continuous feedback for position or intensity correction is crucial to ensure even better stability. Its development will be pursued in the field of hardware/software integration and sensors such as diamond, silicon carbide or silicon.

To complement these developments, there is a need for standardised tools to monitor the degree of coherence of the beam to allow an assessment of the beamline optical systems either during the commissioning phase or as an easily inserted diagnostic device during standard beamline operation. Exact strategies have yet to be determined but measurements of the lateral coherence length or effective source size based upon the diffraction pattern developed by known standard objects are possible approaches. The availability of tools and methods (*e.g.* I_0 monitors) to quantitatively assess the effects of phenomena affecting beam and source stability, such as storage ring current top-up, which can be used routinely at all beamlines, will be

of major importance.

Control aspects (see also Section 4.4): Improved beamline alignment software tools to assist in the adjustment of the X-ray optics need to be envisaged. These are increasingly being coupled with the development of diagnostic tools such as those described in the previous section. Moreover, the development and application of beam stabilisation protocols based on feedback from appropriate sensors may yield significant benefits in terms of beamline usability and data quality. The possibility of using the information from white beam position monitors as the input for small, slow corrections of the electron orbit for X-ray beam steering/stabilisation will be assessed.

Vacuum technologies and related phenomena (BT3): Traditional vacuum technologies already in use at the ESRF should suffice for the beamline systems. Some efforts are still required to reduce the in-service contamination of reflective (mirrors and multilayers) and diffractive (crystal monochromators and grating) surfaces by carbon. In the case of coherently illuminated reflective optics, the build-up of inhomogeneous carbon contamination can introduce significant phase errors into the outgoing wavefront, even for rather small C layer thicknesses (*e.g.* at 17 keV, for a grazing angle of 3 mrad, a 25 nm-layer of carbon introduces a phase shift of 0.4 λ).

In many cases, improved vacuum in the upstream optical sections should significantly slow down the observed contamination rates. Additional approaches to be explored are the use of self-healing techniques, such as the introduction of a low oxygen partial pressure into the vacuum chamber during X-ray exposure. This was originally proposed at SLAC (Warburton & Pianetta, 1992) and more recently applied routinely at Soleil (Yao-Leclerc *et al.*, 2011). In parallel, remediative methods (*e.g.* oxygen plasma cleaning) may be implemented, allowing the regeneration of high-value optics either in a centralised cleaning facility at the ESRF or, ultimately, following feasibility testing, *in situ* in the vacuum chamber.

Fully integrated optomechanical systems: Due to the scale of the engineering resources required to fulfil the requirements of the Phase I beamline renewal programme, a cornerstone of the optomechanical instrumentation strategy has been the development of generic technologies consisting of well characterised building blocks, sub-assemblies and protocols. These elements can readily be used to construct the tailor-made systems necessary to satisfy the diverse requirements of the beamline portfolio. A brief description of the key systems and targeted developments is given below.

Mirror/multilayer systems (BO3, BO4): Mirror and multilayer systems have been developed for white- and monochromatic-beam applications offering both high thermal and vibrational stability (Baker *et al.*, 2013). These objectives have been fulfilled whilst guaranteeing the alignment accuracy necessary for precise beam positioning for end stations that can be up to 180 m downstream. This has involved the development of a generic system architecture (**Figure 4.03**) which can be adapted to the specific needs of individual beamlines. These systems should remain compatible with the requirements of the proposed source upgrade and no major review of the system architecture is considered necessary. The expected improvements of the slope and figure errors of the mirrors and substrates to the 0.1 µrad rms and 1 nm peak-to-valley scale present significant challenges for the mounting and cooling technologies in order to preserve these qualities in the final integrated system. Continued efforts will be required to keep apace of optical manufacturing capabilities.

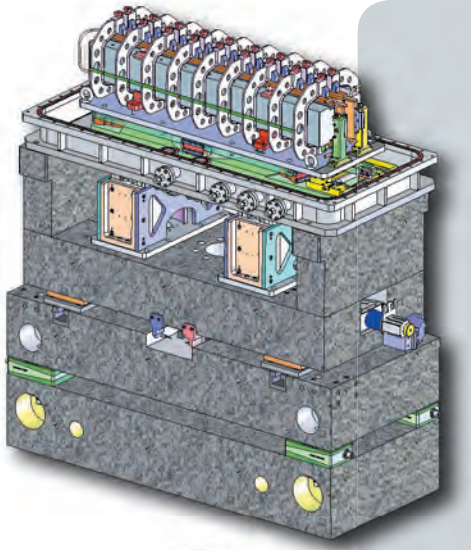

Figure 4.03: Generic white-beam mirror support system.

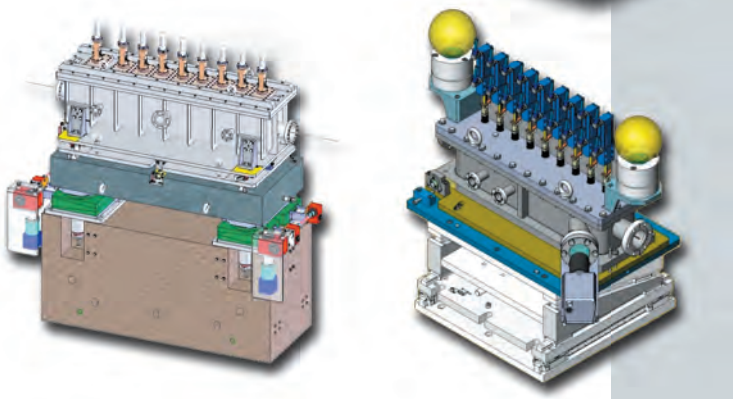

Figure 4.04: Generic refractive lens transfocator systems for white-beam (left) and monochromatic-beam (right).

Refractive lens transfocators (BO5): Similar generic technologies have been developed for compound refractive lens transfocator systems (Vaughan *et al.*, 2010), allowing the focusing behaviour of the devices to be flexibly adapted according to the X-ray energy or specific experimental requirements. Existing in formats suitable for either white beam or monochromatic beam applications (**Figure 4.04**), these systems have been widely deployed in many

Phase I Upgrade Programme beamlines (UPBLs). Although similar solutions will be applied for Phase II, a particular effort will have to be made for the integration of transfocators into front-ends (see **Section 4.1.3**). One of the new constraints is the limited access to this zone during a beam delivery period and the associated need of high reliability.

Crystal monochromator systems (BO6): Significant developments are envisaged for crystal monochromator systems. Most of the double-crystal 'fixed-exit' systems currently deployed at the ESRF, which allow energy scanning whilst keeping the monochromatic beam trajectory constant, were specified and installed in the 1990s. Apart from overall ageing, these systems are underspecified with respect to the new performance requirements (see **Chapter 03**: *Impact on Beamlines*). Recent years have seen dramatic improvements in the source characteristics and a consequent evolution towards the application of spectroscopic techniques requiring extreme stability of the selected photon energy coupled with the need for demanding levels of angular and offset stability of the outgoing beam. The increasing application of these spectroscopic techniques for studies of heterogeneous or small samples means that they are frequently combined with micro- or nano-probe forming optics, for which movements of the incoming photon beam can give rise to instabilities in the focused beam position and/or intensity fluctuations. The improved flux offered by Phase II may also drive a requirement for increased energy scanning speeds either for improved sample throughput or improved time resolution in dynamic studies. Initial assessments of the future requirements indicate that they fall beyond the current capabilities of commercial suppliers. Strategies of the optimal approach to achieving the necessary specifications are being developed. In this domain, there are undoubtedly significant opportunities for common developments between light-sources and/or instrumentation manufacturers.

For applications not requiring fixed-exit and fast energy scanning, there is scope for improvement of the currently widely used ESRF generic channel-cut crystal monochromators. These systems are attractive due to their inherent stability and relatively cost-effective mechanical implementation, but, in particular with a significant degree of spatial coherence in the illuminating beam, are not particularly well suited to imaging or nano-focusing applications due to the intrinsic difficulties of polishing the channel-cut crystal geometry. Development of a generic pseudo-channel-cut monochromator design (whereby two discrete crystals are mechanically mounted in a channel-cut configuration) would overcome these limitations.

Choppers and shutters for controlling time structure and sample dose (BT4): The increased flux available to micro- and nano-probe experiments will give the opportunity for measurements with shorter acquisition times. Depending upon the scientific cases that are to be developed, it may be that tailoring the X-ray pulse structure via the use of fast chopper systems could become a powerful technique. This will require synchronisation with the storage ring radio frequency and bunch clock, particularly in non-uniform filling modes that produce µsec time structure in the X-ray beam. Similarly, developments for fast-shutters or chopper systems for controlling sample dose while synchronised with detectors at the sub-ms level are to be envisaged.

4.1.4. X-RAY OPTICS DEVELOPMENT

Huge progress has been made in the quality of X-ray optics and their implementation since the advent of third-generation synchrotron sources. Nevertheless, the continual improvements in source characteristics (in particular, reductions in emittance) have meant that, often, the optical systems limit the beamline performance. Significant improvement of the underlying X-ray optics technologies is necessary to allow optimal exploitation of the Phase II storage ring source. A comprehensive review of the anticipated future needs for X-ray optics developments has recently been published by the US DoE (D. Mills & H. Padmore, 2013). This report (to which ESRF staff have contributed) addresses many of the key issues for X-ray optics developments common to all sources and particularly relevant to Phase II of the ESRF Upgrade Programme. The principal lines of development for X-ray optics envisaged for the beam conditioning systems are described below. Often these developments overlap with those necessary for micro- and nano-focusing optics (see **Chapter 4.3**).

Refractive lenses: With the reduction in the undulator harmonic energy-width, the use of the strong dispersion properties of refractive lenses in combination with an energy-selecting aperture placed at the achromatic focal point may offer an effective method to create a high-throughput broadband monochromator. Exploration and modelling of the applicability of such schemes to future beamline designs will be required. The new beam parameters will open up a unique opportunity to build up a new concept for loss-free beam transport and conditioning systems based on in-line refractive optics. Taking advantage of the substantially reduced horizontal source size and the beam divergence, these new systems integrated into the front-end can transfer the photon beam almost without losses

from the front-end to any further secondary optical systems (mirrors, crystals, lenses, etc.) or directly to the end stations. This development would be a logical step after the successful implementation during Phase I of transfocators, which are tuneable devices based on refractive lenses. Since 2007, a large variety of transfocators and lens changers were installed in half of the ESRF beamlines. In addition, these optics might play an important role in filtering out the unwanted power developed by the source in order to alleviate thermal deformation or radiation damage of downstream optical components such as mirrors and crystals. The pre-focused beams with smaller sizes/footprints might significantly reduce the length of mirrors and crystals.

More generally, an investigation of alternative raw materials (X-ray homogeneous/amorphous materials (Be, diamond, B)) and methods for both linear/planar and rotationally symmetric lens manufacture will be motivated by the quest for lenses generating reduced levels of absorption, coherent- (speckle contrast), and diffuse-scattering. This selection of ad-hoc materials will rely on the development of appropriate metrology and qualification methods.

Mirrors: For all but the soft X-ray regime, where single particle photon emission divergence dominates the beam size, the reduced horizontal emittance of the Phase II storage ring source leads to a typical reduction in the aperture size (for equivalent flux), ranging from 30% (3 keV) to 65% (100 keV). For mirror optics this translates either to a reduced useful mirror length or improved flux collection following the lattice upgrade. For the former case, this offers the possibility for more compact and higher stability systems coupled with the improvements in the optical quality (slope and figure errors) achievable for shorter optics. Commercial fabrication methods (often using deterministic sub-aperture corrective figuring) currently permit the routine manufacture of long-plane mirrors with sub-0.3 µrad rms slope errors by several manufacturers. The ability to produce plane mirrors with higher tolerance as well as toroidal and spherically curved surfaces is often limited by the precision of the optical metrology techniques available in the manufacturing facility. The production of flat, highly curved and aspheric mirrors with sub-0.1 µrad rms slope errors is significantly more challenging and is currently under the monopoly of just one company. For focusing mirrors with incoherent or partially coherent illumination, the attainable vertical focus size will continue to be dominated by the effects of the slope errors even for values at the 50 nrad rms scale. For horizontal focusing, slope errors of ~100 nrad rms will generally suffice to ensure that focused beam sizes are limited by the source size. For applications exploiting coherent illumination, figure errors will introduce wavefront distortions, which need to be minimised. For the typical hard X-ray wavelengths employed at the ESRF, application of the Maréchal criterion (Hignette *et al.*, 2001) indicates figure error requirements in the sub-1 nm range. Nevertheless, in many apparently less demanding applications, there is a significant incentive to reduce the slope and figure errors to the sub-0.1 µrad rms and sub-1 nm peak-to-valley scale in order to reduce the contrast of the intensity inhomogeneities that are typically observed in the reflected beams from mirrors in either unfocused or defocused beams. Whilst the manufacture of these elements is essentially the preserve of industrial suppliers, the ESRF will continue to explore corrective figuring methods by subtractive (*e.g.* ion beam figuring) or additive (*e.g.* differential deposition) techniques as well as mechanical correction techniques.

Phase II will provide resources to retain and develop capabilities in the measurement of slope and figure errors with appropriate accuracy and precision, both for acceptance procedures and, equally importantly, to validate the mechanical mounting of the optics prior to their integration into the beamlines. Routine protocols allowing the characterisation of the performance of the systems prior to, and/or after, installation using at-wavelength methods will need to be promoted. These tools are also of relevance for the characterisation of diffractive (crystals and gratings) and multilayer optics components.

Monochromator, polarisation and analyser optics: Based on the power management considerations (see **Section 4.1.2**) it is probable that the majority of monochromator applications will continue to be satisfied by float zone silicon material. The crystal processing techniques to be applied to silicon monochromator crystal production are rather mature. However, improvements are still possible, in particular, for the production of bent crystal optics and crystals for ultra-high energy resolution and energy analyser applications. Diamond crystal, in particular as used in semi-transparent beam splitters and for polarisation control, will continue to be a strategic material. We should continue to be active in ensuring the availability of the appropriate crystals. To preserve the reduced horizontal emittance on beamlines implementing such beam-splitters, it may be necessary to expend extra effort in developing the thin plates of the required quality to operate in the symmetric Bragg 111 reflection. The quest for ever higher energy resolution or access to soft X-rays both for monochromators and analyser crystal applications (see **Section 4.2)** may require the development of processing methods for alternative materials (*e.g.* quartz, sapphire). The preservation of the in-house diffractive crystal processing capabilities is a critical element of the ESRF strategy in this field and yields significant benefits for optimal beamline operation. After 20 years of operation, some of the equipment is ageing and a replacement plan has to be considered. Strain-free mounting of the crystals in their final system is a critical aspect that has already been well studied,

but improvements are still possible. Continued access to appropriate characterisation techniques and especially X-ray topography for quality control provides the foundation for all developments in this domain. Soft X-ray applications using diffraction gratings are marginal at the ESRF and no specific optics developments are foreseen. However, we should retain our expertise in the *ex situ* characterisation of these elements.

Multilayers: As for the mirror systems, the use of multilayer-based optical elements will benefit from the post-Phase II reduced horizontal beam size in the sense that the optics can become shorter and/or intercept a larger fraction of the incoming beam. The downside of the reduced horizontal source size will be an increased sensitivity to figure errors even under horizontal deflection. A critical development line will therefore concern the procurement of substrates with lower figure errors while maintaining a very low level of micro roughness. Figure correction within the coating system prior to multilayer deposition may be a potential approach. Shorter but more precisely manufactured multilayers may require a dedicated, downscaled deposition system to complement the existing facilities. The goal would be to attenuate line artefacts from the reflected X-ray beam generated by substrate figure errors. Such equipment will also become mandatory for very short nano-focusing multilayer optics (see **Section 4.2**) and may even permit the fabrication of the recently developed multilayer Laue lenses or multilayer zone plates. The increased brilliance and coherent fraction of the source to higher photon energies open new avenues to the use of multilayers at very high energies, often coinciding with very high energy resolution of 0.5% or less. The fabrication of such multilayer coatings requires a perfect control of stable deposition conditions and an efficient strategy to mitigate intrinsic stress in the layer stack.

4.1.5. X-RAY TEST FACILITIES

X-ray test facilities are essential to all of the X-ray optics (and X-ray detector) development programmes. With the increased demands upon operational beamlines to deliver beam for user experiments, they are rarely accessible for the full performance characterisation of developmental and prototype optics. In particular, pre-testing of white-beam optical systems such as monochromators is generally precluded for operational beamlines and consequently it is important to guarantee access to additional sources for instrumentation testing. Currently complementary needs are satisfied by access to beamtime at two different sources. **ID06** allows tests of: i) high heat-load optics; ii) micro- and nano-focusing optics; iii) new optical configurations; iv) at-wavelength metrology; v) diagnostic systems. **BM05** allows tests of: i) diffractive crystal quality; ii) multilayer and mirror reflectometry; iii) at-wavelength metrology; iv) diagnostic systems. Flexible access to these facilities is also critical for supporting detector development and it is essential that these or equivalent facilities remain available during and after Phase II.

References:

Warburton W.K. and Pianetta P. In Situ Optical Element Cleaning with Photon Activated Oxygen, Nuclear Instruments and Methods in Physics Research Section A: Accelerators, Spectrometers, Detectors and Associated Equipment **319**, no. 1–3: 240–43(August 1, 1992). doi:10.1016/0168-9002(92)90560-Q.

Yao-Leclerc I., Brochet S., Chauvet C., De Oliveira N., Duval J.-P., Gil J.-F., Kubsky S. *et al.,* Handling the Carbon Contamination Issue at SOLEIL, Proceedings of SPIE **8077, no. 1** (May 5, 2011): 807712–807712–9. doi:doi:10.1117/12.886970.

Mills D. and Padmore H., 2013, X-ray Optics for BES Light Source Facilities, http://science.energy.gov/~/media/bes/pdf/reports/files/BES_XRay_Optics_rpt.pdf.

Hignette O., Peffen C., Alvaro V., Chinchio E., and Freund A. K., Towards the Preparation of Optical Surfaces Preserving the Coherence of Hard X-Ray Beams, *X-Ray Mirrors, Crystals, and Multilayers*, edited by A. K. Freund, T. Ishikawa, and A. M. Khounsary, 4501:43–53. San Diego, CA, USA: SPIE, 2001. http://link.aip.org/link/?PSI/4501/43/1

Baker R., Barrett R., Clavel C., Dabin Y., Eybert-Berard L., Mairs T., Marion P. *et al.,* New Generation Mirror Systems for the ESRF Upgrade Beamlines, Journal of Physics: Conference Series **425, no. 5** (March 22, 2013): 052015. doi:10.1088/1742-6596/425/5/052015.

Vaughan G., Wright J., Bytchkov A., Rossat M., Gleyzolle H., Snigireva I., and Snigirev A., X-Ray Transfocators: Focusing Devices Based on Compound Refractive Lenses, Journal of Synchrotron Radiation **18, no. 2,** 125–33(December 21, 2010) doi:10.1107/S0909049510044365.

4.2. END STATION INTEGRATION

4.2.1 OBJECTIVES AND DELIVERABLES

Phase II Deliverables

- Mechatronics platform
- Development of online metrology instrumentation
- Development and procurement of X-ray optics for nano-focusing

The unprecedented beam characteristics in terms of beam size, brightness and coherence are expected to influence the design of new end stations. In all likelihood, there will be an increasing number of applications requiring access to sub-micrometre spatial resolutions. Furthermore, while the increased flux will directly benefit photon-hungry experiments, radiation damage will certainly become a common issue for most of the beamlines. In both cases, faster experiments with deployment of on-the-fly acquisition modes will have to be developed with the general objective of zero dead-time experiments. Finally, the trend towards multimodal end stations will continue to develop. The combination of several analysis techniques available on a single end station and the use of ancillary instruments (*e.g.* AFM/STM, visible light spectroscopy such as Raman, UV-VIS and infrared) is expected to be increasingly common. Similarly, enhanced automation will be instrumental for beamlines performing repetitive measurements while requiring highly stable and easily reproducible acquisition conditions.

To meet these objectives, the development programme will aim primarily to build on Phase I achievements, in particular capitalising on the know-how acquired from recent Phase I Upgrade Programme beamlines. In contrast, Phase II will offer the unique opportunity to complement our expertise and capacities with new developments in mechatronics and high-resolution online metrology, two fields that are currently underdeveloped at the ESRF and identified as highly strategic for future, state-of-the-art beamlines. Table 4.02 provides an

	#	Technology	Development objectives	Type	Phase II
Nanoprobes	EN1	Environmental stability	Temperature control and optimised design of dynamic response of mechanical stages	G	
	EN2	High resolution mechanics	Optimised integration of commercial components	A	
	EN3	On-line metrology	Develop adequate integration of interferometers	G	✓
	EN4	Advanced control system	Multi-axis closed loop fast control system	G	✓
	EN5	Beam/sample visualisation	Full integration of compact, long-distance, visible light microscope	G	
	EN6	Nano-focusing optics	Development and procurement of high-resolution X-ray optics	A	✓
Zero-dead-time experiments	EZ1	On-the-fly continuous scan	Mechanical system and metrology	G	
	EZ2	Automation	Development of ad-hoc technologies and control strategy	A	

Table 4.02: Overview of development programmes in the nanoprobe (EN) and zero-deadtime (EZ) technology programmes. # = R&D programme reference ID. Type: G = General purpose technologies; A = Application-specific development. Projects dependent on Phase II are marked in the last column.

overview of this programme, including all activities foreseen over the next decade, most of which are integral to the core mission within the regular facility operation. The table also highlights projects that are expected to be funded by Phase II.

The following sub-sections detail the planned development programmes listed in Table 4.02, which again follows the logic of a beamline design rather than project priorities. The reference ID (column 2) is used to identify each programme within the different sub-sections.

4.2.2. ENABLING TECHNOLOGIES FOR NANO END STATIONS AND FAST EXPERIMENTS

Over the past 20 years, the ESRF has built up solid expertise in high precision systems. As exemplified by the developments triggered by the UPBL4-NI end station project (see Figure 4.05), the Upgrade Programme Phase I offered the ideal context to strengthen these activities and further develop the technical capabilities dedicated to micro-mechanics (*e.g.* assembly lab, clean rooms, etc.). Indeed, several projects from Phase I required acquisition and implementation of advanced engineering, which now provides a solid base for the next generation of nanoprobe end stations. However, even more challenging requirements must be anticipated for Phase II beamlines, when end stations will have to be compatible with a sub-10 nm beam size. To cope with these new challenges, two engineering areas – currently underdeveloped at the ESRF – have been identified as critical: advanced control and online metrology. These two new areas will be addressed by an expert group on mechatronics.

As already explored in the Upgrade Programme Phase I Purple Book, the design of state-of-the-art nanoprobes relies on the mastering of several technologies and parameters. Developing these technologies further is part of the ESRF's basic operation programme and includes (see Table 4.02 for reference):

Thermal and vibration stability (EN1): Stability, both thermal and vibrational, is a prerequisite to a successful design. We have developed advanced modelling capabilities to optimise air-conditioning systems, heat sources, etc., as well as vibrational behaviour of mechanical systems. Similar methods will be deployed for the beamline refurbishment programme as well as for the design of new nanoprobes in Phase II.

High-resolution positioning and scanning stages (EN2): An expert group constantly assesses the performance of commercially available systems and the way these systems can be integrated into complex and highly customised end stations, in terms of resolution, compactness, stability and electronics. All Phase II projects will benefit from this approach.

Creation of a mechatronics and advanced online metrology laboratory (EN3, EN4): State-of-the-art nanoprobes require nanometric positioning of the sample in 3D. Very often this sample also has to be scanned along several axes (translation and rotation). When dealing with nanometric resolution, the very high precision of the mechanical system is not sufficient to achieve the requested resolution and it must be completed in a feedback loop with ad-hoc online metrology. This so-called mechatronics approach, involving high-resolution mechanics, advanced controllers, and ad-hoc control software will be one of the main areas of development in Phase II. The new control system must be able to pilot several axes according to the signals from several sensors in local and global fast closed loops (several kHz), with the possibility to mathematically combine several sensor signals. Although some exploratory projects have been initiated recently for Phase I Upgrade beamlines (*e.g.* UPBL4), the ESRF expertise in this area is still relatively low and a wider dissemination of this technology will require significant investment.

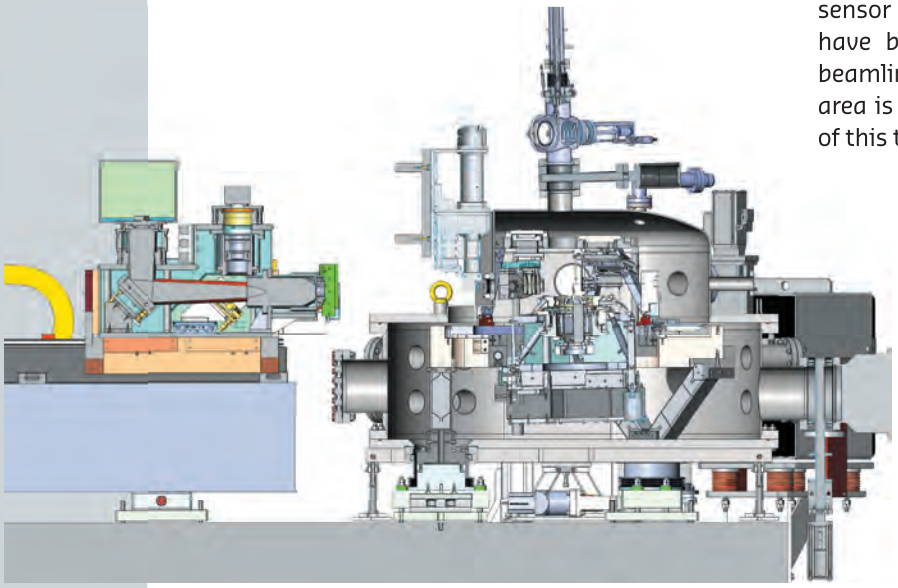

Figure 4.05: The UPBL4-NI end station – an example of a highly integrated endstation for nanoprobe applications.

Phase II is expected to provide adequate resources to create an expert group and a laboratory dedicated to the integration of this technology within the future end station designs.

High resolution visualisation systems (EN5): The operation of nanoprobes will increasingly rely on the ability to fully control the sample position relative to the probe. This will be even more challenging when sample sizes reach the micrometre scale. This new constraint has led to the development of new strategies for sample and beam visualisation. Most of the methods rely on the long-working-distance optical microscope and fluorescence screen coupled to fiducial markers. The full integration of this type of instrument into the end station prevents the use of commercial microscopes, most often requiring the design of fully customised optical systems. Such an approach has been successfully implemented for UPBL4, with an on-axis, visible microscope capable of nanometric precision (see **Figure 4.06**). However, further development in this engineering is foreseen to promote the integration of such a visible light microscope into new end stations.

Nano-focusing optics (EN6): It is becoming increasingly important for optical systems for focusing at the sample to be integrated into the end station design. This approach favours stability and, in the case of nano-focusing, is also motivated by the need to operate with optic-to-sample working distances of typically <0.5 m. Steady progress in the performance of the different classes of optics (see **Figure 4.07**) and the need to adapt to the particular experimental requirements (photon energy, flux, achromatic focusing...) indicate that no unique optical device will satisfy all the ESRF needs. Sub-10 nm resolution using focused beams has been demonstrated using both reflective (Mimura *et al.*, 2010) and diffractive (zone plate) (Vila-Comamala *et al.*, 2009) optics. Significant work is still required, both in the technical implementation and in the optical performance, to be able to offer these capabilities routinely to the user community. The continued close collaboration between the different engineering and beamline groups has proved effective for the successful implementation of diverse nano- and micro-focusing systems within the existing beamlines and it will be important to leverage the acquired know-how and expertise to ensure that the new capabilities of the underlying optics are fully exploited. A significant step in this direction is the ID16 beamline (UPBL4) of the ESRF Upgrade Programme Phase I.

The two applications of X-ray nano-focusing optics are condensing or probe-forming optics upstream of the sample on one hand, and image-forming optics downstream of the sample on the other. For probe-forming optics, apart from near-field approaches such as wave guides or capillaries, the optical systems image the photon source into a fine probe through

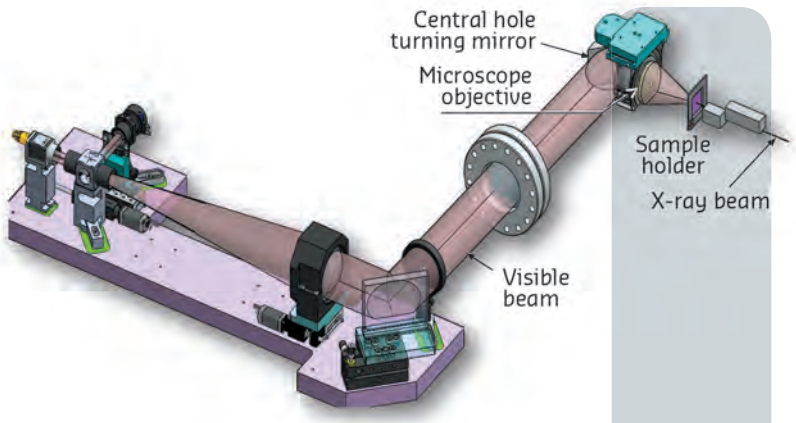

Figure 4.06: The UPBL04-NI sample/beam visualisation device.

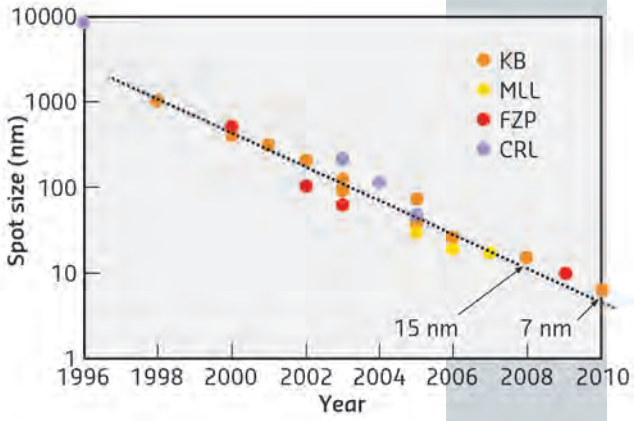

Figure 4.07: Historical evolution of the smallest measured spot size for different hard X-ray focusing elements (KB: Kirkpatrick-Baez focusing mirrors, MLL: multilayer Laue lens, FZP: Fresnel zone plate, CRL: compound refractive lens).

which the sample is generally either translated within the focal plane (scanning probe microscopy) or placed in the diverging radiation downstream of the focal plane (projection microscopy). Compared with the ID sources of Phase I, Phase II offers a photon source of significantly increased circularity. Nevertheless, the ratio of horizontal to vertical source size remains greater than 6:1 over the entire hard X-ray spectrum implying that for an ideal optical system, the formation of a symmetric 'round' probe requires a matching asymmetry between the horizontal and vertical demagnifications. The key to achieving small probe sizes is to maximise the numerical aperture of the optics whilst illuminating with spatially coherent X-rays. The maximum achievable numerical aperture depends primarily upon the focusing optic while the spatial coherence is determined by the source properties. Following the source upgrade the coherent fraction of the beam will be increased by more than 1 order of magnitude in the hard (>10 keV) X-ray regime offering the potential for equivalent increases in the flux in diffraction-limited probes. The formation of probes with a high degree of spatial coherence (*i.e.* close to or at the diffraction limit) is also of importance for the application of ptychographic techniques. The motivation for many of the X-ray optics developments described below is either to increase the numerical aperture, the throughput and/or the efficiency or to reduce manufacturing artefacts

to ensure that the performance is diffraction limited (see **Figure 4.07**).

As described in **Section 4.1.4**, the evaluation of the tolerances for manufacturing the focusing systems with the required performance requires the continued development of appropriate modelling tools. This is particularly true for coherently or partially coherently illuminated optics. The principal X-ray focusing optics developments are:

Reflective optics: The production of highly aspherised mirrors for nanofocusing is technologically complicated and various routes towards rendering these devices accessible to a wider number of beamlines are to be explored. The integration of these mirrors into compact, stable alignment mechanics is a critical aspect in which the engineering groups have gained significant experience during the Upgrade Programme Phase I. We have a well-established development programme for mechanically bent mirror systems for micro- and nano-focusing (see **Figure 4.08**). Used in combination with laterally graded multilayer coatings, these systems offer large acceptance apertures even with rather short focal lengths. The achromatic focusing and wide energy band pass of the multilayer means that these systems can typically accept the photon flux from the entire energy width of the undulator peak. These capabilities will be further developed for Phase II.

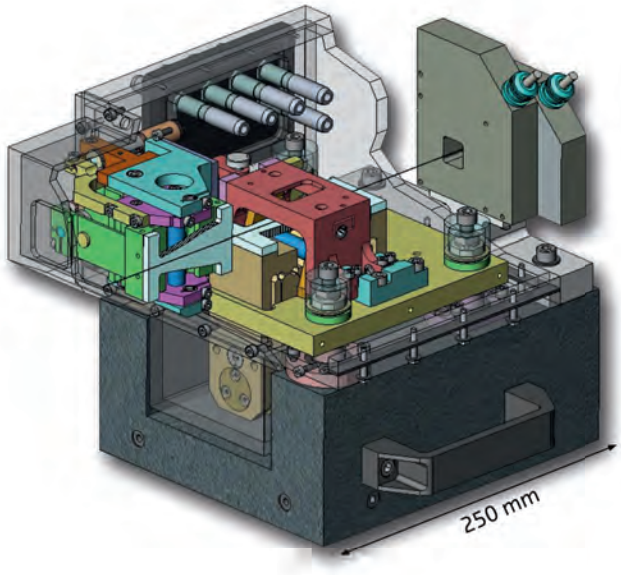

Figure 4.08: Advanced compact Kirkpatrick-Baez mirror system for nano-focusing applications.

Both the development and the application of focusing reflective optic systems can only be efficient if supported by state-of-the-art metrology facilities. The particular challenges are to measure figure and slope errors at the sub-1 nm and sub-0.1 µrad level on a highly aspherical surface and will require the continued development of enhanced measurement techniques.

Refractive optics: The on-axis focusing of refractive lenses renders them an attractive solution for beamlines requiring a flexible and rapid means to alternate between a focused and unfocused beam. This versatility is enhanced by the development of a compact transfocator device (**Figure 4.09**) at the ESRF. This system can be used with either 1D or 2D (rotationally symmetric) parabolic lens elements and is designed to be readily introduced close to the experimental station, allowing the focal length or system chromaticity to be flexibly adapted in seconds by modulating the number of lens elements inserted in the beam path. Principle developments currently foreseen (conducted externally with ESRF collaboration for characterisation) are concentrated upon the quality of the individual lens elements to reduce parasitic scattering through alternative materials and processing.

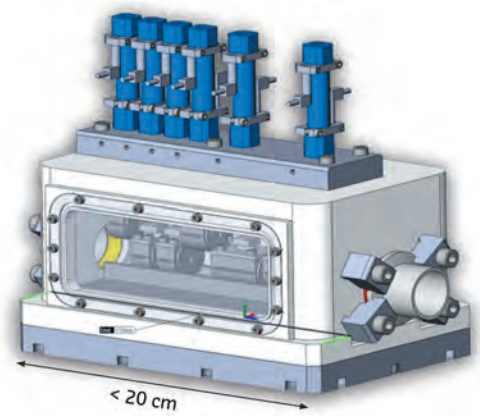

Figure 4.09: Compact transfocator.

Principal improvements in the focusing performance of planar lens technologies for nano-focusing application stem from the desire to increase numerical apertures (currently absorption limited) and to increase the sagittal acceptance. Potential pathways towards improved apertures are through the replacement of the more commonly used silicon lenses by diamond or beryllium technologies, the use of adiabatic (*e.g.* Schroer & Lengeler, 2005) or kinoform lens profiles (*e.g.* Aristov *et al.*, 2000 or Evans-Lutterodt *et al.*, 2003). The improvement of pattern transfer methods to manufacture high aspect-ratio structures with smooth and vertical side walls is essential to the improvement of the sagittal acceptance. As for reflective optics, the availability of non-X-ray based characterisation and metrology techniques is primordial for the efficient development of improved lens processing and capabilities in this field should be developed.

Diffractive optics: Continued improvements in spatial resolution capabilities and efficiency through techniques such as zone doubling and stacking of zone plates mean that these optics are competitive for applications in the multi-keV energy range. Their application is relatively straightforward but investment in zone plate fabrication through

lithographic techniques remains costly. No internal developments for zone plate fabrication are foreseen and activity in this field will be concentrated on the integration of externally sourced optics into the end stations. Principal developments of interest for our applications would be efficiency improvements allowing effective use in the harder X-ray regime. The availability of high resolution (sub-50 nm) kinoform lenses (Di Fabrizio *et al,* 1999) would be a significant advance in this direction.

Other approaches towards the fabrication of diffractive nanofocusing optics such as multilayer Laue lenses or multilayer zone plates are potentially better suited to high energy photon focusing. Internal developments in this direction would fit closely with acquired expertise in multilayer deposition and the necessary capabilities could be incorporated in the new deposition tool proposed in **Section 4.1.4**. In the case of multilayer Laue lens developments, appropriate optomechanical alignment systems would need to be implemented prior to beamline deployment.

Towards zero-dead time experiments: With the expected increase in photon flux, and the availability of faster detectors, the time devoted to acquisition is becoming shorter and shorter while dead time associated to beam alignment, sample positioning and scan, energy tuning, etc., still determines to a large extent the actual duration of an experiment. The overall goal of minimising these sources of dead time addresses several aspects of the beamline operations and aims at multiple objectives: i) better use of beamtime, ii) minimising radiation damage, and iii) minimising the acquisition time per sample when a large number of samples have to be analysed under stable and reproducible conditions.

It is foreseen to address this issue by developing ad-hoc engineering solutions. The R&D programme will be structured around two mains axes of development:

Modernisation of the beamline control: **Section 4.4** gives an exhaustive description of this programme. In this section, it is worth noting that we plan to develop a generic solution for on-the-fly acquisition modes with complex sample trajectories. The required precise control of the sample trajectory will rely on motors controlled in a fast feedback loop by sensors. Adequate motors and sensors must be selected to cope with the dynamic requirements and the mechanical system must be designed for a sufficient dynamic response. As for high precision systems, the central need for fast motion systems is a multi-motor/multi-sensor control system. Major efforts will be invested in this topic during Phase II.

Automation: Structural biology is one of the main drivers for advanced automation. Most of the protein crystallography beamlines worldwide rely on an integrative approach from sample alignment to data analysis allowing high throughput experiments in which a very large number of crystals can be screened and measured. In Phase I, the project *MASSIF* exemplified this approach with a high level of automation and optimisation of the data collection process. Other fields, including powder diffraction and Xray tomography, follow the same trend by the integration of automated sample changers. Phase II will favour the dissemination of such a strategy across a broader range of beamlines. In particular, experiments relying on statistical analysis over a large number of samples will benefit from much shorter acquisition times per sample. Automation of these measurement-oriented beamlines will allow acquisition to be carried out with minimum dead-time and with highly reproducible experimental conditions. Automation processes are by nature case-dependent and require a thorough analysis of the adopted strategy. However, generic technologies can be implemented and in a second stage, tailored into specific solutions. The development of those generic technologies will be an integral part of the mechatronics programme.

References

Schroer C. G. and Lengeler B., Focusing Hard X Rays to Nanometer Dimensions by Adiabatically Focusing Lenses, Physical Review Letters **94, no. 5** (February 10, 2005): 054802. doi:10.1103/PhysRevLett.94.054802.

Aristov V., Grigoriev M., Kuznetsov S., Shabelnikov L., Yunkin V., Weitkamp T., Rau C. *et al*., X-Ray Refractive Planar Lens with Minimized Absorption, Applied Physics Letters **77, no. 24** (December 11, 2000): 4058–60. doi:10.1063/1.1332401.

Di Fabrizio, E., Romanato F., Gentili M., Cabrini S, Kaulich B., Susini J., and Barrett R.. High-Efficiency Multilevel Zone Plates for keV X-Rays, Nature **401, no. 6756** (October 28, 1999): 895–98. doi:10.1038/44791.

Evans-Lutterodt K., Ablett J., Stein A., Kao C-C., Tennant D., Klemens F., Taylor A. *et al.*, Single-Element Elliptical Hard X-Ray Micro-Optics, Optics Express **11, no. 8** (April 21, 2003): 919–26. doi:10.1364/OE.11.000919.

Vila-Comamala J., Jefimovs K., Raabe J., Pilvi T., Fink RH., Senoner M., Maaßdorf A., Ritala M. and David C., Advanced Thin Film Technology for Ultrahigh Resolution X-Ray Microscopy, Ultramicroscopy **109, no. 11** (October 2009): 1360–64. doi:10.1016/j.ultramic.2009.07.005.

Mimura H., Handa S., Kimura T., Yumoto H, Yamakawa D., Yokoyama H., Matsuyama S. *et al.*, Breaking the 10 Nm Barrier in Hard-X-Ray Focusing, Nat Phys **6, no. 2** (February 2010): 122–25. doi:10.1038/nphys1457.

4.3. X-RAY DETECTORS

4.3.1. OBJECTIVES AND DELIVERABLES

Phase II deliverables

- Consolidation of enabling technologies for detector integration
- New, small-pixel, noise-free 2D detectors
- New high dynamic range CMOS detectors

Over the years, the increasing degree of specialisation of beamlines and highly focused scientific applications requires a matched specialisation of X-ray detectors. For this reason, a diversity of detection technologies and concepts have been developed, with each different type of detector satisfying a particular set of characteristics that are critical for a family of applications. Unavoidably, the less critical detector features are thus compromised. The Phase II storage ring source enhancement will increase beam intensity, and boost coherent diffraction techniques. From this perspective, the main challenges for new detector developments are:

4.3.1.1. MANAGEMENT OF HIGHER PHOTON FLUXES AND SHORTER TIME SCALES

The increased photon flux of the Phase II source will require detectors with extended dynamic range and able to cope with shorter timescales. Increased flux will result in a substantial reduction of the total time required to perform a complete sample scan, which promotes the application of fast mapping techniques. The detectors will have to operate with shorter readout times and at increased frame rates, which will require pushing intrinsic time resolution to the limits. Implicitly, the higher time resolution and detector frame rates must be upheld by very high throughput readout systems in order to make adequate use of the available photons.

4.3.1.2. REACHING HIGHER SPATIAL RESOLUTION FOR SINGLE-PHOTON SENSITIVE DETECTORS

A sufficient detection angular resolution is mandatory for all experiments with coherent beams. The same is true for most of our high resolution wavelength dispersive spectrometers using 1D or 2D detectors. In both types of experiments, single-photon sensitivity is also crucial to produce noise-free data. The Phase II source will accentuate the angular resolution requirements of detectors due to the ability to coherently illuminate samples of larger size and the completely new possibility of applying coherent beam techniques at shorter photon wavelengths in order to image samples in absorbing environments such as high pressure cells. Although the angular resolution in coherent scattering applications can be improved by moving the detector far from the sample, some experiments today are already limited by the minimum pixel size of the existing detectors. This is particularly the case in experiments in which the maximum sample-to-detector distance is bounded. In Phase II, the practical ability of extending coherent beam techniques in optimum conditions to a diversity of scientific cases, experiment set-ups and higher photon energies will depend crucially on the availability of efficient and sensitive 2D detectors with spatial resolution beyond 55 µm, the minimum pixel size of current photon counting area detectors.

4.3.1.3. IMPROVEMENT OF DETECTION EFFICIENCY

The increased brilliance and coherence over the whole spectral range provided by the Phase II source will make it possible to perform experiments with very hard X-rays that are today restricted to lower photon energies. Furthermore, moving to high energies to reduce sample radiation damage will be an important trend. Unfortunately, detection of Xrays above 20 keV in most cases suffers from severe efficiency limitations that worsen very rapidly as the photon energy increases. Poor detection efficiency is usually the result of the weak absorption of the Xray sensor which must be kept thin enough to preserve the spatial resolution of the detector. Improving the trade-off between spatial resolution and efficiency is one of the long-standing challenges of the ESRF and other high energy light sources.

Technology developments that improve detection efficiency are also expected to have a very positive impact on all experiments, including those at lower energies. Efficiency improvement efforts must address not only the limited absorption of the X-ray sensors but also aim at other important matters such as minimising detection dead areas or suppressing readout dead time.

4.3.2. MAIN DEVELOPMENT AREAS AND ACTIVITIES

While generic detectors may be adequate for some experiments, 20 years of experience at the ESRF and elsewhere shows the value of application-specific detector development with a focus on customisation, integration and optimisation of complete detector systems. Nevertheless, given the number and variety of experiments performed at large facilities such as the ESRF, as well as the timely and costly development cycles of detector technologies, beamline-specific developments must be restricted to short-term projects of moderate cost. This kind of development projects in the past at the ESRF have typically involved integrating off-the-shelf or commercially available sensors, electronics and opto-mechanical devices and have relied heavily on the available manpower and know-how in the facility.

This approach (see **Figure 4.10**) will be pursued in the future but must be complemented with a programme aimed at state-of-the-art detectors using the most up-to-date technologies.

Therefore, a continuous survey and access by the ESRF technical staff to the latest technical advances will continue to be instrumental in the design of new beamline-specific detectors, as well as the constant upgrading of existing devices. Additionally, the new source will offer many new experimental opportunities, which existing X-ray detectors may be unable to exploit. Therefore Phase II will offer the unique context to launch the long-term development of full, new, advanced detector systems that will boost the scientific capabilities of the facility.

Based on these considerations, the Phase II detector programme will focus on three types of activities: a) customisation and integration of application-specific detectors, b) accessing key and strategic detection technologies, c) the development of new advanced detector systems. While the former may be considered as recurrent activity involving relatively short-term beamline specific projects, the latter two types of activities involve generic developments that require long-term planning and funding. This programme will also seek additional funding and partnerships with other synchrotron radiation facilities or expert teams throughout Europe. **Table 4.03** provides a summary of these activities, which are presented in the following sections.

The following sub-sections detail the developments listed in **Table 4.03**.

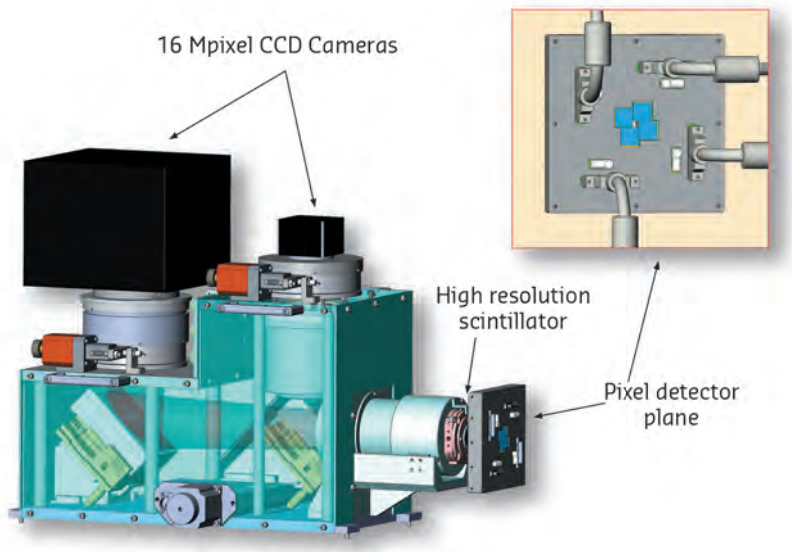

Figure 4.10: Composite detector built for UPBL04 during Phase I. The detector has been designed for X-ray imaging and ptychography applications and integrates two indirect detection imaging cameras and a pixel detector based detector plane to collect the high-q coherent scattering. The instrument includes both generic and modified ESRF components such as the high spatial resolution scintillators, full custom design lenses, a FReLoN 16 Mpixel camera and four special Maxipix modules.

	#	Technology	Development objectives	Type	Phase II
Key technologies and main components	DT1	Improved X-ray sensors	Pixellated semiconductor sensors	G	
	DT2		Scintillator screens	G	
	DT3	Beamline integration of existing detector technologies	Integrating hybrid pixel detectors	G	✓
	DT4		Photon counting pixel detectors	G	
	DT5		Multichannel fluorescence detectors	G	✓
	DT6		Indirect detection technology	G	
	DT7	Data acquisition	High throughput data readout schemes	G	
New detector systems	DP1	Single-photon sensitivity detectors	Small pixel noise-free 2D detectors	G	✓
	DP2	High dynamic range CMOS detectors	Large format CMOS panels X-ray imaging cameras	G	✓

Table 4.03: Overview of development programmes in the key technology (DT) and new detector (DP) programmes.
= R&D programme reference ID.
Type: G = General purpose technologies;
A = Application-specific development. Projects dependent on Phase II are marked in the last column.

4.3.3. KEY TECHNOLOGIES

Improved X-ray sensors: The final performance of any detector system is critically dependent on the characteristics of the element that converts the incident X-ray photons into a more easily measurable quantity. Detection efficiency, spatial resolution and time response determine final detector performance. Scintillating materials (X-rays to visible light) and semiconductors (direct conversion to electrical charge) are the two main focuses for development programmes. As the interest for other converter materials, such as gases or photocathodes, is limited to very specific applications, they have not been included.

Pixellated semiconductor sensors (DT1): The need to overcome the efficiency limitations of silicon is the motivation behind our ongoing development of high-Z sensors for pixel detectors. Monocrystalline CdTe is available on an industrial scale and is today considered the most suitable material for room-temperature, high energy applications. However, this material suffers from inherent defects and is only available within certain limits of homogeneity, thickness and size (Owens *et al.*, 2004). Although it is not expected to influence improvements in the inherent quality of the material, it is possible to refine its function as a sensor. Phase II foresees the following actions:

- Pursue ongoing work on monocrystalline CdTe sensors to improve contact technology, hybridisation methods and edge processing while also developing usage and correction procedures aimed at improving time stability and compensating residual intrinsic imperfections.
- Follow, evaluate and capitalise on progress achieved with other high-Z materials such as GaAs, CZT or Ge.
- Develop thinner sensors optimised for energies ~30 keV. Such sensor developments could be crucial to permitting pixel detectors to reach their ultimate spatial resolution.
- Assess alternative technologies. For instance GaAs/InAlAs superlattice quantum-well structures offer interesting options to increase the detection signal by charge multiplication but could also be investigated as X-ray-to-light photon converters with high time response, no afterglow and tuneable wavelength.

Scintillator screens (DT2): Scintillating screens are critical components for both very high energy and high spatial resolution X-ray detectors (Nikl, 2006; Derenzo *et al.*, 2003). Opportunities for improving the spatial resolution are somewhat limited as high-resolution screens are already near the theoretical limit of 0.4 µm that is achievable with visible light optics. However, it is still very important to enhance the detection efficiency by increasing the stopping power, to improve the time response as well as to improve the time stability by reducing thermal and memory effects such as afterglow or brightburn that are serious handicaps for any quantitative measurement. The main objectives, all rather challenging, and the planned development paths are:

- Increase the stopping power for high and medium spatial resolution applications using either epitaxial scintillators, nanotechnology or powder screens with new scintillating materials such as Lu_2O_3:Eu, GdI_3:Ce or LuI_3:Ce (see **Figure 4.11**). One of the methods that

will be explored is to vary the chemical composition by partial substitution to boost the X-ray absorption above K-edges (*i.e.* Y, In, I, Gd, Lu).

- Improve the time response of all systems by selecting the optimum doping and chemical composition to reduce the decay time, afterglow and brightburn.
- Increase the hardness of the scintillators to heavy irradiation and mechanical stress, and the stability of the luminiscence yield versus temperature variations.

This programme also plans to explore and evaluate other techniques based on surface structure and coating as a means to increase the detection efficiency of the indirect detection schemes.

Beamline integration of existing detector technologies: One of the strengths developed at the ESRF over the past decades is the in-house expertise and capability to integrate current detector components into fully customised detection systems. This integration requires specific know-how in mechanics, electronics and software as well as characterisation and test methodologies. Phase II will see a further consolidation of this integration effort and will include the following sub-programmes:

Integrating hybrid pixel detectors (DT3): With the substantially increased intensity of the Phase II source, the count rate capabilities of current pixel detectors such as PILATUS, MAXIPIX, XPAD or EIGER will be unable to cope with the higher photon fluxes. By replacing the photon counting electronics with individual charge integrators at each pixel, it is possible to build new detectors that are not limited to a maximum photon rate but that can still combine single photon sensitivity, *i.e.* noise free operation, with very fast readout. These detectors cannot discriminate the energy of the incident photons, but this is usually not a major drawback for most experiments using monochromatic beam.

Photon integrating detectors are mandatory instruments for many free-electron laser applications and in the last decade several development initiatives have begun looking into the design and construction of integrating detectors based on hybrid pixel technology. For instance, detectors like JUNGFRAU (Mozzanica *et al.*, 2014) and ongoing projects for the European XFEL (Sztuk-Dambietz *et al.*, 2013) will be excellent candidates to equip certain of our beamlines in the future. However, the restricted range of application of photon integrating detectors compared to pixel detectors may compromise the dissemination of this technology. It will therefore be strategic to establish collaborations and devote

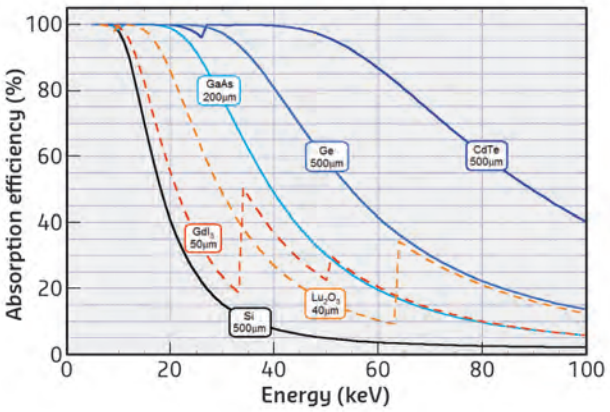

Figure 4.11: Absorption efficiency calculated for various high stopping power Xray sensor materials. The figure shows how highZ semiconductors (GaAs, Ge, CdTe, in solid lines) and high density scintillators (GdI_3, Lu_2O_3, in broken lines) compare to 500 µm thick silicon typically used in pixel detectors today.

resources to develop technical solutions to integrate and customise those detectors for the ESRF beamlines.

The technologies used in photon integrating detectors can also be applied to build detectors with higher spatial resolution – a key requirement for many coherent scattering and diffraction experiments, particularly at high photon energies. As high spatial resolution is not covered by the aforementioned FEL detector developments, significant effort and resources for Phase II will be dedicated to such a development programme (see DP1).

Photon counting pixel detectors (DT4): Despite the intrinsic count rate limitation of photon counting pixel detectors (Llopart *et al.*, 2002), this type of device is expected to continue to be the workhorse for many diffraction and scattering experiments, particularly for the most photon-hungry techniques. Over the last ten years, we have developed our own in-house capabilities to build and customise pixel detectors based on the Medipix readout chip. This strategy has proven to be very successful; today, the family of MAXIPIX detectors equips more than a dozen beamlines, providing superior spatial resolution and frame rates similar to commercial devices (Ponchut *et al.*, 2011). MAXIPIX has also served as the basis

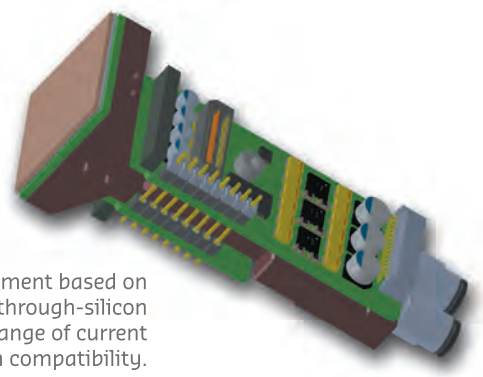

Figure 4.12: CAD view of a SMARTPIX 512×512 module under development based on the Medipix3 readout chip. The module, based on edgeless sensor and through-silicon via technologies, will increase the frame rate and extend the energy range of current MAXIPIX modules whilst providing smaller dead areas and vacuum compatibility.

for developments of highly integrated and optimised experimental set-ups such as those used on Phase I beamlines UPBL4 and UPBL6 (Figure 4.10). Maintaining these in-house capabilities is crucial for the future of the ESRF and the next generation of our detectors, SMARTPIX built on the Medipix3 readout chip, is currently under development (Figure 4.12). The ESRF is also contributing to the EIGER project (Dinapoli *et al.*, 2011), with the purpose of speeding up the development and to gain access to high performance non-commercial modules built by PSI. SMARTPIX will also serve as a development platform for customisation of specialised hybrid pixel devices and will be instrumental in pursuing strategic R&D projects such as the in-house programme on high-Z sensors (see DT1 above) or used as a test-bed for integration of new sensors (edgeless), new sensor materials or more advanced interconnection schemes.

Multichannel fluorescence detectors (DT5): Silicon drift diodes (SDDs) have become the detector of choice for fluorescence measurements using synchrotron beams in the X-ray energy range from 0.2 to 25 keV despite their moderate absorption for the higher energies. This is due not only to the good energy resolution of these devices and the possibility of operation at high count rates, but also to the maturity of the silicon processing technology (Lechner *et al.*, 2001), much more advanced and stable than that of other potential materials of spectroscopic grade. Although SDDs are now produced industrially, specialist suppliers only offer single- or few-channel systems. Therefore, the ESRF will invest Phase II resources into developing multi-channel SDD spectroscopy detector modules, based on existing sensor technology. The modules will be independently operable but easy to combine and customised for specific end station needs. It is expected that, in parallel with beamline control developments, full systems built with several of these modules will be capable of similar count rates to fast existing systems (Ryan *et al.*, 2010) while offering twice as good resolution at the X-ray emission lines of transition metals.

Indirect detection technology (DT6): The detector systems for hard X-ray indirect detection are built by assembling a converter screen, a scintillator, an optical system and a high quality visible-light camera, usually based on a CCD or a CMOS imaging sensor (Figure 4.13). The role of the scintillating screen is fundamental but the overall performance of the detector critically depends on the optimisation and matching of all the components forming the electro-optical system (Gruner *et al.*, 2002). During Phase II, in addition to optimising scintillators (see DT1), resources will be dedicated to improving the integration of indirect X-ray detection systems by selecting and characterising new scientific cameras and developing customised lenses. Through such customisation, it has been possible to overcome the limitations of off-the-shelf optical components and achieve the maximum range of pixel size (from 100 nm to 100 µm) with the same imaging camera.

Data acquisition

High throughput data readout framework (DT7): The planned improvements, both of the light source and the X-ray detectors, will challenge even more the capacity of backend computing systems that receive, manage, store and process the high throughput data streams expected to be produced in the future. A sizeable programme is therefore envisaged for data management and analysis capabilities including the required IT associated

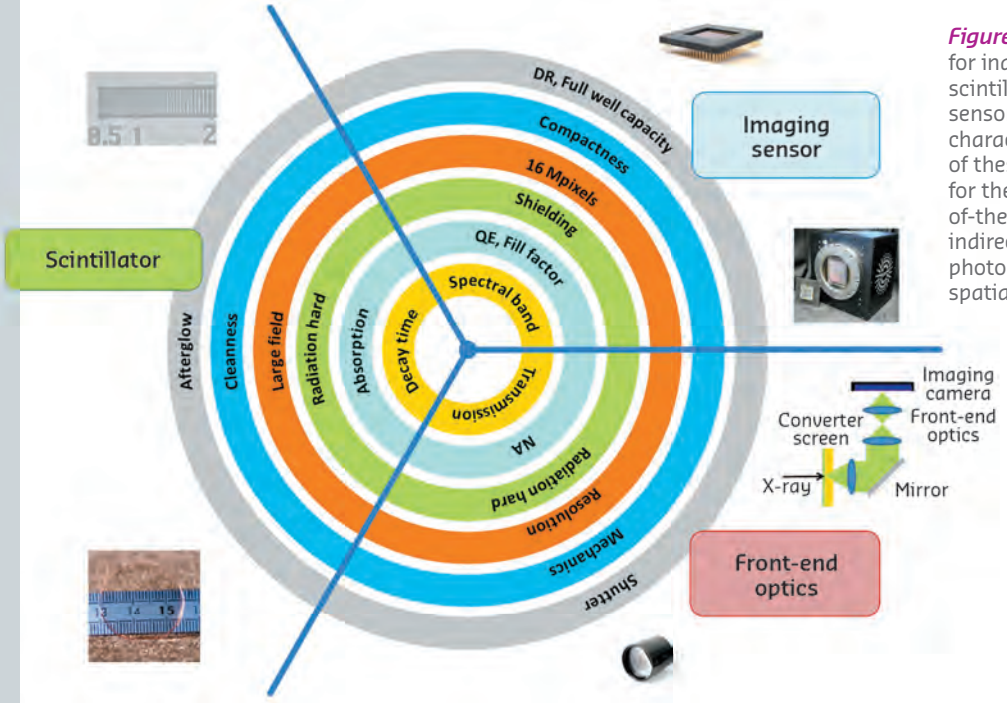

Figure 4.13: Key technologies for indirect X-ray detection: scintillators, optics and imaging sensors. The proper matching of characteristics and specifications of these components is essential for the construction of state-of-the-art high performance indirect Xray detectors for high photon energies or very high spatial resolution.

infrastructure (see **Sections 4.4, 4.5** and **4.6**). From the perspective of the detectors, the problem consists of increasing the capabilities of producing and transferring large data volumes at a high rate while minimising the steps and latency in the subsequent data management chain. With this purpose and under the funding of the CRISP EU project (www.crisp-fp7.eu/about-crisp/), the ESRF started a programme in 2012 aimed at defining a generic framework for data transfer and detector readout that is planned to be further developed and completed during the first years of Phase II. This framework consists of a series of generic software and hardware components that should equip new detectors. The framework will be compatible with our generic detector control software (see **Section 4.4** on LIMA platform) and is destined for advanced high performance detectors, but will be scalable for implementation in less demanding and inexpensive devices. The key features are:

- Data is transferred by operation of an arbitrary number of physical data links in parallel with an effective data throughput above 1 GByte/second per link.
- The data transfer protocols make maximum use of zero-copy techniques, *i.e.* sending the data directly from the source (the detector) to the final destination.
- Although not exclusively, the framework is highly optimised for segmented detectors and in particular for those producing trains of 2D images. Some operations such as reconstruction of full images, mirroring and rotation of image segments, or extraction of regions of interest are managed directly from the detector front-end, which simplifies data manipulation considerably.
- It facilitates the management of the data by implementing simultaneous transfer from the detector to multiple different destinations in parallel, for visualisation, storage or data processing, etc.

4.3.4. NEW DETECTOR SYSTEMS

In parallel to the strategic detection technologies detailed in the previous section, the development of two new detector systems will be a fundamental pillar of the Phase II detector programme. The proposed projects are expected to provide solutions that do not exist today in the specific context of novel applications inspired by the new source characteristics. Phase II will provide significant resources for these two projects. Furthermore, as this programme is of a wider interest, we expect to foster new partnerships with other European facilities and open opportunities for additional funding.

4.3.4.1. SMALL PIXEL NOISE-FREE 2D DETECTORS (DP1):

This project aims at developing area detectors that combine single photon sensitivity with spatial resolution of the order 20 µm or better, a value that goes beyond that achievable by existing photon counting pixel detectors (**Table 4.04**). Such detectors should be able to provide effective noise-free operation and the high angular resolution required by several experimental techniques while keeping the detection plane at a convenient distance from the sample. For instance, the application of coherent scattering techniques for a variety of beamlines and experimental conditions, particularly with sample environments requiring short wavelengths for high X-ray penetration or coherent experiments at Bragg reflections, will be very much facilitated by these new detectors (Hoshino *et al.*, 2012).

By selecting the appropriate material and improving sensor manufacturing processes, it will be possible to build detectors able to operate efficiently at different photon energies up to 30 or 40 keV. Reaching much harder X-rays without spoiling the spatial resolution is not envisaged in the scope of this programme as it will require new concepts in sensor technology that are still to come. Given the inherently lower noise associated with the smaller pixels, the possibility of using these detectors down to energies below 1 keV should not be discarded. However, this would require additional effort for the development of soft X-ray sensors.

DP1 : Small pixel noise-free 2D detectors		
Target experimental techniques	• CDI, XPCS • High energy ptychography • High resolution spectroscopy • USAXS • Soft X-ray 2D detection • Low dose X-ray radiography	**Technology areas involved: DT1, 2, 3, 4 and 7** Performance goals: • Effective pixel size: ≤ 20 µm • Noise-free operation • Energy range: 500 eV to 30 keV • Flux: < 10^6ph/s/pixel @10 keV • Frame rate: > 1000 fps • Module size: 40×40 mm^2
Scientific applications	• Materials science • In-vivo imaging • Protein crystallography • ...	

Table 4.04: Summary of goals of DP1: the project aims at building very sensitive X-ray detectors for scattering applications providing simultaneously high spatial resolution and noise free operation.

As the detectors will be unable to sustain direct illumination by intense monochromatic beams, they will not be well suited to conventional X-ray tomography or similar imaging techniques. However, due to their small pixel size, they could potentially be used in particular cases for medium resolution very low dose X-ray radiography at moderate photon energy.

Related detector technologies and current projects

Noise-free 2D detectors in use today at synchrotron facilities are direct detection devices using semiconductor sensors. Noise-free operation is achieved due to the high sensitivity of the semiconductor materials combined with the discrete nature of the X-rays; each single photon produces an amount of signal that is sufficiently intense to be distinguished from the readout electronics noise. This fact enables photon counting schemes and it is also the reason why charge integrating hybrid detectors, as those currently under development for free-electron lasers, discussed in DT3, can also reach single photon sensitivity (**Figure 4.14**).

Without using a photon position refinement algorithm, the spatial resolution of the detectors is the resulting combination of the intrinsic resolution of the sensor and the actual pixel size. The spatial resolution in the pixel detectors used in synchrotron facilities today is dominated by the pixel size. The maximum resolution has been achieved by the MAXIPIX detectors due to its small pixel pitch of 55 µm inherited from the underlying Medipix2 readout chip. At such a pixel size, the signal starts getting spread across neighbouring pixels and it is generally accepted that the same simple photon discrimination mechanism used in those devices cannot be scaled down to pixels significantly smaller in size. Detectors under development based on the more recent Medipix3 integrated circuit maintain the same pixel size and will not provide better spatial resolution. However, this new readout chip has demonstrated how the signal from neighbouring pixels can be combined to refine the information about a single photon detection event and this principle could be exploited in future designs to improve the spatial resolution of the detected photons.

Another method to reach high spatial resolution is the application of centroiding algorithms on the coarsely sampled charge distributions generated by individual photons (Schubert *et al.*, 2012). This method requires measuring the signal distribution across the pixels and has been used in the past with direct detection CCDs, usually for soft X-ray detection. The same techniques have recently been demonstrated with prototypes of charge-integrating hybrid pixel detectors of 25 µm pitch (Dinapoli *et al.*, 2014) as illustrated in **Figure 4.12**. So far centroiding techniques have been implemented by transferring the image data and running the position refinement algorithms in a computer or a dedicated fast programmable electronic device, limiting the method to very low photo flux applications. Building a detector based on this method that is able to deal with acceptable photon rates for synchrotron applications will require implementing the algorithms at the detector front-end.

Direct detection in semiconductor sensors is not the only option to achieve single photon sensitivity with hard X-ray detection. Recent progress with medium resolution structured scintillators and 2D visible photon detectors such as silicon photomultipliers makes it also possible to consider indirect detection schemes for this project. In this scheme, the incoming X-rays would be absorbed by a scintillator screen, probably a scintillating fibre optics faceplate. The visible light thus generated is transmitted by the fibre optics to a sensitive 2D light sensor. The spatial resolution would be determined by the diameter of the fibres and the light propagation in the faceplate as well as the pixellation of the sensor. The development of silicon photomultipliers has

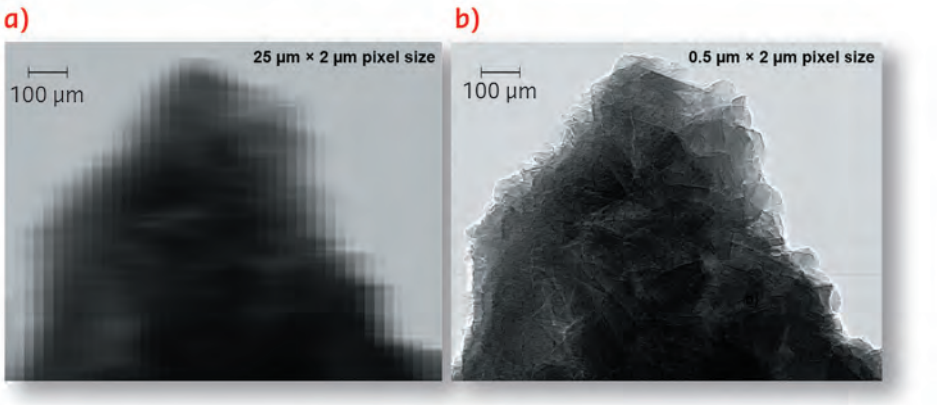

Figure 4.14: X-ray radiography of a kidney stone obtained with 15 keV photons at the TOMCAT beamline of SLS with a charge integrating hybrid strip detector based on the Gotthard chip by vertically scanning a 2 µm beam. a) Image obtained by full direct charge integration showing the 25 µm pixelation of the detector in the horizontal direction. b) The result of applying an off-line photon position refining algorithm. Similar results have been also obtained with a 2D pixel detector based on the Mönch chip (Cartier *et al.*, 2014).

Table 4.05: The project addresses the development CMOS panels optimised for synchrotron diffraction experiments and cameras for X-ray imaging designed to fill the gap between the slower "high image quality" CCD detectors and the faster low/medium image quality obtained with commercial CMOS cameras.

DP2 : High dynamic range CMOS detectors		
		Technology areas involved: DT2, 6 and 7
Target experimental techniques	• Powder diffraction • High energy single crystal diffraction • Pair distribution functions • Diffraction tomography • Microtomography • X-ray radiography	Performance goals (CMOS panel): • Energy range: > 30 keV • Pixel size: 100 µm • Noise: < 1 photon @ 30 keV • Dynamic range: 20 bits • Frame rate: > 500 fps • Module size: 100×100 mm^2
Scientific applications	• Materials science • Extreme conditions • Materials chemistry • Palaeontology • Medical imaging	Performance goals (CMOS camera): • Pixel size: 15 µm • High quantum efficiency (backthinned) • Dynamic range: 16 bits • Number of pixels: 2048×2048 • Frame rate: > 200 fps

been encouraged in the last few years because of the interest for industrial and medical applications. However a detector with the characteristics we require has yet to be constructed. Achieving good time response and sufficient sensitivity combined with the high spatial resolution will be challenging but this technology pathway should not be discarded.

Implementation considerations

As mentioned above, three technological approaches have been identified as potential candidates to serve as a basis for the implementation of a high spatial resolution noise-free area detector. These are charge integrating hybrid devices with very small pixels, photon counting pixel detectors with position interpolation at the detector front-end and indirect detectors based on structured scintillators and very sensitive light sensors. The first phase of the project, that is expected to extend over three years, will include a thorough analysis of the ultimate performance that could be achievable with each of the technological approaches and a comparative study of the three. The technical evaluation will not be restricted to simulations and on-paper calculations; they will include prototyping on a small scale of some of the most critical components in order to validate the key concepts, estimate limiting factors and decide on the system architecture. The study will not be limited to technical matters and other practical aspects related to the prototype development phase, such as the prospection and qualification of the technological partners. Development risks as well as critical matters related to the subsequent production of the detectors, such as costs and availability of the required fabrication processes will also be carefully analysed.

The work on the complete detector system will start by the end of 2018 and the development of the final front-end components will be based on the technology finally selected. The project will also profit from advances achieved in sensor development (DT1, DT2) and in the data acquisition (DT7) programmes. Additionally, the technological approaches that will not be retained after the evaluation phase may eventually offer very interesting possibilities to meet the requirements of more specialised applications. Despite this fact, it will not be possible to pursue those alternative development paths unless additional funding sources are found that will allow those projects to run in parallel.

4.3.4.2. HIGH DYNAMIC RANGE CMOS DETECTORS (DP2)

This project aims at developing integrating area detectors based on indirect X-ray detection with CMOS image sensors designed to operate with very high photon energies and able to achieve a dynamic range substantially higher than that attainable with existing devices (**Table 4.05**). These detectors would be able to operate in the range of a few hundred to one thousand frames per second while providing multimegapixel images. The technology will be scalable in order to produce detectors of variable size and number of pixels. The project will address two families of applications: high energy diffraction techniques requiring very large detection area and X-ray imaging with resolution in the micrometre range. Even if some of the overall detector specifications for these two application families are quite different, both can be addressed to a larger extent by sharing technology, components and overcoming similar challenges. Both detectors will require very different optical and mechanical construction schemes, but the developments are planned to be carried out in a way that the sensor technology, the functional architecture, the readout and data acquisition scheme including the software integration will be the same.

Indirect detection schemes are particularly important for very hard X-rays, with photon energies starting from 30 keV. While photon counting pixel detectors

with high-Z sensors are expected to be the reference technology for small pixel and moderate size devices for very sensitive scattering experiments, usually at medium photon energies, large format panels able to record full intense powder or single crystal diffraction patterns at high energy are essential for many experiments in a diversity of material science applications. In the case of X-ray imaging, the detectors must be able to image the direct beams after some attenuation by the sample. Indirect detection is the only scheme able to cope with the huge intensities of the Xray beams while providing micrometre spatial resolution.

The project aims therefore to develop detectors with two types of opto-mechanical approach. The CMOS panels for high energy diffraction will integrate fibre optical coupling between the scintillating screen and the optical sensor. These detectors will have relatively large pixels whose size will be fixed by detector construction. Conversely, the CMOS cameras will be designed to accommodate a large variety of optics that along with the adequate converter screens will be the base components to build a diversity of different Xray imaging detectors of variable pixel size and field of view.

Related detector technologies and current projects

CMOS imaging sensors are 2D monolithic silicon detectors that are sensitive to visible light in which each pixel has an integrated sensor element, usually a photodiode, and its own charge-to-voltage conversion. The sensor includes signal amplifiers and occasionally noise correction and digitisation circuits (Bigas *et al.*, 2006). A huge effort has been put into the development of CMOS sensors for consumer electronics such as digital cameras and these devices have found their place in industrial imaging and in the medical market. In the last five to ten years this technology has also evolved towards the development of sensors specifically designed for scientific purposes, and today they are used in applications. CMOS image sensors have also replaced CCDs for certain astronomy instrumentation and they are particularly suitable for high speed imaging. The possibility of implementing active components in each pixel and at the periphery of the sensor opens the door to a level of signal processing that can substantially enhance the detection performance and the functionality of the devices.

Large format X-ray detectors based on CMOS sensors cannot be considered new devices (Turchetta *et al.*, 2011). In the last few years advances in sensor manufacturing have allowed wafer scale large size sensors to be produced and several companies have developed and put on the market CMOS panels developed for mammography and other medical applications (**Figure 4.15**). Those devices have good efficiency and sensitivity for hard X-ray detection and although some of them are being used at synchrotron facilities, they do not produce sufficiently good quantitative information as required, for instance, in diffraction experiments. That situation is not expected to change in the coming years as medical imaging CMOS panels are designed to produce images for visual analysis, use simple pixel structures and target low cost to compete with the amorphous silicon flat panels that still dominate the medical market today.

The area of imaging cameras has also seen the appearance of sensors designed for scientific purposes in the last five years. Those sensors, sometimes called scientific CMOS or simply sCMOS, offer improved sensitivity, low noise, high frame rate capabilities as well as interesting functional features such as flexible electronic shutter operation. They also present rather good dynamics for imaging applications but they are optimised for operation with visible light. This fact makes the cameras built around those sensors not ideal for the detection of hard X-rays where each single incident photon may produce ten or more visible light photons that reach the sensor plane.

Implementation and technology considerations

The sensors developed by this project will be CMOS imaging devices optimised to operate with X-ray to light converters. They should have a sufficiently high saturation level to cope with very hard X-rays and multiple signal gain selectable on a pixel by pixel basis to maximise detection sensitivity (Spivak *et al.*, 2009). This possibility, already demonstrated although not yet optimised, is the essential basis to build detectors with the large "intra-image" dynamic range targeted by the project. The sensors for CMOS

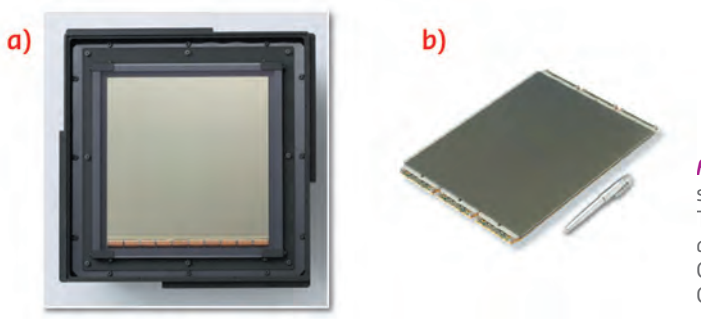

Figure 4.15: a) 300 mm wafer scale CMOS imaging sensor developed by the company CANON Inc. The active area of this single device optimised for astronomy applications is 202×205 mm. b) Six tile CMOS panel for X-ray medical imaging applications. Credit: Teledyne DALSA.

panels and for imaging cameras will be designed with different pixel sizes and active areas to match the rather different specifications, however, it is planned that they will use the same concept to enhance the dynamic range and share the same readout architecture, including the analogue-to-digital conversion scheme. While the large format sensors for CMOS panels will accommodate three progressive gain ranges, the devices for X-ray imaging will have smaller pixels and are expected to accommodate only two gains. This difference is still acceptable given the specific requirements for the two families of applications.

As each pixel is responsible for the charge to voltage conversion and some of the analogue signal processing, the readout can be parallelised to a great extent. This makes it possible to reach high frame rates but it is also the reason why the uniformity across the image area will be lower than achieved with CCDs. Therefore, a substantial effort will be put into the stabilisation and correction of pixel non-uniformities. This will require an efficient temperature regulation scheme, the development of proper calibration procedures and the integration in the detector electronics of the required machinery for fast onthefly data correction.

This project requires partnerships to be established with experienced designers of CMOS sensors for scientific applications, and also with detector manufacturers that have developed the know-how for the construction of large format tiled flat panels. The development of the X-ray imaging camera will benefit from the experience accumulated at the ESRF over more than 20 years.

References

Bigas M., Cabruja E., Forest J., Salvi J., Review of CMOS image sensors, *Microelectronics Journal* **37**, 433451 (2006).

Cartier S., Bergamaschi A., Dinapoli R., Greiffenberg D., Johnson I., Jungmann J., Mezza D., Mozzanica A., Schmitt B., Shi X., Stampanoni M., Sun J., Tinti G., Micron resolution of MÖNCH and GOTTHARD small pixel charge integrating detectors with single photon sensitivity, *Journal of Instrumentation* **9**, *C05027* (2014).

Derenzo S.E., Weber M.J., Bourret-Courchesne E., Klintenberg M.K., The quest for the ideal inorganic scintillator, *Nucl. Instr. and Meth. A* **505,** 111–117 (2003).

Dinapoli R., Bergamaschi A., Henrich B., Horisberger R., Johnson I., Mozzanica A., Schmid E., Schmitt B., Schreiber A., Shi X., Theidel G., EIGER: Next generation single photon counting detector for X-ray applications, *Nucl. Instr. Meth. A* **650**, 79 (2011).

Dinapoli R., Bergamaschi A., Cartier S., Greiffenberg D., Henrich B., Johnson I., Mozzanica A., B.Schmitt, Shi X., Tinti G., MÖNCH, a Small Pitch, Integrating Hybrid Pixel Detector for X-ray Detection, *Journal of Instrumentation* **9**, *C05015* (2014).

Gruner S.M., Tate M.W., Eikenberry E.F., Charge-coupled device area Xray detectors, *Rev. Sci. Instrum.* **73**, 2815-2842 (2002).

Hoshino T., Kikushi M., Murakami D., Harada Y., Mitamura K., Ito K., Tanaka Y., Sasaki S. Takata M., Jinnai H., Takahara A., X-ray photon correlation spectroscopy using a fast pixel array detector with a grid mask resolution enhancer, *J. Synchrotron Radiat.* **19**, 988-993 (2012).

Lechner P., Fiorini C., Hartmann R., Kemmer J., Krause N., Leutenegger P., Longoni A., Soltau H., Stötter D., Stötter R., Strüder L., Weber U., *Silicon drift detectors for high count rate X-ray spectroscopy at room temperature*, *Nucl. Instr. and Meth. A* **458**, 281-287 (2001).

Llopart X., Campbell M., Dinapoli R., SanSegundo D., Pernigotti E., Medipix2: a 64-k pixel readout chip with 55 μm square elements working in single photon counting mode, *IEEE Trans. Nucl. Sci.* **49**, 2279-2283 (2002).

Mozzanica A., Bergamaschi A., Cartier S., Dinapoli R., Greiffenberg D., Johnson I., Maliakal D., Ruder C., Schädler L., Schmitt B., Tinti G., Shi X., Prototype Characterization of the Jungfrau Pixel Detector for SwissFEL, *Journal of Instrumentation* **9**, *C05010* (2014).

Nikl M., Scintillation detectors for X-rays, *Meas. Sci. Technol.* **17**, R37-R54 (2006).

Owens A., Peacock A., Compound semiconductor radiation detectors, *Nucl. Instr. and Meth. A* **628**, 18-37 (2004).

Ponchut C., Rigal J.M., Clément J., Papillon E., Homs A., Petitdemange S., MAXIPIX, a fast readout photon-counting X-ray area detector for synchrotron applications, *Journal of Instrumentation* **6**, C01069 (2011).

Ryan C.G., Kirkham R., Hough R.M., Moorhead G., Siddons D.P., de Jonge M.D., Paterson D.J., De Geronimo G., Howard D.L., Cleverley J.S., Elemental X-ray imaging using the Maia detector array: The benefits and challenges of large solid-angle, *Nucl. Instr. and Meth. A* **619**, 3743 (2010).

Schubert A., Bergamaschi A., David C., Dinapoli R., Elbracht-Leong S., Gorelick S., Graafsma H., Henrich B., Johnson I., Lohmann M., Mozzanica A., Radicci V., Rassool R., Schädler L., Schmitt B., Shi X., Sobott B., Micrometre resolution of a charge integrating microstrip detector with single photon sensitivity, *J. Synchrotron Radiat.* **19**, 359365 (2012).

Spivak A., Belenky A., Fish A., Yadid-Pecht O., Wide-Dynamic-Range CMOS Image Sensors—Comparative Performance Analysis, *IEEE Trans. Electron Devices* **56**, 24462461 (2009).

Sztuk-Dambietz J., Hauf S., Koch A., Kuster M., Turcato M., Status of detector development for the European XFEL, *Proc. SPIE 8778, Advances in X-ray Free-Electron Lasers II: Instrumentation*, 87780U (2013).

Turchetta R., Guerrini N., Sedgwick I., Large area CMOS image sensors, *Journal of Instrumentation* **6**, C01099 (2011).

www.crisp-fp7.eu/about-crisp/

4.4. BEAMLINE CONTROL

4.4.1. OBJECTIVES AND DELIVERABLES

Phase II deliverables

- Major modernisation of the beamline control (*e.g.* replacement of SPEC, new hardware, etc.)

The Phase II beamline control system needs are driven by the higher brilliance of the source, the smaller beams, faster detectors and improved computing infrastructure. To make optimal use of the improvements brought by Phase II, the beamline control system will evolve considerably, pursuing four main objectives, outlined in the Table 4.06 :

The following sub-sections detail the development programmes listed in Table 4.06.

The objectives address the need to take more data, faster, for longer while at the same time making it easier. How each of these objectives addresses the specific requirements of Phase II will be described in more detail below.

	#	Technology	Development objectives	Type	Phase II
Lower latency	CL1	Software framework	Continuous scanning	G	
	CL2	Hardware renewal	Synchronisation, sequencing	G	
	CL3	Data analysis	Online analysis	A	
Timing	CT1	Timing and synchronisation	Improve beamline and source synchronisation	G	✓
Higher data management throughput	CD1	Software framework	Data acquisition and management	G	
	CD2	Standardisation	Data format	G	
	CD3	Database	Metadata	G	✓
Control platforms	CP1	Software framework	New experiment sequencer	G	✓
	CP2	Standardisation	Hardware & software platforms	G	
	CP3	Hardware	Motion control platform	G	
	CP4	Hardware	DAnCE (general purpose platform for data acquisition and control electronics)	G	
	CP5	Software framework	LIMA (library for image acquisition)	G	
	CP6	Software renewal	Moving from TACO to TANGO	G	✓
	CP7	Software development	GUI (graphical user interface)	G	
	CP8	Platform development	Real time control and acquisition	G	✓

Table 4.06: Overview of development programmes in the beamline control programme, focusing on lower latency (CL), timing (CT), data throughput (CD) and modernisation of control platforms (CP).
= R&D programme reference ID.
Type: G = General purpose technologies;
A = Application-specific development. Projects that are dependent on Phase II are marked in the last column.

4.4.2. DEVELOPMENT STRATEGY FOR THE MODERNISATION OF BEAMLINE CONTROL

Lower latency: Latency refers to the delay between a stimulation and the time it takes to respond. In the case of beamline control this refers to the time it takes to move motors and readout acquired data while the sample is not being exposed. This latency is sometimes referred to as *dead-time* because it is time when no data are being acquired. The new source will significantly increase the number of useful photons, which in combination with powerful new detectors, will permit sampling times to be reduced significantly. To ensure the control system does not affect the overall acquisition time, it is crucial to reduce the dead-time by at least the same factor. The ultimate goal is to reduce dead-time to zero.

Continuous scanning (CL1): The basic scanning mechanism in the current ESRF experiment sequencer (SPEC) is a so-called step scan. In a step scan, no data are acquired while the motors are being moved. This can result in a large fraction of the overall time being dead-time (**see** Figure 4.16).

In a step scan, the dead-time stays the same while the count-time is reduced. The increased brilliance of the Phase II source will, in many cases, allow the count-time to be reduced by a factor of 100 compared to today's count-time. This will exacerbate the problem of latency, as a large proportion of the overall experiment time will be dead-time. The solution to this problem is continuous scanning whereby the motors do not stop during the scan and counting is uninterrupted. However, as SPEC does not support continuous scanning inherently, extra software and hardware are required to acquire data continuously. The advantages of continuous scanning have been recognised for some time at the ESRF and a number of customised solutions have been developed over the years. Although they have been effective in reducing dead-time and have enabled many experiments, these tailor-made solutions require a lot of resources in their development and are difficult to maintain. The upgrade of the beamline control system during the Upgrade Programme Phase II will develop a generic continuous scanning framework which will replace the existing step scanning used by most experiments and will enable new experiments to be performed with much higher sampling rates and zero dead-time. The new continuous scanning framework will be easy to configure, will support multiple detectors with different sample station setups, will replace the existing custom-built continuous solutions and will implement a common solution for common needs such as data aggregation and file writing and metadata collection.

The increase in brilliance as a result of Phase II will enable very short integration times to be used – milliseconds down to microseconds. Special hardware is required to synchronise all motors, sensors and detectors at this timescale. Where appropriate, hardware will be developed to help the software detect any timing delays (microseconds to seconds) and/or frame losses during a continuous scan. New software will be developed to provide a generalised buffering system to read out data during the scan and to aggregate them. The new framework will provide support for different scan types and triggering mechanisms:

- Linear and trajectory continuous scan with time as trigger base
- Linear and trajectory continuous scan with position as trigger base

Trajectories can be in real or reciprocal space.

Timing and synchronisation: Timing and synchronisation are two crucial elements when acquiring precision data. To enable generalised, time-based continuous scanning a new high-precision timing protocol based on IEEE-1588 (also known as precision timing protocol – PTP) will be introduced and generalised. Computers are currently synchronised with NTP which can achieve millisecond accuracy at best. PTP provides microsecond (software only) to nanosecond (with additional hardware) accuracy for synchronising computer and embedded hardware clocks.

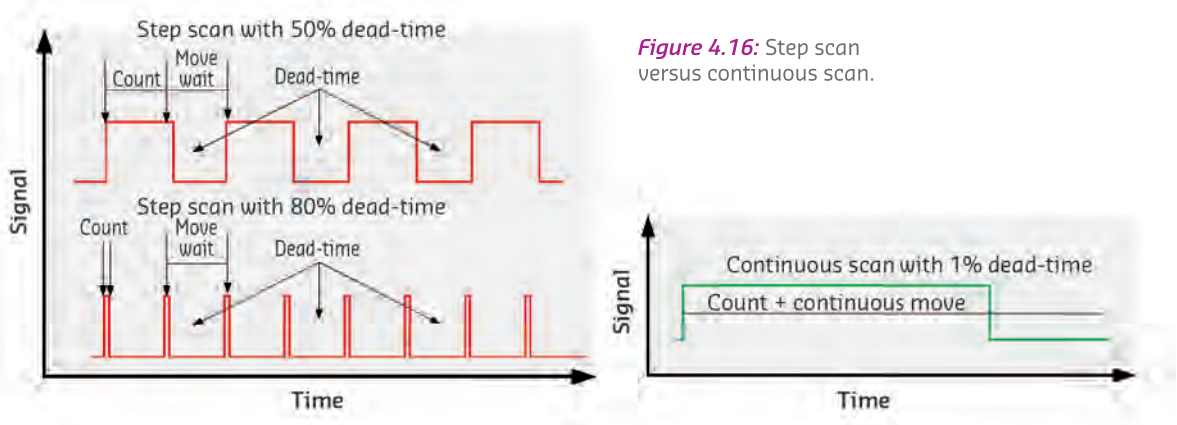

Figure 4.16: Step scan versus continuous scan.

Storage ring timing and source synchronisation (CS1): The time structure of the storage ring bunches will become critical for an increasing number of experiments post Phase II. This is because of the shorter integration times that will be used. The time structure of the source will increasingly need to be taken into consideration in the data acquisition. Improved synchronisation between the electron beam time structure and experiment will be implemented. Hardware synchronisation between the bunch clock and the detectors and shutters will be generalised. Techniques like gating of the detector counting by the electron beam time structure will be employed. Improved synchronisation between the insertion devices and monochromators will be implemented. Adopting the same motor controller (the IcePAP motion controller developed in-house is already the standard solution on all the ESRF beamlines) on the insertion devices as on the beamline optical elements will enable better synchronisation when scanning monochromators and insertion devices. Using the same motor controller will allow experiments to make faster, more accurate measurements. An alternative solution to synchronise the source time structure with the experiment is to use choppers. This option is discussed in more detail in the **Section 4.1**.

During topping up, experiments will have to cope with potential source parameter variations during injection. This will require additional hardware and timing synchronisation. It is foreseen to first implement an improved clock synchronisation with the introduction of the precision timing protocol (PTP) on both beamline and accelerator control systems.

Synchronisation, sequencing (CL2): A new generation of synchronisation and sequencing modules will replace the aging cards currently in use. This new generation will implement features for continuous scanning and will allow a significant improvement of performances (higher speed, higher data throughput, optimisation of hardware resources, extension of number of inputs/outputs, adaptation to modern communication links).

The new modules will be highly programmable and will offer functionalities that will cover a wide range of the requirements found at the beamlines in terms of synchronisation of control instruments and trigger pattern generation. High speed counters for data acquisition and multiplexers will also be available on-board.

Some of the applications that will benefit from these features are: continuous scan at constant or variable step, 2D mapping, synchronous operation of shutters or fast scans with detectors, synchronisation of control instruments.

Online analysis (CL3): Phase II will produce even more data per experiment than Phase I due to the higher sampling rate and multiple and larger detectors. The data explosion problem [cf. J. Berkowitz, 2013] is well recognised as being a problem common to all light sources and the huge quantities of data will make it increasingly difficult for users to take raw data away with them. There is an increasing need for data to be reduced automatically. The time it takes to interpret the results also needs to be reduced. For these reasons, it is important to continue the move towards online data analysis, *i.e.* data reduction routines executed online automatically. Online data analysis started in Phase I (ref: Purple Book) and is part of the move to shorten the delay between data acquisition and first scientific interpretation. We propose to introduce online data analysis as early as possible in the data acquisition pipeline on all beamlines. This means systematically collecting metadata so that the data analysis can be started as soon as possible. Frame-by-frame data correction (*e.g.* flat fielding) and data reduction (*e.g.* azimuthal integration) will be integrated into the processing chain. To ensure that the online data analysis executes at the same speed as the data acquisition, high performance computing (HPC) resources will be dedicated to each beamline (see **Section 4.6**). Human resources are foreseen in the data analysis unit to develop and port data reduction to HPC hardware, *e.g.* GPU's, FPGAs and/or co-processors. Online data analysis requires optimisation of the data transfer and management to ensure raw data is made available for analysis in real-time (see **Section 4.6**). To be able to do online data analysis, experiments will need to ensure calibration runs are performed before starting the experiments. The new experiment sequencer (cf. below) will ensure that calibration is performed before the sample data runs and the necessary metadata are collected for doing online data analysis.

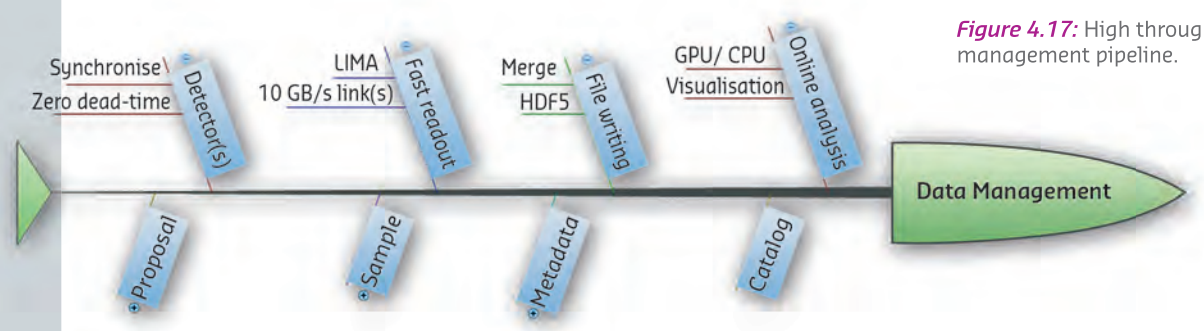

Figure 4.17: High throughput data management pipeline.

Higher throughput data management: The output of experiments is scientific data. The role of the beamline control system is not only to sequence and synchronise data taking but also to manage the data from the detector until it is stored for offline data analysis.

Phase II will see a change in the standard data size units from terabytes to petabytes. At the end of Phase I, the ESRF will be generating 1 to 2 petabytes a year. This will increase by at least a factor of 10 by the end of Phase II, which means the speed of the data pipeline must be increased to manage hundreds of terabytes/day and tens of petabytes/year.

Data acquisition and management (CD1): With the development of the LIMA framework during Phase I, we have standardised the detector readout software for the wide variety of detectors used. The number and variety of detectors will certainly not decrease in Phase II. On the contrary, more and more detectors with ever-increasing performances will need to be interfaced. LIMA will continue to be the main framework for detectors. Phase II will see a huge increase in data production due to the improvements in the source and detectors. An area where standardisation is still lacking is data management. During Phase I, data management for structural biology was improved with developments being made in ISpyB for the MASSIF and BioSAXS beamlines. Most other beamlines saw no significant changes. Phase II will standardise the data management process; A standard pipeline for high data rate beamlines will be developed and generalised and a scaled-down version will be used on medium data rate beamlines.

Data management involves combining the raw data coming from the detectors with the metadata coming from the proposal, sample, environment, source and beamline and storing it in an easily accessible form so that online and offline analysis can be performed. The data management pipeline must be able to deal with high speed data rates (gigabytes per second) and be flexible enough to adapt to different beamlines and experiments (**Figure 4.17**). The metadata will be stored in a database and made available to authorised users to search and download.

With the increase in multi-resolution and multi-technique experiments, more and more experiments will use multiple detectors. The beamline control system needs to synchronise multiple detectors and combine the resulting data into one data set. The LIMA and continuous framework will be extended to enable flexible configuration of one or more detectors with simultaneous readout. Phase II will see the introduction of detectors with data rates of 1 gigabyte/s and more, requiring a dedicated network and computing infrastructure for each high data rate beamline. The data acquisition readout and transfer will go directly from memory to buffer storage independent of the sequencer. The

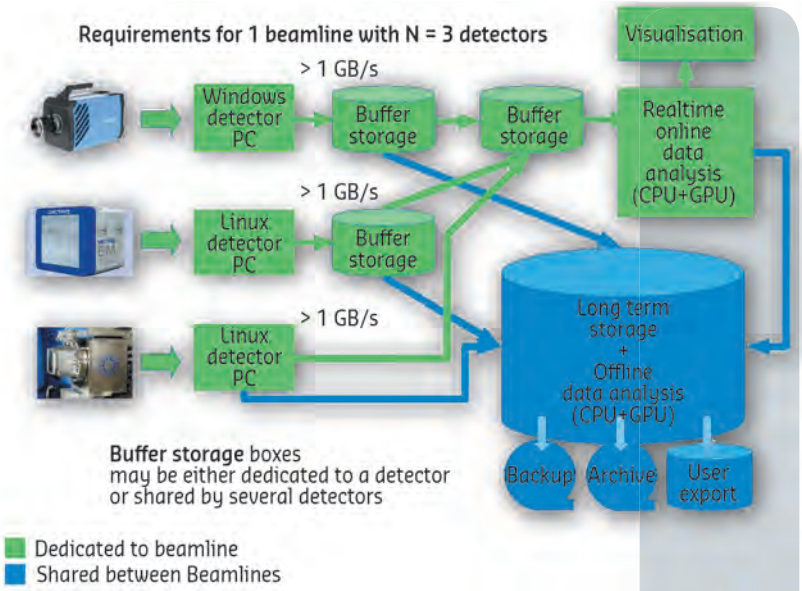

Figure 4.18: Schematic showing dedicated network links, compute resources and storage for multiple high speed detectors.

sequencer's job will be to prepare the detector(s), motors and sample environment hardware and then trigger the start of the continuous scan. A critical part of the data management is to guarantee the speed of the data acquisition. This will be solved with network links, storage and compute resources dedicated to the beamline. As described above, Phase II will see the generalisation of online data analysis on all beamlines. Raw data therefore has to be made available for online data analysis as soon as possible. In some cases this can be done by integrating the online data reduction in the LIMA pipeline using the *ProcessLib* mechanism. Analysis programs which require access to a full or partial dataset will need to run later in the data pipeline, after LIMA. Data must be made accessible from compute resource(s) (GPUs and/or CPUs) in an appropriate format – memory or disk. The Phase II computing infrastructure will need to be optimised to avoid online concurrency problems (see **Figure 4.18**).

One way of reducing the bandwidth and increasing the data rate is to implement realtime data compression. This technique is used by detectors from Dectris, *e.g.* Pilatus 6M, and Eiger. Phase II will implement compression for other commercial and in-house detectors using fast (*e.g.* FPGA) hardware to do the compression. The proposed data format HDF5 has compression built in and accepts external filters for doing compression. Compressing data will be essential for some experiments.

Data format (CD2): Data is written to disk by the beamline control system either by device servers close to the detectors or by the sequencer. The de facto data format for 2D datasets, which has been in use at the ESRF since the beginning is called EDF (ESRF data format). It is a simple binary format that suffers from a lack of definition and support. More and more experiments have needs which

are not served with a simple binary file. Scanning microscopy, coherence diffraction and many other experiments produce hundreds of thousands of EDF files which are difficult to analyse, store and backup. Phase II will have many more experiments which need to store and analyse large datasets (terabytes) from more than one detector. We propose to build on the trend that was started in Phase I and move from EDF to HDF5. HDF5 is a well-supported data format which allows large datasets of different dimensions and types to be stored efficiently in one file. HDF5 has many additional features which EDF does not have such as internal organisation capable of storing many datasets of different dimensions, data compression, multi-platform support, metadata (Nexus), chunking, parallelisation etc (**Section 4.4.2**). Phase II will generalise the use of HDF5 to replace EDF as the de facto data format for the ESRF. The organisation of the data and metadata in the HDF5 will follow Nexus conventions. This is in line with trends in other light sources around the world.

Metadata (CD3): Metadata are data about data that qualify the raw data and are used to describe the conditions under which the experiment was performed. Metadata are essential for online data analysis. Metadata about calibration runs must be stored with the raw data so that online data analysis can be performed automatically. Phase II will generalise the systematic collecting of metadata on all beamlines. Metadata will be stored in a permanent database for online and offline consulting by users. The ICAT (**Section 4.4.5**) metadata catalog selected during Phase I will be deployed on beamlines and, if successful, will be put into operation during Phase II. A copy of the metadata will be stored in HDF5 files for data analysis. The beamline control system will be extended to automatically generate the necessary metadata and pass them to a metadata manager.

Modernise control platforms and standards: The objectives for the beamline control system for Phase II are ambitious and will need modern hardware and software platforms to achieve them. Some of the platforms being used for the beamline control system are showing their age and will need to be replaced; others are more recent and will continue to be used and improved. The dismantling of the storage ring and implementation of its replacement will translate into a 12-month shutdown followed by a long commissioning period. This dark period offers a unique opportunity to significantly modernise and adapt the hardware and software platforms to achieve new performance goals.

All experiments at the ESRF are sequenced with SPEC or have SPEC controlling some part of them. Although SPEC has served our needs for 20 years and all experiments have been done with SPEC, it has become increasingly cumbersome when developing macros for complicated experiments. The development and maintenance of SPEC macros are time-consuming and the limitations of the SPEC macro language make it less and less useful for new sequences. SPEC is too limiting as a platform to build the new control system and therefore we have decided to replace it with a modern sequencer. This follows the trend in other light sources – no new light sources are using SPEC. The long shutdown is a unique opportunity to replace SPEC on a large number of beamlines.

New Experiment Sequencer (CP1): A new sequencer for the beamlines will be developed to replace SPEC. One of the main reasons is to have a more modern software platform for developing the experiment sequences for Phase II. There are three big challenges – (1) ensuring that the new sequencer has at least the same functionality as SPEC, (2) extracting the logic from the hundreds of SPEC macros to implement them in a mixture of device servers and the new sequencer, and (3) testing and commissioning the experiments with the new sequences. The new sequencer will be based on Python. Python is a scripting tool often used in scientific computing as a high-level language to analyse data and develop applications. The new sequencer will rewrite the experiment macros so that they are easier to maintain. To use the long shutdown optimally, the new system has to be developed and tested on as many different kinds of experiments as early as possible beforehand. This means starting the development of the new system as soon as possible. Extra resources will be hired to help with the development and installation during the long shutdown.

Hardware and software platforms (CP2): The "ideal" hardware components should be specialised (with a well defined functionality), high performance (to suit the requirements of increasingly demanding experiments), versatile/adaptable (meaning functionally rich and able to cope with multiple requirements) and flexible in the sense that it should be easy to interface with other devices. The ideal hardware components should also be highly reliable and present convenient cost and packaging.

Similar to other light sources, the ESRF faces the challenge of optimising the effort needed to deploy, support and maintain the hardware equipment installed on both the beamlines and the accelerator complex. Standardisation must therefore be as widespread as possible. It is in this spirit that the IcePAP motion controller was developed over the past years at the ESRF. Today, more than 3000 motion axes are controlled by IcePAP on almost all the ESRF beamlines as well as part of the accelerator complex. A campaign to systematically replace the old VPAP/DPAP controllers with IcePAPs is underway and will be completed during Phase II. Phase II will provide the opportunity to capitalise on the existing platforms and push the development of new platforms, supporting new needs in terms of beamline control.

Motion control platform (CP3): Phase II will also provide a chance to share common standards such as IcePAP from beamline to machine control system (*e.g.* insertion devices) and then capitalise on the expertise acquired by the hardware and software support teams. Use of the IcePAP standard on the insertion devices will enable better synchronisation when scanning monochromators and insertion devices.

DAnCE general purpose platform for data acquisition and control electronics (CP4): New hardware developments increasingly require the integration of intelligent embedded controllers and the implementation of generic communication interfaces. The use of high performance controllers (Linux based) and standard ubiquitous interfaces (Ethernet) is an approach already successfully adopted in various ESRF development programmes such as the motion controller IcePAP. DAnCE targets the preparation and adoption of a new generic platform to be used systematically for new in-house development of control equipment as well as X-ray detectors (specifically data acquisition). DAnCE will make use of real-time Linux. The DAnCE platform will, notably, support the development of the new synchronisation and sequencing modules mentioned above.

Library for image acquisition (LIMA) (CP5): LIMA, started during Phase I, is a project aimed at unifying the control of 2D detectors. The goal of the LIMA project is to clearly separate hardware specific detector code from common software configuration and features, like setting standard acquisition parameters (exposure time, external trigger), file saving and image processing. Phase II will give the opportunity to integrate all detectors into LIMA, establishing it as the standard used right across the ESRF.

Real-time control and data acquisition (CP8): Phase II will see an increasing number of control applications that need real-time control. A good example of this is nano-positioning, which will be needed on all beamlines working with nano-beams (see **Sections 4.1** and **4.2**). Real time needs can be broken down into three regimes (see **Table 4.07**).

The first regime will be solved with programs written in C/C++ or Python running under Linux on a CPU which is clocked sufficiently fast and has sufficient resources. On multi-core CPUs, a core can be dedicated to the soft real-time application. The second regime will be solved with real-time Linux using hard-real-time extensions. The third regime will be solved with FPGA's. All three regimes are compatible with the DAnCE platform. In those cases where a more user-friendly programming environment is required a commercial platform will be considered.

	Applications sampling	Timing constraints
Soft real-time	Hz to 1 kHz	Flexible
Hard real-time	Hz to 10 kHz	Strict
Fast real-time	10 kHz to MHz	Strict or flexible

Table 4.07: The three different domains of real time control.

Moving from TACO to TANGO (CP6): A large number of device servers on the beamlines are still in the legacy control system TACO. The TANGO control system (see **Section 2.4.10**) has been developed to replace TACO and is being used for all new developments. The porting of TACO servers to TANGO will be completed at the beginning of Phase II. Guidelines and rules for designing the device servers in TANGO will be defined to ensure best use of the additional features in TANGO. TANGO provides high-speed, event-based communication. This mode of communication will be used for the continuous scan and sample environment controllers.

Graphical user interface (GUI) (CP7): GUIs are essential for user friendliness, and, as many users of the ESRF come to the beamline for only a few days and sometimes only hours, they cannot be expected to learn how to operate the beamline without a user friendly interface. The best examples of beamline GUIs are MxCube on the structural biology beamlines and applications for microscopy (ID21) and clinical trials (ID17) on the imaging beamlines. Many beamlines however do not have GUIs for doing experiments. Phase II will generalise the use of GUIs on all beamlines in order to allow users to draw maximum profit from the new source, new detectors and new beamline control sequencer.

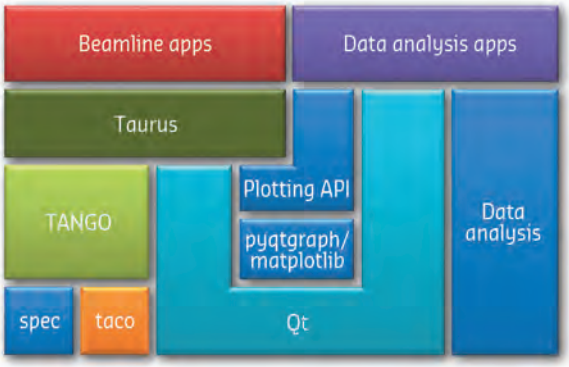

Figure 4.19: Diagram of desktop GUI technology stack.

The short- and medium-term strategy for Phase II is to provide a stable platform for developing desktop GUIs for all beamlines. In order to build upon the trend towards Python with the new sequencer, the GUI toolkit must be Python-friendly. The GUIs will be based on Taurus and Qt (see **Figure 4.19** for a schematic of the technology stack). Taurus is a graphical toolkit for TANGO, co-developed with ALBA and other light sources. The technology stack allows a

maximum of sharing with data analysis applications. Plotting and visualisation will be implemented via a plotting interface with different backends for the low-level plot widgets. The plotting interface and backends will be the same as those used for the data analysis applications.

The long-term strategy for graphical user interfaces is to follow the trend towards web technologies and browser-based applications.

4.4.3. IMPLEMENTATION SCHEDULE

The long shutdown of the machine is instrumental in the way in which the migration to a new control system will be implemented. A tentative timeline is presented in Figure 4.20.

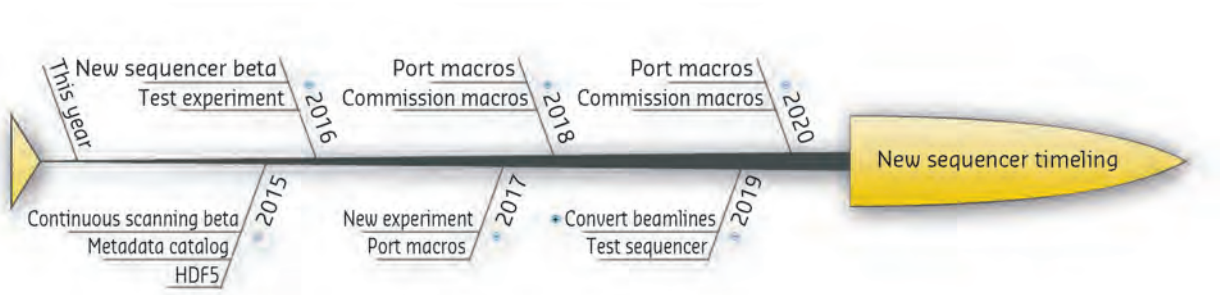

Figure 4.20: Timeline for implementing the new sequencer.

References

Jerkowitz J., Big Data hits Beamline, DEIXIS Magazine (2013)

http://www.hdfgroup.org/HDF5/

http://lima.blissgarden.org/overview.html

http://www.nexusformat.org/

http://icatproject.org/

http://www.certif.com/

4.5. DATA ANALYSIS

4.5.1 OBJECTIVES AND DELIVERABLES

Phase II Deliverables

- A new platform to enable service oriented data analysis, both on-site and off-site.
- Phase II specific science driven projects.

Data analysis presents a growing challenge for all user facilities. Data analysis is not a purely algorithmic problem and includes many aspects of scientific computing in general and of high performance computing in particular. For this reason, the Phase II data analysis programme will address a broad range of scientific and computing areas (see Table 4.08)

The following sub-sections detail the development programmes listed in Table 4.08.

One of the main issues users will face with Phase II is the huge volume of data produced by certain experiments. It could prove very difficult if not impossible for them to take their data away with them for analysis, and it is clear that, in the future, data analysis will have to be done increasingly on-site. Phase II will prepare the future "Data Analysis as a Service" (DaaS) by setting up a platform. Data analysis as a service is a paradigmatic shift in the way data analysis is managed at the ESRF. In certain domains, beamline scientists have traditionally reduced and partially analysed the raw data on behalf of the users, but this has not been the case for most beamlines. Providing a data analysis service to users will only be possible with extra financial and human resources in the form of external collaborations.

	#[1]	Technology	Development objectives	Type[2]	Phase II[3]
Scientific algorithms	AS1	Tomography	Incorporate new, faster analysis algorithms	A	
	AS2	XRPD, SAXS, WAXS	Real time online data reduction Integration of multiple, high-speed detectors Increase modelling capacities	G	
	AS3	For structural biology	Serial crystallography Screening Very high sample throughput Workflows	A	✓
	AS4	Coherent diffraction imaging	Install and develop software packages	A	✓
	AS5	Hyperspectral imaging and multivariate data analysis	Extend to multi-technique mode	G	
Computing	AC1	Data visualisation	Develop complete set of tools for 1D, 2D, 3D, 4D ...	G	✓
	AC2	Data formats	Generalise use of HDF	G	
	AC3	Parallelisation of algorithms	Speed up algorithms by porting to general purpose GPUs and multicore CPUs	G	

Table 4.08: Overview of development programmes in the data analysis programme, including scientific algorithms (AS) and computing technologies (AC). # = R&D programme reference ID. Type: G = General purpose technologies; A = Application-specific development. Projects dependent on Phase II are marked in the last column.

4.5.2. MAIN AREAS FOR SCIENCE-DRIVEN DEVELOPMENTS

Tomography and imaging (AS1): In recent years, advanced X-ray imaging has made significant progress pushing the limits of spatial, time resolution, and image contrast far beyond what can be accomplished by current commercial scanners. Besides absorption contrast, other techniques are becoming commonplace such as phase contrast and 3D X-ray imaging modes, the latter based on the collection of fluorescence and diffraction signals emitted from the sample.

To perform 3D imaging at ultra-high resolutions, state-of-the-art X-ray imaging devices must be combined with tomography capabilities. However, many algorithmic problems emerge when reaching the bleeding edge of tomography. Customised reconstruction algorithms are needed, capable of reconstructing images from a small number of noisy projections acquired in fast scans. These algorithms should incorporate nonlinear image formation models and be robust with respect to experimental instabilities. Novel reconstruction algorithms that have been developed in the mathematical tomography community are able to provide these advantages, yet are typically not well suited for direct application to complex nonlinear reconstruction problems.

The key problem that the experimental X-ray community is currently facing is how to turn this algorithmic development into novel computational tools that can be used in the experimental workflow.

Conversely, adapting the experimental setups to the specific capabilities of advanced reconstruction methods could potentially lead to improved data. To unleash the full potential of the advances, more advanced theory and algorithms are needed to achieve new breakthroughs in the field, especially for limited data reconstructions.

A model for an international centre for scientific computing: During Phase II, experimentalists will be faced with huge quantities of data and formidable computing challenges that can only be overcome by direct collaboration with computational scientists. It is hence extremely important to create an international centre for scientific computing in advanced X-ray tomography at the ESRF during Phase II. This centre would host visiting computer scientists and provide them with training, access to experimental data and software, and direct intensive collaboration opportunities with experimental scientists. Direct feedback from the experiments will provide a unique opportunity for streamlined collaborative development of algorithms. An initiative, which could serve as a model for the future, is currently endorsed by the EU COST Action EXTREMA (MP1207), a network of international researchers on both experimental and computational aspects of X-ray tomography, which runs from 2013-2017. The ESRF will profit from this momentum, and make effective use of the available funding opportunities.

The main areas that an enlarged data analysis community should address are:

- Software and data exchange, *i.e.* establishing a common software platform facilitating the exchange of datasets and experiments with different types of algorithms
- Quantitative models of X-ray image formation promoting efficient computation while also accurately modelling the underlying physics
- Novel reconstruction algorithms that can deal with the specific (often non-linear) problems of various X-ray imaging techniques
- Conventional transmission imaging
- Phase contrast imaging, which allows reconstructing the refractive index of the object
- Advanced phase retrieval algorithms
- 2D and 3D diffraction imaging aimed at reproducing shape, orientation and strain of individual grains in polycrystalline samples
- Fluorescence imaging, to perform chemically sensitive X-ray imaging

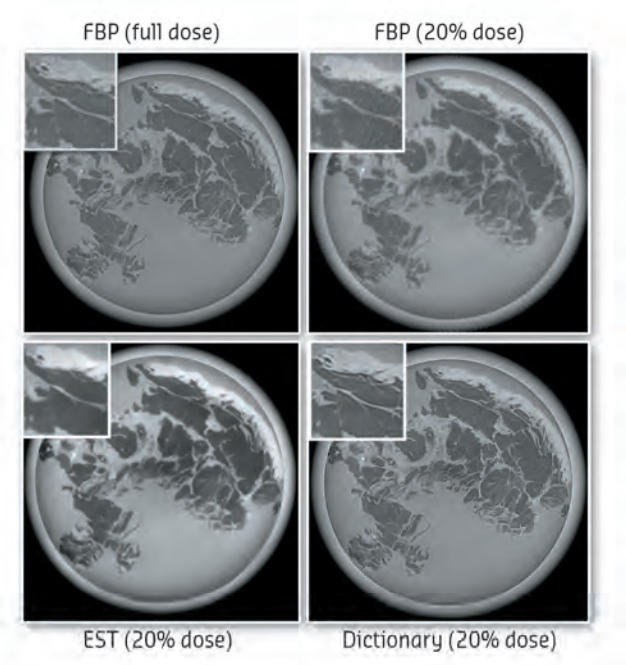

Figure 4.21: Comparison of the reconstruction obtained with Filtered Back Projection (FBP) at full dose, *i.e.* 1000 projections (top left) and the reconstructions made with 20% of the full dose using FBP (top right), Equally Sloped Tomography (EST) (bottom left) and the dictionary learning methods (bottom right) for a human breast. Note that only the dictionary method resolves clearly the small veins. Credit: A. Mirone, E. Brun, and P. Coan *et al.*, ESRF/ Ludwig Maximilians University.

The expected increase of speed in data acquisition with Phase II, combined with algorithmic advances and continuous scanning, will allow experiments to be performed on much shorter timescales than is currently the case. Solving the formidable algorithmic challenge of tomographic reconstruction of objects with a limited number of projections (**Figure 4.21**) will also be useful for a vast class of samples, typically found in medical, life and soft matter science, which are radiation sensitive.

X-ray powder diffraction (XRPD) (AS2): The ESRF operates a beamline dedicated to high resolution XRPD (ID22, relocated from ID31 during Phase I of the ESRF Upgrade Programme). This beamline will take advantage of new area detectors like the high-Z pixel detector (*i.e.* CdTe-MaxiPix) to collect more photons.

The introduction of 2D detectors means the region of interest needs to be adjusted dynamically depending on the position of the moving 2-theta arm in order to remove the peak shaped asymmetry. This integration and normalisation has to be performed almost in realtime and will require a specific data analysis code to be developed and integrated into the LIMA server.

WAXS and SAXS online (AS2): Most other beamlines performing SAXS and WAXS are already using a setup based on large area detectors.

The trend for Phase II will be:

- Overall migration from CCDs with taper (*e.g.* FReLoN) to pixel detectors (*e.g.* Eiger)
- Larger detectors 4 MP => 16 MP detectors
- Faster detectors 1 GBit/s to multiple 10 GBit/s links (used at full capacity)
- Multiple detectors to collect photons over a wider solid angle with consequences on the synchronisation of these detectors (and data)

The main consequence of this trend is the foreseeable bottleneck in accessing the data for processing. One option is to treat data while they are still in the memory of the computer. This requires dedicated computing power located next to the source of data (detector) or at the junction of all data fluxes. A large effort has already been made to parallelise azimuthal and radial integration algorithms, reaching 200 MP/sec with PyFAI (Kieffer & Wright, 2013). However, such a library is merely a building block and still needs to be integrated into the data acquisition pipeline to treat the data on-the-fly. Finally, many users need algorithms like those in PyFAI to be integrated into user-friendly interfaces.

Technological survey: Many new algorithms are being developed in other fields of science such as computer vision and neurosciences, some of which have already proven to be useful for synchrotron radiation experiments:

- Automatic sample centring for protein crystallography
- Image alignment based on SIFT algorithms.

These new algorithms allow unprecedented kinds of experiments to be performed at synchrotron sources (*e.g.* full-field XANES technique). This requires an active technological survey to be carried out and manpower to implement them locally and fully understand their limitations.

SAXS offline: SAXS online data analysis for macromolecules in solution has reached a very high level of automation at the ESRF, especially at BM29, where the users can go home with the reconstructed models of their scattering samples, typically proteins. This is made possible thanks to two extremely fast data reduction PyFAI-based pipelines and one *ab initio* modelling pipeline. However, the results are reliable only if the solutions are well diluted and have to a large extent uniform dispersity. For an in-depth post-experiment analysis of collected data, new modelling software needs to be developed.

Today more than ever, the visibility and reliability of the internal structure of software packages needs to be verified by the scientific communities. This means a common effort towards transparency of process. The source code for the software to be developed during Phase II will be open source (Pernot *et al.*, 2013 and De Maria Antolinos *et al.*, under review).

Structural biology (AS3): Phase II of the Upgrade Programme will define a new paradigm for structural biology. The increase in X-ray brilliance and new detector technologies will make it possible to collect huge sets of data (TB) in a very short time (minutes). Phase II will not only permit an evolution of the current experiments, but it will also open a whole new area of experiments such as serial crystallography. In both cases, data analysis software must be further developed in order to take full advantage of the increased source quality. A few examples of exciting new scientific techniques enabled by new MX beamlines and their data analysis software needs:

- Combining MX with other techniques
- Fragment screening
- Serial crystallography
- Multi-crystal data collection
- Remote data analysis

Combining MX with other techniques: Structural biology is evolving rapidly towards a new level of complexity by addressing the association of biological macromolecules into higher-order structures up to sub-cellular structures. One of the crucial steps for solving 3D structures of bio-macromolecules is the combination of macromolecular X-ray crystallography, nuclear magnetic resonance (NMR) and electron microscopy (EM). This objective demands a huge increase in computing capacity and will have

a profound impact from basic to clinical research. It also requires synergistic integration of the above three techniques and also other complementary techniques such as spectroscopy and small angle scattering. All this will require a transition from the need to analyse data collected at a single experimental facility to the need to analyse data collected at several locations. These issues render structural biology ideally suited to an e-Science environment. This transition provides an opportunity for the European structural biology community to drive the evolution of the field and ultimately contribute to the cutting edge of cell and systems biology. A combination of ESRF local HPC and Cloud technologies would permit the integration of IT resources, experimental data, and applications of the major European structural biology centres. This infrastructure should be made available for users permitting them to process, elaborate, analyse and visualise their own data, regardless of their origin. To sustain its service activities, the proposed environment should also link up to national and European initiatives and possibly also build upon the collaborative network of the ESFRI-INSTRUCT infrastructure. Finally, research activities should be envisaged to optimise services and provide new solutions for the integration of structural biology data.

Fragment screening: Pharmaceutical industrial users and academic laboratories that study mammalian receptors (such as GPCRs) need to perform ligand (protein interaction) studies. The upgraded source, along with the novel automation under development in Phase I (UPBL10) will make fragment screening a routine tool for this kind of research. New toolkits for automatic data reduction and fragment analysis, relying on the combination and sorting of different outputs and techniques (*e.g.* BioSAXS, spectroscopy, etc.) must be developed.

Serial crystallography: Serial crystallography is currently being pioneered at coherent X-ray sources (LCLS, XFEL, SACLA, etc.). Thousands of crystals are exposed to a pulsed X-ray beam and a single (still) diffraction pattern is recorded from each one, before Coulomb explosion occurs. Software to reduce these new kinds of data is currently under development (Gati *et al.*, 2014 and Sauter *et al.*, 2013). ESRF will join this effort during the commissioning of Phase II in order to be able to sort, index and integrate these data sets on-the-fly, where possible. The data analysis needs to be intrinsically linked with new data acquisition software.

Multi-crystal data collection: Hierarchical cluster analysis (HCA) has proven to be an extremely powerful tool, whereby extremely low anomalous signals can be exploited by merging data sets from different crystals that are correlated. The current goal is to perform this analysis on partial datasets and develop and implement the tools enabling this. With UPBL10 it is conceivable to collect tens or even hundreds of partial datasets from different positions in the same crystal or from different crystals, both at cryo- and room temperature. All collected datasets are automatically processed. Tools to rank the results of processing and to apply HCA in order to "build-up" a complete dataset will be investigated and eventually applied.

Remote data analysis: Currently, the results of each characterisation and related processing are stored in a LIMS (laboratory information management system) database (ISPyB) dedicated to structural biology (Delagenière *et al.,* 2011). The new data production rate and the new type of datasets require ISPyB to be extended from an electronic logbook to an active tool used to launch and drive data evaluation remotely. It should enable re-launching of automatic processing and combination of data across different experiments belonging to the same user ID and project. This development will pave the way for a new approach to data analysis "Data analysis as a service" (DaaS) where the amount of data collected will not be exportable.

Workflow tools: Progress in macromolecular crystallography and in structural biology at synchrotron radiation facilities in terms of automation and beam delivery has been constantly boosted by software development for crystal evaluation, automatic data reduction and real-time combination of data collection and data analysis.

The ESRF has been a leading facility on this front. Present tools allow the best possible datasets to be collected using automated pipelines ([Incardona *et al.,* 2009) where each dataset is automatically reduced using two levels of processing, in order to better meet users' requirements. Currently, the data reduction is being expanded to perform the automatic determination of unknown structures and the identification of protein-ligand complexes of known structures.

The recent implementation of a workflow tool (Brockhauser *et al.,* 2012) has revealed new opportunities for processing the data in real-time and uses the results while a crystal is still in the beam, hence enabling complex experiments (see **Figure 4.22**). For example, the automatic X-ray centring workflow locates the crystal in an opaque medium by measuring its diffracting power and then positions the sample in an optimal manner in the beam for data collection.

For Phase II, data will be collected at kHz rates, meaning that data must be very rapidly reduced and analysed in order to assess on-line the data quality and obtain feedback for further data collections. Also, the amount of data collected will be so huge that users will not have obvious solutions to transfer experimental data to their home labs. Therefore, the development of rapid data reduction software,

benefitting from large arrays of processing units and possibly powerful GPUs, is of paramount importance. Moreover, to make provision for automation of complex experiments, workflow tools will be developed further.

Coherent diffraction imaging (AS4): The recent developments of X-ray methods for biophysical and materials science have experienced breathtaking progress owing to the advent of coherent synchrotron radiation. Scanning nano-diffraction, ptychography with simultaneous object probe and phase retrieval, full field phase contrast imaging and tomography are promising techniques to uncover new frontiers of knowledge on the nanoscale. Well-known examples are the reconstruction algorithms, which will need to be adapted and optimised in view of the weak signal coming from cellular diffraction in order to avoid radiation damage. For nano-diffraction, advanced algebraic techniques will be employed, based on statistical and computational techniques to reveal hidden factors in real and reciprocal space. It would be highly desirable to represent data in an automated and model independent manner. This approach will be complemented by model building, similar to existing SAXS analysis software packages, however with appropriate adaptation/generalisation to nanoscale beams. These activities will lead to a *data analysis platform* and knowledge-base that will be made available to the ESRF community through already planned international collaborations.

A software package will be further developed on the basis of an existing platform contributed by the University of Göttingen. Ptychographic and iterative phase contrast reconstruction, as propagation methods, represent two examples where the existing software could be improved for the user community. Other groups in Europe are promising collaborators in this area and if possible their code should be integrated into a single software package.

Hyperspectral imaging and multivariate data analysis (AS5): Spectroscopic imaging techniques producing hyperspectral data sets are increasingly common at the ESRF. Their high spectral resolution enables material identification via adequate analysis. Through Phase II, we will develop a set of innovative tools by building on existing tools (see Figure 4.23 for an example of a well-known tool – PyMca – developed at the ESRF) for analysing XRF, XRPD, XANES, EXAFS, IR, UV and Raman spectral data.

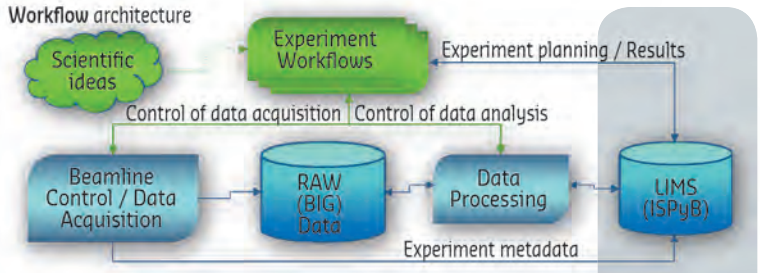

Figure 4.22: The use of a workflow tool facilitates the implementation of scientific ideas into interactive scientific workflows which control both data acquisition and data analysis. The use of a LIMS is mandatory for experiment preparation and follow-up.

The tools to be developed during Phase II will implement:

- Map alignment with different map resolution and orientation handling using *e.g.* GPU-accelerated algorithms like the scale invariant feature transform (SIFT)
- Algorithms showing hidden correlations combining information obtained by each technique
- Evaluation and implementation of blind source separation techniques
- A reference compound and database search engine based on principal component analysis (PCA) or akin (a very common technique in XANES and IR)
- Descriptive tool of huge datasets in terms of their, *e.g.*, PCA decomposition (very important for dimensionality reduction)
- Data format writing utility based on HDF5 and with multipurpose scope to make allowance for generic fitting routines with user defined functions

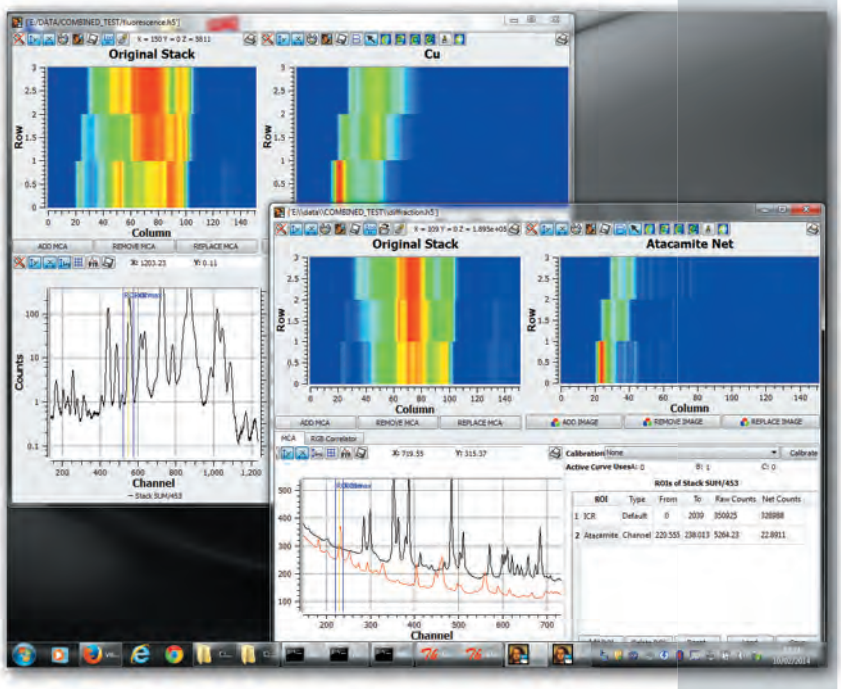

Figure 4.23: Fluo-diffraction imaging, an example being analysed with PyMca.

4.5.3. MAIN AREAS FOR COMPUTING DEVELOPMENT

The scientific objectives for data analysis in Phase II are ambitious and all extremely demanding in terms of human resources and computing infrastructure. The data analysis problem goes well beyond a purely algorithmic one. The main computing areas that need to be worked on during Phase II are:

On-line data analysis: Almost all beamlines require the implementation of a quick data processing user front-end capable of providing, visualising and manipulating data effectively on-line in order to help in the decision process of the running experiment. This step has been universally recognised as being of crucial importance for determining the success of an entire measurement campaign, since the scientist can decide the right strategy at an early stage based on a pre-analysis of the experimental data.

Data visualisation framework (AC1): The interactive presentation of N-dimensional data as projections, sections or iso-surfaces is central to the scientific interpretation of results from complex experiments possibly combining different techniques. Among the challenges to be faced, efficient recognition algorithms for correlations in the data and automated search strategies for clustering and classification are high on the list of missing features. Implementing these would enable the identification of scientifically meaningful sections of the sample parameter space.

HPC algorithms (AC3): The HPC techniques and technologies for data-intensive science are different from traditional computational science and can be seen as a new paradigm for scientific exploration. In terms of specific data analysis objectives to be realistically pursued at the ESRF, it will be essential to exploit the potential of novel architectures such as massively parallel and distributed systems capable of providing the analysis necessary to extract meaningful information from huge data streams. This must be done whilst addressing the bottlenecks which restrict the flow of data within and between these systems and thus limit the potential for handling big data.

The challenges to be faced while undertaking the next generation data analysis are:

- Port existing algorithms to highly parallel environments
- Incorporate reusable algorithms within a generic problem solving environment
- Automate workflows involving several analytical steps
- Adapt the software as a service (SaaS) model to data analysis as a service (DaaS) and provide easy access via a browser

The use of novel architectures supporting highly-parallel data analysis leads to the challenge of how to programme the hardware devices efficiently. There is a need to rewrite existing codes to exploit parallel architectures using libraries like OpenCL, which is the currently dominant open general-purpose GPU computing language.

Research using big data requires software capable of giving efficient scientific insight into that data. A typical experimentalist without expert software knowledge will not be able to analyse their data with standard tools and algorithms, since they were not specifically designed to cope with such high data rates and volumes and often exhibit problems with runtime memory usage and/or may have unacceptably long execution times. An important goal is to develop a scientific computing framework that will transparently handle tasks such as parallelisation, workflow management, load-balancing, GPU (typically NVIDIA) enabled image processing, etc., in the context of big data flows. A collaborative effort with other facilities and the targeted enrolment of young researchers within a Horizon 2020 Proposal will be, if successful, focused on optimising massively parallel systems.

Recent products in mainstream computing such as micro-servers, accelerators, low power x86 processors and other low power architectures such as 64-bit ARM and even Xeon Phi servers offer interesting opportunities to explore new ways of benefitting from the new generation of high performance, power optimised devices for high throughput data processing. In particular, the platforms to be developed must deliver a combination of ease-of-programming and enhanced performance comparable with or improving on purely hardware-based solutions such as FPGAs.

Data Formats (AC2): Most European synchrotrons have adopted the Nexus format, which consists of a set of conventions and a library to write data mainly in HDF5 binary format. HDF5 is particularly well suited to dealing with large datasets. New generation detectors (*e.g.* EIGER) are natively recording data in this format. However, at present, most ESRF beamlines are still generating data in SPEC and ESRF format (EDF), which causes problems for users (experimental data spread across different files with different formats), for system administrators (thousands of small files) and for data analysis code developers due to the inability to keep together the data and metadata. Currently, two ESRF beamlines (BM29 and ID21) are regularly generating HDF5 files as a first step after automatic data reduction. Three other beamlines (ID02, ID16NI and ID16NA) are expected to follow shortly. One important objective

is to generalise the use of HDF5 to the rest of the ESRF beamlines, giving priority to those generating large amounts of data. Most data analysis codes written by the ESRF can already import and export HDF5 files (see Figure 4.24).

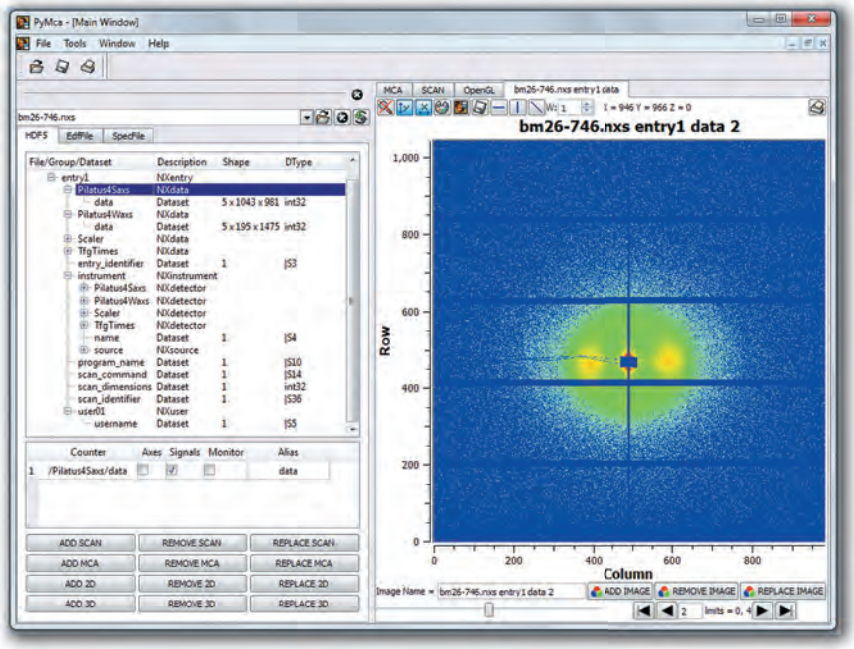

Figure 4.24: PyMca is regularly used at several synchrotrons for HDF5 data visualisation and analysis.

References

Brockhauser S. *et al.*, The use of workflows in the design and implementation of complex experiments in macromolecular crystallography, Acta Crystallogr D Biol Crystallogr. **68**, 975–984 (Aug 2012).

Delagenière S., Brenchereau P., Launer L. *et al.*, ISPyB: an information management system for synchrotron macromolecular crystallography, Bioinformatics **27,** Issue: 22 , 3186-3192, (Nov 2011).

De Maria Antolinos A., Pernot P., Brennich M., Kieffer J., Bowler M., Delagenière S., Ohlsson S., Malbet Monaco S., Ashton A., Franke D., Svergun D., McSweeney S., Gordon E. and Round A., ISPyB for BioSAXS: the gateway to user autonomy in solution scattering experiments, Journal of Applied Crystallography (under review).

Gati C., Bourenkov G., Klinge M., Rehders D., Stellato F., Oberthür D., Yefanov O., Sommer B.P., Mogk S., Duszenko M., Betzel C., Schneider T.R., Chapman H.N. and Redecke L., Serial crystallography on in vivo grown microcrystals using synchrotron radiation, IUCrJ **1**, 87-94 (2014).

Incardona MF., Bourenkov GP., Levik K., Pieritz RA., Popov AN., Svensson O., EDNA: a framework for plugin-based applications applied to X-ray experiment online data analysis, Journal of Synchrotron Radiation **16**, 872-9. (Nov 2009).

Kieffer J., Wright J.P., PyFAI: a Python library for high performance azimuthal integration on GPU, Powder Diffraction **28 Supplement 2**, S339-S350, (2013).

Mirone A., Brun E., Gouillart E., Tafforeau P., Kieffer J., The PyHST2 hybrid distributed code for high speed tomographic reconstruction with iterative reconstruction and a priori knowledge capabilities, Nuclear Instruments and Methods in Physics Research B (*in press*).

Pernot P., Round A., Barrett R., De Maria Antolinos A., Gobbo A., Gordon E., Huet J., Kieffer J., Lentini M., Mattenet M., Morawe C., Mueller-Dieckmann C., Ohlsson S., Schmid W., Surr J., Theveneau P., Zerrad L. & McSweeney S.: Upgraded ESRF BM29 beamline for SAXS on macromolecules in solution, Journal of Synchrotron Radiation **20**, 660-664 (2013).

Sauter N.K., Hattne J., Grosse-Kunstleve R.W. and Echols N.I.: New Python-based methods for data processing, Acta Cryst. **D69**, 1274–1282 (2013).

Sole V.A., Papillon E., Cotte M., *et al.,* A multiplatform code for the analysis of energy-dispersive X-ray fluorescence spectra, Spectrochimica Acta Part B-Atomic Spectroscopy **62**, 63-68, (2007).

https://github.com/kif/pyFAI

http://en.wikipedia.org/wiki/Dispersity

http://opensource.org/

http://www.desy.de/~twhite/crystfel/

4.6. COMPUTING INFRASTRUCTURE

Computing infrastructure is driven by the need to transfer, store, process, and export data produced at the ESRF beamlines. Until recently the infrastructure was dimensioned for the provision of all required services in a generic manner. With the advent of high speed and high resolution pixel and CCD detectors, the generic approach has reached its limit and it has now become mandatory to implement solutions specifically designed for high throughput during Phase II. This was already the case for the Pilatus and pco.dimax detectors in 2012/13 and will be even more so with the delivery of Eiger detectors in the second half of 2014.

The average ESRF data production stood at 2.5 TB/day in 2013. This number will quickly evolve with new detectors finding their way to the beamlines. The Eiger 4M detector will soon be used on the Massif beamline complex (ID30) and ID13, and is capable of generating images of 12 Mbytes at a maximum rate of 750 images per second. This corresponds to an internal data rate of 9 GBytes/sec. After data compression, a single 10 Gbps Ethernet link will send the data to disk for uncompressing and analysis. Even assuming a duty cycle as low as 1% (*i.e.* 15 minutes/day), each Eiger detector would still produce 1 TB/day of compressed data. The Eiger detector examples show the level of chellenges to be faced in the near future, not only by the IT infrastructure but also by the scientists having to deal with such volumes of data.

4.6.1. OBJECTIVES AND DELIVERABLES

Phase II deliverables

- Bandwidth optimised dedicated storage solutions for beamlines using fast high resolution detectors
- High performance centralised storage systems based on parallel file systems

The selection and integration of high performance components on the beamlines and in the data centres will require additional human resources during Phase II. The new systems will only partly replace existing systems or techniques and complement core functions with their high performance counterpart (Table 4.09). Already during early investigations, our experts concluded that it will not be possible to find high performance systems that preserve compatibility with all the existing computing hardware at ESRF. Specific stand-alone solutions tailored to a single or a group of beamlines are required to achieve the performance levels for Phase II beamlines and detectors. These systems will be complex to design and integrate into the beamline operation and proper integration and optimisation of the systems means that the engineers specialised in networking, Linux and Windows systems administration, beamline control, and data analysis will have to work closely together to be successful. An important aspect to be taken into account for all developments is the reliability of the components and ultimately the reliability of the full data management and analysis chain.

Over the duration of Phase II, it is estimated that an additional 15 person-years, *i.e.* an average of 3 full-time employees over a five year period, are required to work on the selection and integration of local buffer storage solutions, central storage systems, and co-processor architectures. The equivalent of 2 full-time employees will work on local buffer storage solutions beamline after beamline and 1 full-time employee on central storage systems, batch processing and data access mechanisms. This is expected to be complemented by human resources from manufacturers for *in situ* testing of specific equipment on the beamlines or the data centres.

The ESRF IT infrastructure is kept up-to-date by an annual operation capital investment of about 1 M€. During Phase II, this will be complemented by 420 k€/year to allow for additional investments in IT-components, notably high-performance storage and backup systems.

	#	Technology	Development objectives	Type	Phase II
Lower Latency	ITL1	Platform development, procurement and operation	Develop IT solutions in terms of bandwidth, storage capacity, and computational capacity, dedicated to specific detectors/beamlines to guarantee bandwidth for fast data writing and simultaneous reading for on-line data analysis	G	✓
	ITL2	Platform development, procurement and operation	Explore and provide new concepts for central storage systems for increased bandwidth in line with the expected data flow from the beamlines and the requirements for fast data analysis with massively parallel clusters.	G	✓
	ITL3	Platform development	Explore new co-processor architectures for potential gains in price, performance and power consumption	G	✓
	ITL4	Platform development	Optimised batch processing environment for small jobs	G	✓
	ITL5	Platform development	Investigate new hardware and software solutions for data export	G	✓
Higher capacity/additional functionality	ITC1	Procurement and operation	Procurement and operation of high performance compute clusters	G	
	ITC2	Procurement and operation	Extension of tape based backup and archival systems	G	
	ITC3	IT security	Fine grain data access control coupled to an authentication, authorisation and accounting (AAA) infrastructure	G	✓
	ITC4	Procurement and operation	Continuous upgrade of data communication network	G	

Table 4.09: Overview of development programmes in IT infrastructure, focusing on lower latency (ITL), higher capacity (ITC). # = R&D programme reference ID. Type: G = General purpose technologies; A = Application-specific development. Projects that are dependent on Phase II are marked in the last column. ITC1, ICT2, and ICT4 are not further developed in this chapter.

4.6.2. BIG DATA

The new source will deliver much brighter and time-structured X-ray beams that will enable new science. The evolution of the machine will be accompanied by a constant development of new detectors, capable of faster frame rates, higher resolution and wider dynamic range. All this will result in more data that needs to be processed on-line and off-line, with adequate and dedicated processing power and with suitable software, tailored to the different scientific domains at ESRF.

All beamlines will experience increased data rates. While photon flux, resolution and in some cases detectors are limiting factors today, the new diffraction limited source as well as advances in detector technology will overcome most of these limitations. From this point onwards the human factor will be the new bottleneck because of the time needed to produce, exchange or modify samples and to analyse the huge amount of data recorded during an experiment. Some of these limitations may evolve further, thanks to the implementation of new robotics (*e.g.* MASSIF UPBL10 for structural biology) or by automatic pre-analysis of data (as, for example, done nowadays for structural biology and X-ray imaging). An estimation of the future data rates and storage requirements on some of the ESRF beamlines, assuming a data retention time of 200 days, is presented in **Table 4.10**.

The computing infrastructure has not only to guarantee write performance to keep up with the detector read-out, but the data must also be instantaneously available for pre-processing and analysis and be stored in a common file-system where users have access for further processing and data export.

Currently, fast detectors, such as the Pilatus6M, are connected via a private link to a so-called local buffer storage (LBS) system where data is written before being transferred to the centralised file-system

(NICE). This has been implemented such that data can be written to disk at a guaranteed speed. For Phase II, an enhanced version of such a setup is required which will extend the role of LBS further by linking it with an on-line data analysis server, equipped with appropriate processing units. Recorded data and analysed data are mirrored to long-term storage (today NICE). Long-term storage permits access to data and pre-analysed data for further analysis and data backup/data archival.

Beamline	Average output (TByte/day)	Max burst (MByte/s)	Storage space needed (TBytes)
ID19	15.0	2 000	3 000
ID16	5.0	2 000	1 000
ID02	2.0	240	400
ID09b	0.6	90	120
ID10	1.0	4 000	200
ID13	3.5	4 000	700
ID01	40.0	4 000	8 000
ID03	40.0	4 000	8 000
ID11	17.0	2 000	3 400
ID15a	2.0	2 000	400
ID31 (old ID15)	2.0	2 000	400
ID22 (old ID31)	2.0	2 000	400
ID23-1	3.0	155	600
ID23-2	5.0	2 000	1 000
ID29	3.0	155	600
MASSIF-1	5.0	2 000	1 000
MASSIF-3	5.0	4 000	1 000
ID30B	5.0	620	1 000
BM29	2.0	4 000	400
TOTAL	158.1		31 620

Table 4.10: Estimated data rates and storage requirements for some of the ESRF beamlines.

The sub-micrometre beams will permit finer sampling, and together with time-framed experiments, will result in much more data. The amount of data that can be produced during an experiment indicates that manual data analysis may become unsustainable in many cases and therefore on-line data analysis should be reinforced by developing pipelines and software for automatic pre-analysis and/or data sorting.

It appears unlikely that all home laboratories of visiting scientists will have the capacity to store and analyse the raw data collected at the ESRF. The current data storage policy (to keep visitor data for 6 months) should continue to be sufficient following Phase II, but for some experiments this may need to be extended. A possible evolution for the ESRF would be to extend its mission further from being purely a photon facility by offering computing services for its user community. This encompasses both the need for dedicated computing power and the development of data analysis software and pipelines that can provide users with an efficient remote interaction with their data (*cf.* De Sanctis *et. al.*, 2013).

Pre-treated or processed data should be available for a longer time span (at least for certain groups) than raw data. Furthermore, because of the large amount of data, the need of accessing data remotely and to sort through data in function of experimental parameters (*e.g.* temperature, pH, sample origin, etc.) makes the development and implementation of databases and electronic logbooks compulsory.

4.6.3. DATA MANAGEMENT

Data from ESRF experiments is currently kept on disks for 50 days and all data is saved on a daily basis to tape. Data on backup tapes are kept for about six months, after which the tapes are re-used, *i.e.* after a period of about six months experimental data disappears from ESRF.

The situation is different for in-house research data where users manage their disk space individually. No automatic expiry of data is configured. In-house research data is copied to tape in an incremental fashion and in addition a full backup is performed every two months and kept for six months.

Retention times for external user data may need to be reviewed if large data sets need to be kept for a longer time period at the ESRF. A prerequisite of keeping data at the ESRF is fine grained management of access rights (ITC3). Today, public research data is easily accessible internally by persons other than those having performed the experiment. This is clearly no longer acceptable in the future and work is ongoing to remedy this situation. Protecting data from unauthorised read access will mean that visiting scientists no longer use a generic account but a personal account which is persistent and ideally the same in all photon and neutron infrastructures. Once such personal user accounts are in place, it will be possible to implement access control lists (ACLs) to access the data. Individual user accounts are the core issue of a federated identity management system and in one of the work packages in the PaNdata-ODI FP7 project. A gradual implementation at the ESRF is foreseen over the next few years and will enable the way data is accessed to be changed.

As already mentioned, long-term archiving of in-house research data is possible on request. In addition publicly accessible data catalogues are being built up and will increase in size and significance (*e.g.* the ESRF paleontology database: http://paleo.esrf.eu).

4.6.4. DATA STORAGE, BACKUP, DATA EXPORT (ITL1/ITL2)

The next generation of fast detectors will impose stringent requirements on data storage systems. On one hand bandwidth must be guaranteed because many detectors do not have enough built-in buffer space and, on the other hand, potentially conflicting requirements such as for on-line data analysis, power and cooling, flexibility, and cost of ownership are increasingly important.

Guaranteed bandwidth can only be achieved with dedicated storage systems directly coupled to the detector systems. On-line or quasi on-line data analysis may require copying the data on-the-fly to another storage system which is used to access the data with a CPU and/or GPU/co-processor cluster. The increased data flow from the detectors will make on-line data analysis and visualisation an essential requirement not only to determine whether the experiment is successful but also to reduce datasets as early as possible. Data must then be copied to a large central storage system for successive backup and off-line data analysis.

Central disk-based storage systems will continue to be the main work horse for most of the data processing needs during Phase II, because of the complexity, cost, and lack of flexibility of local beamline storage systems. The central storage has to be large enough to provide storage space at all times, compatible with legacy operation systems of client computers accessing the space, sufficiently fast to avoid bottlenecks in writing and even more so in reading the data from compute clusters. Current NFS/CIFS based network attached storage systems used at the ESRF provide maximum compatibility and flexibility, but lack the required performance. Different storage solutions need to be explored to complement our NFS/CIFS based systems and provide performance levels in line with future detectors and data analysis needs.

First investigations show that it will be difficult to find solutions offering a very high peak performance for single thread reading or writing and high load resilience for parallel access from compute clusters. StorNext, a shared disk file system made by Quantum Corporation that we tested at the beginning of 2014, provides high speed data transfer through link aggregation, whereas it seems that the object based Lustre file system is better suited for compute clusters. Object storage architectures manage data as objects, as opposed to file systems which manage data as a file hierarchy and block storage which manages data as blocks within sectors and tracks. Each object typically includes the data, a variable amount of metadata, and a globally unique identifier. Cloud storage providers like Google, Amazon, Facebook, and many of the Top 500 supercomputers use object storage products.

Other solutions like PanFS or GPFS must be explored. To fully satisfy needs in terms of throughput and capacity, it will be unavoidable to implement several central storage solutions and let them co-exist. However, heterogeneous systems require significant additional human resources to make on-site tests, install, and operate them.

Automatic duplication of data to a high-performance scratch area for access by compute clusters needs to be explored. Such a scratch area for data analysis could have the advantage of off-loading the central storage systems from the massive I/O activity of compute clusters.

Managing the backup infrastructure is not simple and its importance will probably increase over the next decade. Fortunately backups are rarely used for disaster recovery but constitute nevertheless a much appreciated insurance policy. Most frequently backups are used for data recovery due to accidental deletion of data (human error). Tapes remain the most cost effective and also the most reliable way of storing data. After the initial loading of tapes into our tape robots, the tapes are no longer touched by humans and the data on the tapes has a life-span of 30 years according to the manufacturer's specification. Each file on tape has an entry in a relational database constituting the backup catalogue. Because each image from a detector is currently saved in an individual file, the size of the backup catalogues becomes a potential bottleneck. Already today some of our backup catalogues are several hundred Gigabytes in size because they contain several hundred million file entries. Generating large files containing a suite of images, instead of a single file per image, will be essential. The move to HDF5 and multi-image files is necessary to alleviate this problem.

4.6.5. DATA EXPORT (ITL5)

Data export for large datasets (>1 TB) is challenging. Currently users mainly export data to USB-2 or USB-3 disks. Performance is often limited by disk format, brand, file size, directory structure, and performance of reading from NICE under Windows. Backup is mainly done on Windows PCs, which have lower

performance when accessing the centralized file-system compared to Linux PCs. The internet is not usually used because the end-to-end performance is generally very low (1 TB would for instance take 28 hours to transfer at 80 Mbps). Even using the fastest available portable NAS systems would still require significantly more time than the experiment itself. Clearly USB is not a sustainable option for the future because of the limited transfer speed. New industrial standards need to be investigated during Phase II considering that such standards can evolve quickly with time. For the same reason, the option of ESRF purchasing portable storage devices for users is not a sustainable solution due to the quick evolution of such devices. As stated above, it looks unlikely that users will retrieve all raw data in the future but, with a significant development of data analysis capabilities, data export could be limited to reduced or pre-processed data.

Reference

De Sanctis D., *et. al*., ESRF Internal communication, January 2014.

Notes

1 R&D programme reference ID.

2 GP = General purpose technologies;
AS = Application-specific developments.

3 Funded by Phase II.

The milestones for the shutdown, the restart of the accelerator complex, and the restart of the beamlines for full user operation in June 2020 is summarised below.

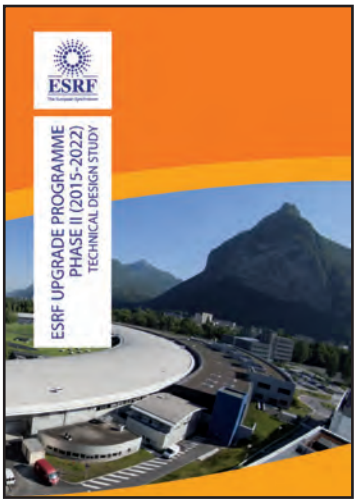

Cover
Cover design by M. Scandella

We gratefully acknowledge the help of the following people in the preparation of this document:
C. Argoud, C. Clavel, M. Dhez, P. Gaget, S. Gerlier, M. Glueckert, L. Graham, A. Joly, C. Mary, M. Scandella, L. Stone, E. Dancer.

Editors
G. Admans, P. Berkvens, A. Kaprolat, J.-L. Revol
Layout
Pixel Project
Printing
Imprimerie de Pont de Claix

© ESRF • December 2014

Communication Group
ESRF
CS40220 • 38043 Grenoble cedex 9 • France
Tel. +33 (0)4 76 88 20 56
Fax. +33 (0)4 76 88 25 42
http://www.esrf.eu

The European Synchrotron
CS 40220 - F38043 Grenoble Cedex 9, France
www.esrf.eu